APPLICATION OF ANN IN STRONG GROUND MOTION PREDICTION

Ph.D. THESIS

by

RAJIV SACHDEVA

DEPARTMENT OF EARTHQUAKE ENGINEERING
INDIAN INSTITUTE OF TECHNOLOGY ROORKEE
ROORKEE – 247667 (INDIA)
DECEMBER, 2014

APPLICATION OF ANN IN STRONG GROUND MOTION PREDICTION

A THESIS

Submitted in fulfilment of the
requirements for the award of the degree
of

DOCTOR OF PHILOSOPHY

in

EARTHQUAKE ENGINEERING

by

RAJIV SACHDEVA

DEPARTMENT OF EARTHQUAKE ENGINEERING
INDIAN INSTITUTE OF TECHNOLOGY ROORKEE
ROORKEE – 247667 (INDIA)
DECEMBER, 2014

I dedicate this thesis

in honor of my son,

SARVAANSH SACHDEVA

INDIAN INSTITUTE OF TECHNOLOGY ROORKEE
ROORKEE

CANDIDATE'S DECLARATION

I hereby certify that the work which is being presented in this thesis entitled **APPLICATION OF ANN IN STRONG GROUND MOTION PREDICTION** in partial fulfilment of the requirements for the award of the Degree of Doctor of Philosophy and submitted in the Department of Earthquake Engineering of the Indian Institute of Technology Roorkee, Roorkee is an authentic record of my own work carried during a period of January, 2008 to December, 2014 under supervision of Dr. Ashok Kumar, Professor and Dr. M.L. Sharma, Professor of Department of Earthquake Engineering, Indian Institute of Technology Roorkee, Roorkee

The matter presented in this thesis has not been submitted by me for the award of any other degree of this or any other Institute.

(Rajiv Sachdeva)

This is to certify that the above statement made by the candidate is correct to the best of our knowledge.

(Ashok Kumar)
Supervisor

(M.L. Sharma)
Supervisor

Date:

The Ph.D. Viva-Voce Examination of **Mr. Rajiv Sachdeva**, Research Scholar, has been held on ……

Chairman, SRC

Signature of External Examiner

This to certify that student has made all the corrections in the thesis

Signature of Supervisors

Head of the Department

Abstract

Strong Ground Motion (SGM) record at a particular site during an occurrence of earthquake is a result of complex – non linear combination of many factors. For design of engineering structures for a specified region the information about the characteristics of strong ground motion is of paramount importance. Peak Ground Acceleration (PGA) is most frequently used parameter to characterize such ground motions. Ground Motion Prediction Equations (GMPE's) are commonly used for estimating these loading conditions by using strong ground motion data from previous recorded earthquakes. A very little agreement has been reached in the past 30 years of ground motion estimation relation studies and the scatter could not be reduced to requisite level. This is more because the relations not only depends upon data selection, characterization of source, path or site or the regression technique employed but also on the purpose for which equation is intended to be used. So the process of determining the regression relation much depends upon the appropriate judgment of scholar. The duration of strong ground motion is another parameter of paramount importance during an earthquake occurrence. In last few decades numerous definition of duration has been purposed by number of authors. Most popular is the time interval in which significant contribution to the integral of the square of acceleration ($\int a^2 dt$) referred to as the accelerograms intensity takes place. Further, local site conditions also play a very critical role to understand damage assessment during an earthquake, since site effect also amplify or de-amplify the ground motion at recording site due to complex phenomena in various layers of soil in top 30 m of recording site. The uncertainties due to both physical as well as computational aspects in GMPE's to predict SGM, its duration and the local site effects lead to significant residuals/errors and therefore, expose inability to predict the observed values. The inherent uncertainties and limitations of mathematical models make inroads for newer methods to predict SGM. It is in this context an endeavor has been made to search for methodologies for prediction of SGM, duration and local site effects in the present study.

The main objective was to develop ANN's (i.e. Artificial Neural Networks) to predict PGA, duration of SGM and local site condition from the observed SGM at a given site using different combination of inputs i.e. magnitude, hypo-central distance, average shear wave velocity, focal mechanism, average primary velocity, average soil density, average Standard Penetration Test (SPT). Artificial Neural Networks (ANNs) are efficient computing models which have shown their strengths in solving many complex problems in numerous fields. They have the versatility

to approximate a wide range of complex functional relationships between sets of input and output data. The purpose of this study is to predict strong ground motion parameters using ANN that are of primary significance in earthquake engineering. In this study, sets of Multilayer Perceptron (MLP) neural network model are trained to predict the PGA, duration of strong motion, and site characteristics. The ANN model is intended to be developed for Indian region but due to lack of strong motion data, the database used in the study is taken from Kyoshin Net (K-NET) database of Japan. Later, developed ANN model is indigenised its use in Indian context. NeuroIntelligence (Neural Network Simulator) software has been used to model ANN and the standard back-propagation supervised training scheme is used to train all networks.

The strong motion data set consists of records from Japanese earthquakes of magnitude more than 4.5 and hypo-central distance less than 200 km for various sites which are classified on the basis of average shear wave velocity calculated using FEMA (356, 2000). In this study, averaged horizontal components of time histories have been used. Basic information such as earthquake magnitude, hypo-central distance, and focal mechanisms, average values of Standard Penetration Test (SPT) blow count, primary wave velocity, shear wave velocity, and density of soil have been used as seven input variables to train the neural network. Since at most locations in world, only average shear wave velocity is used for site characterization, therefore, an attempt has also been made to train the neural network with magnitude, hypo-central distance, focal mechanism and average shear wave velocity as four input variables and magnitude, hypo-central distance and average shear wave velocity as three input variables using Japanese records.

For ANN model developed with seven inputs to predict PGA for all site class, the correlation coefficient ‘R’ has been observed to be almost ~0.8 for all the cases showing a good correlation between observed and predicted data. However, it may be noted that values of ‘R’ are becomes minimum i.e., less than 0.8 in case of 4 inputs showing that either the reported focal mechanisms do not match with the actual physical process or this parameter is least correlated showing its relatively lesser influence on the predicted value. The testing scatter plot of predicted PGA to target PGA for all site classes with 7 inputs reveal that the prediction is good for PGA up to 40 cm/s^2. A similar trend is observed with 4 and 3 inputs cases for all the three classes. Based on the observation a conclusion of good prediction in lower range of PGA values can easily be drawn.

In case of ANN model developed with seven inputs to predict duration for all site class, the values of 'R' is almost more than 0.8 for all the cases showing a good correlation between observed and predicted data except for two cases with 4 inputs and 3 inputs for Class A. The scatter diagram reveals that the duration between 10 to 50 seconds can be predicted faithfully from this approach. The duration definition and its formulae used by various workers generally show much more scatter than the one seen in the prediction diagrams using ANN.

ANN model has been developed with eighteen inputs to predict average shear wave velocity for class site A which shows a good agreement with value of 'R' about ~0.9 with tested dataset. The inputs include magnitude, hypo-central distance, PGA and normalized response spectral ordinates ranging from 0.01 sec to 4 sec. This trained network with eighteen inputs has been tested for few significant earthquakes where average shear wave velocity recorded at stations were taken from NGA Flat File version 7.3. ANN model made a successful attempt to predict $\overline{V}_{S30}$ for those sites having $\overline{V}_{s30}$ between 750 - 1100 m/sec. Finally trained model was use to predict $\overline{V}_{S30}$ for those Indian Himalayan sites where at least 4 past earthquake records are available and classified as Class A site. The prediction of $\overline{V}_{S30}$ is first order estimation and need to be validated in future by borehole data at these sites. An alternate methodology for prediction of Strong Ground Motion has been developed in the present study. The method can be used to predict strong ground motion in terms of PGA and duration for its use in earthquake engineering. Further, the site characteristics can also be estimated using the recorded ground motion which is otherwise not worked out for the sites. The present thesis has concluded the successful use of ANN in earthquake engineering.

ACKNOWLEDGEMENT

The research work presented in this thesis was carried out from January, 2008 to December, 2014 in the Department of Earthquake Engineering, Indian Institute of Technology Roorkee, Roorkee, India. As it is said, darkness labours the whole light to bloom the rose and remain silent take the daylight credit. Likewise, many people contributed their best to the successful completition of this research work and stepped aside for me to take the credit. I wish to graciously acknowledge each one of them for the constant encouragement and support given to me that made it possible for me to do this work to the extent of my satisfaction.

In the first place I would like to record my gratitude to **Prof. Ashok Kumar**, Department of Earthquake Engineering, IIT Roorkee, for his supervision, advice, and guidance from the very early stage of this research as well as giving me extraordinary experiences throughout the work. Above all and the most needed, he provided me unflinching encouragement and support in various ways. His truly scientist intuition has made him as a constant oasis of ideas and passions in science, which exceptionally inspire and enrich my growth as a student, a researcher and a scientist want to be. I am indebted to him more than he knows.

I gratefully acknowledge **Prof. M.L. Sharma**, Head Department of Earthquake Engineering, IIT Roorkee, for his, supervision, advice and crucial contribution, which made him a backbone of this research and so to this thesis. His involvement with his originality has triggered and nourished my intellectual maturity that I will benefit from, for a long time to come. He is most responsible for helping me complete the writing of this thesis as well as the challenging research that lies behind it. He taught me how to write basic things, had confidence in me when I doubted myself, and brought out the good ideas in me. (More importantly, he taught me how to work hard and play hard, and how to ski to reduce stress!) Without his encouragement and constant guidance, I could not have finished this thesis.

I am thankful to **Prof. J.P. Narayan**, Department of Earthquake Engineering, IIT Roorkee, and **Dr. Kamal**, Department of Earth Sciences, IIT Roorkee, for their guidance, constructive comments and inventive suggestions at every step of this work

I express my gratitude to my fellow researchers Dr. Himanshu Mittal, Dr. Arjun Kumar, Dr. Govardhan Bhatt, Dr Vijay Khose Dr. Putul Haldhar, and Mr. Anshu Tomar, Mr. Sanjay Jain, Mr. Nitesh Ahir, Mr. Roshan Kumar, Mr. Bhanu Chamoli, Mr. Bhavesh Panday, Mr. Arup Sen for their sincere support and help during the process of this research work.

I would like to specially thank the non teaching staff from my lab Shri Babu Ram, Shri Rakesh Gondi, Shri Ramesh Chand, Shri Rishi Chand, Shri Amit Srivastav, Shri Ganshyam Tiwari, Shri Sandeep Kumar, Shri Dinesh Kumar, Shri K.G. Mittal and Shri Samiullah and other staff members from department who had helped a lot during my entire work.

I wish to express my love and gratitude to all my buddies Dr. Vivek Acharaya, Dr. Satya Prakash Singh, Dr. Ajay Khushwa, Dr. Vikas Chawala, Dr. Balwinder Raj, Dr. Vinod Kumar, Dr. Santosh Kumar, Dr. Rituraj Dubey, Mr. Jai Meena, Mr. Davinder Singh all my buddies made my stay pleasant in roorkee.

I wish to thank, all the faculty members of Department of Earthquake Engineering, IIT Roorkee for their support and Cooperation.

I wish my sincere regards to **Kyoshin Net** strong motion network of Japan for providing me with the vast and excellent strong motion data for carrying my studies.

Financial support by the **DST**, **MoES** grants and data set provided by the Department of Earthquake Engineering, IIT Roorkee is highly acknowledged. The use of the software namely **NeuroIntelligence** are greatly acknowledged.

I wish to express my love and gratitude to all my family. I'd particularly like to thank my parents, my grandmother (Dadi ji) and my loving brother and cousins for advising me. They had more faith in me than could ever be justified by logical argument. These pages wouldn't be sufficient to mention their enormous support, encouragement and especially invaluable untiring patience displayed. I owe my whole life to them. I wish to express my love, affection to my Late grandfathers (Dada ji and Nana ji) and grandmother (Nani ji) for their unconditional love, support and blessings throughout my journey of life.

I would like to thank my wife, **Ruchi Sachdeva**. Without my wife's encouragement, I would not have finished the degree. Her unending love, patience, understanding and constant personal support has shown this work the light of the day.

Finally, I wish to thank all those whose names have not figured above but have helped me directly or indirectly during the course of my research work. Really this thesis would not have been written without any of you.

Last but not least I express my gratitude to the Almighty for this divine favor, whose blessings helped me in working for this thesis and giving it the present shape.

(Rajiv Sachdeva)

CONTENTS

LIST OF FIGURES

LIST OF TABLES

LIST OF NOTATIONS

SGM	Strong Ground Motion
PGA	Peak Ground Acceleration
PHA	Peak Horizontal Acceleration
ZPA	Zero Period Acceleration
PVA	Peak Vertical Acceleration
PGV	Peak Ground Velocity
PHV	Peak Horizontal Velocity
PGD	Peak Ground Displacement
FAS	Frequency Amplitude Spectrum
FPS	Fourier Phase Spectrum
f_c	Corner frequency
f_{max}	Cut Off Frequency
m_o	Seismic Moment
PSD	Power Spectral Density
RVT	Random Vibration Theory
RS	Response Spectra
SDOF	Single Degree of Freedom
$x(t)$	Maximum Absolute Value of the Displacement
$\dot{x}(t)$	Maximum Absolute Value of the Velocity

$\ddot{x}_T(t)$	Maximum Absolute Value of the Acceleration
S_D	Spectral Displacement
S_v	Spectral Velocity
S_a	Spectral Acceleration
ω_n	Undamped Natural Frequency
ξ	Damping Ratio
PSV	Pseudo Spectral Velocity
PSA	Pseudo Spectral Acceleration
T_n	Undamped Natural Period
a_o	Threshold Acceleration Value
a(t)	Ground Acceleration Time History
t_o	Total Duration of Earthquake
g	Acceleration due to Gravity
μ	Shear modulus
V_s	Shear Wave Velocity
V_p	Primary Wave Velocity
MASW	Multichannel Analysis of Surface Waves
SPT	Standard Penetration Test
GMPE	Ground Motion Prediction Equation
ANN	Artificial Neural Network
AI	Artificial Intelligence

NN	Neural Network
PE	Processing Element
MLNN	Multilayer Neural Network
BP	Back Propagation
BPN	Back Propagation Network
RBFN	Radial Basis Function Network
MLFFNN	Multi-Layer Feed Forward Neural Network
MLP	Multi-Layer Perceptron
RL	Reinforcement learning
FFBPN	Feed Forward Back Propagation Network
E	Global Error
MSE	Mean Squared Error
η	Learning Rate
α	Momentum
GP	Geometric Progression
R	Coefficient of Correlation
MAE	Mean Absolute Error
RMSE	Root Mean Squared Error
DST	Department of Science and Technology
SMA	Strong-Motion Accelerographs
IITR	Indian Institute of Technology Roorkee

K-NET	Kyoshin Net
EW	East-West
NS	North-South
M_{JMA}	Japan Meteorological Agency Magnitude
M_w	Moment Magnitude
t_D	Duration of Strong Ground Motion
M	Earthquake Magnitude
D_{hyp}	Hypo-central distance
FM	Focal Mechanism
$\overline{V}_{S30}$	Average shear wave velocity in top 30m of surface layer
$\overline{N}$	Average Standard Penetration Test (SPT) blow count
$\overline{V}_{P30}$	Average P-wave velocity in top 30m of surface layer
$\bar{\rho}$	Average density of soil.
X	actual numeric value of real data
X_{min}	actual minimum numeric value in data base
X_{max}	actual maximum numeric value in data base
SR_{min}	lower scaling range limit
SR_{max}	upper scale range limit
SF	scaling factor
X_p	pre-processed value
X_i	observed value at i^{th} record

Y_i	predicted value at i^{th} record
n	total number of data points
$\overline{X}$	mean of X_i
$\overline{Y}$	mean of Y_i
NE	Network Error
SS	Sum of Squares

Chapter 1

INTRODUCTION

1.1 PREAMBLE

The occurrence of large earthquakes in most part of the Indian continent and the subsequent heavy loss of life and damage to the property make it imperative to actively seek reasons and remedial measures. One of the most active zones of the world, namely Himalayan tectonic zone, being a collision plate boundary, is manifested with very high level of seismicity with great earthquakes visiting the region very often in geological time scale. The ongoing northwards drift of Indian plate makes the Himalaya geo-dynamically active. Here, the seismic activity concentrated along these major thrusts is characterized with relatively larger magnitudes occurring with longer return periods which fall beyond the known catalogue. Thus, one of the major challenges is to predict strong ground motion in this very fast developing region. Structural engineers have long been interested in the response of civil structures to ground motions resulting from an earthquake. The response of structures under earthquake ground motions can be calculated either using a response spectrum or an acceleration time history. For design purposes, seismic codes provide a design spectrum, i.e. a smooth response spectrum that takes into account every possible earthquake likely to occur in a given zone with a certain probability of occurrence. The response spectrum contains all information on ground motion amplitudes and frequencies and hence can be directly used to design the structure for earthquake loads.

The strong ground motion is described using many parameters including Peak values of acceleration, velocity and/or displacement, the spectral ground motion and various parameters related to its amplitude and frequency. Peak Ground Acceleration (PGA) has been generally considered as a parameter representing the severity of shaking at a site and has been widely used to scale earthquake design spectra and acceleration time histories. Further, among many other parameters, duration of strong motion has also been considered as having pronounced effect on the severity of shaking. The prediction of such parameters has been carried out either using empirical formulation (based on the past observed data) or theoretically synthesizing such data based on various contemporary earthquake models. However, such endeavours have

resulted in large scatter in the predicted data and hence other approaches have made inroads in such studies.

Artificial Neural Networks (ANNs) have proved to be efficient tools and have been successfully applied for the solution of complex problems in many fields. They have the versatility to approximate a wide range of complex functional relationship between sets of input and output data.

The present study is dedicated to search for newer methods to be used for prediction of strong ground motion and an attempt has been made to develop efficient neural network based models to predict strong ground motion parameters, which are of significance in earthquake engineering applications. Further, the modification of strong ground motion data due to local soil conditions is also explored. The ANN approach has also been explored to predict the local soil conditions in terms of shear wave velocity to include the effect of local site in strong ground prediction at the surface.

The present chapter introduces the strong ground motion along with very brief introduction of the local site effects and ANN. It also contains the objectives of the present study and enumerates the chapters following very brief description of their contents.

1.2 STRONG GROUND MOTION PREDICTION

Prediction of Strong Ground Motion (SGM) has remained one of the main research focus in the past few decades due to lot of damage to human life and its assets being impelled by the damaging earthquakes. Knowing the characteristics of ground motions in a specified region is vital for the design of engineering structures. Loading conditions appropriate for a particular type of structure are expressed in terms of ground motion. Such studies have gained their paramount importance not only because of the recent spurt in the seismicity and the need for earthquake resistant design of structure for safe societies but also due to complex nature of its source, propagation, recording and its use in such endeavours.

Generally, Peak Ground Acceleration (PGA) is used to describe the SGM albeit spectral acceleration is more useful for engineers. The prediction of PGA is made through Ground Motion Predictive Equations (GMPE's) developed using regression analysis, which implicitly assumes to have considered the linear and nonlinear behaviour of source, path and recording. In the regression analyses, the PGA is generally calculated as function of independent variables like magnitude, source to site distance (including combined effect), local site conditions, type

of faulting and wave propagation (Kramer, 1996; Douglas, 2003). However, these independent variables generally present uncertainties in the construction of database for the recording station, because they often oversimplify reality.

In addition to PGA, the duration of strong motion is also an important parameter. A ground motion with moderate peak acceleration and a long duration may cause more damage than a ground motion with a larger acceleration and a shorter duration (Naeim, 2001). A typical earthquake accelerograms is generally composed of rise, strong motion, and decay part. For all engineering application, only strong motion portion of an accelerograms is of interest. Strong motion duration play an important role in assessing the damage potential of earth ground motion. In past several authors proposed various methods for computing the strong motion duration of an accelerograms (Trifunac et al., 1982; Boomer et al., 2009; Toflampas et al., 2009; Shoji et al., 2005;). In literature, there are more than 30 definition of strong motion duration (Boomer et al., 1999). Bracketed duration (Bolt, 1969), is defined as the time interval between the first and last exceedance of a specified acceleration (usually 0.05 g). The most commonly used (Trifunac et al., 1975) is time interval in which significant contribution to the integral of the square of acceleration ($\int a^2 dt$) referred to as the accelerograms intensity take place. In present study the strong motion duration is defined as the interval between the times at which 5 % and 95 % contribution of the total integral is achieved.

1.3 LOCAL SITE EFFECTS

Local site conditions have a profound influence upon the strong ground motion characteristics. They are markedly found as the primary reason of the structural damage in many previous studies, in the earthquakes of 1985 Mexico City, 1989 Loma-Prieta, 1994 Northridge, 1995 Dinar, 1995 Kobe, and 1999 Chi-Chi earthquake. The local soil conditions of a site may substantially alter the subsurface characteristics of earthquake ground motion by (1) amplifying the ground motion, (2) elongating its duration, (3) generating differential motions (aggravation) (Seed et al., 1976; Chang et al., 1996; Bard, 1997; Sun et al., 2005). The local site effects can be estimated using experimental and numerical methods based on the analysis and treatment of earthquake records. The literature for these methods is extensive and can be found for a review in Aki (1988). Generally, the most accepted soil response that reflects the site effects within the methods is the shear wave velocity (V_S) define for top 30 m of the subsurface soil under the

accelerograph station (Boore et al., 1993, 1994). This parameter has been adopted in many structural codes to incorporate the local site conditions with the structural characteristics under the design ground motion (BSSC 2003; TSC 2007). The shear-wave velocity profile by in-situ seismic geotechnical tests (cross-hole, down-hole, up-hole, the surface wave testing, etc.) and detailed site description are not available for majority of accelerograph stations installed all over world. The analytical solution for the site description has not been sufficiently studied due to highly nonlinear behaviour of soil.

1.4 ARTIFICIAL NEURAL NETWORK

To overcome the limitations of the classical methodology, newer methods like Artificial Intelligence have been explored for solving highly complex and nonlinear phenomenon. Artificial Neural Networks (ANNs) are computational models derived from the biological structure of neurons which imitate the operation of human brain. Artificial Neural Networks are nonlinear information (signal) processing devices, which are built from interconnected elementary processing devices called neurons. ANNs like people learns by data examples presented to them in order to capture the fine functional relationship among the data even if underlying relationships are unknown or the physical meaning is difficult to explain. It has advantaged over the most traditional empirical and statistical model, which require prior information about the nature of the relationships among the data. Back Propagation algorithm (Hertz et al., 1991; Zurada, 1992; Haykin, 1999) is the most popular Neural Network used particularly for prediction applications and data modelling. Back Propagation Network (BPN) was first introduced in 1986 (Rumelhart et al., 1986). Back Propagation is a systematic method for training multi-layer ANN using extend gradient-descent based delta-learning rule, commonly known as Back Propagation (of errors) rule. Back propagation provides a computationally efficient method for changing the weights in a feed forward network, with differentiable activation function units, to learn a training set of input-output examples. The use of ANN has been made in the present context to replace our lack of knowledge with the use of Artificial Intelligence. An endeavour has been made to predict the strong ground motion and the local site effect using a relevant vast data set.

1.5 MOTIVATION BEHIND THE RESEARCH

The uncertainties due to both physical as well as computational aspects in predicting SGM, its

duration and the local site effects lead to significant residuals/errors and therefore, reveal inability to predict the observed values. The inherent uncertainties and limitations of mathematical models make inroads for newer methods to predict SGM. It is in this context an endeavour has been made to search for methodologies for prediction of SGM, duration and local site effects in the present study.

1.6 OBJECTIVE OF STUDY

The main objective of the present research work is to explore an alternate methodology instead of GMPE's for prediction of Strong ground Motion which is highly complex and non linear in nature. In recent years with advancement in the field of Artificial Intelligence (i.e. ANNs) offer new insights to solve the problem in most complex systems utilizing different algorithms and models and can be used to remove uncertainties in predictive equations. The objectives are enlisted as follows:

1. To develop alternate methodology for prediction of Strong Ground Motion that is highly complex and nonlinear in nature.
2. To study the feasibility of using Artificial Intelligence to predict Strong Ground Motion.
3. To develop ANN to integrate methodology to predict SGM, local site conditions and duration of SGM from the observed SGM at a given site.
4. To compile strong ground motion data set for Indian region and collate it with other such regions in the world to develop a single data set for analyses to be carried out to train ANN for the above said objectives.
5. To propose ANN for prediction of strong ground motion for Indian region for various soil classes for inclusion of local site effects.

1.7 THESIS OUTLINE

Chapter 1 contains a general introduction to the thesis. The problem description is also briefly discussed. In addition to the brief introduction to SGM, local site effects and ANN, motivation, objective and the organization of the thesis are also included in the first chapter.

Chapter 2 presents a brief review of literature about strong ground motion prediction parameters selection criteria, and methodology like GMPE’s and ANN used by numerous authors to predict ground motion in term of PGA, Duration and its site effects.

Chapter 3 describes a brief background of the most important characteristics of strong ground motion that are of engineering significance. The amplitude and the frequency content parameters are briefly discussed. At the end of the chapter, the concepts of Arias intensity and duration of strong motion are explained.

Chapter 4 presents a review on Artificial Neural Networks and the network architecture. A discussion on the different learning rule and training algorithm is done. The chapter concludes with a discussion on the various issues of training the ANN model and parameters used to check the generalization capability of model.

Chapter 5 deals with the compilation and processing of strong motion data from Indian sites and K-NET database of Japan. In addition to provide justification for use of K-NET data set for a more than exercise. This chapter also discusses the influence of soil condition on the shape of response spectra. The chapter also contains the classification of Japanese earthquake records as per FEMA 356, 2000 as well as IS 1893 (Part 1): 2002.

Chapter 6 belong to study about the development of ANN for generating Peak Ground Acceleration and Duration of strong motion for various site classes namely Class A, B, and C defined on the basis of average shear wave velocity. This chapter also discusses about the prediction capability of ANN in terms of correlation coefficient, mean absolute error and root mean squared. Finally chapter has been concluded with results and discussion.

Chapter 7 contains information about the development of eighteen input based ANN model to predict average shear wave velocity of site. This chapter also discusses and presents the capability of ANN to learn from trained networks and to predict average shear wave velocity for India Himalayan sites which fall in category of class A.

Chapter 8 finally presents a summary of the outcome of the work conducted in this study and conclusion drawn, followed by some suggestions for future work.

Chapter 2

LITERATURE REVIEW

2.1 INTRODUCTION

Over 59 per cent of India's land area is under threat of moderate to severe seismic hazard as per the current seismic zone map of the country (IS 1893: 2002). Specifically, entire Himalayan belt is considered prone to great earthquakes of magnitude exceeding 8.0; and in a relatively short span of about 50 years, four such earthquakes have occurred: 1897 Shillong (M8.7); 1905 Kangra (M8.0); 1934 Bihar-Nepal (M8.3); and 1950 Assam-Tibet (M8.6). The hazard becomes many folded due to a spurt in developmental activities driven by urbanization, economic development and the globalization of India's economy.

India has a long history of earthquakes with earliest earthquake described in "The Mahabharata" the great Indian epic, which occurred about 1500BC in Kurukshetra, Haryana (Bilham, 2004). One of the most seismically active belts of the world namely, Himalaya is the outcome of convergence of continent-continent boundaries where the Indian plate is under thrusting the Eurasian plate. The earthquake activity in Himalaya and other regions of Indian plate is therefore related to build up of stress and release of energy from time to time inform of small, large and great earthquakes. Therefore the Himalayan belt has considerable potential for generating large and great earthquakes. Many studies related to seismic hazard assessment of the Indian region have already shown the seismic hazard to be very high (Khatri et al., 2000; Sharma, 2003; Iynger, 2004; Kumar et al., 2008, 2011; Anbazhagan et al., 2008a, b; Sharma et al., 2009; Mahajan et al, 2010, 2011; Kanagarathinam et al, 2010; Manisha et al., 2011)

Studies concerned with evaluating seismic hazards related to ground shaking require the prediction of strong ground motion from earthquakes that pose a potential threat to public, either by injury or damage to property. To make such a prediction, one must know certain fundamental characteristics of these earthquakes, as they relate to the source of the seismic waves, the medium through which the waves propagate, the local geology of the site, and the structures located at the site. If a sufficient number of strong-motion recordings from earthquakes and sites having the same or similar characteristics as those being evaluated are

available, then it is straightforward to select an ensemble of these recordings for evaluating or designing structures located at these sites for seismic loads (Fallgren et al., 1974; Guzman and Jennings, 1976; Werner, 1976; Bernreuter, 1984; Kimbal, 1983; Heaten et al. 1984;). Estimates of strong ground motion using this approach are referred to as site-specific.

For most applications, site-specific procedures are not feasible because a sufficient number of recordings with appropriate characteristics are generally unavailable. This is especially true for probabilistic analyses, where a wide range of earthquake sizes and locations are hypothesized, or for analyses where near-source estimates of ground motion are required. In such cases, a predictive model is needed. Such a model, commonly referred to as an **attenuation relation**, and is expressed as a mathematical function. These equations have a handful of independent parameters, such as magnitude and source-to-site distance, and a dependent parameter, such as peak ground acceleration, and the coefficients in the equation are usually found by regression analysis. Although the equations are often referred to as attenuation relationships, attenuation relations or attenuation equations, they predict more than how ground motion varies with distance. Hence over the past 30 years ground motion estimation equations have been much studied and many versions published.

A number of reviews of ground motion estimation studies have been made in the past which provide a good summary of the methods used, the results obtained and the problems associated with such relations. Trifunac and Brady (1975, 1976) provide a brief summary and comparison of published relations. Idriss (1978) presents a comprehensive review of published ground motion estimation relations up until 1978, including a number which is not easily available. Boore and Joyner (1982) provide a review of ground motion estimation studies published in 1981 and comment on empirical prediction of strong ground motion in general. Campbell (1985) contains a full survey of ground motion estimation equations up until 1985. Joyner and Boore (1988) give an excellent analysis of ground motion prediction methodology in general, and ground motion estimation relations in particular; Ambraseys and Bommer (1995) provide an overview of relations which are used for seismic design in Europe although they do not provide details about methods used. Joyner and Boore (1996) update this by including more recent studies. After these studies were completed, many more equations were derived. Campbell (2003a, b, c) are three excellent recent reviews of equations for the estimation of strong ground motions and include the coefficients of, and comparisons between, 14 well used equations. Douglas (2001, 2002, and 2011) summarizes over 150 studies that derived equations

for the estimation of peak ground acceleration. It seeks to compliment the recent reviews by Campbell by focusing on the methods used to derive the equations.

This chapter presents a review on the various characteristics of SGM used in earthquake engineering along with the detailed discussions of independent and dependent parameters being used in regression models. A brief review to attenuation relationships (also called as Ground Motion Prediction Equations lately) has been given in the present chapter. The dataset and the methodology for regression have been found to be unable to reduce the inherent variability which requires newer methods to be adopted for such endeavours. The following sections also provide a prelude to the new methods such as Artificial Neural Networks.

2.2 STRONG GROUND MOTION PARAMETERS

The quantification of ground motion requires a good understanding of the ground motion parameters that characterize the severity and the damage potential of the earthquake and the seismological, geological, and topographic factors that affect them.

Although, the SGM can be described using many parameters but in the present context focus has been made on peak ground acceleration only. Peak ground acceleration (PGA) is still often used as a parameter to describe strong ground motion. PGA is simply the amplitude of the largest peak acceleration recorded on an accelerogram at a site during a particular earthquake. PGA is the simplest strong-motion parameter and hence more than 150 equations (Douglas, 2001, 2002) have been derived in the past to predict it.

In statistical terminology, the parameter to be predicted – in this case a strong-motion parameter is referred to as a dependent variable. The parameters used to predict the variable are referred as independent variable. Some of the details of development of such pediction relationships is given below:

2.2.1 Dependent Variables

Horizontal peak ground acceleration is the usual choice, because ground motions usually are recorded on three orthogonal components, a further needed decision is how to treat these three components. The motions in the horizontal plane are of greater engineering significance than those in the vertical direction, and therefore most studies have dealt with horizontal motions only; three approaches are common: (1) use the larger of either horizontal component; (2) use both components; or (3) use the mean of the estimates from both components.

2.2.1.1 Combination of Horizontal Components

Most accelerograms consist of three mutually orthogonal components: two horizontal and one vertical. Seven different ways of combining the horizontal components have been investigated, these are given below.

- Arithmetic mean: a_M=[max1a_1(t)1$_{for\ t}$ + max1a_2(t)1$_{for\ t}$]/2.

1. Both: $a_{B,1}$= max1a_1(t)1$_{for\ t}$ and $a_{B,2}$ = max1a_2(t)1$_{for\ t}$.
2. Geometric mean: a_G =$\sqrt{[max1a_1(t)1_{for\ t} + max1a_2(t)1_{for\ t}]}$.
3. Note that: log a_G= {log [max1a_1(t)1$_{for\ t}$] + log [max1a_2(t)1$_{for\ t}$]/2.
4. Largest component: a_L = max [max1a_1(t)1$_{for\ t}$, max1a_2(t)1$_{for\ t}$].
5. Random: a_r = max1a_1(t)1$_{for\ t}$ or a_r = max1a_2(t)1$_{for\ t}$, chosen randomly.
6. Resultant: a_R = max[max1a_1(t)cosθ + a_2(t)sinθ1$_{fort}$]$_{for\ \theta}$. Correct calculation of this combination requires that the two horizontal components records are perfectly aligned with respect to time and that they are exactly mutually perpendicular. This may not always be true, especially for digitized accelerograms from mechanically triggered analogue instruments.
7. Vectorial addition: a_V= max1a_1(t)^2$_{for\ t}$ + max1a_2(t)^2$_{for\ t}$: This assumes that the maximum ground amplitudes occur simultaneously on the two horizontal components; this is a conservative assumption.

Using either horizontal components or the geometric mean of the two components leads to exactly the same regression coefficients when logarithms of the ground motion measurements are used. This can be demonstrated by considering the normal equations which are solved to give the least squares estimate of the coefficients Douglas (2001).

2.2.2 Independent Variables

Ground-motion predictions are almost always a function of the independent variables. Most commonly used independent variables are earthquake source, distance to the source and geophysical properties of the site.

2.2.2.1 Source Effect

The parameter most commonly used to characterize earthquake source in strong-motion attenuation relations is earthquake magnitude. Magnitude is the only source parameter routinely

reported by seismographic networks. Other source parameters used in the past have included source dimensions (Bernreuter, 1981), seismic moment or moment magnitude (Hanks, 1970; McGuire and Hanks, 1980; Hanks and McGuire, 1981; Joyner and Boore, 1981, 1982; McGuire et al., 1984), and stress drop (Hanks and Johnson, 1976; Hanks, 1979; Bernreuter, 1981; McGuire et al., 1984). While stress drop is an important source parameter from a theoretical point of view, in practice its estimation is associated with a large degree of uncertainty.

Early studies (Esteva, 1970; Donovan, 1973), did not state which magnitude scale they use. Many authors use local magnitude (also called Richter magnitude), M_L, to derive their ground motion estimation relations (McGuire, 1977; Campbell, 1989; Tento et al., 1992; Mohammadioun, 1994). This may be because these are the only magnitude estimates available for the chosen earthquakes. Mohammadioun (1994) uses M_L because it is generally available and is uniformly determined but states that it may not be the best choice. Ambraseys (1995) does not use M_L because there are no M_L estimates for many of the earthquakes in his set and many estimates of M_L are unreliable. Boore (1989) states that M_L is difficult to predict for design earthquakes because catalogues of historical earthquakes often contain unreliable M_L estimates.

Another magnitude scale which is commonly used is surface-wave magnitude, M_s (Dahle et al., 1990; Ambraseys and Bommer, 1991; Ambraseys, 1995; Ambraseys et al., 1996; Crouse and McGuire, 1996; Bommer et al., 1998). Dahle et al. (1990) use M_s because it is reasonably unbiased with respect to source dimensions and there is a globally consistent calculation method. Theodulidis and Papazachos (1992) mainly use M_s but for the foreign earthquakes in their set they use Mw or M_{JMA} which they state to be equivalent between 6.0 and 8.0.

Japanese Meteorological Agency magnitude, M_{JMA}, has been employed in many Japanese ground motion estimation relations (Kawashima et al., 1984; Kamiyama et al., 1992; Fukushima et al., 1995) although Kawashima et al. (1984) notes that it may not necessarily be the most suitable parameter to represent magnitude but it is the only one which exists for all earthquakes in their set of records. Peng et al. (1985) use Chinese surface-wave magnitude but also use m_b and M_s and find larger residuals.

Recently most equations have been derived using moment magnitude, M_w, (Boore et al., 1993; Lawson and Krawinkler, 1994; Sadigh et al., 1997; Kobayashi et al., 2000) The other major advantage of M_w is that it does not saturate for largemagnitudes, and can be calculated for

small magnitudes, and hence provides a good measure of the energy released over the entire magnitude range. The other main technique for providing a homogeneous magnitude scale for all sizes of earthquakes is to use one magnitude scale for small earthquakes, usually M_L and one scale for larger earthquakes; usually M_s. Campbell (1981) introduced this idea to develop magnitude estimates that are generally consistent with M_w.

Almost all studies include a factor which has an exponential dependence on magnitude, expaM, this is because the energy released by an earthquake is exponentially dependent on magnitude (Richter, 1958). Trifunac (1976) was the first to include a factor to model magnitude saturation, by using a factor that is exponentially dependent on the magnitude squared, i.e. exp bM_2, in addition to the normal factor expaM. Other authors (Joyner and Boore, 1981; Kawashima et al., 1984; Crouse et al., 1988; Crouse, 1991) incorporate factors like exp bM_2 into their equations but find that the coefficient b is not statistically significant or that it does not improve the adjusted multiple correlation coefficient so remove the factor.

The records in earthquake catalogues are mostly presented by one of the magnitude scales such as surface, body, duration, local and moment. Ulusay et al. (2004) stated that the best scale used in Attenuation relations are the moment magnitude (M_w) due to related with rupture parameters. However, M_w scales may not be always available for all catalogues. In this case, the other scales of events are converted into the moment magnitude by correlations. But, this indirect way of obtaining the magnitude data may cause significant variations on the PGA estimations.

Another earthquake source parameter found to be related to strong ground motion is focal mechanism. Campbell (1983, 1984c), in his empirical analysis of near-source ground motion, found that reverse and reverse-oblique mechanisms are associated with ground motions approximately 30-40 percent larger than strike-slip mechanisms. Young (1980a) attributes such differences to regional variations in stress drop. Other source effects found to influence strong ground motion are source radiation pattern, source directivity, and geometry of the fault plane (Berrill, 1975; Arnold and Vanmarcke, 1977; Bureau, 1978; Boatwright and Boore, 1982; Anderson and luco, 1983; Singh, 1983), Focal depth (McGarr, 1984). The latter effect is especially significant for sites located near the fault.

2.2.2.2 Path Effect

Propagation parameters characterize the effects of wave scattering, geometrical attenuation, and inelastic attenuation of ground motion as it travels from the source to the site. The independent variable universally used to characterize these parameters is distance.

The use of distance measures which contain information on the depth of the source, i.e. hypo-central distance, rupture distance, seismogenic distance, centroid distance, energy centre distance, equivalent hypo-central distance or surface projection distance with focal depth (as used by Ambraseys and Bommer, 1991; Sigbjornsson and Baldvinsson, 1992; Ambraseys, 1995) forces deeper earthquakes to predict smaller ground motions than shallower shocks. This is actually a path effect.

The source distance to a particular site directly affects the PGA. This distance is variously measured such as the epi-central and hypo-central distances, the distance to the zone of highest energy release, the closest distance to the zone of rupture and the closest distance to the surface projection of the fault rupture (Kramer, 1996; Abrahamson and Shedlock, 1997). However, each of them can be considered as a source of uncertainty due to unclear effects of earthquake source mechanism. In addition, the lack of a standard usage of the distance in attenuation relations makes difficulties and leaves a doubt in the PGA reliability. Therefore, the most acceptable distance should be utilized particularly by understanding the source mechanism well.

The distance travelled from the source to the site, d, is the parameter used in all ground motion estimation relations to characterise the path, although many different definitions of this distance are used.

Definitions of Source to Site Distance

Joyner and Boore (1981) state that the correct distance to use in ground motion estimation relations is the distance from the origin of the actual wave, which produced the measurement of ground motion (for example PGA or SA), to the station but this is difficult to determine for past earthquakes and impossible to predict for future earthquakes. To overcome this difficulty, 10 different measures have been proposed to characterise the distance to the earthquake source:

1. *Epi-central distance, d_e***:** distance to the epicentre of the earthquake, i.e. the distance to the horizontal projection of the rupture's starting point. This is the easiest distance

measure to use because the epicentre is the location information given for all earthquakes.

2. *Hypo-central distance, d_h*: distance to the hypocenter of the earthquake, i.e. the distance to the rupture's starting point. Like epicentres, hypocentres are reported for most earthquakes but accurate measures of focal depth are often difficult to obtain unless there is a good distribution of stations with distance from the source (Gubbins, 1990). Most damaging earthquakes occur within a shallow region of the crust (about the top 30 km) and hence de and dh become equal at intermediate and large distances.

3. *Rupture centroid distance, d_c*: distance to the centroid of the rupture. This distance measure requires an estimate of the dimensions of the rupture plane so that the centroid can be defined; it can be difficult to define this plane. However, because it is measured to point source uncertainties in defining the exact location of the rupture plane will have less of an effect on rupture centroid distances than for line or surface measures.

4. *Centre-of-energy-release distance, d_E:* distance to a point on the fault rupture where energy considered being concentrated (Crouse et al., 1988; Crouse, 1991). This distance is similar to rupture centroid distance.

5. *Surface projection distance* (also called Joyner– Boore or fault distance), d_f: distance to the surface projection of the rupture plane of the fault (Joyner and Boore, 1981); for a point within the projection df=0. Surface projection distances can have large uncertainties (up to 20 km for certain earthquakes and stations) because there are no published studies on the rupture plane or because there are several and no obvious way of deciding which is best. The errors in surface projection distances could be larger for earthquakes occurring during a sequence of similar sized shocks when aftershocks and geodetic data are likely to be difficult to use. The current practice of quoting surface projection distances to one decimal place should not be taken as meaning that the distances are accurately known to 0.1 km.

6. *Surface projection distance with focal depth, $d_{f,h}$*: distance to the projection of the rupture on a plane at the focal depth. The horizontal distance part of surface projection distance with focal depth is obviously associated with the same uncertainty as surface projection distance and errors in focal depths have already been discussed.

7. *Rupture distance (also called source or fault distance)*, d_r: distance to rupture surface. For future earthquakes, rupture distance can be estimated using mapped faults although it requires that the dip and depth of the faults are known.

8. *Seismogenic distance*, d_s: distance to seismogenic rupture surface, assumes that the near-surface rupture in sediments is non-seismogenic (Campbell, 1997). Campbell (1997) believes that seismogenic distance can be 'reliably and easily determined for most significant earthquakes' but, in fact, it has the same difficulties in its determination as rupture distance, which can be large, plus the requirement of defining depth to the seismogenic layer.

- *Elliptical distance D or average site to rupture end distance*, *ASRED*: mean of the distances to the extremities of the fault surface rupture (Bureau, 1978; Zhou et al., 1989), if no surface rupture occurred then the projection of the top of the rupture should be used.

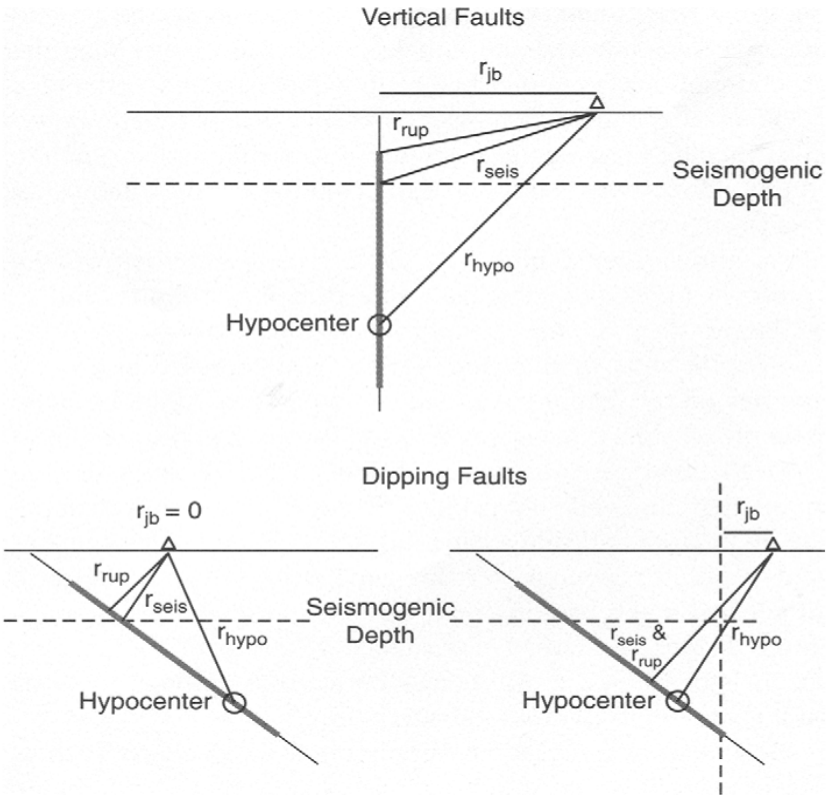

Figure 2.1: Source-to-site distance measures for ground-motion attenuation models (after Abrahamson and Shedlock, 1997).

9. *Equivalent hypo-central distance, EHD:* distance from a virtual point source that provides the same energy to the site as does a finite-size fault (Ohno et al., 1993). Defined by:

$$\frac{1}{EHD^2} = \frac{\sum_{i=1}^{n} M_{0,i}^2 X_i^{-2}}{\sum_{i=1}^{n} M_{0,i}^2} \tag{2.1}$$

Where n is the number of segments on the rupture plane, $M_{0,i}$ is the seismic moment density on the i^{th} segment and X_i is the distance between i^{th} segment and site. It includes the effects of fault size, fault geometry and inhomogeneous slip distribution (Ohno et al., 1993). Ohno et al. (1996), Kawano et al. (2000) and Si and Midorikawa (2000) use EHD to derive their ground motion estimation equations.

10. In many applications, the fault can be identified but the hypocenter or sources of particularly energetic radiation cannot. In these cases, a measure based on the closest distance to the fault seems reasonable.

2.2.2.3 Site Parameters

Traditionally, site parameters have been related to simple geologic descriptions of the recording stations. More sophisticated classification of the site has been based on wave-propagation velocity (Joyner and Fumal, 1984) and depth of deposits (Trifunac and Lee, 1978a, 1979; Campbell, 1984). The diversity of site classifications used in the past attests to the complex and poorly understood relationship between strong ground motion and site characteristics. Campbell (1983, 1984b), found that factors such as fault mechanism, site topography, soil depth, instrument embedment, and structure size, if not properly accounted for in the development of strong motion attenuation relations, can significantly influence the quantification of site effects.

The significant influence of topography was first documented for the 1971 San Fernando earthquake by Boore et al (1973).The most commonly used technique to incorporate site effects into a ground motion estimation relation is to use multiplicative factors between ground motion at one type of site and that at another.

Trifunac (1976) introduces this method; he uses three site categories and the multiplicative factor between basement rock and intermediate type rock is forced to be half the multiplicative factor between solid hard basement rock and alluvium sites thus limiting the generality of the

method. The number of multiplicative factors used is usually one less than the number of site categories used, thus allowing different scalings amongst the site categories (e.g. Boore et al., 1993; Lawson and Krawinkler, 1994; Ambraseys et al., 1996; Sabetta and Pugliese, 1996; Chapman, 1999). Lee (1995) classifies stations into three geological site classes and two local soil classes, although the difference between geological and local scales is not clear, so there are six categories in total but only three factors.

Some studies have insufficient data to derive adequate site category multiplicative factors so they adopt multiplicative factors from previous studies (e.g. Atkinson, 1997; Spudich et al., 1999). If the site categories used in the two studies are similar enough then this is a valid procedure because true site coefficients should only depend on local site conditions at the stations. Ambraseys and Bommer (1991) attribute the apparent small dependence of horizontal PGA on site classification to the lack of available information which compelled them to use a simple binary system. As more site information on strong-motion stations has become available, the number of site classes used has grown, so that there are three or more categories of increasing stiffness (roughly increasing shear-wave velocity) (e.g. Trifunac, 1976; Kawashima et al., 1986; Fukushima and Tanaka, 1990; Lawson and Krawinkler, 1994; Campbell, 1997; Chapman, 1999; Kobayashi et al., 2000).

A single parameter which is a rough combination of shear-wave velocity and depth to bedrock is the natural period of the site, T, which for a single layer equals 4H/Vs. The need to include a term reflecting explicitly local amplification dependent on natural period of the soil is noted by Benito et al (1992). Also the natural period of the site is less available for strong-motion recording sites than is shear-wave velocity and hence it is easier to use shear-wave velocity than natural period of the site.

The most site specific procedure is to use individual coefficients for each station. This idea was introduced by Kamiyama and Yanagisawa (1986) (although Kobayashi and Midorikawa, 1982 developed a method which is similar) and has since been adopted in many Japanese studies (Kamiyama et al., 1992; Fukushima et al., 1995; Molas and Yamazaki, 1995; Shabestari and Yamazaki, 1998; Kawano et al., 2000; Shabestari and Yamazaki, 2000).

Some studies define the boundaries of the categories in terms of shear-wave velocity (e.g. Boore et al., 1993; Ambraseys et al., 1996) but in fact there are no shear-wave velocity measurements for many of the stations they use, so a rough classification is made. Due to the difficulty of finding site information, Theodulidis and Papazachos (1992) examined the

PGV/PGA ratio for some of their Alaskan sites to decide whether they were rock or soil, which is based on empirical formulae which find differences in this ratio due to the local site conditions

One of the shortcomings of existing attenuation relations can be attributed to both the lack of a standard definition of site categories and the lack of detailed geotechnical explorations for the site conditions of recording stations (Somerville and Graves, 2003). This leads to different site classifications for the same station in the prediction of PGA. Others such as Gülkan and Kalkan (2002) and Ulusay et al. (2004) were composed of the site condition parameter; these authors noticed that their equations need to be improved by the actual shear wave velocity and the detailed site description of underlying recording stations.

New data and analysis have provided the basis for more reliable empirical estimates of ground motion in future earthquakes. Theoretical methods have been developed for estimation of ground motion parameters and simulation of ground motion time series. We then consider the choice of parameters for characterizing strong ground motion and the factors affecting ground-motion amplitudes.

2.3 ATTENUATION RELATIONSHIPS

Some of the attenuation models developed in the recent years by considering the various independent parameters for the prediction of PGA. The main aim of the present work is not to develop such relationships but to find the size of variability for their use in ground motion prediction. The general form of the attenuation relation may be considered as

$$\log (a) = f_1 (M) + f_2(r, E) + f_3(r, M, E) + f_4(F) + \varepsilon$$

where a is the peak ground acceleration (horizontal or vertical); $f_l(M)$ is a function of earthquake magnitude; $f_2(r, E)$ is a function of earthquake-to-recording site distance and the tectonic environment; $f_3(r, M, E)$ is a non separable function of magnitude, distance, and tectonic environment; $f_4(F)$ is a function of fault type; and ε is a random variable representing uncertainty in log(a). The models considered in the past are either $f_l(M)$, $f_2(r, E)$, and $f_4(F)$ (Joyner and Boore, 1981) used this model or $f_1(M)$, $f_3(r, M, E)$, and $f_4(F)$ (Campbell,1981) used this model. The first model assumes that the distance and magnitude have separable influence on peak ground acceleration, and the second model considered it to be non separable. Abrahamson and Litehiser (1989) used the hybrid model of Campbell and Joyner and Boore.

The forms of the functions $f_1(M)$, $f_2(r, E)$, $f_3(r, M, E)$, and $f_4(F)$ are discussed by Campbell (1985). Many such relationships have been compiled from time to time viz., Seismological Research Letters 1989 and Earthquake Spectra 2008. Further, the variability has been well proven by Douglas (2011) while considering such relationships from parameters and region wise.

In the above section, entire discussion have been done about the importance of strong ground motion in earthquakes, strong ground motion parameters and the various independent parameters that are considered in the estimation of PGA. Overview of general functional form of the Attenuation relationships used by different researchers is presented.

2.4 STUDY BASED ON ANN AROUND THE WORLD

Over the years, many researchers used artificial neural networks (ANNs) to estimate PGA and to evaluate ground motions spectra. Some of the important milestones are briefly discussed below.

Yamazaki et al., (1994) developed neural network with supervised learning algorithm to predict structures damage. The network used input parameters such as peak ground acceleration, peak ground displacement, spectrum intensity and observed output parameter as three levels of damage extent (negligible, moderate, severe). The authors used training data consist of 79 real earthquake records taken from Japan, USA, and Mexico. The network resulted into good estimation of structure damage due to strong earthquake motions.

Rogers (1994) laid down guidelines to train ANN model with optimal design. This model was used to simulate a structural analysis program in less time. Considering stress constraints, the author presented optimum shape of beam with minimum weight. The study on selection of training pairs shows best approximation of the design space by hypercube method. The author introduced a good approach to take sum of nodes in the input and output layers for selection of number of nodes in hidden layers.

Wang and Teng (1997) identified and automatically picked local and regional S phase from set of three-component seismic data using multilayer perceptron (MLP) neural network. The ANN S-phase picker used input parameters such as the ratio between short-term average and long-term average, the ratio between horizontal power and total power, autoregressive model coefficients, and the short-axis incidence angle of polarization ellipsoid. The network resulted into good accuracy of phase identification by 86%, out of which 74% identification is in less

than 0.1 sec onset time error. The network presented good estimation of onset time and automatic identification of phase.

Dai and Mac Beth (1995) applied a back-propagation artificial neural network (ANN) to collect and find P and S seismic arrivals from local earthquakes data. Giacinto et al. (1997) presented an estimate of earthquake risks for real geological structures using artificial neural networks.

Dai and Mac Beth (1997a) identified arrival of P and S waves from three components recordings of local earthquake data using back-propagation neural network (BPNN). The BPNN used input as onset time of arrivals and trained by nine groups of degree of polarization (DOP) segments to identify P wave's arrival by 82.3% and S waves' arrival by 62.6%. However, BPNN trained by five groups identify P wave's arrival by 76.6 % and S waves' arrival by 60.5%. This network limits to improve its performance.

Dai and Mac Beth (1997b) applied BPNN on local earthquake data that identifies arrival of P and S waves from single component (1-C) recording. The authors used normalized segment (40 samples of amplitude) as input pattern and obtained output values between 0 and 1. The output values represented either background noise or seismic arrivals existence. Although this network can identify seismic arrivals from vertical, horizontal components and other stations but ray paths strong effect and source position varies its performance for all the three components. On comparison with 3-C recording this approach showed more flexibility but less performance.

Ghaboussi and Lin (1998) presented artificial neural networks (ANNs) to design artificial earthquake accelerograms from pseudo-velocity response spectrum. The first replicator neural network (RNN) was trained to compress real and imaginary parts of Fourier transforms of a sample of 30 recorded earthquake accelerograms. The association of ordinates of pseudo-spectral velocity (PSV) spectrum with the compressed parts of Fourier spectrum was done by second multi-layer neural network. This method built similar accelerograms as of training set from either design spectra or pseudo-velocity response spectrum.

Lin and Ghaboussi (2001) produced multiple earthquake spectrum accelerograms from design or response spectra with stochastic neural networks (SNN). The authors combined earlier replicator neural network (RNN) with new stochastic neural network that effectively enhances characteristics extraction and compression of the earthquake accelerogram. A set of 100 recorded earthquake accelerograms was applied to train the network with single design spectrum that resulted in producing real looking and compatible accelerograms.

Pandya et al., (2002) estimated site-specific response spectra using artificial neural network (ANN). The pseudo-velocity response spectrum was estimated with feed-forward back propagation ANN. The training of the network was done with seventy-five distinct spectral ordinates due to two horizontal components of earthquakes. These spectral ordinates were further divided into fifteen sets at five different time periods. The networks with different configuration were trained parallel for alluvium and rock. The pseudo-velocity spectral ordinates at five different time periods were obtained by the network and then converted to pseudo-acceleration. The results were plotted to compare the actual and predicted response spectra.

Lin et al., (2002) introduced neural networks to estimate PGA and bridge damages after major earthquakes in Taiwan. The network for PGA estimation used input parameters such as magnitude, depth and epicentre coordinates of eight major earthquakes, while bridge damage estimation used Chi-Chi earthquake data. The 7-8-8-2 network for bridge damage estimation was trained with sixty-four sets of data. Finally, the combined two networks trained by twenty sets of bridge damage conditions resulted in accurate estimation of bridge damages by major earthquakes.

Lee and Han (2002) introduced a new approach to develop artificial earthquake accelerograms and response spectra using five neural network models. The ANN models utilized input parameters such as magnitude, epi-central distance, site conditions and focal depth. The ANN-I model developed the Fourier amplitude spectrum. The nonlinear power spectral density (PSD) and intensity function parameters were computed after training ANN-II and ANN-III models respectively. The ANN-IV model developed the acceleration response spectrum with input parameters. While, the ANN model V is the inverse version of model IV, developed synthetic ground motion accelerograms compatible with a design response spectrum.

Kerh and Chu (2002) predicted PGA by applying three feed-forward back-propagation neural network models for Taiwan's Kaohsiung Mass Rapid Transit line sections. For training these models input layer used different combinations of input parameters such as epi-central distance, focal depth, and earthquake magnitude. The validation check of estimated results was done by using Nakamura transformation techniques on microtremor measurement. The results were also compared with output of nonlinear regression analysis such as Kanai, Joyner and Boore, and Campbell forms. However, it was concluded that neural networks model provides reliable estimation of PGA values.

Garcia et al., (2003) presented artificial neural networks (ANNs) to estimate the (earthquake) ground surface response of the clayey soil of the Mexico City. In comparison to empirical relative transfer function based method, this network showed better results especially for the Tehuacan seismic event. The authors iteratively used the ANN network with different input functions such as Dot Product (DP) and L1 distance, learning rules such as back propagation (BP), general regression (GR), quick propagation (QP), conjugate gradients (CG) and Levenberg-Marquard (LV), transfer functions such as sigmoid, hyperbolic secant (sech) and hyperbolic tangent (tanh).The accurate ground response for Mexico City was estimated by GR-L1 combination for intraslab earthquakes that occurred at mid distances.

Tehranizadeh and Safi (2004) proposed artificial neural networks (ANNs) that developed design spectra for different site conditions in Iran. These networks classified Iran's 2000 ground motion records based on acceleration and displacement response spectra. The models used competitive and back propagation networks with supervised and unsupervised learning algorithms. The authors compared design spectra based on classification of spectra response with existing code spectra and experimental results. The results obtained by ANNs determine ranges of shear wave velocity and soil characteristics. The ANNs design spectra was more efficient, robust, and require less time and computational efforts. // developed seismic design spectra for Iran utilizing ANN. The authors classified more than 2000 ground motion records based on their characteristics such as linear acceleration and displacement response spectra. The classification problems were solved with competitive and back propagation neural networks with use of both unsupervised and supervised learning algorithms.

Kerh and Ting (2005) applied back-propagation neural network on seismic data obtained from 30 checking stations in Taiwan, to predict peak ground acceleration (PGA) at 10 train stations along high-speed rail line. This network used epi-central distance, focal depth and strong motions magnitude from 8 to 39 data sets as input parameters and peak ground horizontal acceleration as output parameter. The results predicted by neural network were compared with microtremor measurements. It was observed that prediction by neural network provides better results than existing building code values.

Baziar and Ghorbani (2005) estimated the horizontal ground displacement with a neural network model. This model estimated displacement in ground slope and free face conditions due to liquefaction-induced lateral spreading. Alves (2006) estimated earthquake forecasting using neural networks. Barrile et al., (2006) applied radial basis function neural network to

estimate seismic sequences of aftershocks after a great earthquake. Liu et al., (2006) presented an estimate of peak ground velocity (PGV) using neural network for West American region. According to the priority on variations in PGV the authors applied input parameters in input layer as earthquake magnitude, epi-central distance, and soil condition.

Chen and Stewart (2006) proposed multi-window algorithm that automatic detect and pick arrival times of impulsive P-phases of local seismic events with low signal-to noise (SNR) ratio for a single trace. This algorithm is more efficient and reliable for real-time seismic detection and hypocentre location with SNR higher than 3. It requires less than 1 sample to pick P-phase in low *SNR* environments. Further, Lin et al. (2006) also utilized neural network to generate artificial earthquake accelerograms from response spectra for Taiwan area (Taipei basin).

Gullu and Ercelebi (2007) presented an estimate of peak ground acceleration (PGA) values on three sample sets of Turkish strong motion data using Fletcher-Reeves conjugate gradient back-propagation based ANN model. The authors used magnitude, source-to-site distance and site conditions as the input parameters and PGA as the output parameter. This network results in high correlation coefficients (R^2) between the predicted and the observed PGA values. The ANN model showed better correlation values on comparison with values obtained by the regression method. However, this ANN model limits its generalization capability for optimal configuration by the testing method.

Garcia et al. (2007) developed artificial neural networks (ANNs) for Mexican subduction zone earthquakes that predict horizontal (PHA) and vertical (PVA) peak ground accelerations at rock sites. The networks used magnitude, epi-central distance and focal depth as input parameters. The ANNs features such as flexibility, adaptability, prediction capability, etc. resulted in obtaining better PGA responses than other traditional regression techniques. These networks predicted good PGA responses for Japan and North America.

Kerh et al. (2007) checked appropriateness of building code values with back propagation neural network (BPNN) estimations of 209 seismic data records for Taiwan's current conditions. The epi-central distance, focal depth and strong motions magnitude were used as input-parameters and peak ground acceleration (PGA) as output parameter in neural network design. The PGA estimated by the network showed good results in comparison to building code values. It also recognized potential hazardous areas and presented curve fitting model that show relationship between horizontal PGA and the focal distance as $PGA = \frac{(8.96)}{Df}$.

Shahin et al. (2008) presented benefits of ANNs over other mathematical models that solved complex problems in geotechnical engineering. The data driven approach of ANN makes the model training, updating, structure and parameters finding easy. In spite of these benefits, ANNs lack in knowledge extraction, extrapolation and uncertainty

Amiri and Bagheri (2008) built artificial earthquake accelerograms from target spectrum using wavelet analysis and radial basis neural network. The learning feature of network did inverse mapping to build earthquake accelerograms from response spectrum. The neural network was trained by several levels (representing range of frequencies) obtained by splitting earthquake accelerograms using discrete wavelet transform. The trained network was capable to relate response spectrum with wavelet coefficients and therefore built artificial earthquake accelerograms from pseudo-velocity response spectrum.

Gunaydin and Gunaydin (2008) estimated peak ground acceleration from 95 three-component records observed in North-western Turkey for 15 ground motions. The authors utilized feed-forward back-propagation (FFBP), radial basis function (RBF), and generalized regression neural networks (GRNNs) with inputs such as moment magnitude of earthquake, hypo-central distance, focal depth, and site conditions in vertical(U-D), east-west(E-W), and north-south (N-S) directions. The predicted PGA values showed superiority of FFBP over other networks for three directions.

Khameneh and Scherer (2008) proposed two layers feed forward neural networks D-ANN and S-ANN to predict duration of seismic wave phase and strong ground motion signal for first approaching signals. The authors used 10 earthquake data records and applied Fast Fourier Transform (FFT) on data such as shear wave velocity greater than 750m/s, magnitude ranges from 6 to 7.5 and hypo-central distance from 14 to 34km. The predicted signals are retrieved by applying reverse Fast Fourier Transform (R-FFT). This method develops relationship between first beginning signals and earthquake wave's full content.

Derras et al., (2010) applied artificial neural networks (ANN) approach that economically generated free surface acceleration response spectrum for chosen site. The network used inputs such as spectrum value and period and output as acceleration spectrum response. The results estimated by network were compared with KIK-NET accelerograph networks seismic data. It was observed that network behaviour resembles to the real case.

Kamatchi et al. (2010) presented site-specific response spectra and generation of strong bedrock level ground motions for Delhi city in India using feed forward back propagation

neural network. The authors utilized earthquake data records that originated in the Himalayan belts central seismic gap. The network used input parameters such as moment magnitude, shear wave velocity, vibration period, soil stratum depth above the bedrock, damping ratio and output parameter as spectral acceleration. The results obtained by trained neural network are validated on Delhi's two buildings. It was observed that root mean square percentage error for predicted spectral acceleration values is acceptable and hence shows applicability of this methodology on other regions with all information available.

Gullu (2012) presented genetic expression programming (GEP) a new tool to estimate PGA on Turkish earthquake data where moment magnitude ranges from 4.5 to 7.4 and epicenter distance (source-to-site) up to 100 km. The suitable candidate ground motion model was selected by applying likelihood estimation (LH) measure and comparing predictions of GEP with one obtained by regression methods. The attenuation characteristics, strong ground motion data records of Turkey and attenuation equations for Turkey were used to check the validity of GEP with LH and regression methods. It was observed that the PGA models by GEP and regression such as class A and B passes validation and designated as good qualifications while class C fails in validation and ranked as lower levels. For seismic hazards studies of predicting the PGAs, class A and B are the appropriate models of GEP approach with LH method. This approach provides additional assistance in prediction of PGA over conventional regression methods.

Gullu (2013) estimated shear wave velocity in California's 60-accelerograph station sites by applying artificial intelligence (AI) method. This method consists of artificial neural network (ANN) and genetic expression programming (GEP) models. These models utilized input variables such as magnitude, site-to-source distance, different site period's spectral accelerations, peak ground acceleration and predicted shear wave velocity. The AI models provide good estimation of shear wave velocity based on error and correlation criteria for highly nonlinear problems.

The work done by various groups and authors for the use of ANN in earthquake engineering has amply proven its usefulness to predict unknown parameters. None the less, it may not be considered as lack of present day knowledge in terms of physical processes but may be thought of as extra tool to predict such parameters in very complex scenarios.

Chapter 3

STRONG GROUND MOTION CHARACTERISTICS

3.1 INTRODUCTION

During an earthquake occurrence ground vibrate from faint tremor to wild motions necessitating high dynamic range for recording instruments as well as a wide perspective in understating the physical phenomenon and seeking remedial measures. The ground motion that cause severe damage to loss of human life and its habitat is referred as Strong Ground Motion (SGM). Earthquake engineers have keen interest to study these strong ground motions and it characteristics. Peak Ground Acceleration (PGA) is popularly used as a parameter to describe SGM. Ground motion during an earthquake is measured by strong motion instruments, that record the ground acceleration and recorded motion is referred as accelerograms. To completely describe the ground motion at a recording site, three orthogonal components of ground acceleration, and three rotational components are required. Usually, most of accelerograms consist of three mutually orthogonal components: two horizontal and one vertical and neglect the rotational part.

It is of paramount interest to look into the characteristics of strong ground motion before their prediction and use the same for earthquake engineering purpose. The following sections describe the important characteristics of strong ground motion which will be later useful in selecting methodology for the prediction of SGM.

3.2 STRONG GROUND MOTION PARAMETERS

For an earthquake engineering applications, the characteristics of ground motion during an earthquake are of prime significance are classified as follow:

1. The amplitude (i.e. Peak ground motion)
2. Frequency content, and
3. Duration of strong motion.

Peak ground motion used to describe amplitude of vibration, frequency content to describe response characteristics of medium and duration describes time taken by fault rupture to release

energy. To describe these characteristics, number of strong ground motion parameters has been described in literature; these parameters provide information about one or more of these characteristics. For practical purpose a single strong ground motion parameter study is not enough to describe strong ground motion completely (Jenning, 1985; Joyner and Boore, 1988).

3.2.1 Amplitude Parameters

Time history is the most common way to describe the ground motion, as it defines its amplitude as function of time. Ground acceleration, velocity and displacement time histories are the most common time domain parameters of strong ground motion. Acceleration time history show high frequency content of motion, whereas velocity time history shows intermediate and displacement time history emphasis on low frequency content of ground motion. One of these parameters is measured directly with the use of instrumentation; while other can be computed indirectly by using mathematical process i.e. integration or differentiation. Historically, the peak ground motion has been considered as a parameter representing severity of shaking at a site.

3.2.1.1 Peak Acceleration

Peak Ground Acceleration (PGA), most easily obtained and widely used parameter to describe ground motion. Peak Horizontal Acceleration (PHA) mostly used to measure the amplitude of a particular ground motion, since its occurs in most recording in the S wave portion with predominant frequencies between 3 and 8 Hz, and is defined as the absolute maximum amplitude of recorded acceleration. Some time it also called as Zero Period Acceleration (ZPA). Most of time it is measured as vector sum of two orthogonal components, to get maximum resultant PHA. Whereas Peak Vertical Acceleration (PVA) may occur in the P wave portion with predominant frequencies between 5 and 20 Hz. PVA is generally assumed to be two third of PHA for engineering purposes (Newmark and Hall,1982). However, in general peak vertical acceleration, is considered as poor parameter for characterizing ground motion, since it is related to single isolated peak within record and does nor correlate well with the damage potential of the shaking. PHA is more preferable to describe ground motion as compare to PVA due to its natural relationship to inertial forces that are introduced in very stiff structure during ground motion. Therefore; PHA is widely used to scale earthquake design spectra and acceleration time histories.

3.2.1.2 Peak Velocity

Peak Ground Velocity (PGV) associate with longer period motion and can be related with energy release, because kinetic energy is directly proportional to square of velocity. Peak Horizontal Velocity (PHV), is parameter used to characterize the ground motion at intermediate frequencies. It is better indicator of potential damage to structure or facilities (i.e. bridges, tall or flexible buildings etc.) that are sensitive to loading in intermediate frequency range.

3.2.1.3 Peak Displacement

Peak Ground Displacement (PGD) relates the lower frequency components of an earthquake motions and it is obtained by double integration of acceleration time history. According to (Campbell, 1985 and Joyner and Boore, 1988) peak displacement is difficult to measure with great accuracy due to long period noise as well as due to signal processing error in filtering and integration of accelerograms. Therefore, its use is limited as compare to PGA, PVA to characterize the ground motion. Fig. 3.1 (a), 3.1 (b), and 3.1 (c) depicts the acceleration, velocity and displacement time histories respectively along with their peak values for the 180 degrees component of the Northridge Earthquake of January 17, 1994 recorded at the Moorpark Station.

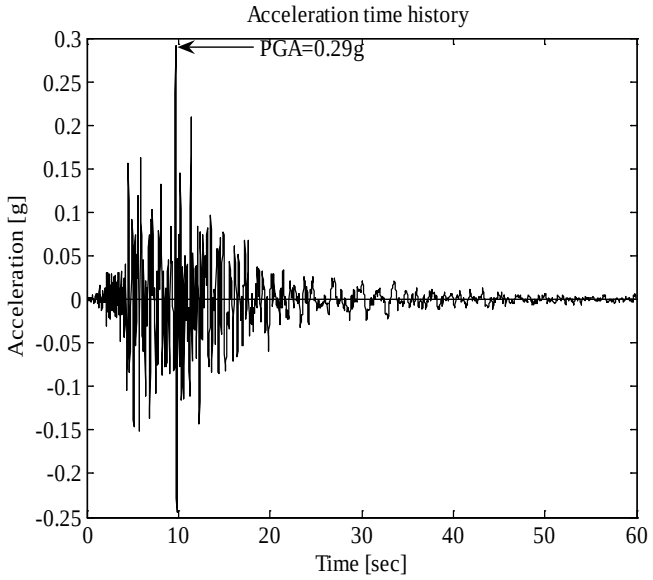

Figure 3.1(a): Acceleration time history recorded at Moorpark station.

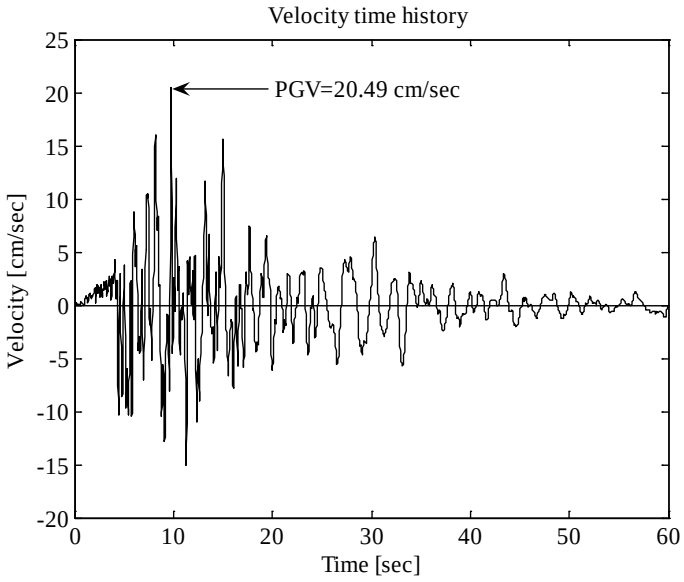

Figure 3.1(b): Velocity time history recorded at Moorpark station.

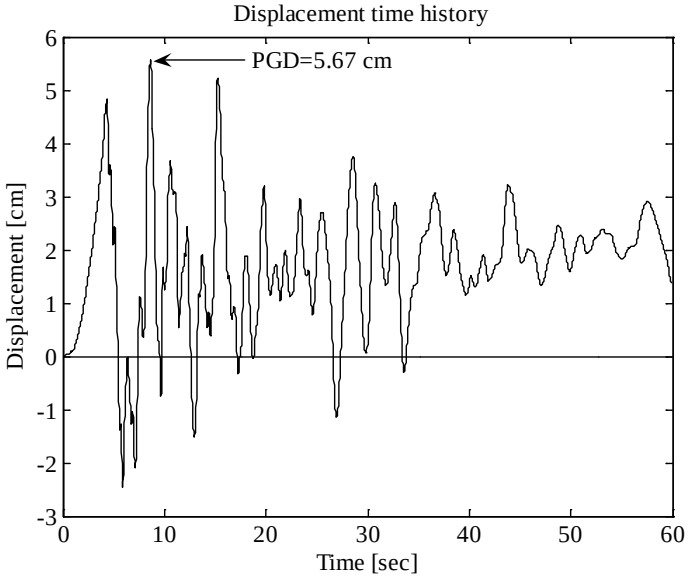

Figure 3.1(c): Displacement time history recorded at Moorpark station.

3.2.2 Frequency Content Parameters

During an earthquake, the dynamic response of structures (i.e. buildings, bridges etc) is very sensitive to the frequency at which they are loaded. Therefore, complete knowledge about the frequencies which is carried by ground motion during an earthquake occurrence has been

critical for research purposes. The frequency content describes how the amplitude of a ground motion is distributed its energy among different frequencies. Ground motion frequency contents can be easily computed by transforming the ground motion from time domain to frequency domain through Fourier transformation. In the frequency domain, the Fourier amplitude, phase spectrum and power spectrum are used in the quantification of strong ground motion. Another very important description of frequency content of earthquake time history is response spectra, which provides peak response values of single degree of freedom system structures having different natural periods and damping.

3.2.2.1 Fourier Amplitude and Phase Spectra

A plot of Fourier amplitude versus frequency is known as Frequency Amplitude Spectrum (FAS). It describes how the amplitude of ground motion is distributed w.r.t frequencies. A plot of Fourier phase angle gives the Fourier Phase Spectrum (FPS) (Kramer, 1996). For sinusoidal like time history, FAS is very narrow, implies the motion has dominant frequency, where as for earthquake like time history FAS is broader since it's contain wide range of frequencies due to jagged and irregular nature of time history. Phase angles control the times at which the peak of motion occur, the FPS influences the variation of ground motion with time. In contrast to FAS, FPS does not display characteristics shape. Fig. 3.2 shows normalized Fourier amplitude spectra for acceleration for the 180 degrees component of the Northridge earthquake of January 17, 1994 recorded at Moorpark station.

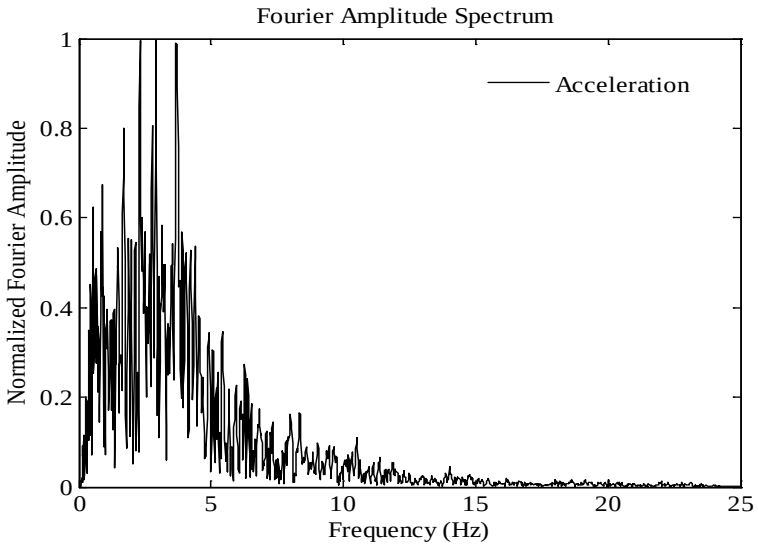

Figure 3.2: Normalized Fourier amplitude spectrum of acceleration at Moorpark station (180 Degrees component).

The characteristics shape of actual earthquake motion is clearly visible when FAS is smoothed and plot on logarithmic scale. Corner frequency (f_c) and cut off frequency (f_{max}) are two attributes of smoothed and well shape spectra. Brune (1970), showed that f_c is inversely proportional to the cube root of seismic moment (m_o) and thus large earthquake produce greater low frequencies motions as compared to smaller earthquakes, where as f_{max} assumed to be constant for particular geographic region is used as parameter to characterize both near site effect (Hank, 1982) and source effect (Papageorgiou and Aki, 1983).

3.2.2.2. Power Spectra

Power Spectral Density (PSD) function is useful not only as a measure of frequency content of ground motion, but also in estimating its statistical properties and help in generating artificial time histories matching a given response spectrum through using Random Vibration Theory (RVT) concept (Vanmarcke, 1976; Yang, 1986; Clough and Penzien, 2003;).

3.2.2.3 Response Spectra

Response Spectra (RS) is the most fundamental engineering tool to characterize ground motion in earthquake engineering and forms the strong basis for most design and analysis of structures. The concept of response spectrum introduced by Biot (1941) and later popularized by Housner (1941) and is defined as the maximum response of a Single Degree of Freedom (SDOF) system to a particular ground motion as a function of natural frequency and damping of the SDOF system. RS is an indirect way of reflecting strong ground motion characteristics, since they are filtered by response of SDOF systems. For design purposes, engineers have to incorporate natural period or natural frequency in the design of a structure using seismic codes, which are developed using response spectrum analysis. Earthquake parameters such as epi-central distance, magnitude, duration, and local soil conditions at the recording station and source characteristics influence the shape and amplitude of response spectra. As illustrated in Fig. 3.3, the ordinates of a response spectrum are given by the maximum absolute value of the displacement $x(t)$, velocity $\dot{x}(t)$ or acceleration $\ddot{x}_T(t)$ of a single-degree-of-freedom oscillator with specified natural period and damping. These are called spectral displacement (S_D), spectral velocity (S_v) and spectral acceleration (S_a) respectively. The equation of motion of SDOF system undergoing base excitation is given as

$$\ddot{x} + 2\omega_n \xi \dot{x} + \omega_n^2 x = -\ddot{u}_g \tag{3.1}$$

Where, $\omega_n(Undamped\ Natural\ Frequency) = \sqrt{\frac{k}{m}}$, $\xi(Damping\ ratio) = \frac{c}{2\sqrt{km}}$ and $\ddot{x}_T(t) = \ddot{x} + \ddot{u}_g$. The solution of Eqn. 3.1 is given as

$$x(t) = \frac{-1}{\omega_n\sqrt{1-\xi^2}} \int_0^t \ddot{u}_g(\tau) e^{-\omega_n \xi (t-\tau)} \sin \omega_n \sqrt{1-\xi^2}(t-\tau) d\tau$$

(3.2)

The maximum value of integral of RHS of Eqn 3.2 is called as Pseudo Spectral Velocity (PSV). Therefore for small value of damping, $PSV = \omega_n * S_D$. Pseudo Spectral Acceleration (PSA) is defined as $PSV * \omega_n$ and therefore Eqn. 3.3 describes relationship between S_D, PSV and PSA.

$$PSA = \left(\frac{2\pi}{T_n}\right) PSV = \left(\frac{2\pi}{T_n}\right)^2 S_D$$

(3.3)

Where T_n is the undamped natural period of a SDOF system. It has been common practice in the past to estimate a design response spectrum from PGA or from, a combination of PGA, PGV, and PGD (Newmark and Hall, 1982). Fig. 3.4 shows the acceleration response spectra of the 180 Degrees component of Northridge earthquake of January 17, 1994 recorded at Moorpark station for 5 % damping.

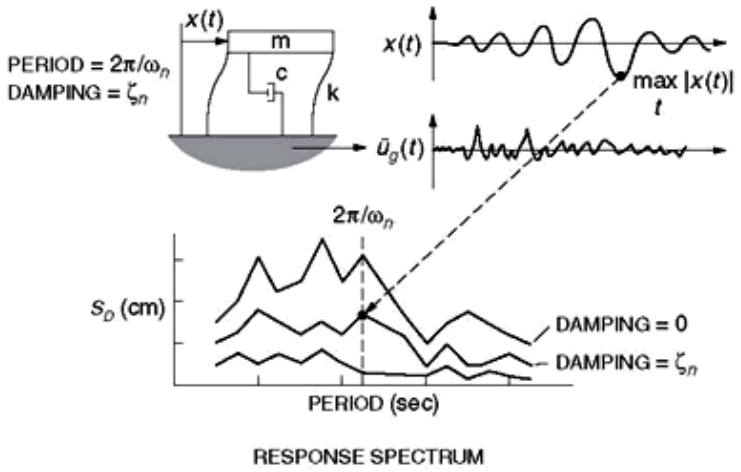

Figure 3.3: Response spectra are determined from the earthquake motion of a SDOF oscillator. The ordinates of the response spectrum are determined by the maximum absolute value of the response quantity of interest as a function of the natural period and damping of the oscillator.

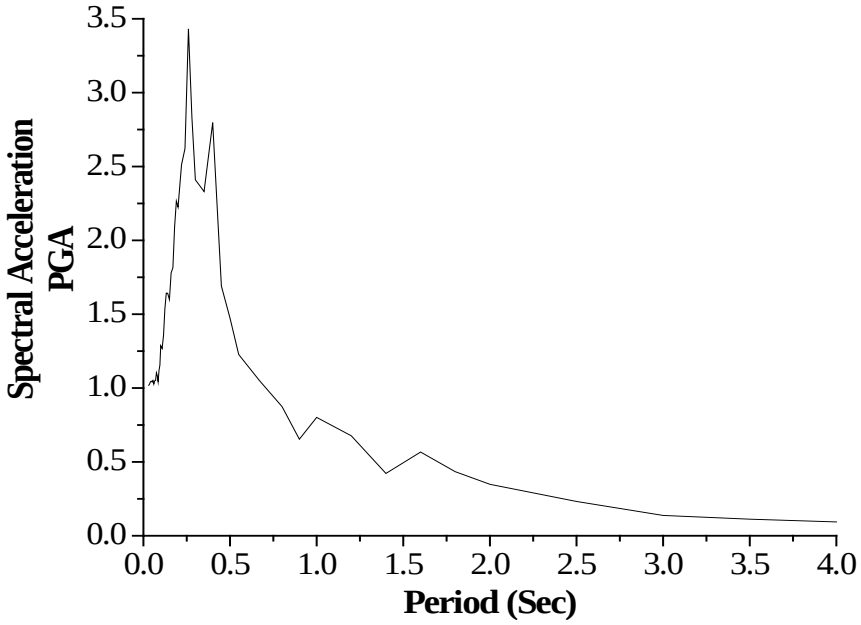

Figure 3.4: Acceleration response spectra at Moorpark station for 5 % damping.

3.2.3 Duration

When an earthquake occur, destructiveness capability of an earthquake lies in its duration which is a function of source parameter: fault size, rupture velocity; path effect: source to site distance; site effect: soft soil, basin effect and directivity. The duration of a SGM is related to time taken by rupture along the fault to release its accumulated strain energy. Larger fault size, result in large duration of SGM with increase in magnitude. The duration of strong ground motion can have a significant influence on damage to structures. For engineering purposes only strong motion portion of the accelerograms is of prime interest. A number of definitions exist in the literature for the duration of the strongest part of shaking (Bommer and Martinez-Pereira, 2000). Perhaps the most widely used definitions of strong ground motion duration are the (1) Bracketed duration and (2) Significant duration.

3.2.3.1 Bracketed Duration

The Bracketed duration (Bolt, 1969) is defined as the time interval between the first and last exceedance of a specified acceleration (usually 0.05g). A disadvantage of this definition is the subjectivity in choice of threshold acceleration value i.e. a_o (it can be absolute or relative e.g. 5% of PGA).

3.2.3.2 Significant Duration

Another definition of duration (Trifunac and Brady, 1975) is the time interval in which significant contribution to the integral of the square of acceleration ($\int a^2 dt$) referred to as the accelerogram intensity takes place.

3.2.3.3 Husid Plot

The accelerogram intensity known as the Arias intensity (Arias, 1970) is defined as the sum of energies dissipated (per unit weight), stored in the undamped oscillators uniformly distributed with respect to their frequencies at the end of earthquake

$$I = \frac{\pi}{2g}\int_0^{t_o} a^2(t)dt \tag{3.4}$$

Where, **a(t)** refers to the ground acceleration time history, $\mathbf{t_o}$ represents the total duration of earthquake and **g** is the acceleration due to gravity. The significant duration is then defined as the interval over which some portion of the total integral is accumulated, which is generally 5% to 95% as shown in Fig. 3.5. The Arias intensity is one of the replacements for PGA as a measure of severity of ground shaking. The Arias intensity is also used for calculating the earthquake destructiveness potential factor defined by Araya and Saragoni (1984). Fig. 3.5 for the Northridge earthquake of January 17, 1994 recorded at Moorpark station (180 Degrees component) on a plot of the built-up of the Arias intensity, known as a Husid Plot (Husid, 1969).

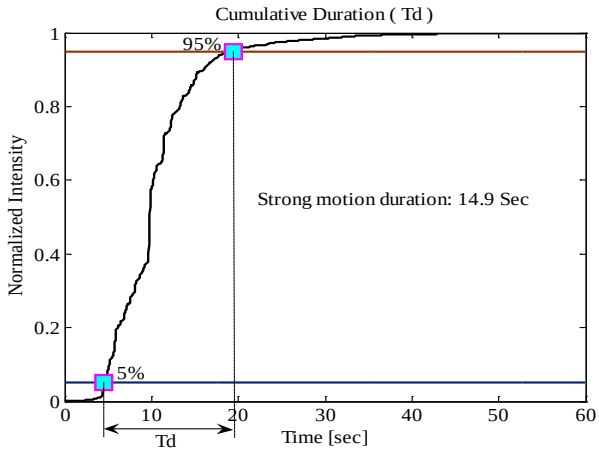

Figure 3.5: Strong motion duration of Northridge earthquake recorded at Moorpark station.

3.3 EFFECTS OF LOCAL SITE CONDITION ON SGM

Site effects are generally referred as variations of ground motion in space, amplitude, frequency content and duration. It has been found in large number of literature that earthquake damage is generally larger over soft sediments than on firm bedrock outcrops (Bessasson and Kaynia, 2002; Yoseph and Ramana, 2008; Boominathan et al., 2008; Boominathan, 2010). This is of prime significance because most of urban settlements have occurred along river valleys over such young, soft surface deposits (Kaynia, 2006; Maheshwari et al., 2012; and Maheshwari et al., 2013). Around the world, large number of densely populated cities as examples: Los Angeles, San Francisco, San Salvador, Kobe, Osaka and Tokyo, Kathmandu, Lisbon, Thessaloniki, Izmit, Mexico City and many more, lies in earthquake prone areas.

Soft soils may have dramatic consequences for the inhabitants of those cities. This provides opportunities to engineering seismologist to perform numerous macro-seismic observations around these cities during the last century (Guttierez and Singh, 1992; Lindholm et al., 1995; Lindholm, 1998; Ortizi et al., 2000; Mahajan and Virdi, 2001; Wirth et al., 2003; and Mundepi et al., 2010). These observations demonstrated very clearly local intensity increase as large as 2, in extreme cases even 3 degrees on the MM or MSK/EMS scale due to damaging effects associated with such soft deposits.

Trapping of seismic waves due to the impedance contrast between soft sediments and the underlying bedrock is the fundamental phenomenon responsible for the amplification of motion over soft sediments. This trapping affects only body waves travelling up and down in the surface layers, when the structure is horizontally layered (which will be referred to in the following as 1-D structures), but in case of the surface sediments form a 2-D or 3-D structure, due to lateral heterogeneities present such as thickness variations, this trapping also affects the surface waves which develop on these heterogeneities, and thus reverberate back and forth.

The phenomena of interference arises between these trapped waves leads to resonance patterns. Geometrical and mechanical characteristics of the structure are closely related to shape and the frequency of resonance pattern. In case of 1-D media (vertical resonance of body waves), these resonance patterns are very simple, they become more complex in the case of 2-D and a fortiori 3-D structures. Therefore, surface geology and geotechnical characteristics of soil deposit at recording site are the salient features that have very profound influence on the nature of strong ground motion, either they amplify or de-amplify the amplitude at all frequencies, which is dependent on physical properties of soil (i.e. Shear modulus (μ), damping ratio, shear wave

velocity (V_s), primary wave velocity (V_p), soil internal damping). The surface geology generally accounted by its categorization as hard rock, rock, stiff soil, alluvium soil etc or by measuring average shears wave velocity in uppermost 30 m of recording site, which can be determined directly by bore holes measurement, using Multichannel Analysis of Surface Waves (MASW*)* method or inferred from empirical relations between shear modulus (μ) and Standard Penetration Test (SPT) blow count, N. To understand physics and spatial variation of ground motion at each particular site, site characteristic in term of shear wave velocity must be known, since average shear wave velocity is most common way to introduce site effect in GMPE's.

3.4 SUMMARY

This chapter documents the various issues involved in the interpretation of strong motion data for engineering applications. The chapter starts with the basic definition of strong ground motion and discusses important characteristics of a strong ground motion from earthquake engineering point of view. The chapter concludes with a discussion on role of site effect on strong ground motion.

Chapter 4

ARTIFICIAL NEURAL NETWORK

4.1 INTRODUCTION

An Artificial Neural Network (ANN), one of subfield of Artificial Intelligence (AI), works on the principle of human brain and nervous system. More specifically, it is an imitator of biological neural system that tries to simulate its learning process. ANN consist of interconnected group of artificial neurons that process and transmit information using various mathematical and computational models as done by biological neurons in the nervous system. Firstly, concept of mimicking the functionality of biological neurons was introduced by McCulloh and Pitts (1943). Later on work of various authors (Hebb, 1949; Minsky, 1954; Neumann's, 1956, 1958; Rosenblatt, 1958; Hopfield, 1982, 1985; Grossberg, 1976, 1988a, 1988b, 1988c; Widrow, 1960, 1985) made the framework of ANN to be very powerful computational tool. From last few decades many authors have described the structure and operation of ANN (Zurada, 1992; Haykin, 1999; Fausett, 1994) but there is no universal accepted definition of an ANN. According to Zurada (1992), ANN is physical cellular systems which can acquire, store, and utilize experimental knowledge. ANN is massively parallel-distributed information processing system whose performance characteristics resemble to biological neural network of the human brain (Haykin, 1999). ANN is information processing systems which have been developed as generalization of mathematical models of human cognition or neurobiology (Fausett, 1994). In recent years ANN have become very popular computational tool and find applications in large number of scientific fields such as pattern recognition, signal processing, medicines, speech recognition, machine learning, market and stock forecasting, weather forecasting, earthquake forecasting, geo-technical engineering, image processing, earthquake engineering etc (Masters, 1993; Welstead, 1994, Alves, 2006).

ANN are highly adaptive in nature and have ability to capture the subtle relationships amongst inputs and outputs for data exemplars presented to them, even if underlying physical relations between inputs and output is not known, in comparison to most statistical and empirical models where physical relation between inputs and outputs must be known, which makes its use a strong case in earthquake engineering. ANN serves as excellent tool for modelling of data that

are known to be complex and often non linear, due to its ability to learn from experience and generalize from examples presented to it. Large numbers of literature can be found (e.g. Zurada, 1992; Haykin, 1999; Fausett, 1994; Mehortra et al., 1996; Gurney, 2005; Galushkin, 2007) to acquire complete information about theoretical background of Neural Network and its applications. Therefore a review of Neural Network (NN) presented in this chapter is limited to only those aspects that are pertaining to this study.

4.2 THE BIOLOGICAL MODEL (REAL NEURONS)

Human beings are successful in performing more cognitive, perceptual (e.g. recognition of face, voice) and control activities (e.g. movement of body parts and its functions) due to massive parallelism, the highly parallel computing structure and imprecise information processing capability of its brain.

A human brain consists of more than 10 billion interconnected computing element called neurons. Each biological neuron or a nerve cell is the fundamental to the construction of the biological neural network that uses biochemical reaction to receive process and transmit the information. A typical structure of biological neuron is shown in Fig. 4.1 that consists of synapses, dendrites, axon and soma (or the cell body).

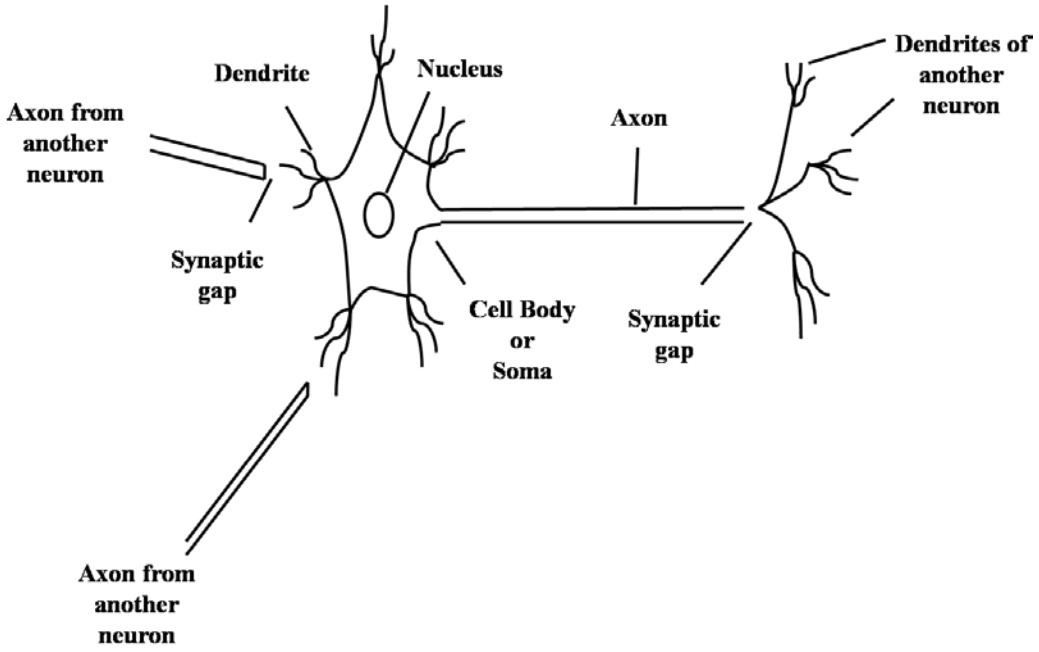

Figure 4.1: A typical structure of biological neuron (Fausett, 1994).

Dendrites are treelike network of nerve fibres connected to the soma or cell body, which sum up all the incoming signals. Dendrites receives information from other neurons through axon which is single long fibre that serve as transmission line and each end part of an axon branches into strands and sub-strands that are further connected to other neurons through synaptic terminal (synaptic gap) or synapses. Synaptic is a junction that allows signal or information transmission between the axon and dendrites. During the transmission of information or signals from one neuron to another, a biochemical process occur at each synapses, in which specific transmitter substances are released by sending end of the junction which has effect either to raise or lower the electrical potential inside the body of receiving cell. When particular threshold potential is achieved, a pulse is sent down to the axon and the cell is fired.

A biological neuron is fundamental to the construction of any neural network that receives input from other sources, summed up them in some way and finally performs some non-linear operation on the result and then output the final result. Fig. 4.2 shows the association of biological network with artificial network.

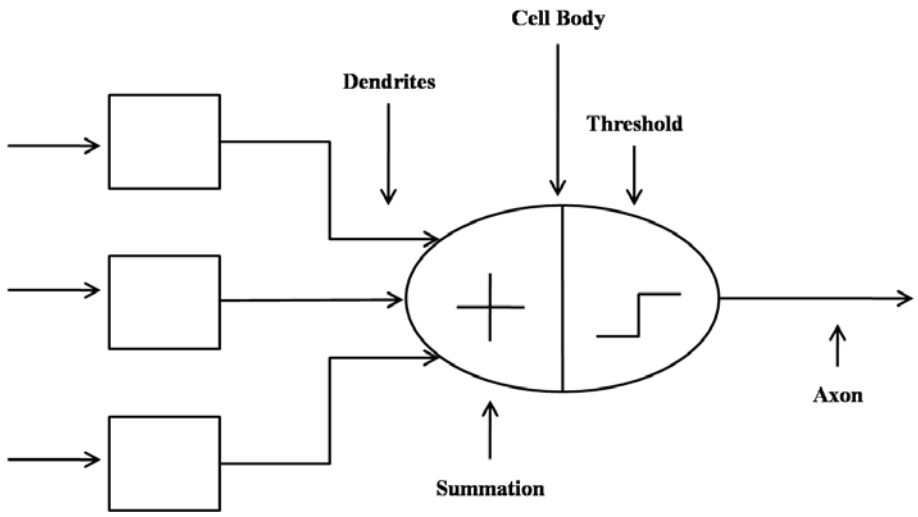

Figure 4.2: Association of biological network with artificial network (Sivanandam et al. 2006).

4.3 THE MATHEMATICAL MODEL

Artificial neuron, or simply neuron known as 'Processing Element' (PE), 'node' or 'unit' are the building blocks of ANN, which are fully or partially connected with other neurons. A typical

model of artificial neuron, which is fundamental to the designing of ANN, is shown in Fig 4. 3. Three basic elemental components of neuron model are:

1. Input and Synaptic weights
2. Adder
3. Activation function or transfer function

Synaptic weight, an adjustable numerical value represents connection between an input and a neuron. Weights can have positive, zero or negative values representing excitatory, no connection or inhibitory connections (Haykin, 1999). All weighted inputs are linearly summed up by adder. The convergence property of a neural network can be improved by adding or subtracting threshold or bias unit that scale all weighted inputs to effective range. In output state, activation function (e.g. logistic sigmoid, hyperbolic tangent) generates output of the neuron for applied weights and biased inputs. Output can attain a value between 0 and 1, or -1 and 1 depending upon which type of activation function is used. For node j, the whole process is illustrated in Fig.4.3 is summarized using Eqns.4.1 and 4.2.

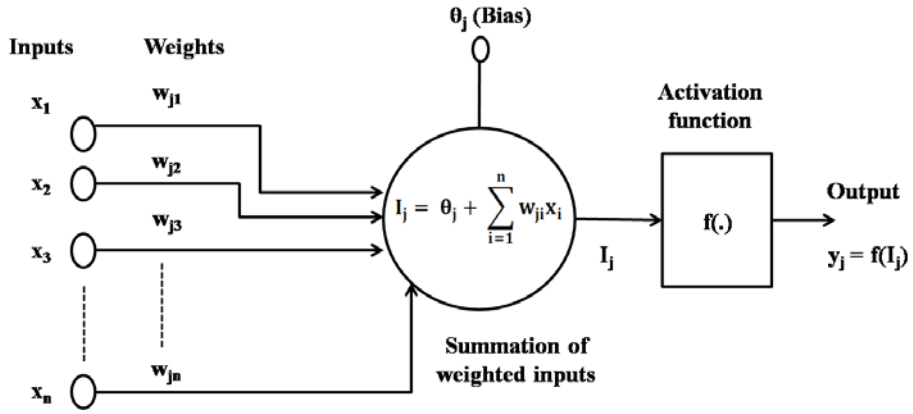

Figure 4.3: Schematic representation of functional structure of a processing element (Haykin, 1999).

$$I_j = \theta_j + \sum_{i=1}^{n} w_{ji}\, x_i \qquad \textbf{(4.1)}$$

$$y_j = f(I_j) \qquad \textbf{(4.2)}$$

Where, I_j = the activation level of node j; w_{ji} = the connection weight between nodes j and i; x_i = the input from node i; i = 0, 1... n; θ_j = the bias or threshold for node j; y_j = the output of node j; and f (.) = activation function or transfer function.

4.4 ACTIVATION FUNCTIONS

The role of activation function is used to transform the activation level of a unit (neuron) into an output signal. In NN each neuron has scalar-to-scalar function (i.e. activation function) that transforms activation level of processing unit for given input or sets of inputs to an output signal known as unit's activation function. Activation function also called as squashing function, has bounded amplitude range of the output. These functions are used to solve both linear and non-linear problems. Most commonly used activation functions (Fausett, 1994) are:

4.4.1 Linear Function

As its name suggest, it satisfies the concept of superposition. It's mathematically expressed as Eqn. 4.3 and shown by Fig. 4.4, where β is the slope of linear function.

$$y = f(x) = \beta x\,;\ \ for\ all\ x \tag{4.3}$$

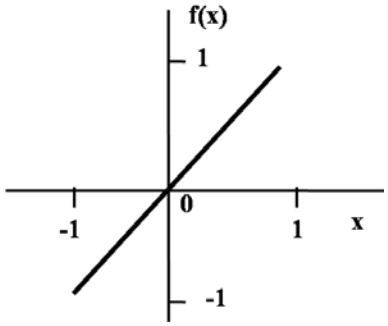

Figure 4.4: Linear function.

Special case:

With β =1, y = f(x) = x is called *Identity function.*

The output y of identity function is same as it input x or simply, just passed the activation level directly as output. The output of linear function is simply a scalar multiplication of input with

some constant. Its output range is [-∞, ∞]. This function is generally used at last step of a Multilayer Neural Network (MLNN).

4.4.2 Step Function

It is also known as *Threshold (Hard limiter)* or *Heaviside function*. It is of two types.

1. Binary
2. Bipolar

It's mathematically expressed as Eqn. 4.4 and shown by Fig. 4.5 and 4.6.

Binary Form

$$y = f(x) = \begin{cases} 1; & if\ f(x) \geq 0 \\ 0; & if\ f(x) < 0 \end{cases} \quad \textbf{(4.4)}$$

Bipolar Form

$$y = f(x) = \begin{cases} 1; & if\ f(x) \geq 0 \\ -1; & if\ f(x) < 0 \end{cases} \quad \textbf{(4.5)}$$

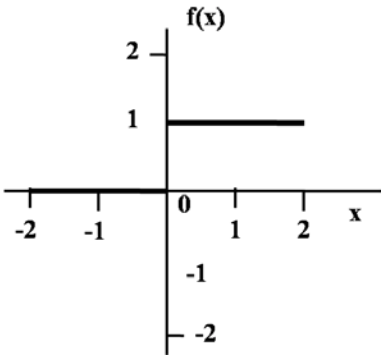

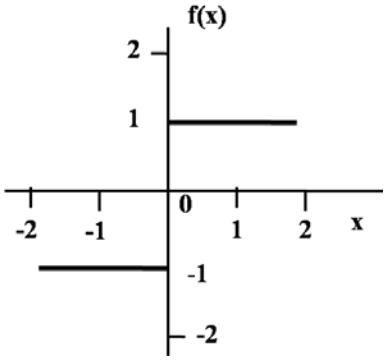

Figure 4.5: Binary step function. **Figure 4.6:** Bipolar step function.

Its
output range is [0, 1] (i.e. binary signal) and [-1, 1] (i.e. bipolar signal). It is commonly used in single layer network. Since it is non-differentiable function, so can't be used with Back Propagation (BP) algorithm in multilayer network.

4.4.3 Piecewise Linear Function

It is also known as *saturating linear activation function*. Depending on saturation limits of the output it can acquire either binary or bipolar range. It's mathematically expressed as Eqn. 4.5 and shown by Fig. 4.7.This activation function output results in -1 for negative weighted inputs sum, proportional to input for range [-1, 1] and 1 for positive weighted inputs sum.

$$y = f(x) = \begin{cases} -1; & if \quad x < -1 \\ x\,; & if \; -1 \geq x \geq 1 \\ 1; & if \quad x \geq 1 \end{cases} \tag{4.5}$$

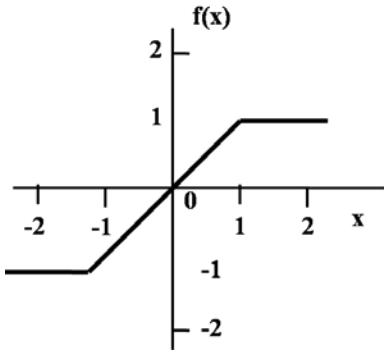

Figure 4.7: Piecewise linear function.

4.4.4 Sigmoid Function

Sigmoid function is nonlinear well behaved, differentiable and strictly increasing function, whose graph is S-Shaped, curves. It is extensively used to construct the Back Propagation Network (BPN) and Radial Basis Function Network (RBFN). *Hyperbolic* and *Logistic* functions are most commonly used.

4.4.4.1 Logistic Function

It is known as *Binary Sigmoid function*. It output range is [0, 1]. It's mathematically expressed as Eqn. 4.6, where, $\boldsymbol{\sigma}$ is steepness parameter. By varying it, different shape of function which is continuous and differentiable can be obtained as shown in Fig.4.8.

$$\boldsymbol{f(x) = \frac{1}{1 + e^{-\sigma x}}} \tag{4.6}$$

4.4.4.2 Hyperbolic Tangent Function

It is also known as *Bipolar Sigmoid function*. It has similar property as Logistic Sigmoid function. It's mathematically expressed as Eqn. 4.7 and shown by Fig.4.9. Its output range is [-1, 1].

$$f(x) = tanh(\sigma x) = \frac{sinh(\sigma x)}{cosh(\sigma x)} = \frac{e^{\sigma x} - e^{-\sigma x}}{e^{\sigma x} + e^{-\sigma x}} \quad \textbf{(4.7)}$$

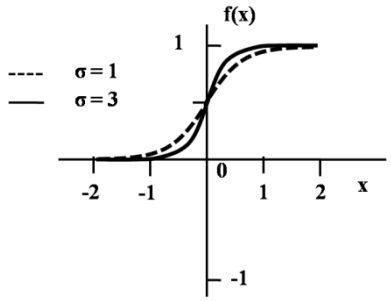

Figure 4.8: Binary logistic function with varying slope.

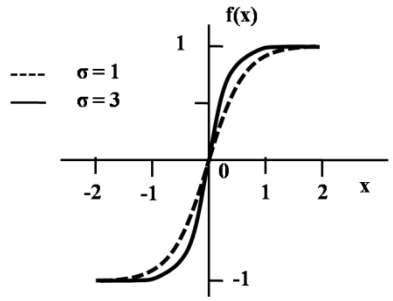

Figure 4.9: Hyperbolic tangent function with varying slope.

Logistic and *Hyperbolic* are easily differentiable that makes them to use as first choice in BPN, because they dramatically reduce the computation burden for training due to well defined relation between the value of function at a point and it derivate value at that point. For hidden units in Multilayer Neural Network (MLNN), a non-linear activation function is used to introduce non-linearity that increases its computational power to solve more complex problems. Any non-linear activation function can be used for this job, but for back propagation learning the activation function must be well behaved, differentiable and must be bounded. Thus, sigmoid functions are the most common choice.

For the output units, based on distribution of the target value, activation function must be chosen. For continuous bounded target value, sigmoid functions are excellent choice with condition that targets to be scaled in the range of the output activation function. But for non-bounded target value, better choice is unbounded activation function, most often identity function. Exponential activation is best choice in case of positive targets value with no upper bound limit (Sarles, 1997).

4.5 NEURAL NETWORK TOPOLOGIES

Neural Network topologies represent way of organizing neuron in different layers and its connection with other neurons. However, connection among neurons can be partial or full depending on input at neurons, topology used for the connections and algorithm applied in the network. Network topologies can be categorized as:

1. Feed forward
2. Feedback or Recurrent

4.5.1 Feed-Forward Networks

The first and simplest fully connected artificial neural network is feed-forward neural network. The term 'feed-forward' signify that the network connections between units, data and calculations travel in one direction i.e. forward direction from input to output. This way of processing data can be extended over multilayer of units, but this network has no directed cycles or loops or feedback. In this network, output values depend on input values, synaptic weights and thresholds. It is also known as top-down or bottom-up. Feed-forward network finds application in pattern recognition, data mining, etc. They are further classifies as single layer and multilayer feed forward network.

Single layer network: The network consists of only one feed forward layer of weighted inputs connected to the output units.

Multi-layer network: The network consists of one or more feed forward layers of weighted inputs connected to the output units. On comparison to single layer network, it is more capable in solving complex problems.

4.5.2 Feed-Back Networks

The most powerful and complicated artificial neural network is feed-backward neural network. In this network, connection between units has directed cycles or loops and data can flow in both forward and backward direction. It is nonlinear dynamic network since their state changes continuously and also changes when input varies, until equilibrium point is reached. It is also known as interactive or recurrent network. Feed-backward network finds application in handwriting recognition, associative memories, etc.

Here our main emphasis is on Multi-Layer Feed Forward Neural Network (MLFFNN), since this network is the main focus of this thesis work. MLFFNN also known as Multi-Layer Perceptron (MLP) has been used in many applications such as Pattern recognition, speech synthesis, stock market prediction etc. Generalization and fault tolerance features of MLP emphasize its use in this study. Multilayer perceptron architecture is composed of input layer, one or more hidden layer and output layer. The input signal processing occurs on layer-by-layer basis. Input signal is transformed by synaptic weights to next layer in forward direction. The output of each layer is transmitted to the input of neurons in the next layer through weighted links. Hidden layer execute complex computation by extracting progressively more meaningful features from the input layer by scaling and normalization of input data, simply it is known as pre-processing of input data. Data pre-processing attempts to fasten learning process in ANN. One hidden layer MLP with I inputs, H hidden and O outputs (MLP (I-H-O)) is show in Fig. 4.10.

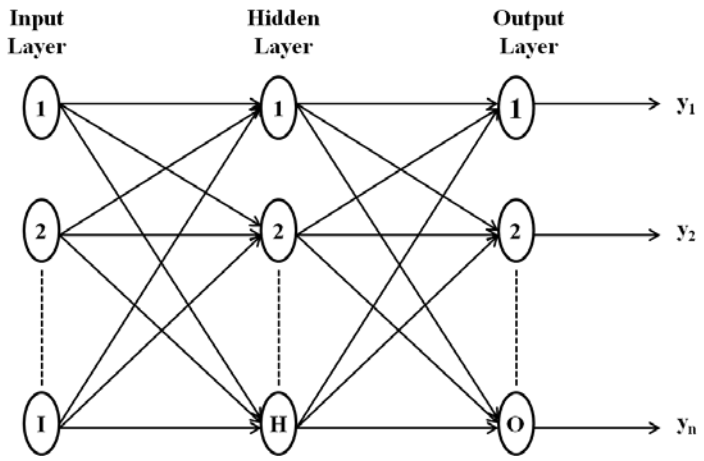

Figure 4.10: Multi-layer perceptron (MLP) with one hidden layer (I-H-O).

4.6. TRAINING OF ARTIFICIAL NEURAL NETWORK

The functioning of ANN is generally defined by the combination of its topology and the synaptic weights of its neurons connections within the network. The topology of ANN is generally held fixed in term of numbers of layers, numbers of neurons per layer and it's synaptic weights , in order to capture subtle relationship between the inputs and desired outputs is called *learning or training*. Trained network shows its ability to vary its input/output corresponding to variation in the surrounding. Actually, value of connection weights possesses

knowledge, altering the knowledge through learning process causes change in value of weights. Hence, neural networks can be classified as fixed or adaptive networks, depending on whether weights are fixed or changeable respectively. The various learning algorithm shown in Fig. 4.11, have been used to train ANN can be categorized as:

1. Supervised learning
2. Unsupervised learning
3. Reinforcement learning

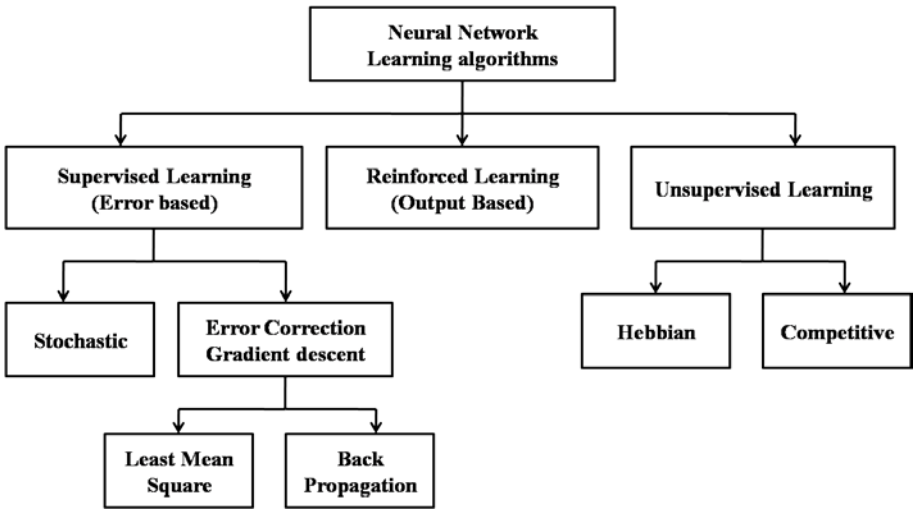

Figure 4.11: Classifications of learning algorithms.

4.6.1 Supervised Learning

Supervised learning also called *associative learning,* in which both inputs and desired outputs (target values) are given. Most popularly known Back-Propagation algorithm using gradient descent based delta learning rule is supervised learning method used for modifying the connection weights. The network processes inputs and results obtained are compared with desired outputs and measured differences (i.e. error vector) are propagated back from output layer to input layer via hidden layer for adjusting the weights. This process of modifying weights is repeated again and again till error measured is minimized, which is one of the prime objectives of BPN (Fig 4.12). So, in this type of learning external teacher is present for providing continuous feedback to results obtained. Examples of supervised learning are pattern recognition, regression, speech and gesture recognition, etc.

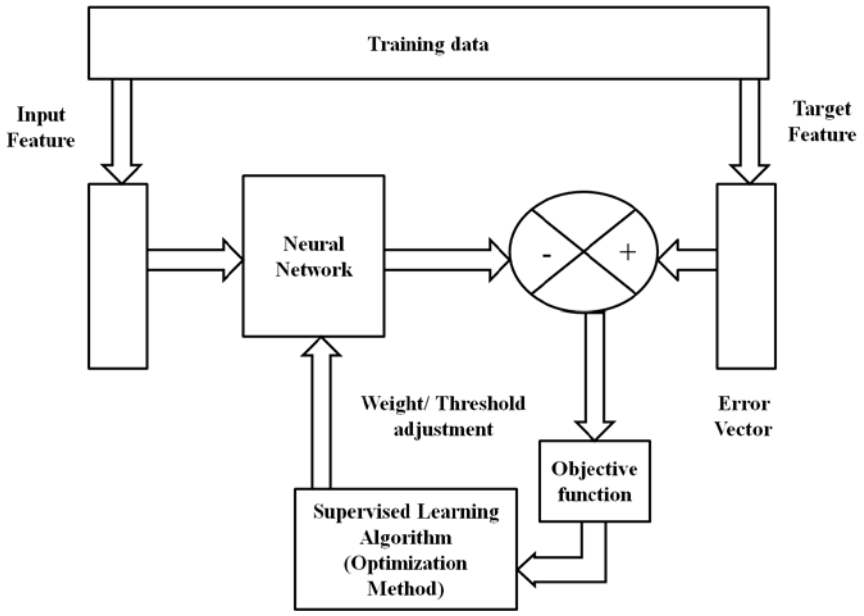

Figure 4.12: Supervised learning algorithm of ANN.

4.6.2 Unsupervised Learning

Unsupervised or adaptive learning also known as self-organization provides only input data, with no desired outputs or external teacher. In this learning, network itself identify patterns and classify them by correlating salient features in the input data. Unsupervised learning can be categorized based on rules applied as Hebbian learning and Competitive learning. Examples of unsupervised learning are clustering, estimation of statistical distributions, compression, filtering, etc.

4.6.3 Reinforcement Learning

Reinforcement learning (RL) is *trial and error* learning where network perform action with the environment and from its response, generates data. Like supervised learning, external teacher is present but network is not provided with right answer. However, only correctness of the output answer is indicated in form of either success (1) or failure (0). RL network adapt itself to actions whose response is good and figure out as reward. This learning tries to maximize amount of rewards and correspondingly modify its parameters so that network is able to learn

input-output mapping. This process of modifying parameters continues and fixes when equilibrium point is reached. Thus, it can solve a specific problem if provided with an adequate amount of information.

4.7 BACK PROPAGATION ALGORITHM

The main objective of all training algorithms is to adjust the weights so that network performs well. A wide range of algorithms have been found in literature for this purpose. Here, the study is limited to the gradient descent algorithm with an addition of momentum factor (i.e. Back Propagation). Back Propagation algorithm is most commonly used systematic method for training of multi-layer neural network (MLNN) for data modelling and prediction applications (Hertz et al., 1991). It is based on a supervised learning technique using extend gradient descent based delta learning rule to adjust the weights in feed forward networks with differentiable transfer functions in order to minimize the error in its predictions on the training set of input-output examples. This training procedure is commonly known as Back propagation of error or in short back propagation. Typically Feed Forward Back Propagation Network (FFBPN) have three layers: an input layer having x_n neurons, hidden layers having h_m neurons and output layer having y_l neurons (Fig. 4.13), where w_{ij} and w_{jk} are named assign to input to hidden, and hidden to output weights, and b_1 ,b_2 are the hidden layer and output layer bias respectively. FFBPN learning process consists of four phases.

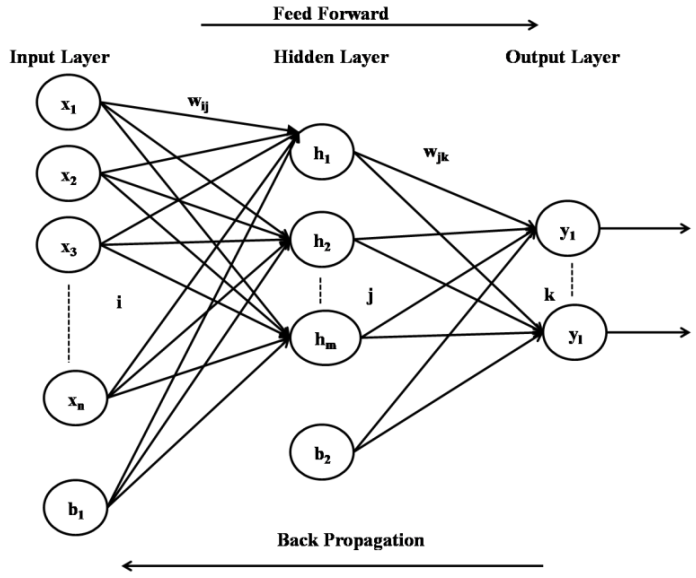

Figure 4.13: Structural diagram of Feed Forward Back Propagation Network.

Initially all its weights and biases are allotted with small random numbers, generally between -0.5 and 0.5 or between -1 and 1. In the second phase input signal flows in only one direction from input i^{th} node through hidden j^{th} node to output k^{th} node that calculates activation function of the total weighted input. In third phase the network determines the Global Error (E) or Mean Squared Error (MSE) between computed activation output y_k and desired output d_k by the Eqn. 4.8, where N represents the numbers of data points considered for training. The weights and biases of the network in forward direction remain same. However, in the final phase the weights and biases are iteratively updated using Eqn. 4.9, so that E can be minimized.

$$E \; or \; MSE = \frac{1}{2N}\sum_{k}(y_k - d_k)^2 \tag{4.8}$$

$$\Delta w_{jk}(n) = \underbrace{\eta\left(\frac{\partial E}{\partial w_{jk}}\right)}_{\text{Gradient Descent Part}} + \underbrace{\alpha \Delta w_{jk}(n-1)}_{\text{Momentum Part}} \tag{4.9}$$

Where $\Delta w_{jk}(n)$ and $\Delta w_{jk}(n-1)$ are weights updation between n^{th} and $(n\text{-}1)^{th}$ epoch respectively between j^{th} and k^{th} nodes, this whole process is known as learning process, its consist of two parts namely gradient descent and momentum part, where **η** is the learning rate and **α** is the momentum rate. Learning rate, **η** play critical role, its assign the upper limit to the amount by which weights can be changed, hence prevent the network to get trapped in local minimum instead of global minimum, so its value must be choose carefully.

Momentum rate provide an advantage over the gradient descent learning in the sense that a momentum term, help in upgrading of weight in a direction that based on the combination of current gradient and the previous gradient, hence speed up training and prevention of oscillation in the weights, in order to stabilize the convergence. Typically values of **α** ranges from 0.5 to 0.9. Momentum learning is a robust method to speed up learning, and it is used as default search rule for all networks in this study. The derivation of the back propagation algorithm can be found in numerous literatures (Zurada, 1992; Bishop, 1995; Haykin, 1999; Fausett, 1994, Adeli, 2001; Anderson, 2003).

4.8 MODELING ISSUES IN ARTIFICIAL NEURAL NETWORK

For better performance of ANN model it must be developed in systematic manner. Typical design of ANN models follows a number of systematic steps as follows

1. Data Preparation
2. Pre-processing of Data
3. Designing of ANN architecture
4. Selection of training algorithm
5. Testing of trained ANN model

4.8.1 Data Preparation

4.8.1.1 Forming Inputs and Outputs

By forming inputs and outputs, simply mean the selection of those input variables and that have the significant effect on output variable. Selections of input variables is always critical to the performance of ANN, a large number of input variables to ANN model result in large size of network, decrease processing speed and reducing the network efficiency (Lachtermacher and Fuller, 1994). So only those input variables which have maximum influence on our output have been choosen.

4.8.1.2 Division of Data

ANN has a limitation that it cannot be extrapolated beyond the range of data used for calibration or training (Flood and Kartam, 1994; Minns and Hall, 1996; Tokar and Johnson, 1999). An interesting feature of ANN is generalization, which means that trained neural network is able to process new data set with minimum error as it performed on data set during training phase. For good generalization, *Cross Validation* (Stone, 1974) approach is most efficient way, which is simply division of entire dataset into multiple data sets, most commonly as *training, validation and testing dataset.* Training set is a part of our dataset, used to adjust the connections and weights during training, where as validation set is used by the network during training to tune the network topology or network parameters other than weights and it help to guard against overtraining of network. By overtraining of network mean network start memorizing the data point used for calibration purpose, instead of finding some trend in it. The performance of validation set will begin to degrade when network is starting to over train

on the training data set. Testing set is a part of our dataset which is not exposed to network during training phase and considered as new data entered by user for neural network application, to check the overall performance of trained network. The primary concerns during division of data set, should be to ensure that: (a) the training set contains enough data, and suitable data distribution to adequately demonstrate the properties which is essential for network to learn, (b) there is no unwarranted similarity between data in different data sets. Shahin et al., (2001, 2004) found that training set constitutes 70 %, validation and testing set each constitutes 15 % of entire data set show better performance with ANN model.

4.8.2 Pre-processing of Data

After completing the division of entire available dataset into multiple sets i.e. training, cross validation and testing set, it is important to pre process the data in a suitable form before it is fed to an ANN. Neural Networks work only with numeric data and numeric values should be scaled before feeding them to the network input because artificial neurons have a limited range of operating value. Therefore, data should be modified before it is fed to a Neural Network which is known as *Data Pre-processing*. The objective of pre-processing is to reduce dimensionality of the input data set and simplify the patterns to ease recognition in order to avoid a huge amount of computation and improve the network's generalization ability. Data pre-processing ensures that all variables get equal importance during the training phase of network (Maier and Dandy 2000). Typically, in pre-processing the whole input parameters are converted in the scaling range of -1 to 1 and output parameters are converted in the scaling range of 0 to 1.

4.8.3 Designing of ANN Architecture

Most critical and tedious task in ANN model development is appropriate selection of numbers of layers and numbers of neurons in each layer. There is no thumb rule for determination of optimal ANN architectures. MLP with single hidden layer using sigmoid activation function is sufficient to solve many complex problems (Hecht-Nielsen, 1989). ANN with more than one hidden layer provides more flexibility to model complex function in many practical situations (Flood et al., 1994; Sarle, 1994). Local feature of inputs is extracted using 1^{st} hidden layer whereas 2^{nd} hidden layer is useful in extracting the global feature of training inputs (Chester, 1990). However, the probability of getting trapped in local minima is increased using two hidden layers concept and it also slows the training speed dramatically (Masters, 1993). For

practical purpose any feed forward network with single hidden layer should be the first choice, until unless a single hidden layer with sufficiently large numbers of hidden nodes does not perform well, and then make shift to second hidden layer with fewer numbers of nodes.

There is no precise way of selecting optimum numbers of neurons in each hidden layer. Lesser number of nodes results in under fitting, whereas large number of nodes results in over fitting. The numbers of input and output units, presence of noise in the targets, the complexity of the error function, the network topology, and the training algorithm all play critical role in selection of hidden nodes. Several authors worked for finding optimum numbers of neurons in hidden layers. Salchenberger et al. (1992) suggested that for single hidden layer the number of neuron should be 75% of the numbers of inputs nodes. Whereas Berke and Hajela (1991) suggested that the number of neurons in single hidden layer should be average sum of input and output nodes. Hecht-Nielsen (1987), suggested that upper limit on the numbers of neurons in single hidden layer should be 2I+1, where I is numbers of inputs. Nawari et al. (1999) described geometric pyramid rule for selection of neurons for two hidden layers network, the number of neurons in each layer should follow a Geometric Progression (GP) with decrease in numbers of neurons from input layer towards output layer. Kudrycki (1988) suggested that number of neurons should be in 3:1 from first to second hidden layer.

Inspite of all the above suggestions hit and trial method is the most popular approach to find the optimal number of neurons. For practical purpose, *forward selection* or *backward selection* can be used to determine the hidden layer size. In forward selection process, start with minimum number of neurons, like two if it is difficult to guess how small it is; train and test the network; record its performance. Repeat this process for some time with slight increase in the number of neurons, until the error is acceptably small, or no significant improvement is noted, whichever comes first. Backward selection is contrary to forward selection. Here initially start with a large number of neurons, and then decreases the number gradually (Masters, 1993 and Ripley, 1996). This process is time-consuming, but it works well.

4.8.4 Selection of Training Algorithm

4.8.4.1 Model Optimization (Training)

The main objective of ANN is optimizing the connection weights; this process of optimization of connection weights is known as *training or learning.* There have been a large number of algorithms found in literature to perform this job. The most popular algorithm to find optimum

connection weights in MLFFNN based on first order gradient descent optimization method is back-propagation algorithm (Rumelhart et al. 1986) which is proven very successful in many applications. Another method such as simulated annealing and genetic algorithm (Hassoun, 1995; Masters, 1993; Reed et al. 1999) have been proposed for global optimization, as these methods have ability to escape local minima in the error surface, thus, produce optimal solutions with slow convergence rate. Major problem with back propagation algorithm is that its convergence tends to be extremely slow. Ultimately, it is performance criteria of model in use for specific problem, which will decide the appropriate training algorithm.

4.8.4.2 Stopping Criteria

During training phase of ANN, the most important task is when the training process should be stopped. For this purpose various stopping criteria have been used in literature. Maier et al. (2000) suggested a stopping criterion to help us to decide whether model has been optimally or sub optimally trained. Training can be stopped; if training error reaches a sufficiently small value and no further slight changes in the training error occur for given fixed number of training records. But this type of stopping criteria lead to the model stopping prematurely or over training. To overcome this problem, cross validation (Stone, 1974) approach is useful and considered as most efficient way to ensure that over fitting does not occur (Smith, 1993). Cross validation approach requires data to be divided into three subset i.e. training, validation and testing set as discussed previously. Bayesian Information Criteria, Akaike's Information Criterion and Final prediction error are some other stopping criteria which can be used. Unlike cross validation, these stopping criteria require division of entire data set into two subsets i.e. training and validation set. Training set used to construct the model and validation set is used to test the validity of model in the deployed environment.

4.8.5 Testing of Trained ANN Model

Once training phase of model has been successfully completed, the performance of the trained model should be validated. The validation procedure ensure that model has ability to generalize within the limits set by training data in a robust manner, rather than memorizing the input - output relationships of data set used for training purpose. The approach most of time in the literature adopted for this purpose is to test the performance of trained ANN's on an independent dataset which is never exposed to the network during training phase. If such performance is adequate, the model is considered have good generalization capability.

The result of testing network is mostly defined in terms of the coefficient of correlation (R), the mean absolute error (MAE) and the root mean squared error (RMSE). The R is a measure of relative correlation and goodness of fit between target and predicted outcome, but extreme values heavily affect it. The value of $|R|$ lies between 0 and 1 and on its value, Smith (1986) suggested following rules: $|R| \geq 0$, strong correlation exists between two set of variables; $0.8 > |R| > 0.2$, correlation exists between two set of variables and $|R| \leq 0.2$, weak correlation exists between two set of variables. The RMSE is the most popular measures of error, which is well suited to iterative algorithms and is a better measure for high value in data set, since it gives a relatively high weight to large errors than small errors (Hecht- Nielsen, 1990). The MAE measure the average magnitude of the errors in a dataset, without considering their direction, gives the same weight to all errors, thus has the advantage that it does not distinguish between the overcome and underestimation and does not get too much influence by higher value (Kalra, 2005; Karunanithi, 1994). Both RMSE and MAE are desirable when the evaluated data are smooth or continuous (Twomey and Smith 1997).

4.9 SUMMARY

In this chapter a brief description of Artificial Neural Networks pertaining to present thesis work is presented. The qualities of ANNs to capture/understand very complex phenomenon and train themselves for prediction form the backbone of generating strong ground motion parameters in this study. The Multilayer Perceptron neural network model is briefly discussed along with back propagation algorithm. The chapter concludes with a discussion on various modelling issues, which should be taken care during implementation of back propagation algorithm in ANN.

Chapter 5

STRONG GROUND MOTION DATABASE

5.1 INTRODUCTION

The prediction of any parameter requires either a good mathematical model to describe fully the physics of the phenomenon or a good data set which can be used for prediction. The complex phenomenon of earthquake occurrence and relatively lesser data has made in roads to the use of such methodologies like ANN. In the present case, ANN methodology has been proposed to be used for prediction of PGA, duration and site conditions which require a relatively larger data set. The paucity of SGM in Indian context has been described in many reports (Singh et al., 1996; Sharma, 1998; Sharma et al., 2006) which leads to initiate a search for a good data set to train the ANN.

The chapter describes the strong motion data acquired for Indian sites. Due to smaller size of strong motion data set from India for the type of ANN analyses required in present case, strong motion data set from other regions has to be worked out for prediction of strong ground motion or the local site conditions. The following sections describe the Indian data set along with the strong motion data set from Japan.

5.2 INDIAN STRONG GROUND MOTION DATABASE

In India, strong motion seismology started in early 80's with the deployment of strong ground motion instrumentation in the Himalayan region. Therefore strong-motion data available for Indian Himalaya is very limited. Department of Science and Technology (DST), Government of India, under its vision of Indian National Strong Motion Instrumentation Network sanctioned a project to the Department of Earthquake Engineering, Indian Institute of Technology Roorkee (IITR), Roorkee, under which three strong-motion arrays in one of the world's most seismically active region of the Indian Himalaya, have been deployed namely, the Kangra array in Himachal Pradesh (North West India), the Garhwal array in Uttrakhand (North Central India), and Shillong array in Meghalaya and Assam (North East India). The Kangra array consists of 50; the Shillong array, 45; and the Garhwal array, 40 analog strong-motion accelerographs (SMA 1). Dharmsala earthquake (M 5.4), 1986 was the first major strong-motion record

recorded by Kangra array. Subsequently, the Uttarkashi, 1991 and Chamoli, 1999 earthquakes of magnitudes 6.8 and 6.4 respectively were recorded.

These arrays produced strong-motion data, which are being used at the national and international level by engineers and scientists. These strong-motion instruments performing well from last three decades and provided good quality recordings. However, due to the unavailability of components/spare parts and to obsolete technology, most of the strong-motion accelerographs installed during this program in 1980s are no longer functional.

Strong motion instrumentation programme in India got major boost in 2004 when DST launched a project titled "National Strong Motion Instrumentation Network" in collaboration with IITR under its mission mode programme. In February, 2004, under this program about 300 state-of-the-art digital strong-motion accelerographs were planned out to be installed in north and north-eastern India to record earthquake activities in seismic zones V and IV and in some heavily populated cities in seismic zone III. This strong-motion instrumentation network of IITR installed 293 strong-motion stations covering the Indian Himalayan range from Jammu and Kashmir to Meghalaya. Average station-to-station distance is approximately kept at between 40 to 50 km which, ensure triggering of at least two or more accelerographs (trigger level of 5 gals) if a magnitude of 5 or larger earthquake occurs anywhere in north and north-eastern India. Until today this network has recorded approximately 250 earthquakes occurring in this region. All installed strong-motion accelerographs consist of internal AC-63 GeoSIGtriaxial force-balance accelerometer and GSR-18 GeoSIG-18 bit digitizer with external GPS. The recording for all instruments is in trigger mode at a sampling frequency of 200 samples per seconds. The triggering threshold was initially set at 0.005 g for all the instruments, which was subsequently reduced to 0.002 g and in some cases even 0.001g depending upon noise level around installation site. All the processed accelerograms of this strong motion instrumentation network of IITR available on strong-motion data bank PESMOS (URL: http\:www.pesmos.in).

5.3 JAPAN STRONG MOTION DATABASE

Kyoshin Net (K-NET) database of Japan provides one of the most extensive enrich features of strong ground motion records. Kyoshin Net is a dense strong-motion networking consisting of approximately 1,035 observatories deployed all over Japan at free-field sites with average station to station distance was about 20 km. All these observatories have same type of strong

motion accelerometers i.e. KNET95 type, which are installed on free ground surface in order to have a systematic uniform recording condition. KNET95 type, are three components digital strong-motion accelerograph having a maximum measurable acceleration of 2000 Gals with a wide frequency-band and wide dynamic range. A map of Japan with all the K-NET station locations is presented in Fig. 5.1.

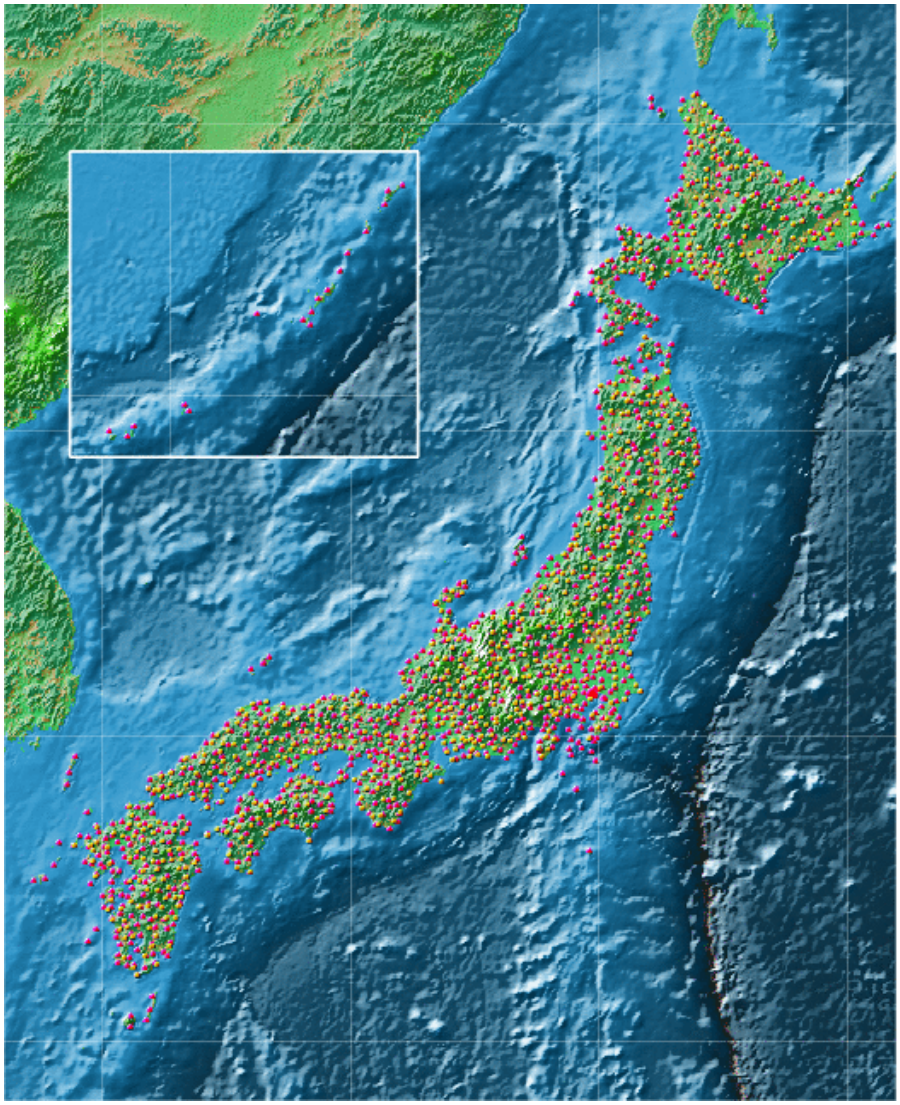

Figure 5.1: Locations of strong motion stations operated by K-NET in Japan (After [http://www.k-net.bosai.go.jp]).

The records obtained from these instruments are acquired at a control centre in Tsukuba by telemetry. Soil profile, including P and S-waves velocity structures, at each recording site are available and has been obtained by down-hole measurement. The control centre makes three

kinds of data files (UNIX, DOS, and ASCII) with a common header including the source parameters determined by the Japan Meteorological Agency (JMA) for each event. The control centre sends one of the three files on the Internet according to the user's request. Also, the control centre maintains a database of strong-motion records and site information which the user can access for scientific studies and engineering applications.

5.3.1 Strong Motion Data Procured

In present study, a total of 225978 time histories (only horizontal components i.e. EW and NS signifying east-west and north-south component of ground motion respectively) from 3571 earthquakes recorded at different observatories in Japan having magnitude of 4 and above and source depth less than 200 Km have been downloaded from the internet. All K-NET strong motion data can be easily downloadable by registration through their Web-site (http://www.k-net.bosai.go.jp). Fig. 5.2 shows a typical strong-motion data recorded (either EW or NS component) format of K-NET.

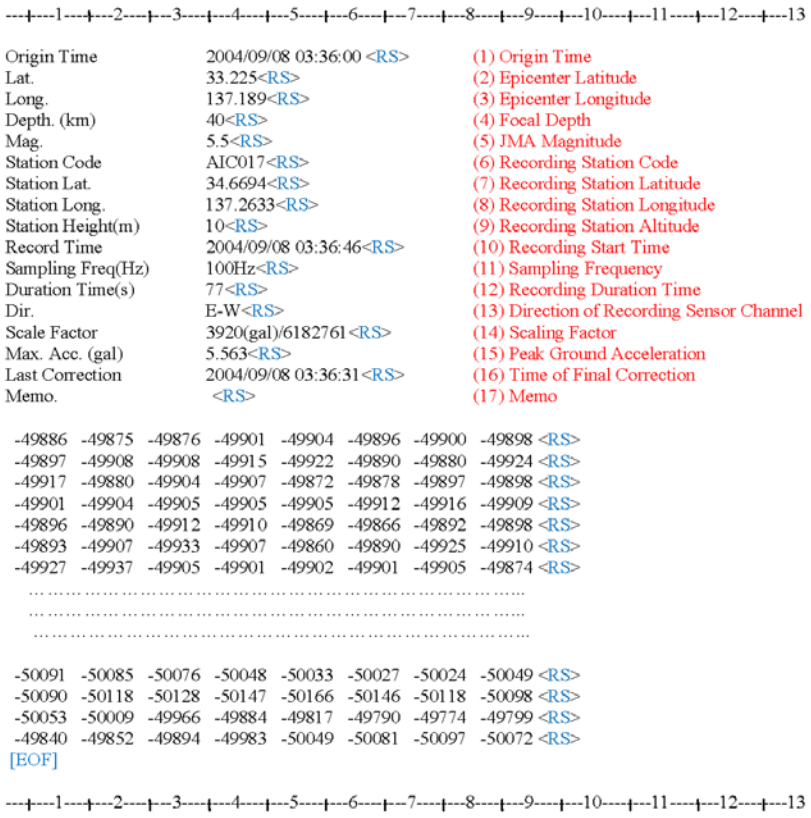

Figure 5.2: Typical data format of K-NET, Japan recorded at Tahara station (After [http://www.k-net.bosai.go.jp]).

5.3.2 Earthquake Magnitude Scale Used by K-NET

Magnitude scale used by K-NET in Japan is M_{JMA}, estimated by the Japan Meteorological Agency (JMA) and it value is mentioned in line no. 5 of Fig.5.2. Katsumata (1996) found that for earthquake magnitude laying in range of 5-7.5, the average difference between M_{JMA} and moment magnitude (M_w) is not significant. Fig.5.3 shows the relationship between moment magnitude and various other magnitude scales.

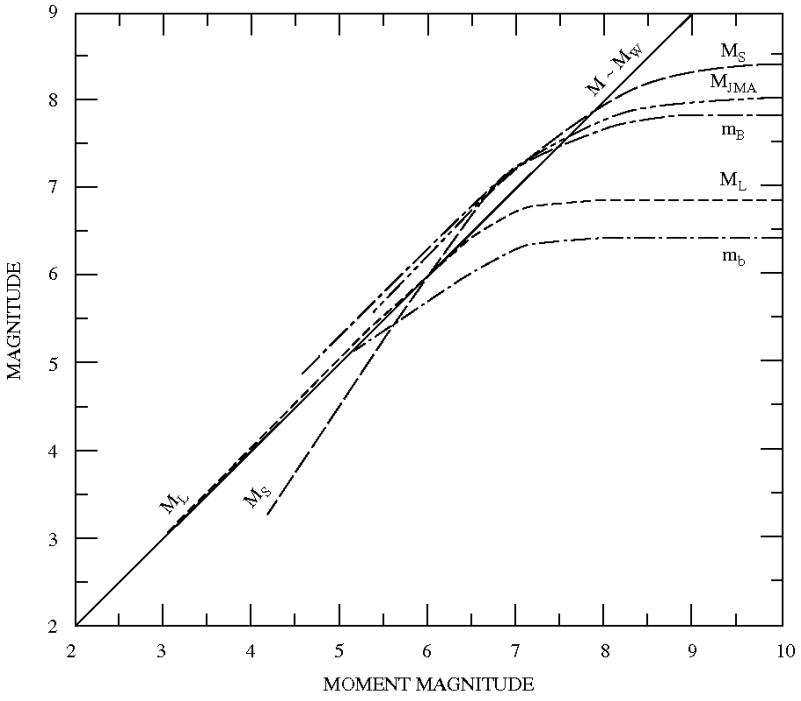

Figure 5.3: Relationship between moment magnitude and various magnitude scales: Mw (moment magnitude); MS (surface-wave magnitude); ML (local magnitude); MJMA (Japan Meteorological Agency magnitude); mb (short-period body-wave magnitude); mB (long-period body-wave magnitude). (After Campbell, 1985).

5.3.3 Soil Condition Data at Strong Motion Stations

Soil profile in term of Standard Penetration Test blow count value, density of soil, including P and S wave velocities structure are available for all recording sites, except a few sites where these soil data are not available. A typical soil data profile at one of the stations is presented in Fig. 5.4. The variation of soil profile along the depth at Tahara station, Japan is shown in Fig. 5.5.

Depth (m)	N – Value	Velocity (m/s)		Density (gm/cm^3)	Soil Column
		P	S		
1m	23	400	220	1.90	0.00 m – 0.70 m F1
2m	25	400	220	1.91	0.70 m – 1.30 m C
3m	15	590	290	1.86	1.30 m – 2.25 m GF
4m	18	590	290	1.83	2.25 m – 7.80 m S
5m	28	590	290	1.83	7.80 m – 8.60 m SF
6m	25	590	290	1.76	8.60 m – 9.30 m C
7m	21	590	290	1.82	9.30 m – 9.90 m SF
8m	5	590	290	1.77	9.90 m – 12.55 m S
9m	23	1160	250	1.71	12.55 m – 14.70 m SF
10m	16	1490	300	1.93	14.70 m – 20.00 m S
11m	17	1490	300	1.89	
12m	24	1490	300	1.98	
13m	50	1490	300	2.02	
14m	34	1750	420	2.18	
15m	32	1750	420	1.99	
16m	50	1670	400	2.04	
17m	39	1670	400	2.07	
18m	48	1670	400	1.95	
19m	34	1670	400	1.97	
20m	46	1670	400	1.98	

Figure 5.4: Typical Soil profile at Tahara Station, Japan (After [http://www.k-net.bosai.go.jp]).

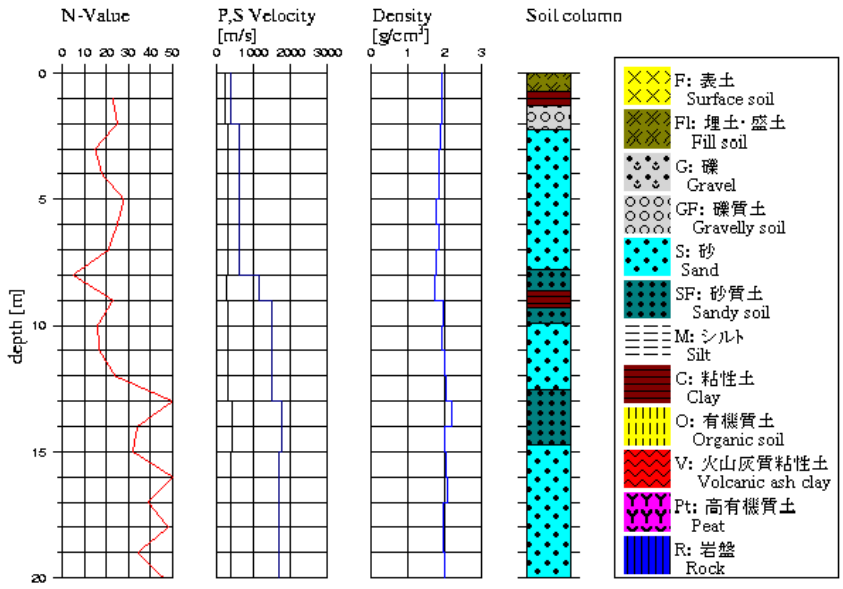

Figure 5.5: Variation of soil conditions at Tahara station, Japan (After [http://www.k-net.bosai.go.jp]).

5.3.4 Processing of Strong Ground Motion Data

All observatories operated by K-NET have K-NET95 accelerometers depicted in Fig. 5.6 and its specification is summarized in Table 5.1.

Table 5.1: Specification of K-NET95 Acceleormeter (After [http://www.k-net.bosai.go.jp]).

Resolution of Accelerometer	15 mGal
Maximum Measurable Acceleration	2000 Gal
Resolution of A/D Converter	18 bit
Dynamic Range	108 dB
Sampling Frequency	100 Hz
Recording Capacity	Approx. 150 minutes with 8 mb flash memory
Communication Port	2 RS-232 C ports
Trigger Level	From 0.1 to 10 Gals

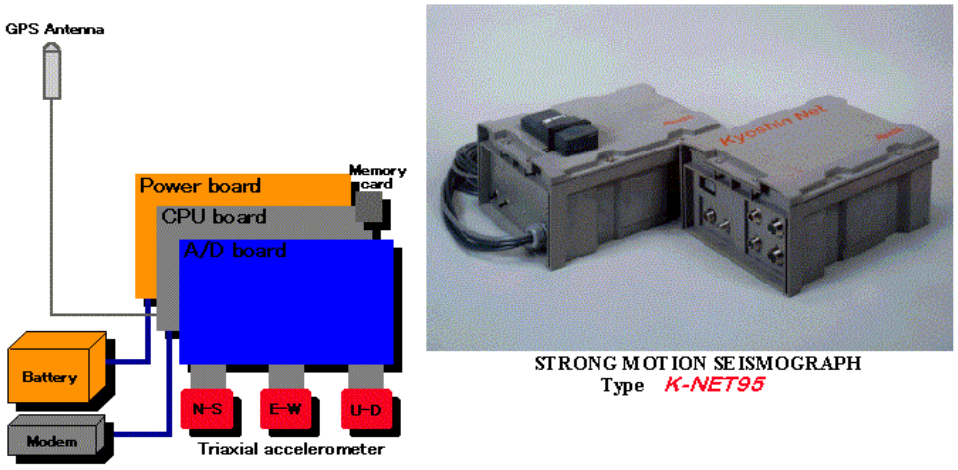

Figure 5.6: Strong-Motion Accelerograph of K-NET95, (After [http://www.k-net.bosai.go.jp]).

All the **225978** horizontal components of earthquake records were viewed manually by plotting the acceleration time history on the screen of the PC, and it was observed that in some of the time histories, two or more events had taken place. Fig. 5.7 shows the E-W Component of the 1999 earthquake of magnitude 5.1 (Origin Time: 1999/02/26 15:18:00) recorded at Honjoh station in Japan, where two events were recorded. In such case only first event was considered

and second event was chopped out by altering it duration time as referred in line no. 12 of Fig.5.2. Some of the time histories based on their shape, frequency content appearance and duration as expected from magnitude and distance combination does not look like an earthquake and have been completely removed. Time histories for which no soil data are available are also removed. After removing all such records from database **218058** horizontal components were used for further processing.

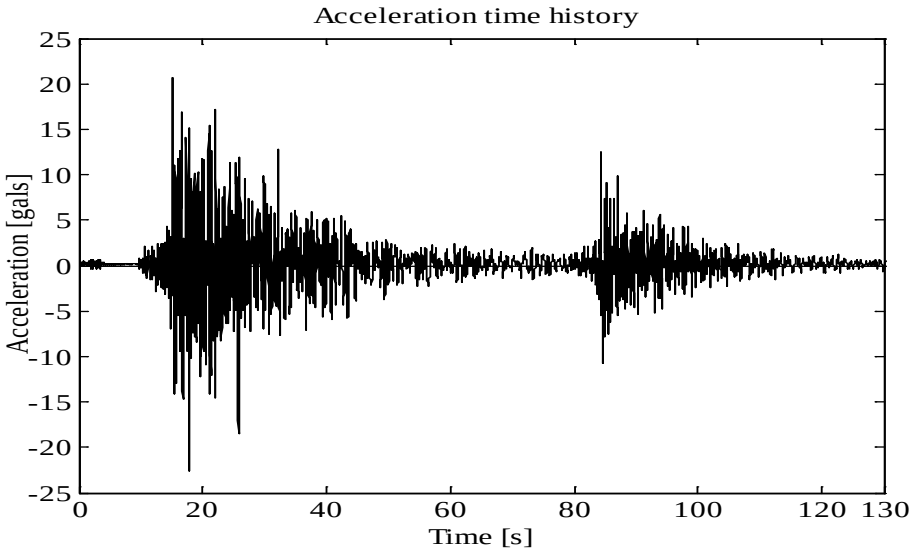

Figure 5.7: Record showing two events recorded at Honjoh station in Japan during the 1999 earthquake of magnitude 5.1 (After [http://www.k-net.bosai.go.jp]).

For processing the strong motion data, various computer programs were developed in FORTRAN to carry out various jobs including sorting, compiling, formatting, filtering, and other time series analyses. All records which have hypo-central distance more than 200 were dropped. As a first step, the raw data available in terms of counts in the data format of K-NET (over 18th line, Fig. 5.2) were converted into acceleration using the scale factor given in the header of data at line no. 14 of Fig. 5.2 and absolute peak value of acceleration was calculated for both components (EW and NS) of each record and finally the geometric mean of their peak acceleration was considered, if geometric mean was less than 5 (cm/sec^2), then record was also dropped.

As natural frequencies of all accelerographs were very high (about 200 Hz), there was no need of instrument response correction. A typical response characteristics curve of a K-NET95 accelerometer is shown in Fig. 5.8. A baseline correction of all acceleration time histories has

been performed using the least square line of the time history. Corrections have also been applied in frequency domain by filtering high and low frequency components of the accelerograms. All accelerograms were band-pass filtered by removing frequencies below 0.1 Hz and frequencies above 30 Hz. A sixth order Butterworth band pass filter was used for the above filtering operation. After complete processing of strong motion database, a total **37046** horizontal components were obtained from 218058 horizontal components.

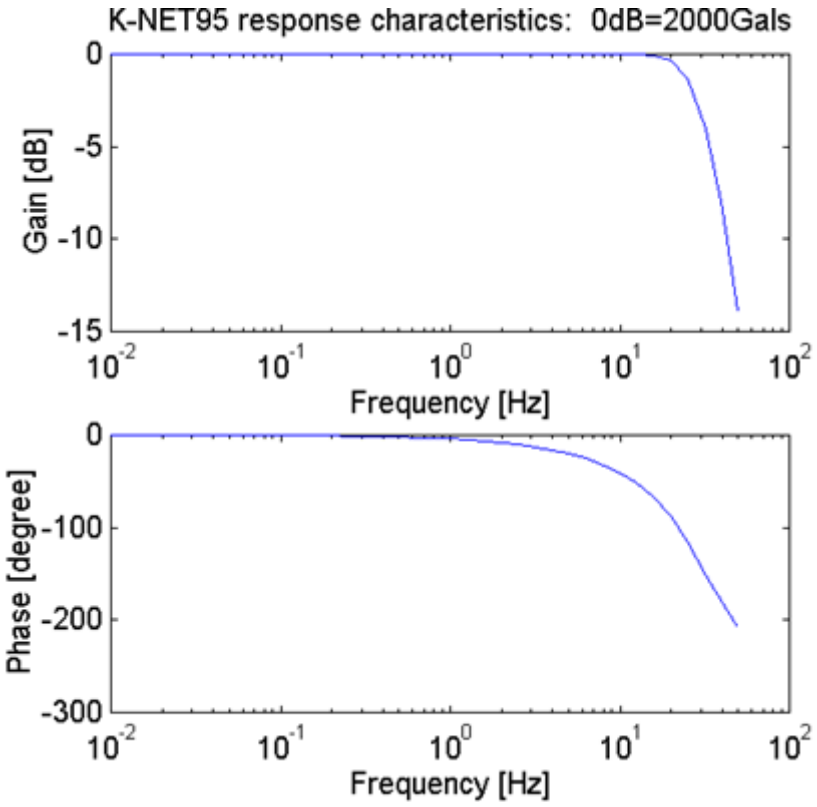

Figure 5.8: Response characteristic curves of K-NET 95 accelerograph, (After [http://www.k-net.bosai.go.jp]).

5.4 CALCULATION OF VARIOUS PARAMETERS

5.4.1 Hypo-central Distance

The basic parameter used in the study is hypo-central distance. The shortest distance (i.e. epi-central distance) over the earth's surface between the site latitude-longitude and the epi-centre latitude-longitude is calculated using the Haversine formula (http://www.movable-type.co.uk/scripts/latlong.html) as given below:

$$D_{epi} = R \times C \tag{5.1}$$

$$C = 2 \times \text{atan2}\left(\sqrt{a}, \sqrt{1-a}\right) \tag{5.2}$$

$$a = \sin^2\left(\frac{\Delta \text{ lat}}{2}\right) + \cos(\text{lat}_1) \times \cos(\text{lat}_2) \times \sin^2\left(\frac{\Delta \text{ long}}{2}\right) \tag{5.3}$$

$$\Delta \text{ lat} = \text{lat}_1 - \text{lat}_2 \text{ and } \Delta \text{ long} = \text{long}_1 - \text{long}_2 \tag{5.4}$$

Where, D_{epi} = Epi-central distance (in km); R = earth's radius i.e. mean radius = 6,371 km); (lat_1, long1) and (lat_2, $long_2$) are coordinates of any two points on earth surface. The shortest possible distance over's the earth surface is used to compute the hypo-central distance as follows:

$$D_{hpy} = \sqrt{\left(D_{epi}\right)^2 + (FD)^2} \tag{5.5}$$

Where, FD = Focal depth in km (as referred in line no. 4 of Fig.5.2.).

5.4.2 Peak Ground Acceleration

In present study resultant peak ground acceleration was considered, which had been obtained by taking geometric mean of largest peak acceleration obtained for horizontal components i.e. east west component (EW) and north south component (NS).

5.4.3 Arias Intensity

In present study Arias intensity had been computed using Eqn. 3.4 as discussed in chapter 3, and resultant arias intensity had been obtained by taking arithmetic mean of arias intensity obtained for horizontal components i.e. east west component (EW) and north south component (NS).

5.4.4 Duration

In present study duration had been defined using Husid Plot concept discussed previously in chapter 3, and obtained by taking arithmetic mean of duration obtained for horizontal components i.e. east west component (EW) and north south component (NS).

5.4.5 Type of Faulting

To assign the type of faulting to these earthquakes, the source mechanism of earthquakes from http://www.fnet.bosai.go.jp have been taken and then matched these earthquake records by comparing their origin-time, latitude-longitude and magnitude with earthquake records taken from http://www.fnet.bosai.go.jp and assumed that the earthquake taken from http://www.fnet.bosai.go.jp is same as taken from http://www.k-net.bosai.go.jp if their origin time match with $\pm$ 1 in mins, latitude and longitude $\pm$ 0.3 degree and magnitude $\pm$ 0.2. Once the matching of earthquake records were completed, then classified these records into three types of faulting i.e. normal, reverse, strike slip with help of Japan tectonic map and focal mechanism parameter like Strike, dip, rake. The numeral value assign to each type of fault i.e. 1 for Normal fault type, 2 for Reverse fault type and 3 for Strike slip fault type respectively.

5.4.6 Average Values of Soil Parameters

In present study, the average values of shear wave velocity, primary wave velocity, Standard Penetration Test (SPT) blow count, and the density of soil had been used. The averaging of these parameters had been done as per FEMA 356, 2000. These values were calculated as

$$\overline{V}_s, \overline{V_p}, \overline{N} = \frac{\sum_{i=1}^{i=n} d_i}{\sum_{i=1}^{i=n} \frac{d_i}{V_{si}}, \frac{d_i}{V_{pi}}, \frac{d_i}{N_i}} \tag{5.6}$$

Where, V_{si} = Shear wave velocity of i^{th} layer; V_{pi} = Primary wave velocity of i^{th} layer; N_i = SPT blow count of the i^{th} layer; d_i = Depth of the i^{th} layer; n = Number of layers of similar soil materials for which data is available. Average density was calculated by taking average of density of each layer. From Fig. 5.4 observation, soil profile is available up to 20 m depth, but commonly average shear wave velocity for 30 m was used in GMPE's, so in order to maintain

uniformity with GMPE's, the value of all parameters mentioned corresponding to last row in Fig 5.4 is extended up to 30 m by assuming the same values.

5.4.7 Spectral ordinate

The response acceleration spectra for 5% damping were estimated using Eqn. 3.3 for both horizontal component at various periods, and then normalized to peak ground acceleration of records. Finally total 15 response spectral ordinate at the time period ranging from 0.03 sec to 4 sec were calculated using geometric mean of both component. Table 5.2 shows the fifteen points of normalized response spectrum selected at discrete time periods ranging from 0.03 to 5.0 seconds.

Table 5.2: Fifteen Time Periods Selected for Response Spectral Ordinates.

Time Period (Sec)	Response Spectral Ordinates	Time Period (Sec)	Response Spectral Ordinates	Time Period (Sec)	Response Spectral Ordinates
0.03	$(S_a/g)_1$	0.3	$(S_a/g)_6$	1.0	$(S_a/g)_{11}$
0.05	$(S_a/g)_2$	0.5	$(S_a/g)_7$	1.25	$(S_a/g)_{12}$
0.07	$(S_a/g)_3$	0.55	$(S_a/g)_8$	2.0	$(S_a/g)_{13}$
0.1	$(S_a/g)_4$	0.67	$(S_a/g)_9$	3.0	$(S_a/g)_{14}$
0.2	$(S_a/g)_5$	0.75	$(S_a/g)_{10}$	4.0	$(S_a/g)_{15}$

5.4.7.1 Influence of Soil Condition on Normalized Response Spectra

A total of **37046** averaged horizontal components of earthquake records were obtained from 2 18058 horizontal components. The 37046 averaged horizontal components of earthquake records were divided into four classes based on the average shear wave velocity i.e. ($\overline{V}_s$) estimation as follow:

1. **Class A:** Hard rock or rock with $\overline{V}_s > 750$ m/s (500 averaged horizontal time histories).
2. **Class B:** Very dense soil or soft rock with 750 m/s $\geq \overline{V}_s > 360$m/s (11,377 averaged horizontal time histories).
3. **Class C:** Stiff soil with 360 m/s $\geq \overline{V}_s > 180$ m/s (21,326 averaged horizontal time histories).
4. **Class D:** Any soil profile with $\overline{V}_s \leq 180$ m/s (3,843 averaged horizontal time histories).

The average and the mean plus one standard deviation (84.1 percentile) normalized acceleration spectra for the different class sites are presented in Fig. 5.9 and 5.10 respectively. From the Fig 5.9 and 5.10, it is clearly demonstrated that soil conditions affect the spectra to a significant degree. The figures show that for period greater than 0.2 sec, the normalized spectral ordinates (amplifications) for hard rock and rock are substantially lower than those for other soil conditions. Fig. 5.11 shows soil classification (namely A, B, C and D) for each site of K-NET location.

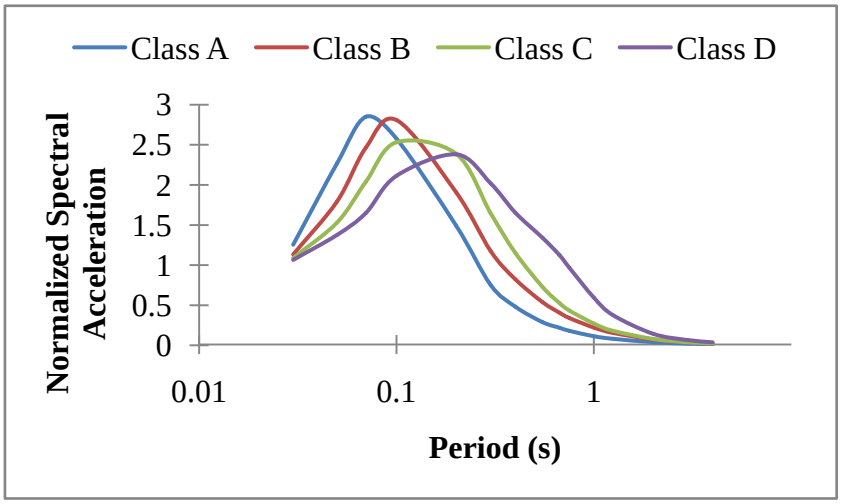

Figure 5.9: Normalized average acceleration spectra for 5 % damping for different soil conditions.

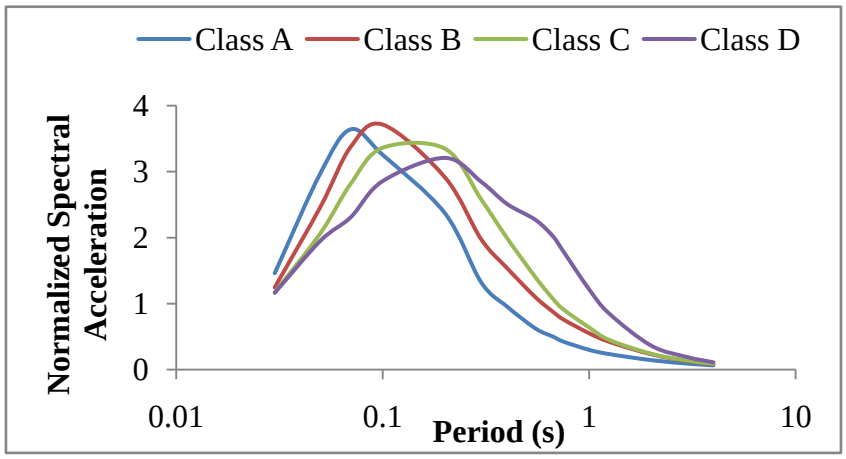

Figure 5.10: Mean plus one standard deviation normalized acceleration spectra for 5 % damping for different soil conditions.

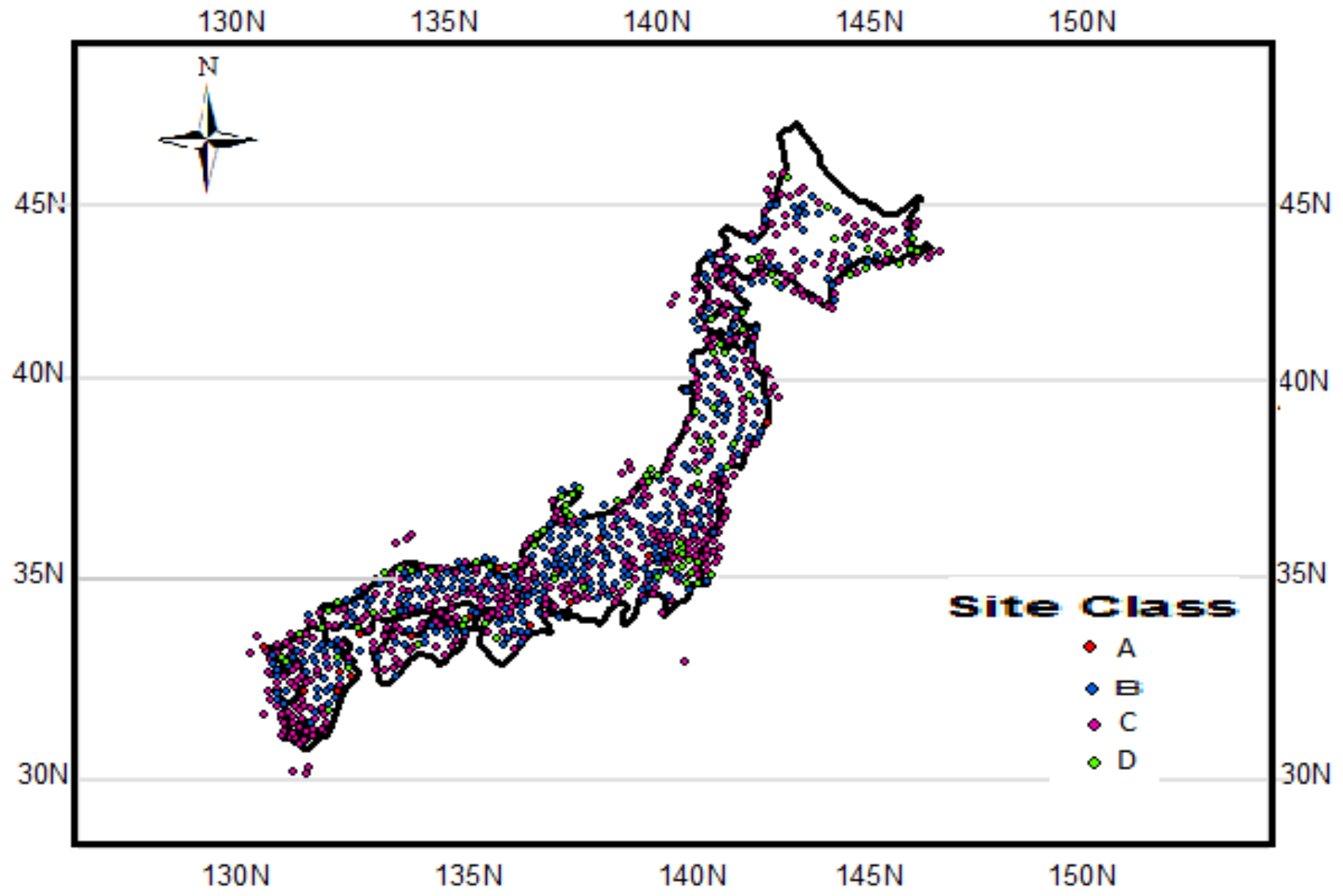

Figure 5.11: Shows soil classification namely (A, B, C and D) for each site of K-NET location.

5.4.7.2 Classification of Earthquake Records Based on IS 1893 (Part1): 2002

The 37,046 averaged horizontal components of earthquakes records were further classified on the basis of Standard Penetration Test (SPT) blow count ($\bar{N}$) as per IS 1893 (Part1): 2002 as follow:

1. **Type I Rock or Hard Soil:** Average Standard Penetration value $\bar{N} > 30$ (10689 time histories).
2. **Type II Medium Soil:** Average Standard Penetration value $30 \geq \bar{N} > 10$ (10897 time histories).
3. **Type III Soft Soil:** Average Standard Penetration value $\bar{N} \leq 10$ (9460 time histories).

In present study , a comparison between IS 1893 (Part1): 2002 normalized response spectra and mean plus one standard deviation (84.1 percentile) normalized acceleration spectra for Japanese earthquake records which were classified into three categories as mentioned above have been done and corresponding plots are shown in Fig. 5.12 to 5.17 respectively.

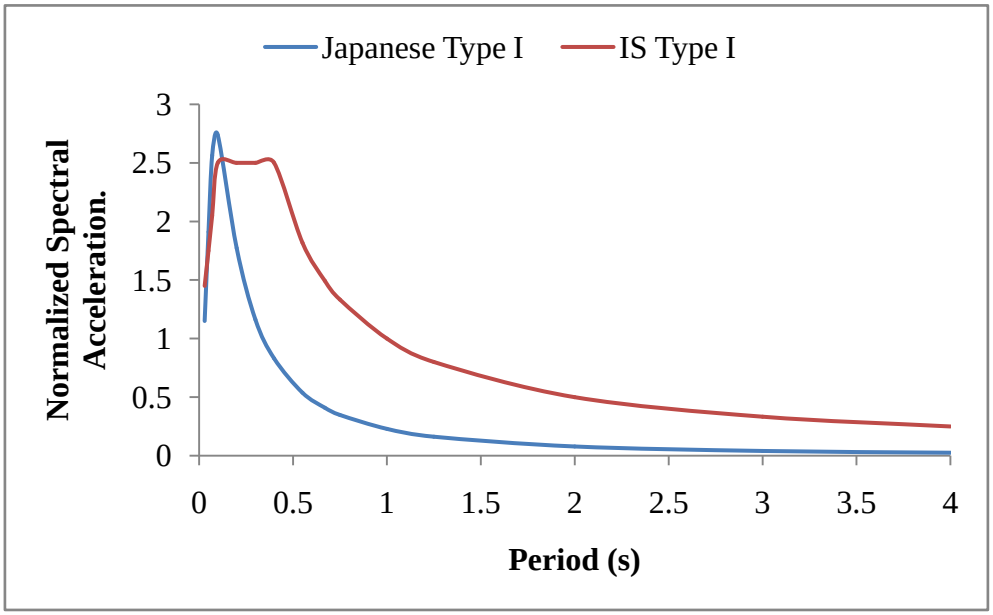

Figure 5.12: Normalized average acceleration spectra for 5 % damping for rock or hard soil condition.

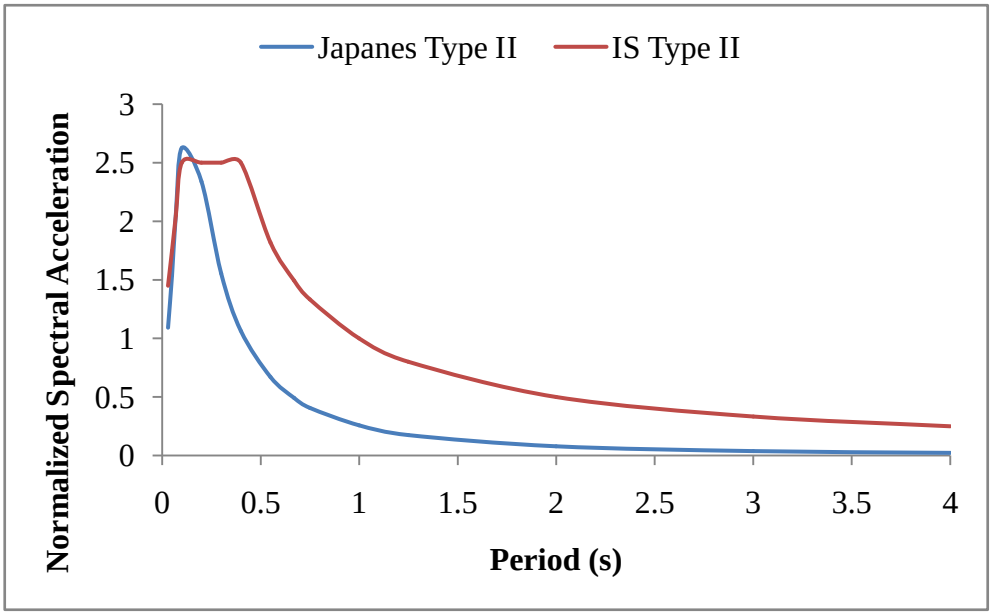

Figure 5.13: Normalized average acceleration spectra for 5 % damping for medium soil condition.

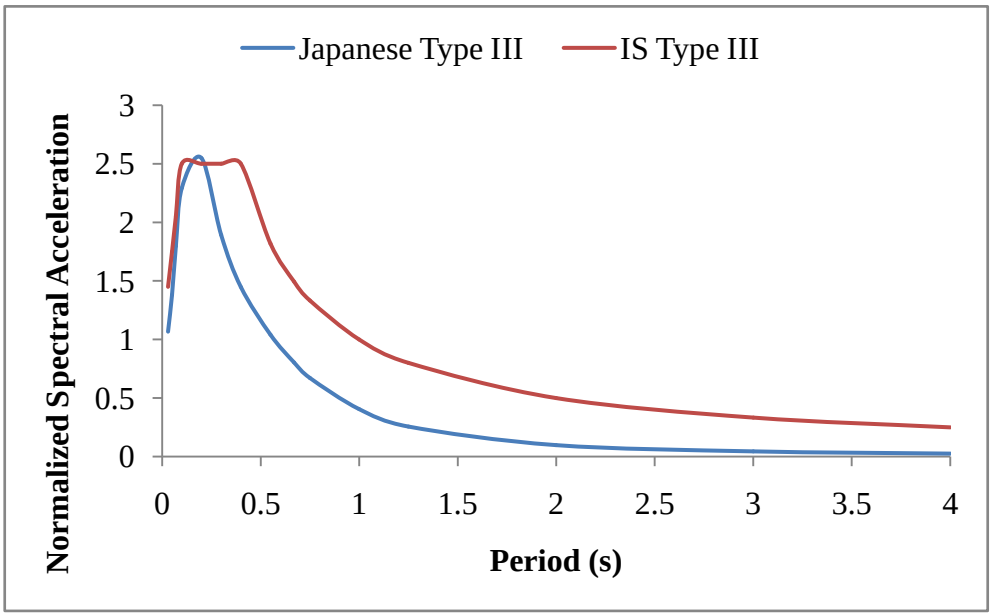

Figure 5.14: Normalized average acceleration spectra for 5 % damping for soft soil condition.

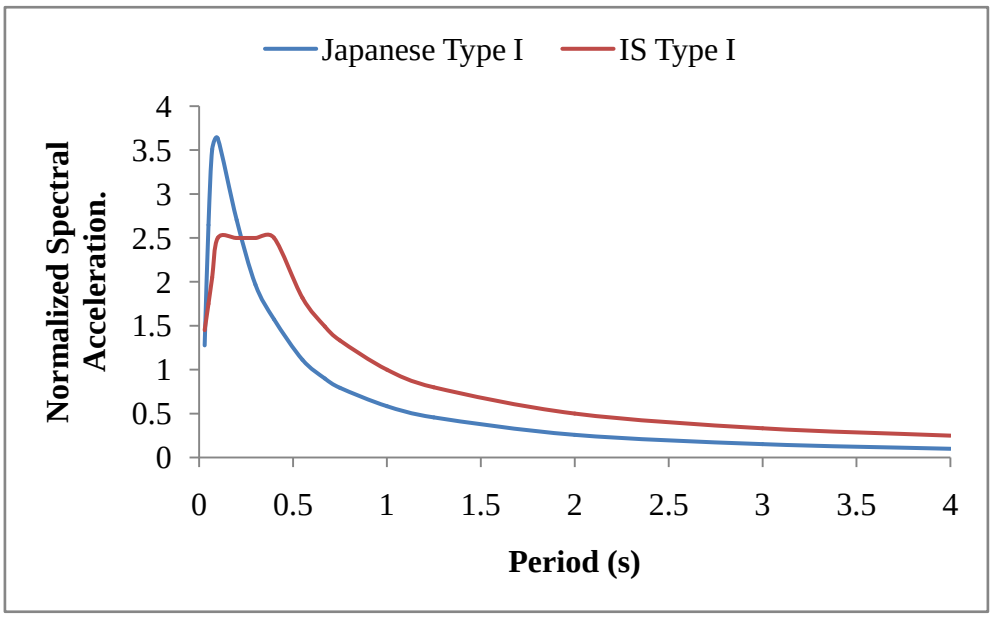

Figure 5.15: Mean plus one standard deviation normalized acceleration spectra for 5 % damping for rock or hard soil condition.

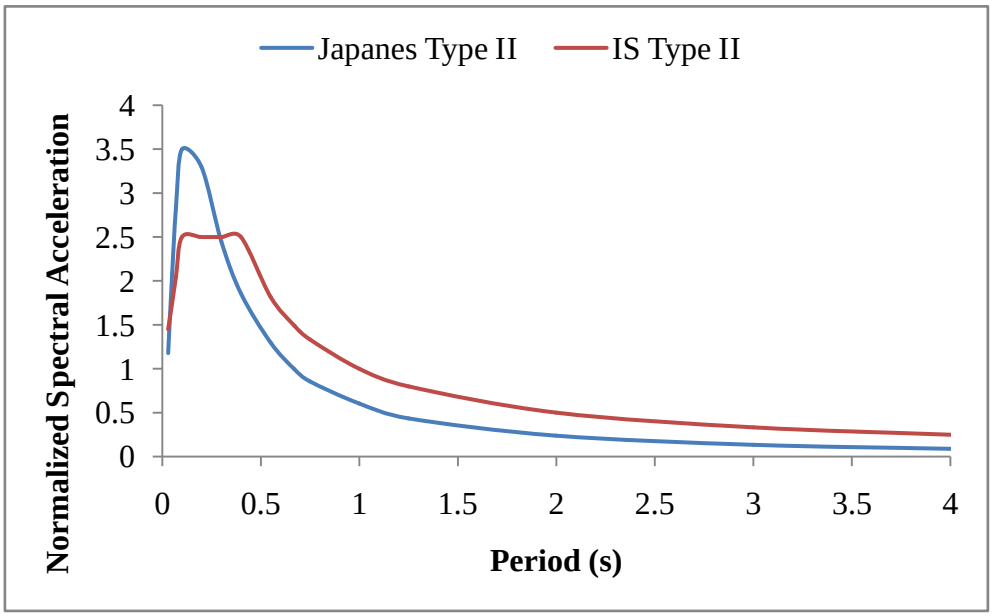

Figure 5.16: Mean plus one standard deviation normalized acceleration spectra for 5 % damping for medium soil condition.

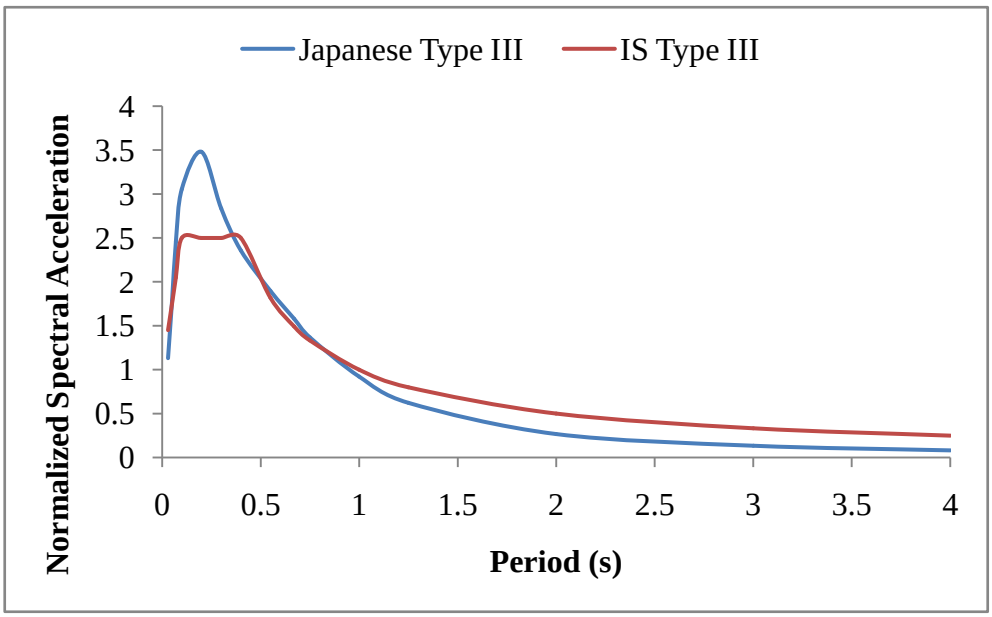

Figure 5.17: Mean plus one standard deviation normalized acceleration spectra for 5 % damping for soft soil condition.

Figs. 5.12 to 5.14 reveal that IS 1893 (Part 1): 2002 response spectra gave conservative results for time periods greater than approximately 0.4 sec. Figs. 5.15 to 5.17 show mean plus one standard deviation response spectra curves of Japanese records along with IS code spectra. This comparison show that IS code spectra is under estimated upto 0.25 s for rock, 0.35 s for medium soil and 1.25 s for soft soil.

5.5 SUMMARY

This chapter presents a brief discussion about Indian strong ground motion database and then shift to the compilation and processing of strong motion data from K-NET database of Japan. It also discusses the influence of soil condition on the shape of response spectra. The classification of Japanese earthquake records as per FEMA 356, 2000 as well as IS 1893 (Part 1): 2002 is presented. The chapter concludes with a comparison between the IS 1893 (Part 1): 2002 response spectra and the average and the mean plus one standard deviation spectra for the Japanese earthquake records.

Chapter 6

ESTIMATION OF SGM USING ANN

6.1 INTRODUCTION

The complex behaviour of earthquake source, attenuating media, instrumental recording, local site effects and above all the paucity of data implicitly made it necessary to use Artificial Intelligence to predict the SGM for future cases. The peak ground acceleration has been considered as a parameter representing the severity of shaking at a site. Researchers in the past have proposed attenuation relationships for peak ground acceleration. The majority of attenuation relationships for predicting peak ground acceleration are presented in terms of earthquake magnitude. A set of accelerograms is generally used to estimate the peak ground acceleration in terms of 1) distance in km between source to site, 2) the moment magnitude, 3) the average shear wave velocity and 4) the fault mechanism. Further, the duration of strong ground motion, another important parameter, can have a significant influence on earthquake damage. Correlations of the duration of strong motion with epi-central distance have been studied by Trifunac and Brady (1975). As discussed in previous chapter 3, several definitions have been proposed for the strong motion duration of an accelerogram. In present study, the definition proposed by Trifunac and Brady (1975) is used to compute the duration of strong ground motion. The duration of strong motion (t_D) is defined as the time interval in which 90 % of the total contribution of the acceleration intensity ($\int a^2 dt$) takes place. The time interval selected between the 5 % and the 95 % contributions is considered as the duration of strong motion.

In this study, an attempt has been made to predict peak ground acceleration and duration by implementing Multilayer Perceptron neural network with back-propagation learning scheme using Japanese earthquake records. A geometric mean of the two horizontal components has been considered for the computation of Peak Ground Acceleration and arithmetic mean for duration of strong motion. This chapter deals the problem of generating the peak ground acceleration and the duration of strong motion using ANN. The effectiveness of neural networks for generating the PGA and the duration of strong motion has been studied.

ANN models are proposed for generating the peak ground acceleration and the duration of

strong motion of an accelerograms using the basic information such as source parameters: magnitude, focal mechanism; path effect: hypo-central distance; and site-effect: soil conditions in term of its density, average SPT blow count, average shear wave and P-wave velocity. The standard back-propagation algorithm has been used for training of ANNs.

6.2 DEVELOPMENT OF ANN MODEL

The basis of prediction of strong ground motion is described in Chapter 2 where the dependent and independent parameters have been described in details. Lot of efforts have been made in last few decades to predict SGM using GMPEs in which the dependent and independent parameters have been worked out thoroughly. The characteristics of SGM have been described in Chapter 3. In the present case the dependent parameter has been taken as the PGA and the duration. The independent parameters considered in the present study consists of magnitude, distance, focal mechanism and local site effects. The predictions of Peak Ground Acceleration (PGA) and Duration of strong ground motion (t_D) using ANN for each respective site namely A, B and C have been taken up for study. For prediction of PGA and Duration entire work has been carried out in three stages as described in the following sections. In first stage 7 input based ANN model, in 2^{nd} stage 4 input based ANN model and in last stage 3 input based ANN model has been developed. As discussed in chapter 5, after filtered out the data on the basis of PGA and hypo-central distance we have left with 37046 averaged horizontal component of earthquake records, this numbers were too large for training the neural networks, and finally a limit on focal depth was imposed and the records which have a focal depth of 35 km or less were considered. A total of 4471 average horizontal components of earthquake records were obtained from 37046 components which were having a focal depth of 35 km or less. These 4471 average horizontal components of earthquake records were further classified on the basis of average shear wave velocity in respective site classes namely A, B, C.

For development of ANN model a large numbers of neural network simulator platforms are available, some of them mentioned as Wolfram mathematical neural network (ver. 1.1.1), Stuttgart neural network simulator (ver. 4.3), NeuroSolution (ver. 6.02), OpenNN (ver. 1.0), NeuronC (ver. 6.44), Neural Designer (ver. 1.0), NetMaker (ver 0.9.5.5), Matlab neural network toolbox (ver. 6.04), NeuroIntelligence (ver. 2.2) and many more. In our entire thesis work Alyuda NeuroIntelligence software version 2.2 (677) developed by Alyuda Research, Inc. has been used for development of ANN models.

6.2.1 Forming Inputs and Output

To develop an ANN model, three different sets of inputs with seven nodes, four nodes and three nodes in the input layer have been used to made prediction of PGA and t_D for each respective site class and the functional form of model for three different combination of inputs are shown in Fig. 6.1 and also described in Eqn. 6.1 (a), 6.1 (b) and 6.1 (c).

$$PGA \ or \ t_D = f\left(M, D_{hyp}, FM, \overline{V}_{S30}, \overline{N}, \overline{V}_{P30}, \bar{\rho}\right) \quad \textbf{(7 Inputs Form)} \tag{6.1a}$$

$$PGA \ or \ t_D = f\left(M, D_{hyp}, FM, \overline{V}_{S30}\right) \quad \textbf{(4 Inputs Form)} \tag{6.1b}$$

$$PGA \ or \ t_D = f\left(M, D_{hyp}, \overline{V}_{S30}\right) \quad \textbf{(3 Inputs Form)} \tag{6.1c}$$

Where, PGA = Peak ground acceleration; t_D = Duration of strong ground motion; M = Earthquake magnitude; D_{hyp}= Hypo-central distance; FM = Focal mechanism; $\overline{V}_{S30}$ = Average shear wave velocity in top 30m of surface layer; $\overline{N}$ = Average Standard Penetration Test (SPT) blow count; $\overline{V}_{P30}$ = Average P-wave velocity in top 30m of surface layer and $\bar{\rho}$ = Average density of soil.

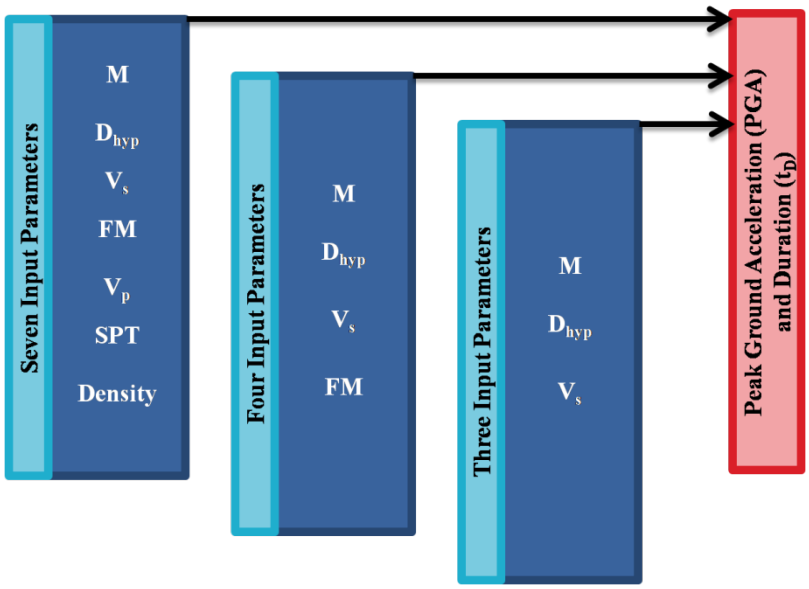

Figure 6.1: Three different combinations of inputs set used for ANN development.

Table 6.1 shows the distributions of dataset in respective site classes namely A, B, and C. The distribution of the dataset w.r.t M, D_{hyp}, PGA and $\overline{V}_{S30}$ is shown in Fig. 6.2(a), 6.2(b) and 6.2 (c) for each respective site class.

Table 6.1: Distribution of dataset for class site A, B, C.

Input Parameters Range				
	Abbreviations used	**Class A**	**Class B**	**Class C**
Earthquake Magnitude	M	4.5-7.4	4.5-7.3	4.5-7.3
Hypo-central distance(in km)	D_{hyp}	21-200	9-200	13-200
Focal mechanism	FM	1 = N fault 2 = R fault 3 = SS fault	1 = N fault 2 = R fault 3 = SS fault	1 = N fault 2 = R fault 3 = SS fault
Average shear wave velocity (m/s)	$\overline{V}_{S30}$	760-1433	362-760	182-360
Average SPT blow count	$\overline{N}$	7-99	6-99	3-93
Average P-wave velocity (m/s)	$\overline{V}_{P30}$	1616-3097	631-2848	434-2211
Density of soil (g/cm^3)	$(\overline{\rho})$	1.967-2.406	1.304-2.630	1.141-2.669
Output parameters Range				
Peak ground aceleration (cm/s^2)	PGA	6.06-211.29	6-709.32	6-886.81
Duration of strong ground motion (s)	t_d	0.766-38.06	2.61-78.44	3.8-121.1

6.2.2 Selecting the Training Pairs

Cross Validation (Stone, 1974) approach as discussed in chapter 4, was used for each class dataset and each dataset was divided into three multiple subsets as: training; validation, and testing set. The training set, which consists of about 68 % of the data set, was used to train the network by adjusting the connection weights and its values; the validation set, consists of 16 % of the data set, and was used for the purpose of monitoring the training process at various stages and to guard against overtraining. The training was stopped when cross validation error begins to increase i.e. the training was stopped when the cross validation errors was reached minimum value. Once the training was over then, the testing set, consists of 16 % of the

remaining data set, and was used to judge the performance of the trained network. The testing set was that part of dataset which were not exposed to ANN during training phase

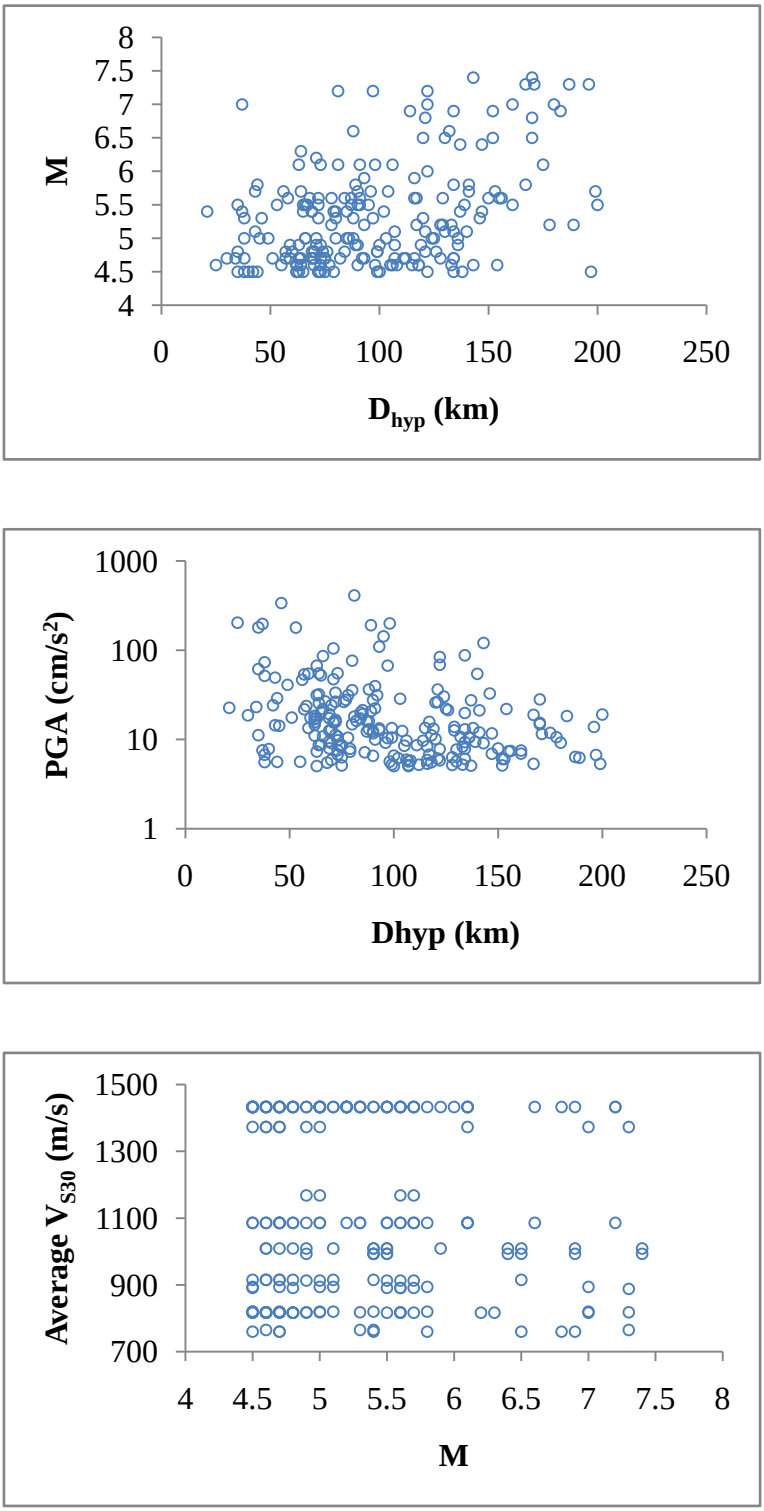

Figure 6.2 (a): Distribution of dataset between M and D_{hyp}, PGA and D_{hyp} , and $\overline{V}_{S30}$ and M for site class A.

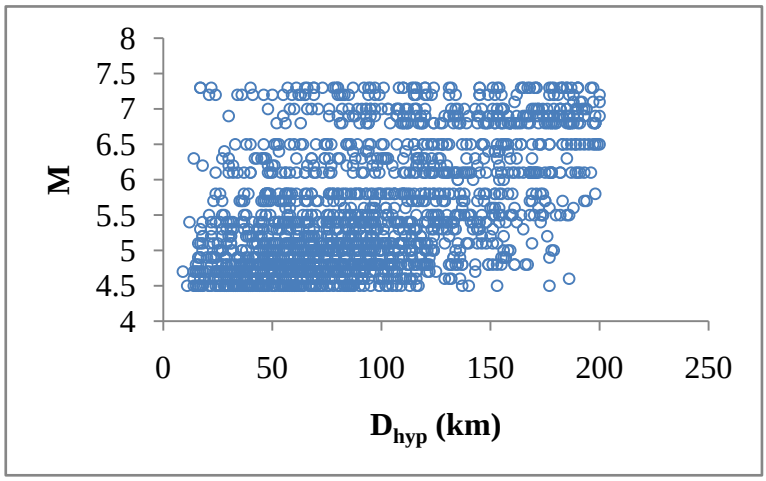

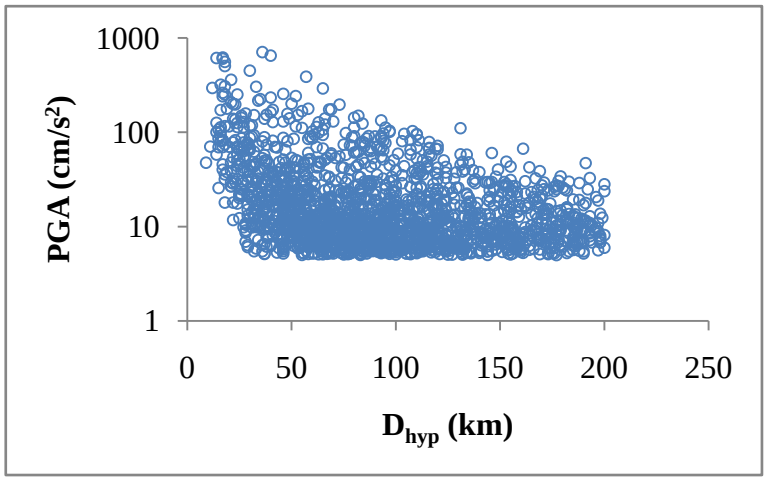

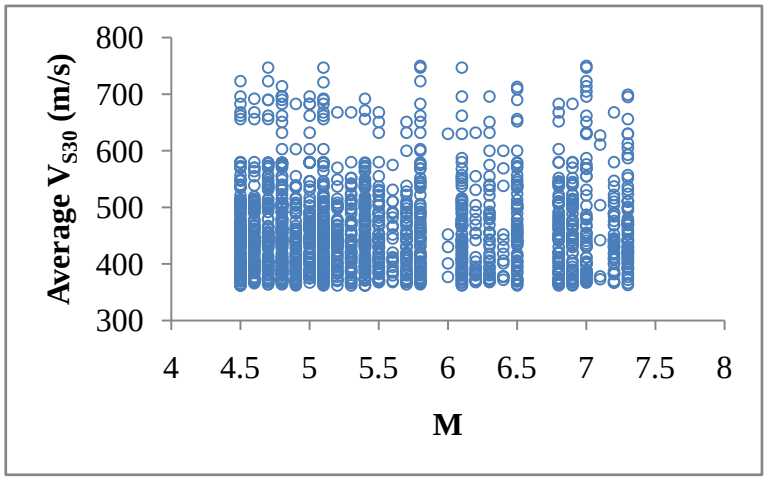

Figure 6.2 (b): Distribution of dataset between M and D_{hyp}, PGA and D_{hyp} , and $\overline{V}_{S30}$ and M for site class B.

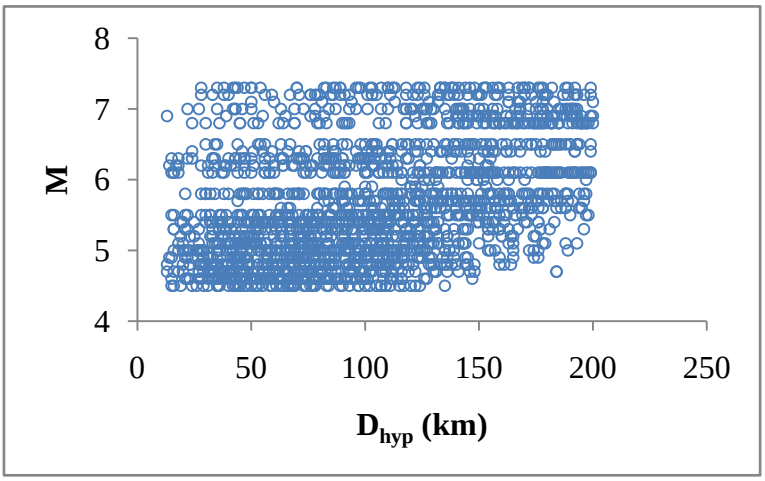

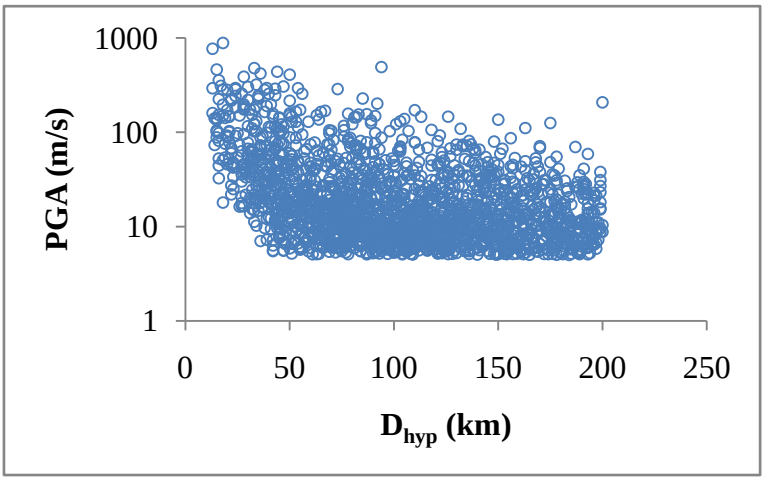

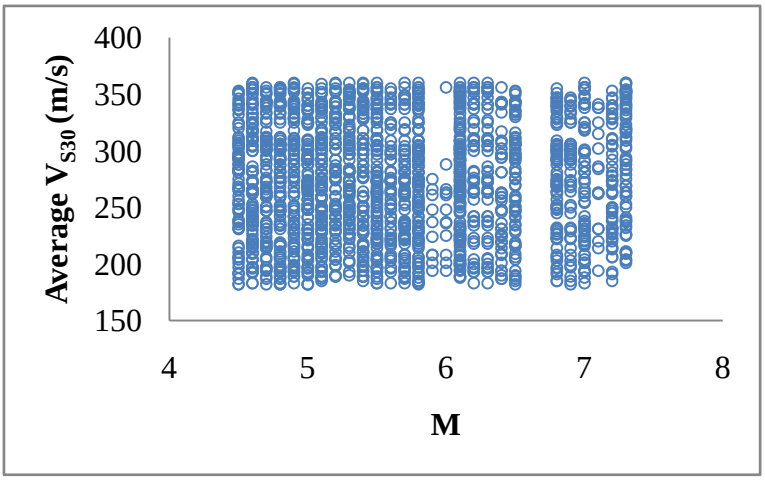

Figure 6.2 (c): Distribution of dataset between M and D_{hyp}, PGA and D_{hyp} , and $\overline{V}_{S30}$ and M for site class C.

6.2.3 Training Phase of ANN

As discussed in chapter 4, the limitation of neural network includes working only with numeric data and has a limited range of operating values. Therefore, entire dataset should be modified before it was fed to a Neural Network. In pre-processing the whole input parameters was converted in the scaling range of -1 to 1 and output parameter was converted in the scaling range of 0 to 1. The conversion of entire data was done using Eqn. 6.2 and 6.3 respectively.

$$SF = \frac{(SR_{max} - SR_{min})}{(X_{max} - X_{min})} \tag{6.2}$$

$$X_p = SR_{min} + (X - X_{min}) * SF \tag{6.3}$$

Where, X = actual numeric value of real data; X_{min}= actual minimum numeric value in data base; X_{max} = actual maximum numeric value in data base; SR_{min} = lower scaling range limit; SR_{max} = upper scale range limit; SF = scaling factor and X_p = pre-processed value. Once the pre-processing of data was finished, next step constitutes the design of ANN architecture by simply providing the required number of hidden layers and nodes in each hidden layer. For this to decide initially an exhaustive search was carried out among a large array of networks with a single and double hidden layer with different number of neurons. From above search, based on correlation coefficient, initially best five performing architectures were chosen. In the second step, the chosen architecture was then trained for higher number of epochs with different momentum and learning rate. In the third step the best performing network in terms of correlation coefficient and network error from the chosen architecture are once again trained for increasing number of epochs, the training was stopped when the validation error was minimum in order to obtain the suitable network model. The correlation coefficients (R) and the network error used to evaluate the accuracy of each model are defined as

$$R = \frac{\sum_{i=1}^{n}(X_i - \overline{X}) - (Y_i - \overline{Y})}{\sqrt{\sum_{i=1}^{n}(X_i - \overline{X})^2 \sum_{i=1}^{n}(Y_i - \overline{Y})^2}} \tag{6.4}$$

Where X_i is observed value at i^{th} record, Y_i is predicted value at i^{th} record, n is total number of data points, $\overline{X}$ and $\overline{Y}$ is the mean of X_i and Y_i respectively. The correlation coefficient (R) is a statistical measure of strength of the relationship between the actual values and network

outputs. The R can range from -1 to +1. The closer R is to 1, the stronger the positive linear relationship, and the closer R is to -1, the stronger the negative linear relationship. When R is near 0 there is no linear relationship. *Network Error (NE)* is a value in terms of *Sum of Squares (SS)*, it is used to rate the quality of the Neural Network training process. The smaller the network's error is, the better the network has been trained. Minimization of the error is the main objective of Neural Network training. *Sum-of-Squares* is the most common error function and is the sum of the squared differences between the actual value (target column value) and Neural Network output.

6.3 ANN BASED PREDICTION OF PGA

6.3.1 Seven Input Based Network

As shown in Fig 6.3, the seven nodes on the input layer for creating the neural network were the earthquake magnitude (M), hypo-central distance (D_{hyp}), focal mechanism (FM), average shear wave velocity ($\overline{V}_{S30}$); average SPT blow count ($\overline{N}$); average shear wave velocity($\overline{V}_{P30}$); and average density of soil ($\overline{\rho}$) and one node on the output layer that was peak ground acceleration (PGA) have been used for prediction of PGA for each site class.

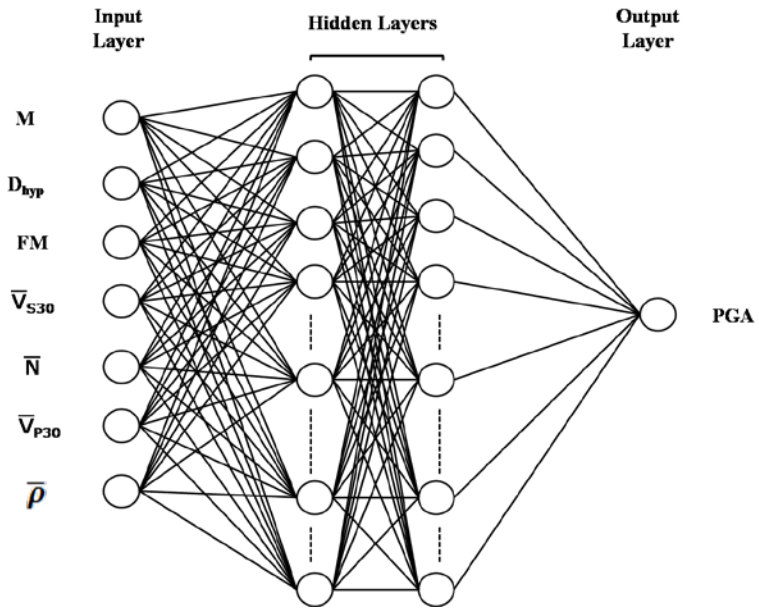

Figure 6.3: Neural network architecture with seven nodes on input layer and one node on output layer.

6.3.1.1 Class A

Class A dataset consist of total 214 averaged horizontal earthquake time histories. A dataset of 178 was selected randomly from the total set of 214 for training and cross validation and the remaining 36 was used to test the performance of the trained network. Three different data sets of 178 were created and randomized. The three data sets were trained independently and the data set, which gave the minimum network error, was considered for testing the network. Finally ANN model with two hidden layer having 40, 36 neurons in each hidden layer respectively, seven input neurons and one output neuron showed the best performance. The trained network results and various parameters used for training are mentioned in Table 6.2 and 6.3 respectively. Fig. 6.4 shows training scatter plot for predicted PGA to target (desired) PGA. Fig. 6.5 shows testing scatter-plot for 36 data points which are used to test the prediction capability of above trained model. The correlation coefficient (R), the root mean square error (RMSE), and the mean absolute error (MAE) as defined by Eqn. 6.4 and 6.5, were used to evaluate the accuracy of model. The result of testing network is defined in terms of R, MAE and RMSE mentioned in Table 6.4. A few test results of seven inputs based network for prediction of PGA are shown in Table 6.5

Table 6.2: Network results for 7-40-36-1 architecture for class A with 7 inputs.

Architecture	Epochs	Correlation	Network Error
7- 40-36-1	10000	0.986	0.000087

Table 6.3: Parameters used for training neural network 7-40-36-1 architecture for class A with 7 inputs.

Description	Hidden Layer	Output Layer
Transfer Function	TanhAxon	SigmoidAxon
Learning Rate	0.08	0.08
Momentum	0.8	0.8

$$\mathrm{RMSE} = \sqrt{\frac{1}{n}\sum_{i=1}^{n}(X_i - Y_i)^2}$$

$$\text{and } \mathrm{MAE} = \frac{1}{n}\sum_{i=1}^{n}|(X_i - Y_i)| \tag{6.5}$$

Table 6.4: R, MAE, and RMSE values of AAN model used in test performance to predict PGA for class A with 7 inputs.

Correlation	MAE	RMSE
0.983	3.86	14.03

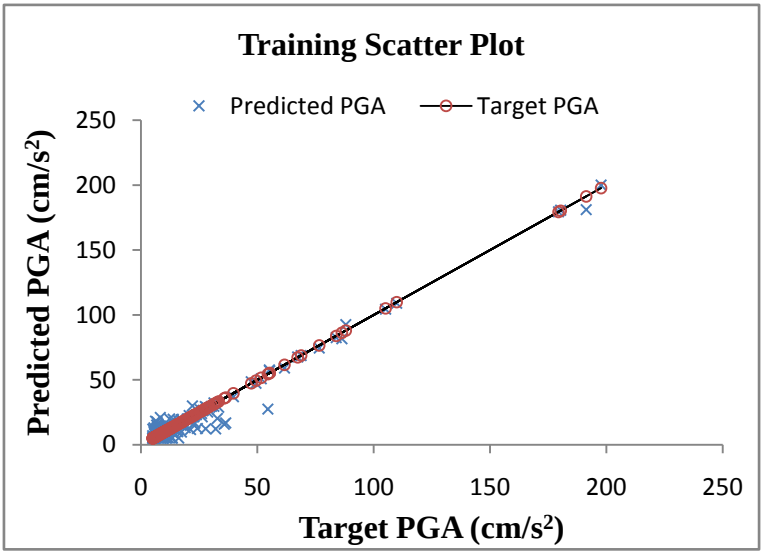

Figure 6.4: Training scatter plot of predicted PGA to target PGA for site class A with 7 inputs.

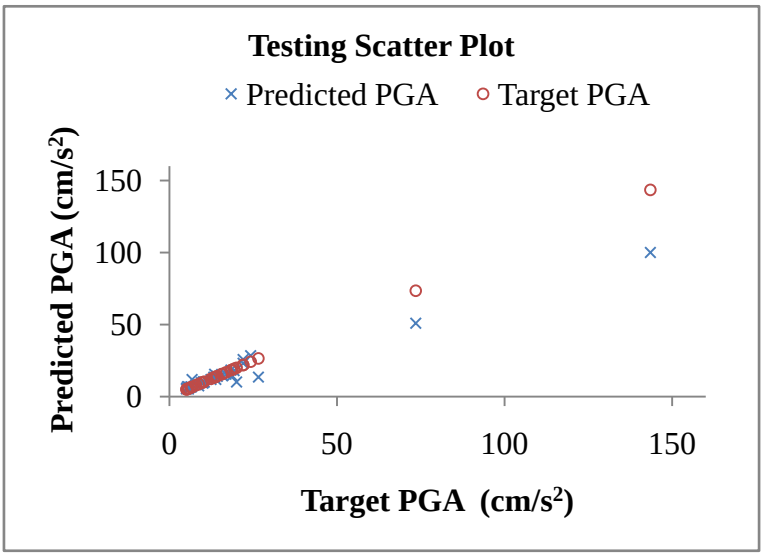

Figure 6.5: Testing scatter plot of predicted PGA to target PGA for site class A with 7 inputs.

Table 6.5: Few test results of 7- input based network (PGA) for class A.

M	D (in Km)	FM	$\overline{V}_s$ (in m/s)	$\overline{N}$	$\overline{V}_p$ (in m/s)	$\overline{\rho}$ (in gm/cm3)	Desired PGA (in cm/s^2)	Network PGA (in cm/s^2)
4.9	107	2	818	62	2006	2.161	6.69	6.27
4.6	90	1	1433	60	3097	2.376	6.68	6.81
6.6	91	3	891	99	2063	2.191	10.02	9.44
7.3	196	3	1373	60	2747	2.234	13.86	12.00
6.6	96	1	1433	60	3097	2.376	143.47	100.06
6	38	1	1433	60	3097	2.376	73.49	60.00
4.6	62	2	1373	60	2747	2.234	16.91	16.67

6.3.1.2 Class B

Class B dataset consist of total 1825 averaged horizontal earthquake time histories. A dataset of 1534 was selected randomly from the total set of 1825 for training and cross validation and the remaining 291 was used to test the performance of the trained network. Three different data sets of 1534 were created and randomized. The three data sets were trained independently and the data set, which gave the minimum network error, was considered for testing the network. Finally ANN model with two hidden layer having 38, 24 neurons in each hidden layer respectively, seven input neurons and one output neuron showed the best performance. The trained network results and various parameters used for training are mentioned in Table 6.6 and 6.7 respectively. Fig. 6.6 shows training scatter plot for predicted PGA to target PGA. Fig. 6.7 shows testing scatter-plot for 291 data points which are used to test the prediction capability of above trained model. The result of testing network is defined in terms of R, MAE and RMSE mentioned in Table 6.8. A few test results of seven inputs based network for prediction of PGA are shown in Table 6.9.

Table 6.6: Network results for 7-38-24-1 architecture for class B with 7 inputs.

Architecture	Epochs	Correlation	Network Error
7- 38-24-1	16000	0.940	0.000260

Table 6.7: Parameters used for training neural network 7-38-24-1 architecture for class B with 7 inputs.

Description	Hidden Layer	Output Layer
Transfer Function	TanhAxon	SigmoidAxon
Learning Rate	0.08	0.08
Momentum	0.8	0.8

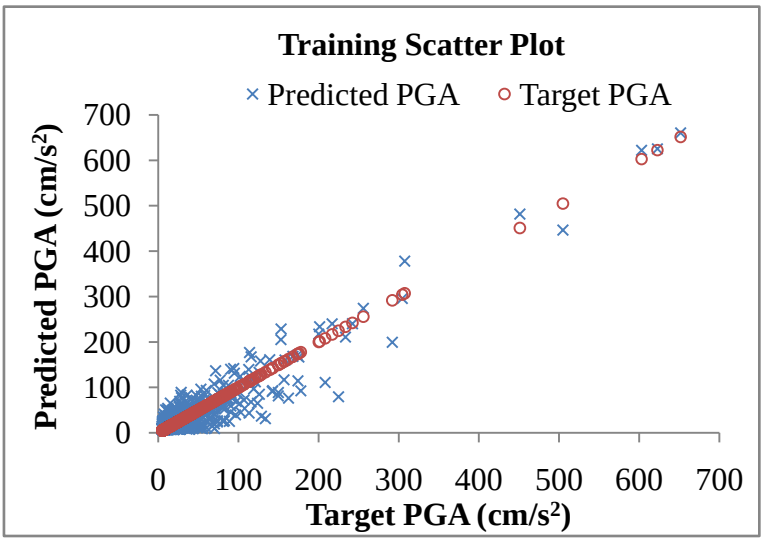

Figure 6.6: Training scatter plot of predicted PGA to target PGA for site class B with 7 inputs.

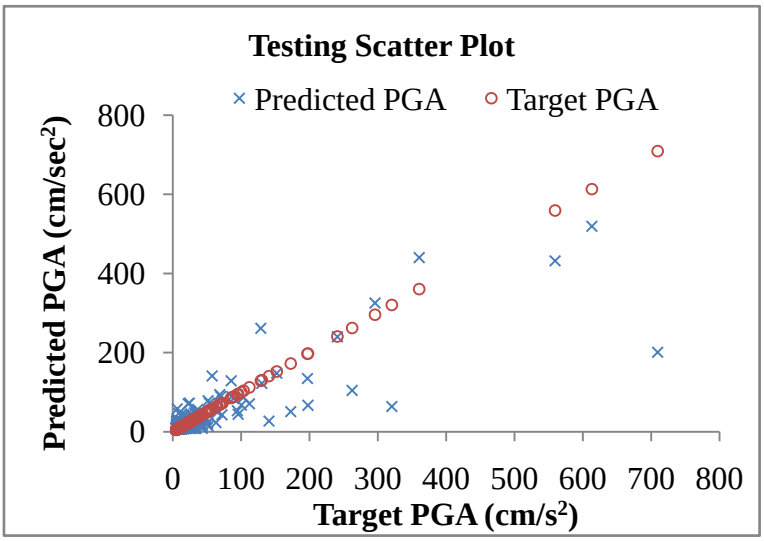

Figure 6.7: Testing scatter plot of predicted PGA to target PGA for site class B with 7 inputs.

Table 6.8: R, MAE, and RMSE values of AAN model used in test performance to predict PGA for class B with 7 inputs.

Correlation	MAE	RMSE
0.845	14.81	55.17

Table 6.9: Few test results of 7- input based network (PGA) for class B.

M	D (in Km)	FM	$\overline{V}_s$ (in m/s)	$\overline{N}$	$\overline{V}_p$ (in m/s)	$\overline{\rho}$ (in gm/cm3)	Desired PGA (in cm/s^2)	Network PGA (in cm/s^2)
4.7	107	3	441	32	1423	1.917	5.30	7.77
5.4	148	1	570	38	2160	1.982	6.91	8.83
4.6	77	1	427	24	1042	1.966	6.99	10.14
6.1	61	1	389	37	1176	1.787	6,57	58.08
7.3	73	3	416	26	1368	2.028	197.01	134.63
6.3	14	3	442	51	1738	2.166	613.13	519.33
5.1	118	2	415	39	1400	2.048	7.21	7.69

6.3.1.3 Class C

Class C dataset consist of total 1926 averaged horizontal earthquake time histories. A dataset of 1618 was selected randomly from the total set of 1926 for training and cross validation and the remaining 308 was used to test the performance of the trained network. Three different data sets of 1618 were created and randomized. The three data sets were trained independently and the data set, which gave the minimum network error, was considered for testing the network. Finally ANN model with two hidden layer having 37, 23 neurons in each hidden layer respectively, seven input neurons and one output neuron showed the best performance. The trained network results and various parameters used for training are mentioned in Table 6.10 and 6.11 respectively.

Table 6.10: Network results for 7-37-23-1 architecture for class C with 7 inputs.

Architecture	Epochs	Correlation	Network Error
7- 37-23-1	16000	0.966	0.000335

Fig. 6.8 shows training scatter plot for predicted PGA to target PGA. Fig. 6.9 shows testing scatter-plot for 308 data points which are used to test the prediction capability of above trained

model. The result of testing network is defined in terms of R, MAE and RMSE mentioned in Table 6.12. A few test results of seven inputs based network for prediction of PGA are shown in Table 6.13.

Table 6.11: Parameters used for training neural network 7-37-23-1 architecture for class C with 7 inputs.

Description	Hidden Layer	Output Layer
Transfer Function	TanhAxon	SigmoidAxon
Learning Rate	0.08	0.08
Momentum	0.8	0.8

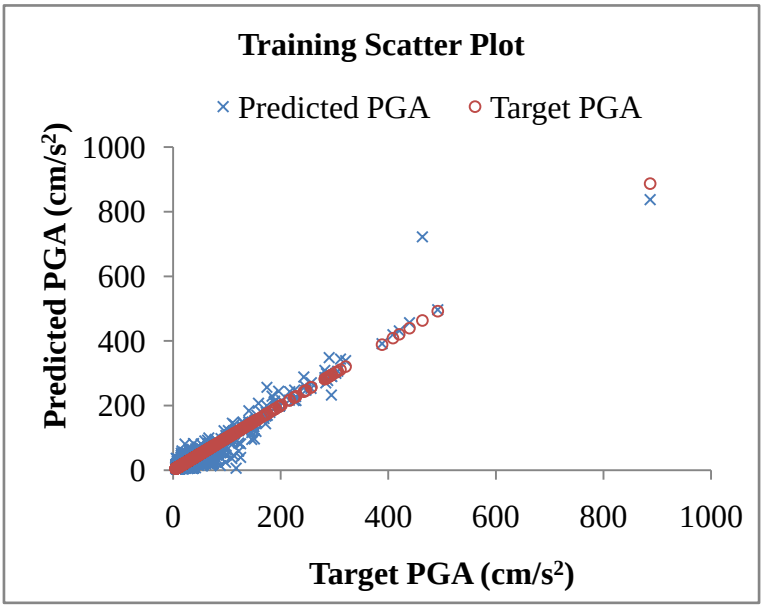

Figure 6.8: Training scatter plot of predicted PGA to target PGA for site class C with 7 inputs.

Table 6.12: R, MAE, and RMSE values of AAN model used in test performance to predict PGA for class C with 7 inputs.

Correlation	MAE	RMSE
0.811	16.53	21.32

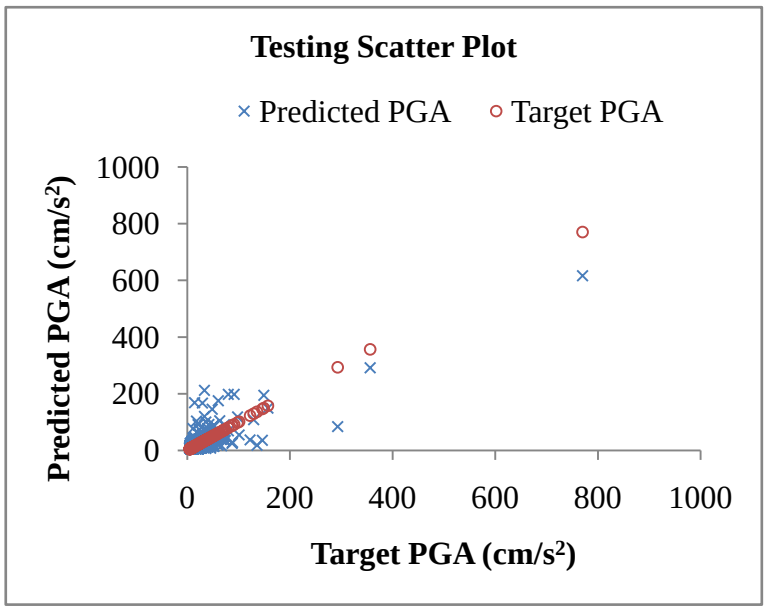

Figure 6.9: Testing scatter plot of predicted PGA to target PGA for site class C with 7 inputs.

Table 6.13: Few test results of 7- input based network (PGA) for class C.

M	D (in Km)	FM	$\overline{V}_s$ (in m/s)	$\overline{N}$	$\overline{V}_p$ (in m/s)	$\overline{\rho}$ (in gm/cm3)	Desired PGA (in cm/s^2)	Network PGA (in cm/s^2)
4.6	91	1	210	18	1017	1.936	5.3	7.63
5	80	1	266	12	803	1.676	7.57	7.06
6.2	145	3	319	33	1499	2.011	13.68	12.53
6.4	87	1	231	27	1474	1.469	29.68	166.97
7.2	123	1	337	19	1899	2.112	54.58	45.01
5.5	21	3	197	10	1101	1.753	149.34	194.45
6.9	13	1	344	23	1087	1.704	770.37	616.50

6.3.2 Four Input Based Network

As shown in Fig 6.10, the four nodes on the input layer for creating the neural network were the earthquake magnitude (M), hypo-central distance (D_{hyp}), focal mechanism (FM), average shear wave velocity $\overline{V}_{S30}$; and one node on the output layer that was peak ground acceleration (PGA) have been used for prediction of PGA for each site class.

6.3.2.1 Class A

Class A dataset consist of total 214 averaged horizontal earthquake time histories. A dataset of 178 was selected randomly from the total set of 214 for training and cross validation and the remaining 36 was used to test the performance of the trained network. Three different data sets of 178 were created and randomized. The three data sets were trained independently and the

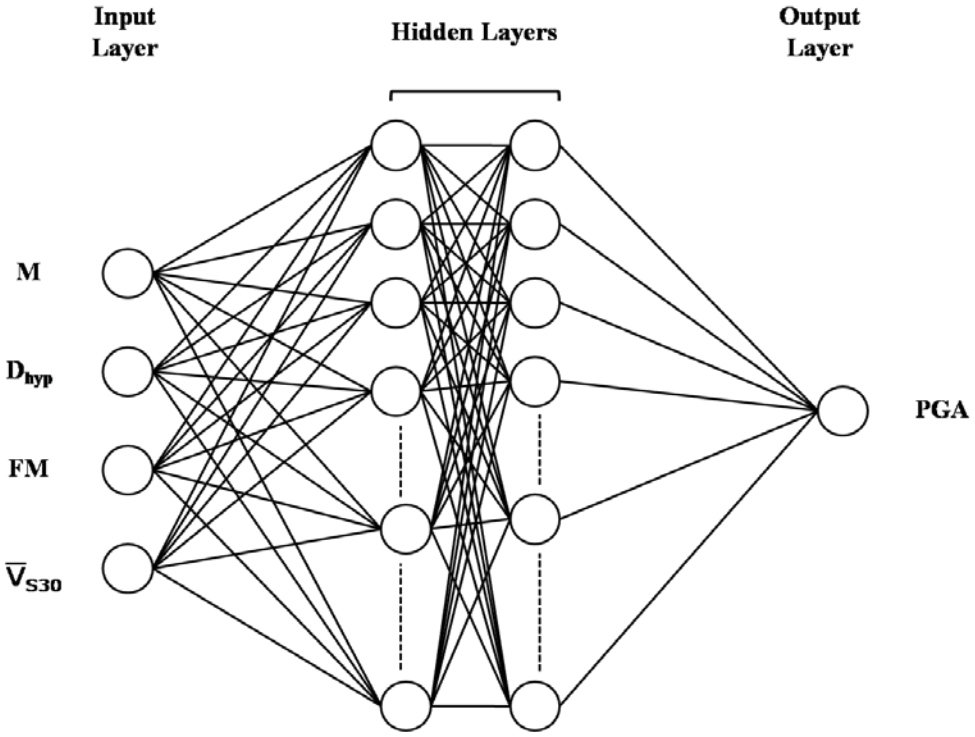

Figure 6.10: Neural network architecture with four nodes on input layer and one node on output layer.

data set, which gave the minimum network error, was considered for testing the network. Finally ANN model with two hidden layer having 40, 32 neurons in each hidden layer respectively, four input neurons and one output neuron showed the best performance. The trained network results and various parameters used for training are mentioned in Table 6.14 and 6.15 respectively. Fig. 6.11 shows training scatter plot for predicted PGA to target PGA. Fig. 6.12 shows testing scatter-plot for 36 data points which are used to test the prediction capability of above trained model. The result of testing network is defined in terms of R, MAE and RMSE mentioned in Table 6.16. A few test results of four inputs based network for prediction of PGA are shown in Table 6.17.

Table 6.14: Network results for 4-40-32-1 architecture for class A with 4 inputs.

Architecture	Epochs	Correlation	Network Error
4- 40-32-1	17000	0.820	0.001918

Table 6.15: Parameters used for training neural network 4-40-32-1 architecture for class A with 4 inputs.

Description	Hidden Layer	Output Layer
Transfer Function	TanhAxon	SigmoidAxon
Learning Rate	0.08	0.08
Momentum	0.8	0.8

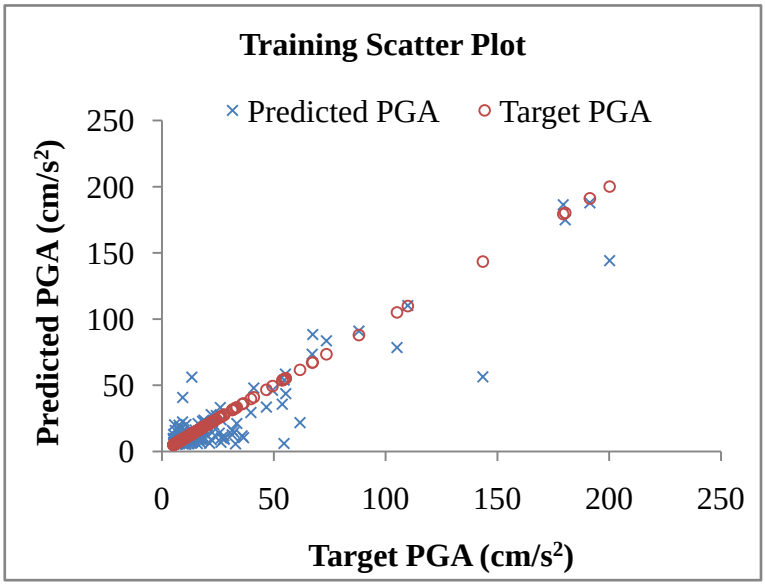

Figure 6.11: Training scatter plot of predicted PGA to target PGA for site class A with 4 inputs.

Table 6.16: R, MAE, and RMSE values of AAN model used in test performance to predict PGA for class A with 4 inputs.

Correlation	MAE	RMSE
0.781	17.30	57.08

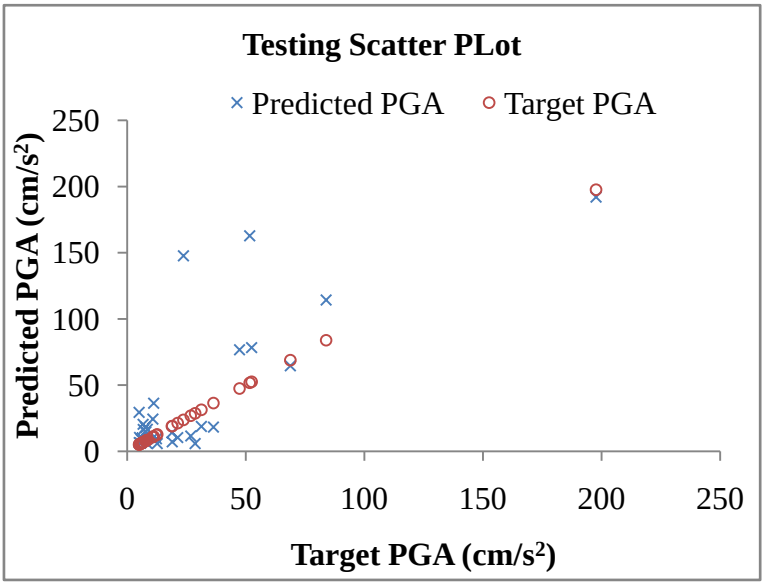

Figure 6.12: Testing scatter plot of predicted PGA to target PGA for site class A with 4 inputs.

Table 6.17: Few test results of 4- input based network (PGA) for class A.

M	D (in Km)	FM	$\overline{V}_s$ (in m/s)	Desired PGA (in cm/s^2)	Network PGA (in cm/s^2)
5.4	137	3	765	5.1	6.54
5.1	130	1	1009	5.69	6.04
4.7	73	2	1373	10.79	9.98
5.3	38	1	1433	51.69	162.83
7.3	187	3	888	6.38	9.87
6.8	121	1	1433	36.39	18.33
5.2	133	1	1433	8.33	6.08

6.3.2.2 Class B

Class B dataset consist of total 1825 averaged horizontal earthquake time histories. A dataset of 1534 was selected randomly for training and cross validation and the remaining 291 was used to test the performance of the trained network. Three different data sets were created and randomized and were trained independently. The data set, which gave the minimum network error, was considered for testing the network. Finally, ANN model with two hidden layer

having 30, 28 neurons in each hidden layer respectively, four input neurons and one output neuron showed the best performance. The trained network results and various parameters used for training are mentioned in Table 6.18 and 6.19 respectively. Fig. 6.13 shows training scatter plot for predicted PGA to target PGA. Fig.6.14 shows testing scatter-plot for 291 data points which are used to test the prediction capability of above trained model. The result of testing network is defined in terms of R, MAE and RMSE mentioned in Table 6.20. A few test results of four inputs based network for prediction of PGA are shown in Table 6.21.

Table 6.18: Network results for 4-30-28-1 architecture for class B with 4 inputs.

Architecture	Epochs	Correlation	Network Error
4- 30-28-1	28000	0.90	0.000380

Table 6.19: Parameters used for training neural network 4-30-28-1 architecture for class B with 4 inputs.

Description	Hidden Layer	Output Layer
Transfer Function	TanhAxon	SigmoidAxon
Learning Rate	0.08	0.08
Momentum	0.8	0.8

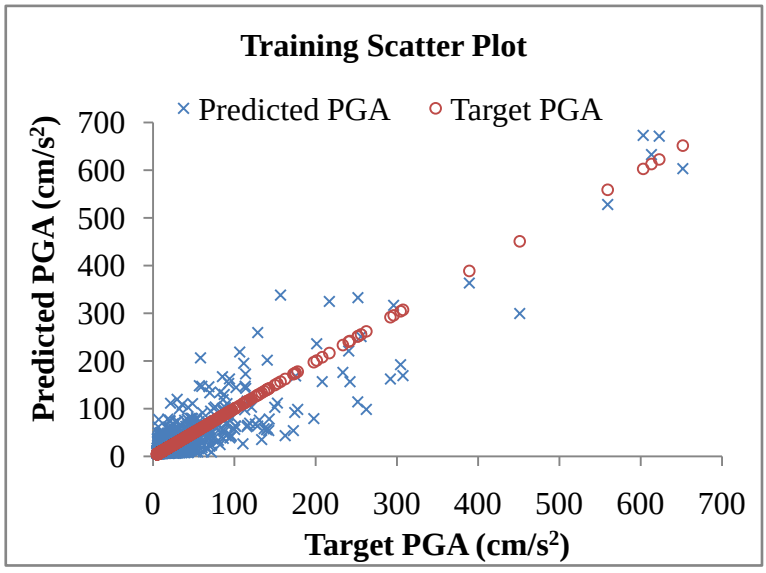

Figure 6.13: Training scatter plot of predicted PGA to target PGA for site class B with 4 inputs.

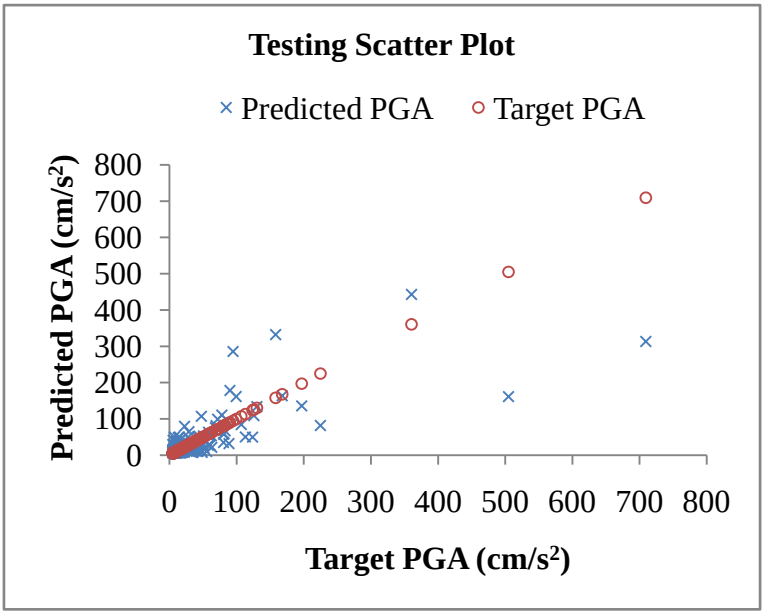

Figure 6.14: Testing scatter plot of predicted PGA to target PGA for site class B with 4 inputs.

Table 6.20: R, MAE, and RMSE values of AAN model used in test performance to predict PGA for class B with 4 inputs.

Correlation	MAE	RMSE
0.764	13.98	36.78

Table 6.21: Few test results of 4- input based network (PGA) for class B.

M	D (in Km)	FM	$\overline{V}_s$ (in m/s)	Desired PGA (in cm/s^2)	Network PGA (in cm/s^2)
4.8	105	3	437	5.21	6.90
4.6	74	1	458	5.27	7.80
6.1	76	1	429	5.6	41.36
4.6	89	1	403	7.49	7.72
6.3	45	3	372	41.71	49.16
6.5	60	1	394	86.36	94.39
7.2	36	1	430	709.32	313.23

6.3.2.3 Class C

Class C dataset consist of total 1926 averaged horizontal earthquake time histories out of which a dataset of 1618 was selected randomly for training and cross validation and the remaining 308 was used to test the performance of the trained network. After carrying out similar exercise as was done earlier, it was observed that ANN model with two hidden layer having 33, 12 neurons in each hidden layer respectively, four input neurons and one output neuron showed the best performance. The trained network results and various parameters used for training are mentioned in Table 6.22 and 6.23 respectively. Fig. 6.15 shows training scatter plot for predicted PGA to target PGA. Fig. 6.15 shows testing scatter-plot for 308 data points which are used to test the prediction capability of above trained model. The result of testing network defined in terms of R, MAE and RMSE is mentioned in Table 6.24. A few test results of four inputs based network for prediction of PGA are shown in Table 6.25.

Table 6.22: Network results for 4-33-12-1 architecture for class C with 4 inputs.

Architecture	Epochs	Correlation	Network Error
4-33-12-1	23500	0.887	0.000761

Table 6.23: Parameters used for training neural network 4-33-12-1 architecture for class C with 4 inputs.

Description	Hidden Layer	Output Layer
Transfer Function	TanhAxon	SigmoidAxon
Learning Rate	0.08	0.08
Momentum	0.8	0.8

Table 6.24: R, MAE, and RMSE values of AAN model used in test performance to predict PGA for class C with 4 inputs.

Correlation	MAE	RMSE
0.806	13.50	22.60

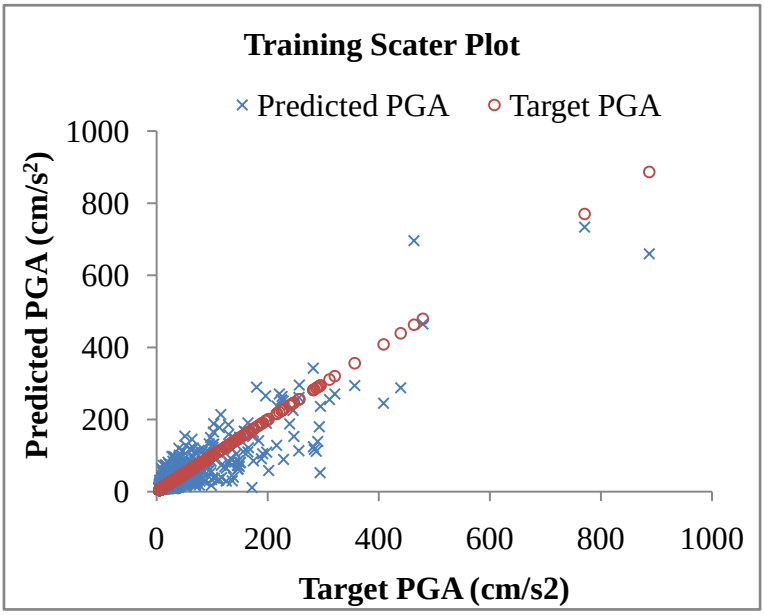

Figure 6.15: Training scatter plot of predicted PGA to target PGA for site class C with 4 inputs.

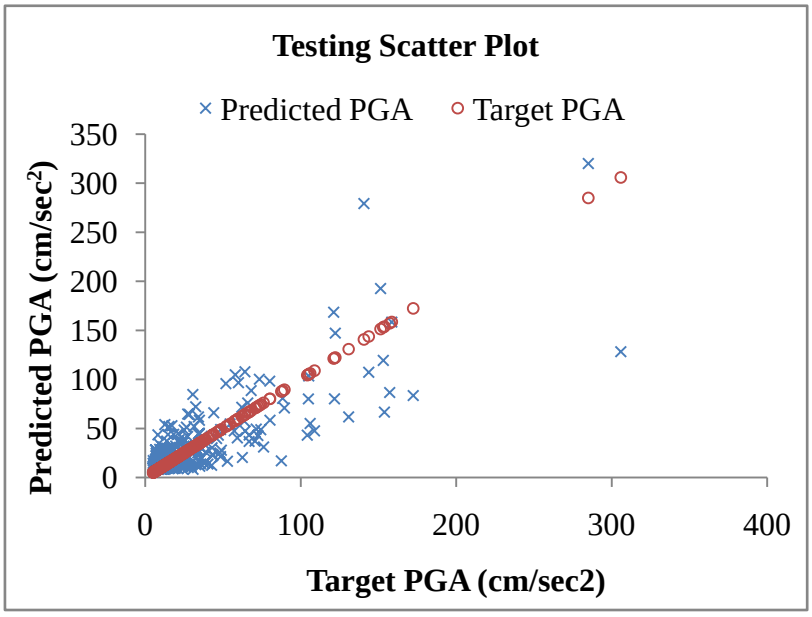

Figure 6.16: Testing scatter plot of predicted PGA to target PGA for site class C with 4 inputs.

Table 6.25: Few test results of 4- input based network (PGA) for class C.

M	D (in Km)	FM	$\overline{V}_s$ (in m/s)	Desired PGA (in cm/s^2)	Network PGA (in cm/s^2)
5.2	124	3	344	7.24	8.16
6.1	182	3	284	7.66	13.60
4.9	110	1	189	8.72	10.85
6.4	103	3	226	70.64	37.06
7.1	50	1	263	158.62	158.45
6.8	24	1	295	285	320
7.3	47	3	302	305.96	128.25

6.3.3 Three Input Based Network

As described above, the three nodes on the input layer for creating the neural network were the earthquake magnitude (M), hypo-central distance (D_{hyp}), average shear wave velocity $\overline{V}_{S30}$ and one node on the output layer that was peak ground acceleration (PGA) shown in Fig 6.17.

6.3.3.1 Class A

This Class of dataset consists of total 214 averaged horizontal earthquake time histories from which 178 was selected randomly for training and cross validation and the remaining 36 was used to test the performance of the trained network.

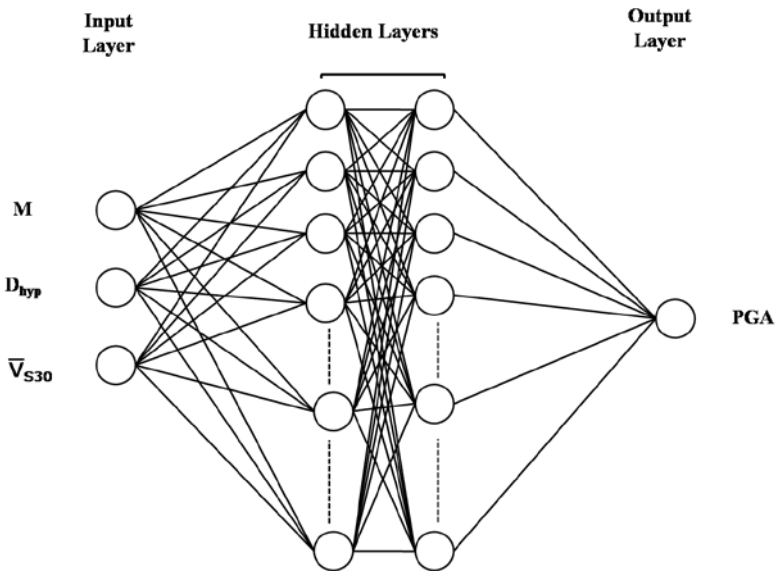

Figure 6.17: Neural network architecture with three nodes on input layer and one node on output layer.

Three different data sets of 178 were created and randomized and trained independently and the data set, which gave the minimum network error, was considered for testing the network. Finally ANN model with two hidden layer having 22, 13 neurons in each hidden layer respectively, three input neurons and one output neuron showed the best performance. The trained network results and various parameters used for training are mentioned in Table 6.26 and 6.27 respectively. Fig. 6.18 shows training scatter plot for predicted PGA to target PGA. Fig. 6.19 shows testing scatter-plot for 36 data points which are used to test the prediction capability of above trained model. The result of testing network is defined in terms of R, MAE and RMSE mentioned in Table 6.28. A few test results of three inputs based network for prediction of PGA are shown in Table 6.29

Table 6.26: Network results for 3-22-13-1 architecture for class A with 3 inputs.

Architecture	Epochs	Correlation	Network Error
3- 22-13-1	30000	0.895	0.000731

Table 6.27: Parameters used for training neural network 3-22-13-1 architecture for class A with 3 inputs.

Description	Hidden Layer	Output Layer
Transfer Function	TanhAxon	SigmoidAxon
Learning Rate	0.09	0.09
Momentum	0.9	0.9

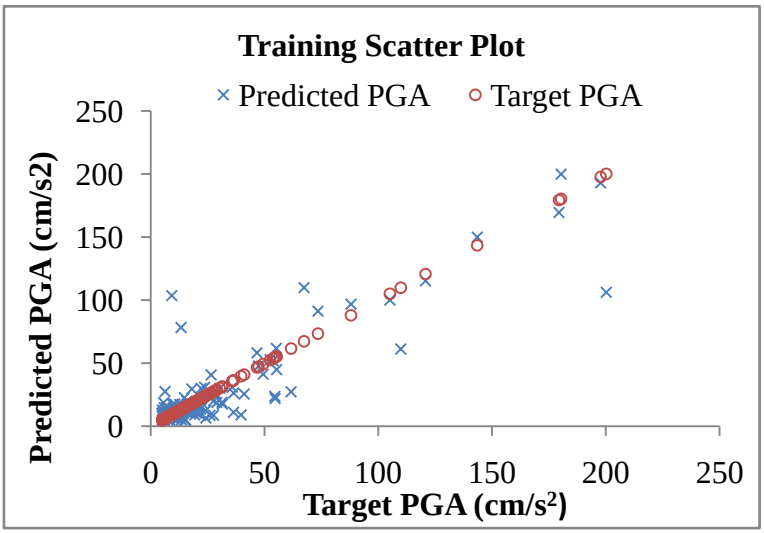

Figure 6.18: Training scatter plot of predicted PGA to target PGA for site class A with 3 inputs.

Table 6.28: R, MAE, and RMSE values of AAN model used in test performance to predict PGA for class A with 3 inputs.

Correlation	MAE	RMSE
0.877	11.20	32.15

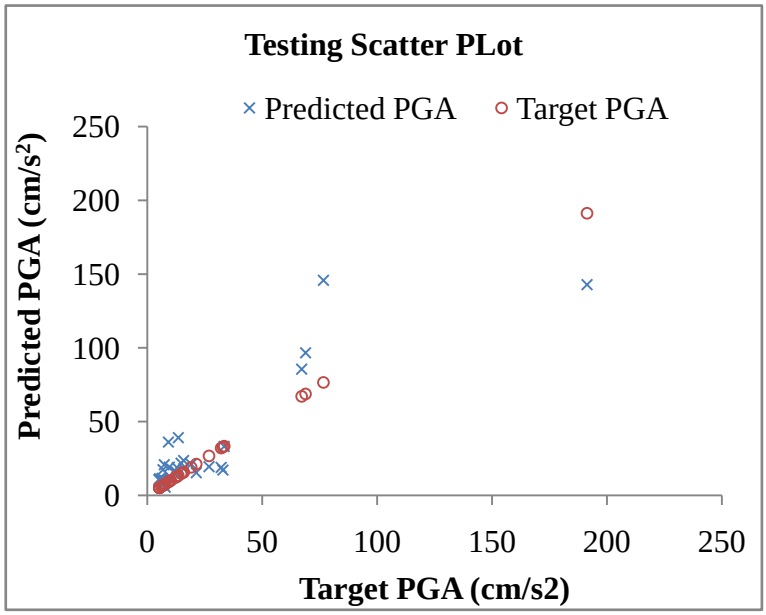

Figure 6.19: Testing scatter plot of predicted PGA to target PGA for site class A with 3 inputs.

Table 6.29: Few test results of 3- input based network (PGA) for class A.

M	D (in Km)	$\overline{V}_s$ (in m/s)	Desired PGA (in cm/s^2)	Network PGA (in cm/s^2)
6.5	130	993	7.72	5.70
7.0	161	817	6.95	7.38
4.6	106	818	9.75	10.93
5.7	141	1433	12.02	14.88
5.5	199	1433	19.05	21.20
7.0	122	894	68.82	96.70
4.9	89	1433	191.3	142.92

6.3.3.2 Class B

Class B dataset consist of total 1825 averaged horizontal earthquake time histories. A dataset of 1534 was selected randomly from the total set of 1825 for training and cross validation and the remaining 291 was used to test the performance of the trained network. Three different data sets of 1534 were created and randomized. Similar exercise resulted in ANN model with two hidden layer having 33, 28 neurons in each hidden layer respectively, three input neurons and one output neuron showing the best performance. The trained network results and various parameters used for training are mentioned in Table 6.30 and 6.31 respectively. Fig. 6.20 shows training scatter plot for predicted PGA to target PGA. Fig. 6.21 shows testing scatter-plot for 291 data points which are used to test the prediction capability of above trained model. The result of testing network is defined in terms of R, MAE and RMSE mentioned in Table 6.32. A few test results of seven inputs based network for prediction of PGA are shown in Table 6.33.

Table 6.30: Network results for 3-33-28-1 architecture for class B with 3 inputs.

Architecture	Epochs	Correlation	Network Error
3- 33-28-1	35000	0.895	0.000362

Table 6.31: Parameters used for training neural network 3-33-28-1 architecture for class B with 3 inputs.

Description	Hidden Layer	Output Layer
Transfer Function	TanhAxon	SigmoidAxon
Learning Rate	0.08	0.08
Momentum	0.8	0.8

Table 6.32: R, MAE, and RMSE values of AAN model used in test performance to predict PGA for class B with 3 inputs.

Correlation	MAE	RMSE
0.846	12.92	44.71

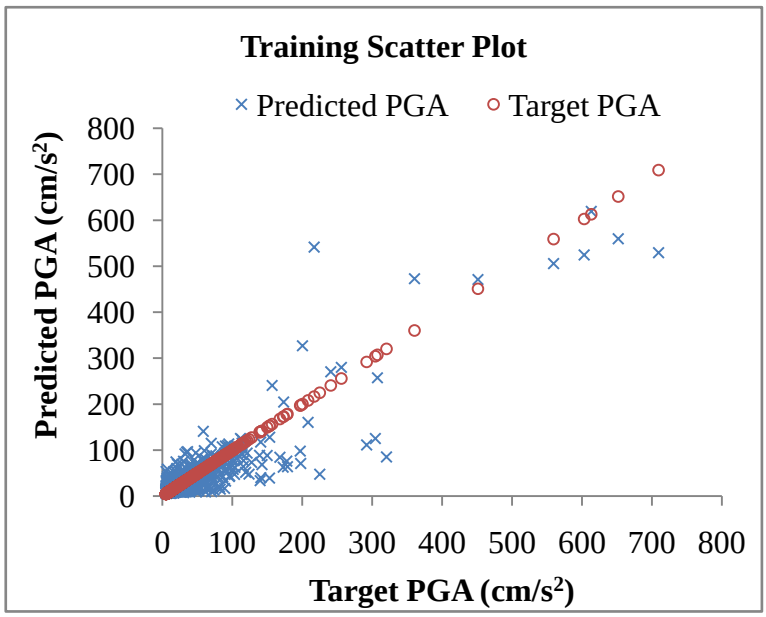

Figure 6.20: Training scatter plot of predicted PGA to target PGA for site class B with 3 inputs.

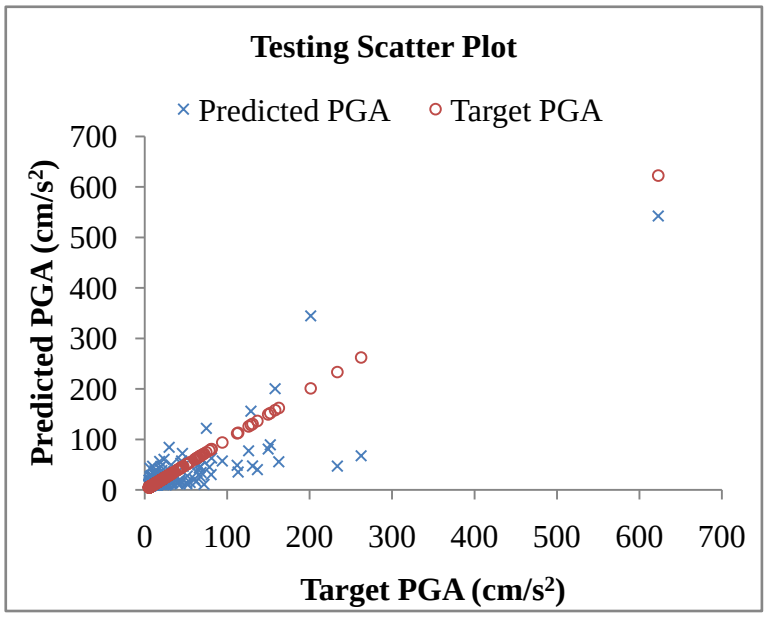

Figure 6.21: Testing scatter plot of predicted PGA to target PGA for site class B with 3 inputs.

Table 6.33: Few test results of 3- input based network (PGA) for class B.

M	D (in Km)	$\overline{V}_s$ (in m/s)	Desired PGA (in cm/s^2)	Network PGA (in cm/s^2)
4.6	109	668	7.30	7.73
5.5	66	368	14.20	14.93
6.1	115	441	9.55	15.18
5.1	25	443	46.71	46.95
6.3	27	369	128.73	156.00
7.3	17	404	622.68	542.70
5.3	31	476	31.42	34.28

6.3.3.3 Class C

Class C dataset consist of total 1926 averaged horizontal earthquake time histories. A dataset of 1618 was selected randomly for training and cross validation and the remaining 308 was used to test the performance of the trained network. Three different data sets of 1618 were created, randomized and trained independently. Finally ANN model with two hidden layer having 33, 28 neurons in each hidden layer respectively, three input neurons and one output neuron showed the best performance. The trained network results and various parameters used for training are mentioned in Table 6.34 and 6.35 respectively. Fig. 6.22 shows training scatter plot for predicted PGA to target PGA. Fig. 6.23 shows testing scatter-plot for 308 data points which are used to test the prediction capability of above trained model. The result of testing network is defined in terms of R, MAE and RMSE mentioned in Table 6.36.A few test results of three inputs based network for prediction of PGA are shown in Table 6.37.

Table 6.34: Network results for 3-33-28-1 architecture for class C with 3 inputs.

Architecture	Epochs	Correlation	Network Error
3- 33-28-1	372000	0.902	0.000248

Table 6.35: Parameters used for training neural network 3-33-28-1 architecture for class C with 3 inputs.

Description	Hidden Layer	Output Layer
Transfer Function	TanhAxon	SigmoidAxon
Learning Rate	0.09	0.09
Momentum	0.9	0.9

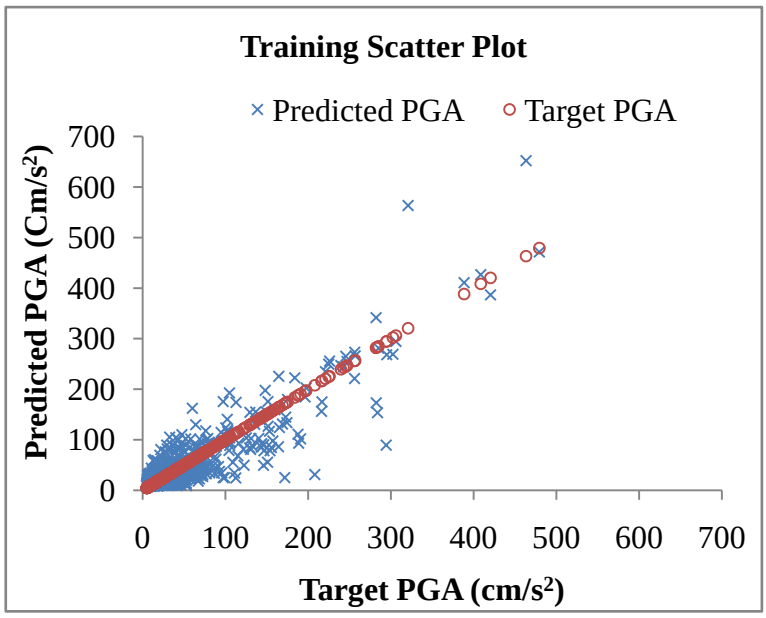

Figure 6.22: Training scatter plot of predicted PGA to target PGA for site class C with 3 inputs.

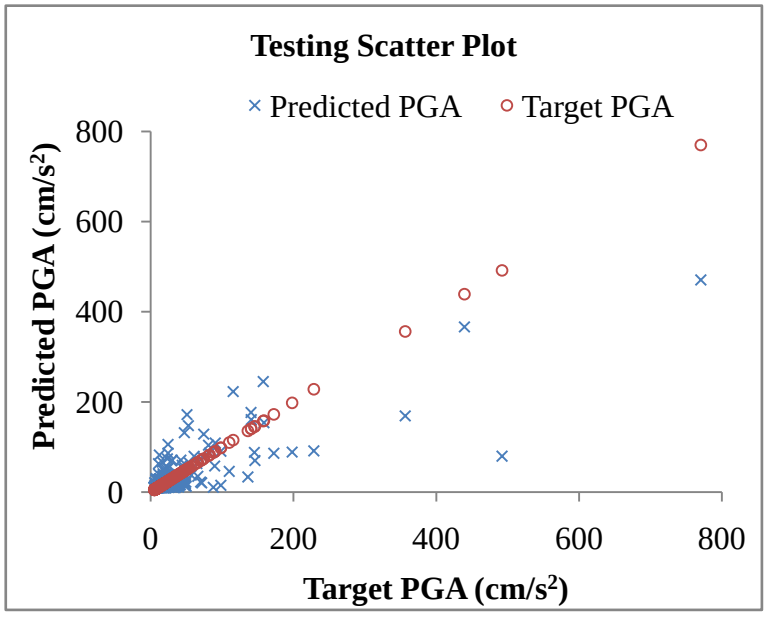

Figure 6.23: Testing scatter plot of predicted PGA to target PGA for site class C with 3 inputs.

Table 6.36: R, MAE, and RMSE values of AAN model used in test performance to predict PGA for class C with 3 inputs.

Correlation	MAE	RMSE
0.805	16.55	31.66

Table 6.37: Few test results of 3- input based network (PGA) for class A.

M	D (in Km)	$\overline{V}_s$ (in m/s)	Desired PGA (in cm/s^2)	Network PGA (in cm/s^2)
4.7	184	301	5.00	9.65
6.4	179	190	8.14	9.52
5.7	124	187	14.60	13.14
7.3	42	323	157.64	245.26
4.5	26	249	73.07	77.35
7.0	156	231	32.93	34.68
6.9	13	344	770.37	470.94

6.4 ANN BASED PREDICTION OF DURATION

6.4.1 Seven Input Based Network

As shown in Fig 6.24, the seven nodes on the input layer for creating the neural network were the earthquake magnitude (M), hypo-central distance (D_{hyp}), focal mechanism (FM), average shear wave velocity $\overline{V}_{S30}$; average SPT blow count $\overline{N}$; average shear wave velocity $\overline{V}_{P30}$; and average density of soil $\bar{\rho}$ and one node on the output layer that was duration (t_D) have been used for prediction of duration for each site class.

6.4.1.1 Class A

Class A dataset consist of total 214 averaged horizontal earthquake time histories. A dataset of 178 was selected randomly from the total set of 214 for training and cross validation and the remaining 36 was used to test the performance of the trained network. Three different data sets of 178 were created and parameters used for training are mentioned in Table 6.38 and 6.39 respectively. Fig. 6.25 shows training scatter plot for predicted duration to target (real) duration. Fig.6.26 shows testing scatter-plot randomized. The three data sets were trained independently and the data set, which gave the minimum network error, was considered for

testing the network. Finally ANN model with single hidden layer having 63 neurons, seven input neurons and one output neuron showed the best performance.

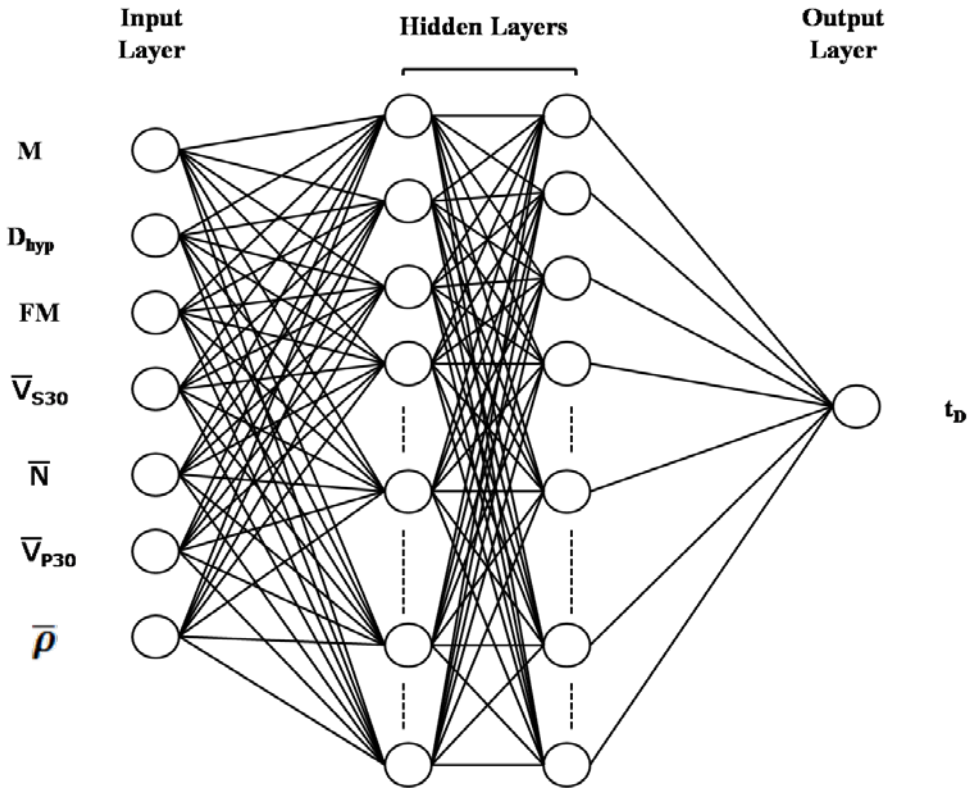

Figure 6.24: Neural network architecture with seven nodes on input layer and one node on output layer.

The trained network results and various parameters used for training are mentioned in Table 6.38 and 6.39 respectively. Fig. 6.25 shows training scatter plot for predicted duration to target (real) duration. Fig.6.26 shows testing scatter-plot for 36 data points which are used to test the prediction capability of above trained model. The result of testing network is defined in terms of R, MAE and RMSE mentioned in Table 6.40. A few test results of seven inputs based network for prediction of duration are shown in Table 6.41

Table 6.38: Network results for 7-63-1 architecture for class A with 7 inputs.

Architecture	Epochs	Correlation	Network Error
7- 63-1	21000	0.954	0.003727

Table 6.39: Parameters used for training neural network 7-63-1 architecture for class A with 7 inputs.

Description	Hidden Layer	Output Layer
Transfer Function	TanhAxon	SigmoidAxon
Learning Rate	0.1	0.1
Momentum	0.6	0.6

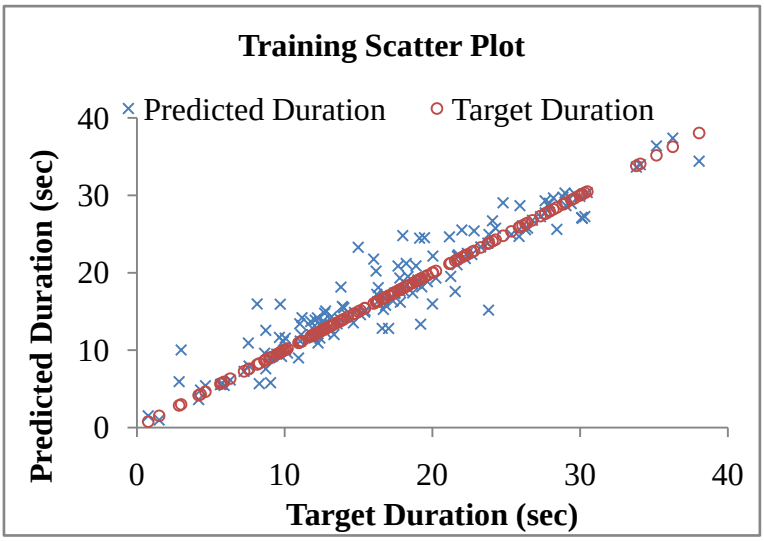

Figure 6.25: Training scatter plot of predicted duration to target duration for site class A with 7 inputs.

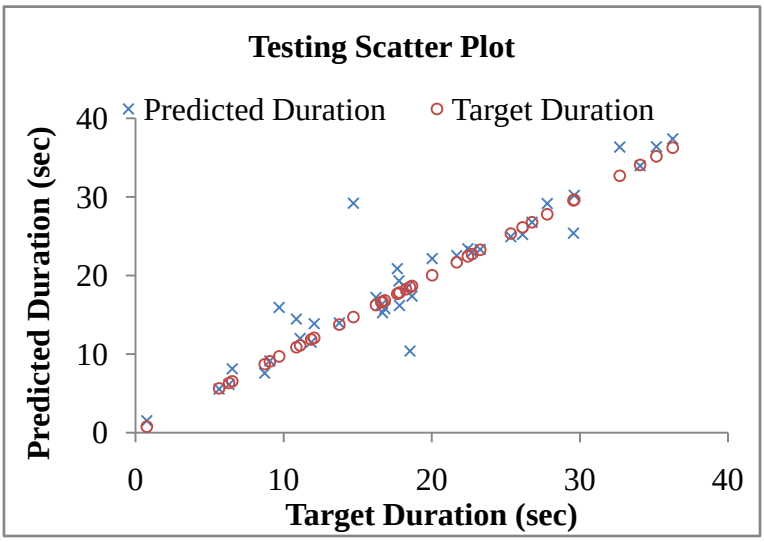

Figure 6.26: Testing scatter plot of predicted duration to target duration for site class A with 7 inputs.

Table 6.40: R, MAE, and RMSE values of AAN model used in test performance to predict duration for class A with 7 inputs.

Correlation	MAE	RMSE
0.936	1.81	4.26

Table 6.41: Few test results of 7- input based network (Duration) for class A.

M	D (in Km)	FM	$\overline{V}_s$ (in m/s)	$\overline{N}$	$\overline{V}_p$ (in m/s)	$\bar{\rho}$ (in gm/cm3)	Desired Duration (in sec)	Network Duration (in sec)
5.3	46	3	818	62	2006	2.151	0.77	1.52
4.5	40	1	760	70	1615	2.232	9.08	9.15
5	45	3	820	55	1915	2.136	11.87	11.51
4.8	99	1	1086	99	2338	1.957	16.24	17.20
6.5	120	1	915	49	1990	2.220	23.28	23.31
7.3	196	3	1373	60	2747	2.234	32.70	36.34
7.0	180	3	1373	60	2747	2.234	36.275	37.38

6.4.1.2 Class B

Class B dataset consist of total 1825 averaged horizontal earthquake time histories. A dataset of 1534 was selected randomly from the total set of 1825 for training and cross validation and the remaining 291 was used to test the performance of the trained network. But we were unable to get convergence of network, so we reduced the data by dividing 1825 averaged horizontal earthquake time histories into 4 equal's data set each having 456 time histories. These four data sets of 456 were randomized. The four data sets were trained independently and the data set, which gave the minimum network error, was considered for testing the network. A new dataset of 382 was selected randomly from the total set of 456 for training and cross validation and the remaining 74 was used to test the performance of the trained network. Finally ANN model with single hidden layer having 53 neurons, seven input neurons and one output neuron showed the best performance. The trained network results and various parameters used for training are mentioned in Table 6.42 and 6.43 respectively. Fig. 6.27 shows training scatter plot for predicted duration to target duration. Fig. 6.28 shows testing scatter-plot for 74 data points which are used to test the prediction capability of above trained model. The result of testing network is defined in terms of R, MAE and RMSE mentioned in Table 6.44. A few test results of seven inputs based network for prediction of duration are shown in Table 6.45.

Table 6.42: Network results for 7-53-1 architecture for class B with 7 inputs.

Architecture	Epochs	Correlation	Network Error
7- 53-1	13000	0.988	0.000551

Table 6.43: Parameters used for training neural network 7-53-1 architecture for class B with 7 inputs.

Description	Hidden Layer	Output Layer
Transfer Function	TanhAxon	SigmoidAxon
Learning Rate	0.1	0.1
Momentum	0.6	0.6

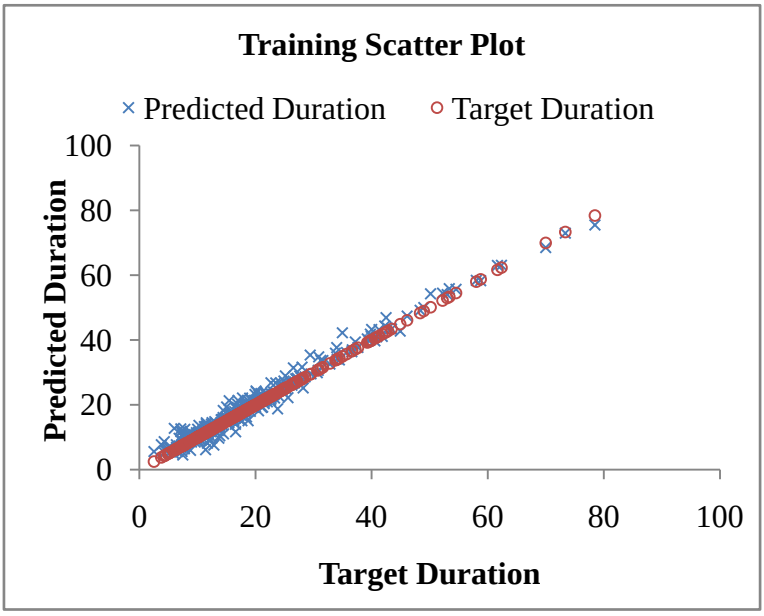

Figure 6.27: Training scatter plot of predicted duration to target duration for site class B with 7 inputs.

Table 6.44: R, MAE, and RMSE values of AAN model used in test performance to predict duration for class B with 7 inputs.

Correlation	MAE	RMSE
0.986	2.82	6.32

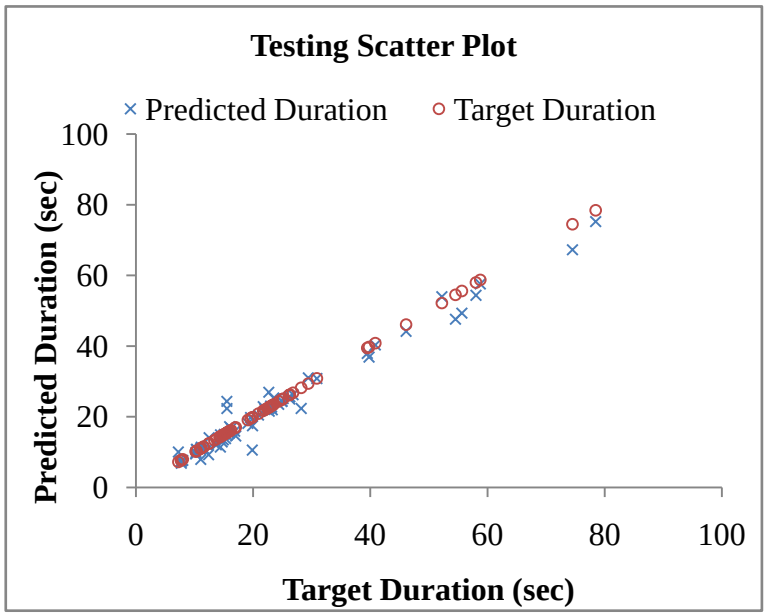

Figure 6.28: Testing scatter plot of predicted duration to target duration for site class B with 7 inputs.

Table 6.45: Few test results of 7- input based network (Duration) for class B.

M	D (in Km)	FM	$\overline{V}_s$ (in m/s)	$\overline{N}$	$\overline{V}_p$ (in m/s)	$\overline{\rho}$ (in gm/cm3)	Desired Duration (in sec)	Network Duration (in sec)
4.7	58	2	389	53	1437	2.360	7.69	7.39
6.1	32	3	587	99	1653	2.138	10.32	10.79
5.4	87	1	537	99	1510	2.066	15.51	24.40
5.5	185	1	370	21	1536	1.926	28.21	22.37
6.4	154	1	430	15	1753	1.304	78.44	75.24
4.7	62	3	408	48	1227	1.94	14.26	13.77
5.0	49	1	461	61	1286	1.785	19.90	17.50

6.4.1.3 Class C

A dataset of 1618 was selected randomly from the total set of 1926 (Class C) for training and cross validation and the remaining 308 was used to test the performance of the trained network. But we were unable to get convergence of network, so we reduced the data by dividing 1926 averaged horizontal earthquake time histories into 4 equal's data set each having 482 time histories. These four data sets of 482 were randomized, trained independently and the data set,

which gave the minimum network error, was considered for testing the network. A new dataset of 405 was selected randomly from the total set of 482 for training and cross validation and the remaining 77 was used to test the performance of the trained network. Finally ANN model with single hidden layer having 67 neurons, seven input neurons and one output neuron showed the best performance. The trained network results and various parameters used for training are mentioned in Table 6.46 and 6.47 respectively.

Table 6.46: Network results for 7-67-1 architecture for class C with 7 inputs.

Architecture	Epochs	Correlation	Network Error
7- 67-1	29000	0.969	0.000756

Table 6.47: Parameters used for training neural network 7-67-1 architecture for class C with 7 inputs.

Description	Hidden Layer	Output Layer
Transfer Function	TanhAxon	SigmoidAxon
Learning Rate	0.1	0.1
Momentum	0.6	0.6

Fig. 6.29 shows training scatter plot for predicted duration to target duration. Fig. 6.30 shows testing scatter-plot for 77 data points which are used to test the prediction capability of above trained model. The result of testing network is defined in terms of R, MAE and RMSE mentioned in Table 6.48.A few test results of seven inputs based network for prediction of duration are shown in Table 6.49.

Table 6.48: R, MAE, and RMSE values of AAN model used in test performance to predict duration for class C with 7 inputs.

Correlation	MAE	RMSE
0.938	2.39	3.21

Table 6.49: Few test results of 7- input based network (Duration) for class A.

M	D (in Km)	FM	$\overline{V}_s$ (in m/s)	$\overline{N}$	$\overline{V}_p$ (in m/s)	$\overline{\rho}$ (in gm/cm3)	Desired Duration (in sec)	Network Duration (in sec)
6.1	16	1	337	22	1471	1.85	7.05	19.34
4.8	144	3	246	5	1499	1.65	7.40	7.58
5.2	64	3	292	29	563	1.96	15.09	13.35
7.3	89	3	345	24	1026	2.02	17.24	15.62
6.1	124	1	352	20	1751	1.96	52.72	60.19
7.2	132	1	286	21	940	1.87	66.27	69.03
6.4	162	3	248	12	1331	1.79	46.91	42.65

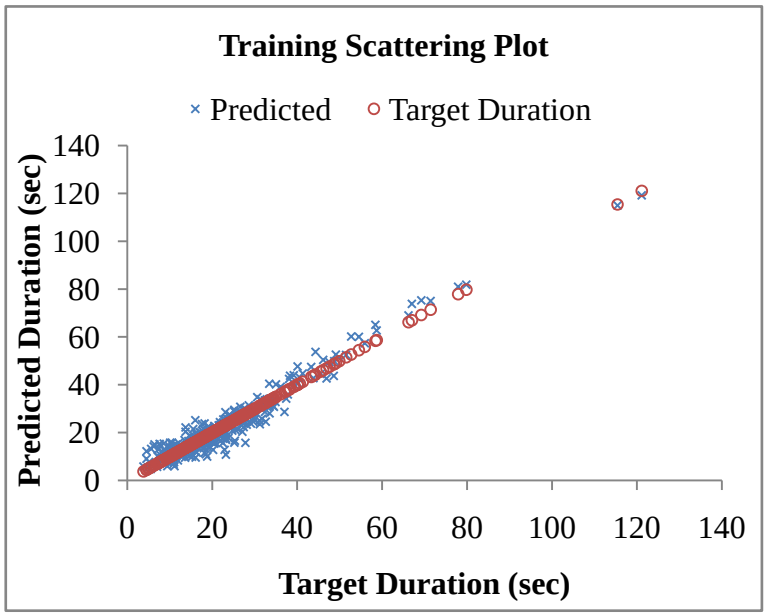

Figure 6.29: Training scatter plot of predicted duration to target duration for site class C with 7 inputs.

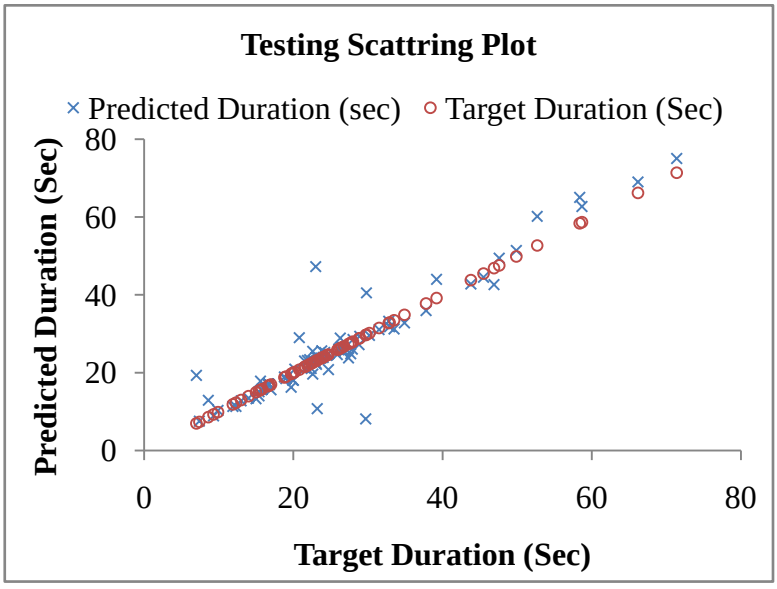

Figure 6.30: Testing scatter plot of predicted duration to target duration for site class C with 7 inputs.

6.4.2 Four Input Based Network

As shown in Fig 6.31, the four nodes on the input layer for creating the neural network were the earthquake magnitude (M), hypo-central distance (D_{hyp}), focal mechanism (FM), average shear wave velocity $\overline{V}_{S30}$; and one node on the output layer as duration (t_D) have been used for prediction of duration for each site class.

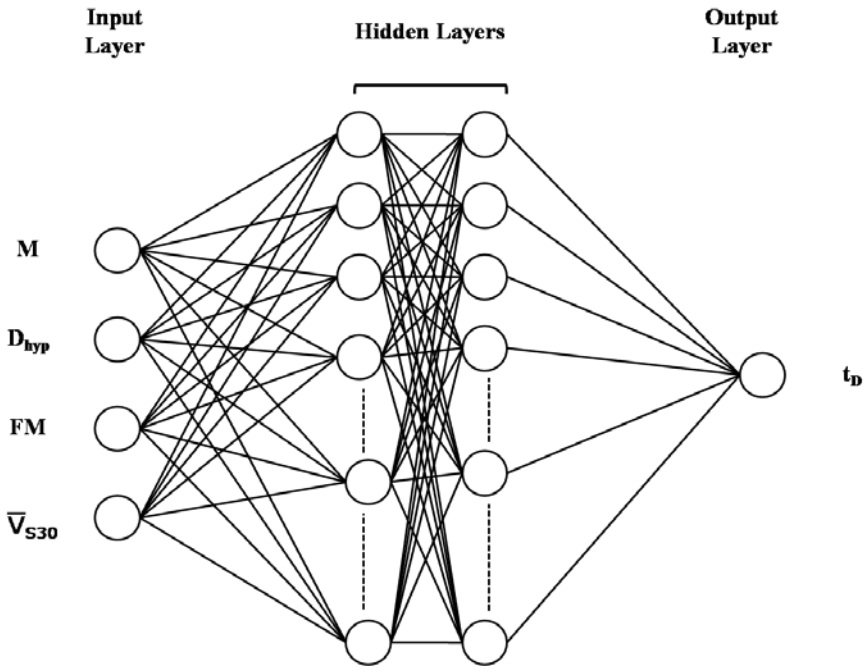

Figure 6.31: Neural network architecture with four nodes on input layer and one node on output layer.

6.4.2.1 Class A

A dataset of 178 was selected randomly from the total set of 214 for training and cross validation and the remaining 36 was used to test the performance of the trained network. Three different data sets of 178 were created and randomized. The three data sets were trained independently and the data set, which gave the minimum network error, was considered for testing the network. Finally ANN model with single hidden layer having 52 neurons, seven input neurons and one output neuron showed the best performance. The trained network results and various parameters used for training are mentioned in Table 6.50 and 6.51 respectively. Fig. 6.32 shows training scatter plot for predicted duration to target duration. Fig. 6.33 shows testing scatter-plot for 36 data points which are used to test the prediction capability of above

trained model. The result of testing network is defined in terms of R, MAE and RMSE mentioned in Table 6.52. A few test results of four inputs based network for prediction of duration are shown in Table 6.53.

Table 6.50: Network results for 4-52-1 architecture for class A with 4 inputs.

Architecture	Epochs	Correlation	Network Error
4- 52-1	35000	0.962	0.00239

Table 6.51: Parameters used for training neural network 4-52-1 architecture for class A with 4 inputs.

Description	Hidden Layer	Output Layer
Transfer Function	TanhAxon	SigmoidAxon
Learning Rate	0.1	0.1
Momentum	0.6	0.6

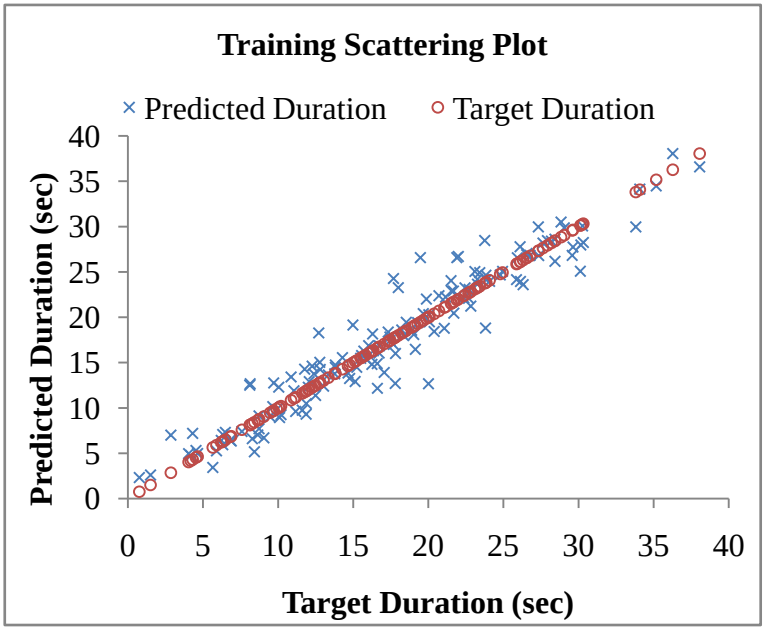

Figure 6.32: Training scatter plot of predicted duration to target duration for site class A with 4 inputs.

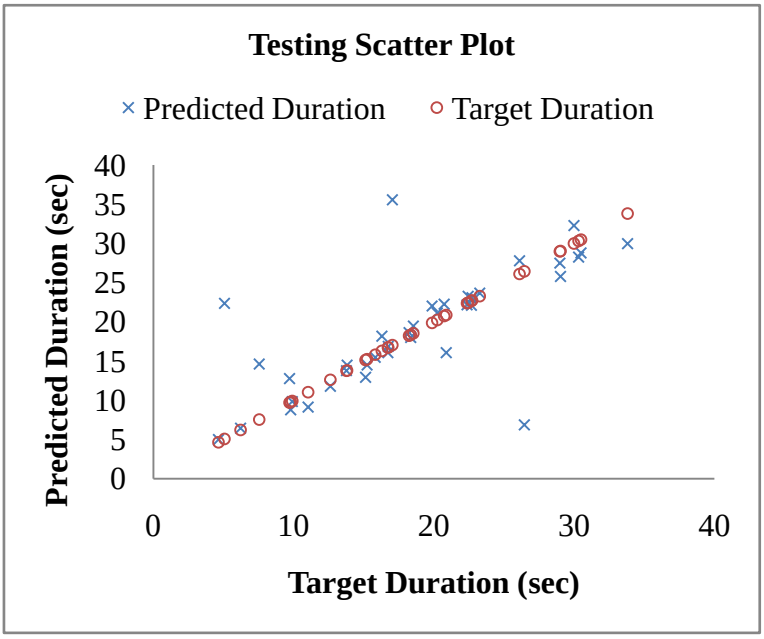

Figure 6.33: Testing scatter plot of predicted duration to target duration for site class A with 4 inputs.

Table 6.52: R, MAE, and RMSE values of AAN model used in test performance to predict duration for class A with 4 inputs.

Correlation	MAE	RMSE
0.720	2.79	3.37

Table 6.53: Few test results of 4- input based network (Duration) for class A.

M	D (in Km)	FM	$\overline{V}_s$ (in m/s)	Desired Duration (in sec)	Network Duration (in sec)
5.5	53	3	1009	4.64	4.97
7.0	161	3	817	33.81	29.96
4.7	69	1	1433	7.545	14.61
5.6	84	1	1086	22.72	23.07
6.9	134	1	1009	29.99	32.25
5.3	120	3	765	5.07	22.34
6.1	73	1	1433	17.04	35.55

6.4.2.1 Class B

Class B dataset consist of total 1825 averaged horizontal earthquake time histories. A dataset of 1534 was selected randomly from the total set of 1825 for training and cross validation and the remaining 291 was used to test the performance of the trained network. But we were unable to get convergence of network, so we reduced the data by dividing 1825 averaged horizontal earthquake time histories into 4 equals data set each having 456 time histories. These four data sets of 456 were randomized. The four data sets were trained independently and the data set, which gave the minimum network error, was considered for testing the network. A new dataset of 382 was selected randomly from the total set of 456 for training and cross validation and the remaining 74 was used to test the performance of the trained network. Finally ANN model with single hidden layer having 58 neurons, seven input neurons and one output neuron showed the best performance. The trained network results and various parameters used for training are mentioned in Table 6.54 and 6.55 respectively. Fig. 6.34 shows training scatter plot for predicted duration to target duration. Fig. 6.35 shows testing scatter-plot for 74 data points which are used to test the prediction capability of above trained model. The result of testing network is defined in terms of R, MAE and RMSE mentioned in Table 6.56. A few test results of seven inputs based network for prediction of duration are shown in Table 6.57.

Table 6.54: Network results for 4-58-1 architecture for class B with 4 inputs.

Architecture	Epochs	Correlation	Network Error
4- 58-1	45000	0.943	0.00445

Table 6.55: Parameters used for training neural network 4-58-1 architecture for class B with 4 inputs.

Description	Hidden Layer	Output Layer
Transfer Function	TanhAxon	SigmoidAxon
Learning Rate	0.1	0.1
Momentum	0.6	0.6

Table 6.56: R, MAE, and RMSE values of AAN model used in test performance to predict duration for class B with 4 inputs.

Correlation	MAE	RMSE
0.887	5.31	5.69

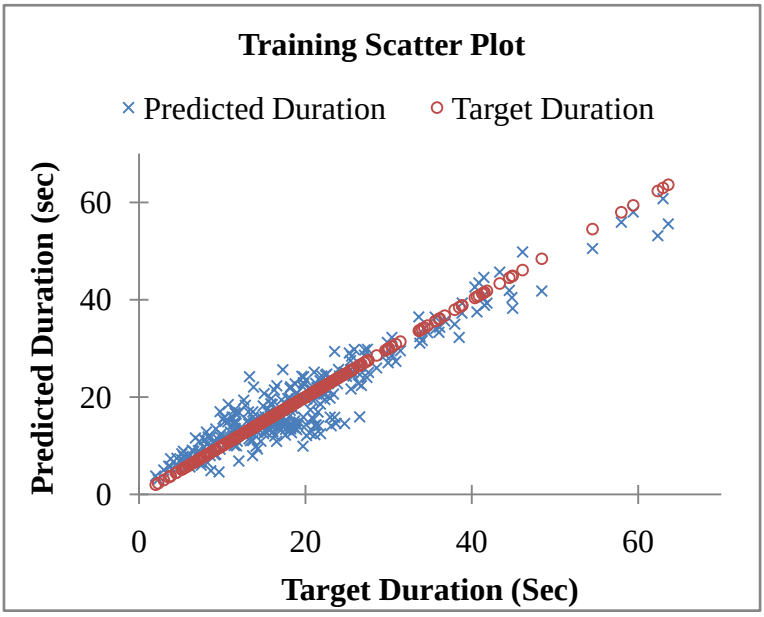

Figure 6.34: Training scatter plot of predicted duration to target duration for site class B with 4 inputs.

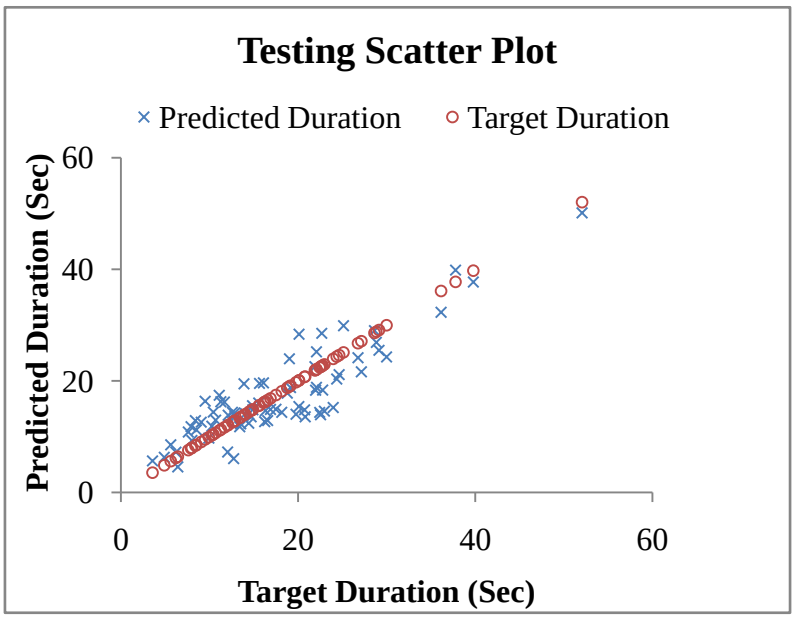

Figure 6.35: Testing scatter plot of predicted duration to target duration for site class B with 4 inputs.

Table 6.57: Few test results of 4- input based network (Duration) for class B.

M	D (in Km)	FM	$\overline{V}_s$ (in m/s)	Desired Duration (in sec)	Network Duration (in sec)
4.5	87	3	439	3.56	5.66
5.4	31	1	508	10.26	11.88
6.1	37	3	530	13.88	19.48
7.3	165	3	695	19.01	23.97
6.2	30	3	382	12.72	6.07
6.9	186	1	500	28.61	29.03
5.7	138	2	431	28.82	26.92

6.4.2.3 Class C

A dataset of 1618 was selected randomly from the total set of 1926 (Class C) for training and cross validation and the remaining 308 was used to test the performance of the trained network. But we were unable to get convergence of network, to improve the convergence we reduced the data and divided 1926 averaged horizontal earthquake time histories into 4 equal's data set each having 482 time histories. These four data sets of 482 were randomized, trained independently and the data set, which gave the minimum network error, was considered for testing the network. A new dataset of 405 was selected randomly from the total set of 482 for training and cross validation and the remaining 77 was used to test the performance of the trained network. Finally ANN model with single hidden layer having 49 neurons, four input neurons and one output neuron showed the best performance. The trained network results and various parameters used for training are mentioned in Table 6.58 and 6.59 respectively. Fig. 6.36 shows training scatter plot for predicted duration to target duration. Fig. 6.37 shows testing scatter-plot for 77 data points which are used to test the prediction capability of above trained model. The result of testing network is defined in terms of R, MAE and RMSE mentioned in Table 6.60.A few test results of seven inputs based network for prediction of duration are shown in Table 6.61.

Table 6.58: Network results for 4-49-1 architecture for class C with 4 inputs.

Architecture	Epochs	Correlation	Network Error
4- 49-1	52000	0.944	0.001493

Table 6.59: Parameters used for training neural network 4-49-1 architecture for class C with 4 inputs.

Description	Hidden Layer	Output Layer
Transfer Function	TanhAxon	SigmoidAxon
Learning Rate	0.1	0.1
Momentum	0.6	0.6

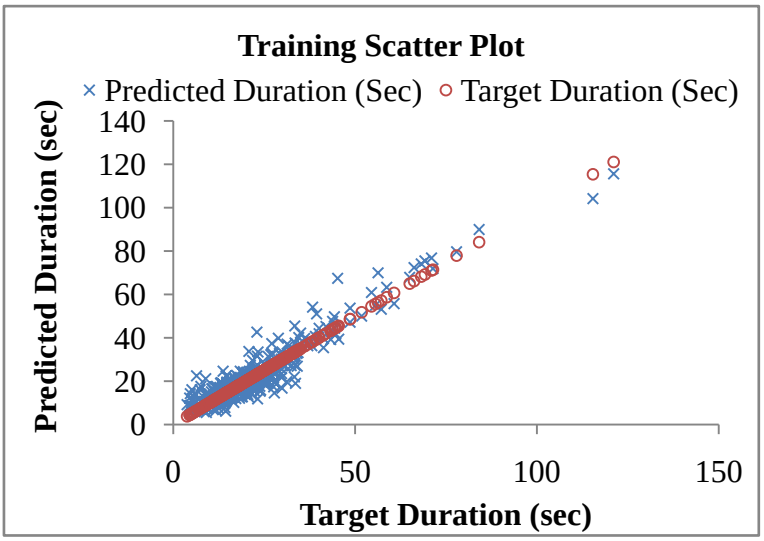

Figure 6.36: Training scatter plot of predicted duration to target duration for site class C with 4 inputs.

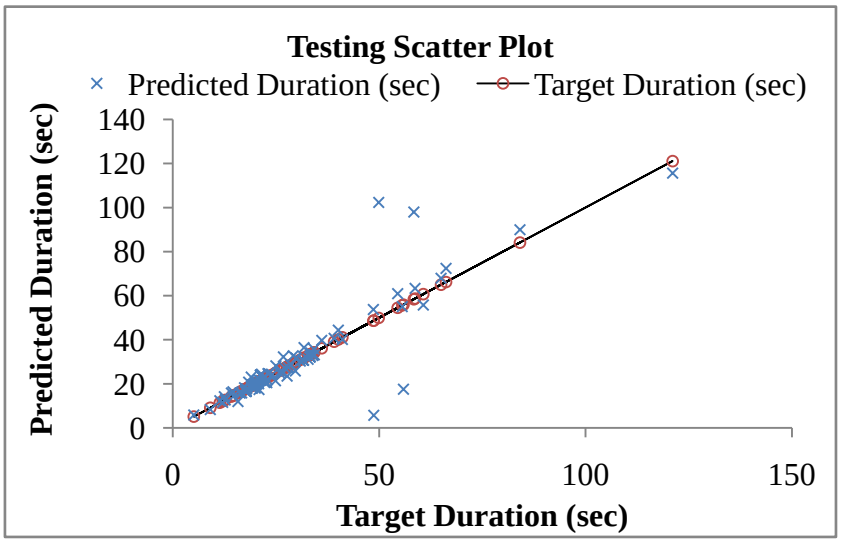

Figure 6.37: Testing scatter plot of predicted duration to target duration for site class C with 4 inputs.

Table 6.60: R, MAE, and RMSE values of AAN model used in test performance to predict duration for class C with 4 inputs.

Correlation	MAE	RMSE
0.878	4.12	4.96

Table 6.61: Few test results of 4- input based network (Duration) for class C.

M	D (in Km)	FM	$\overline{V}_s$ (in m/s)	Desired Duration (in sec)	Network Duration (in sec)
4.6	11	1	329	5.1	5.89
5	139	1	301	15.8	11.97
5.8	61	3	298	18.4	20.81
7.3	43	3	320	19.0	23.12
5.6	87	1	273	26.8	32.27
5.9	103	1	201	48.6	53.77
7.2	93	1	185	121.1	115.67

6.4.3 Three Input Based Network

The three nodes on the input layer for creating the neural network were the earthquake magnitude (M), hypo-central distance (D_{hyp}), average shear wave velocity $\overline{V}_{S30}$ and one node on the output layer as duration (t_D) shown in Fig 6.38.

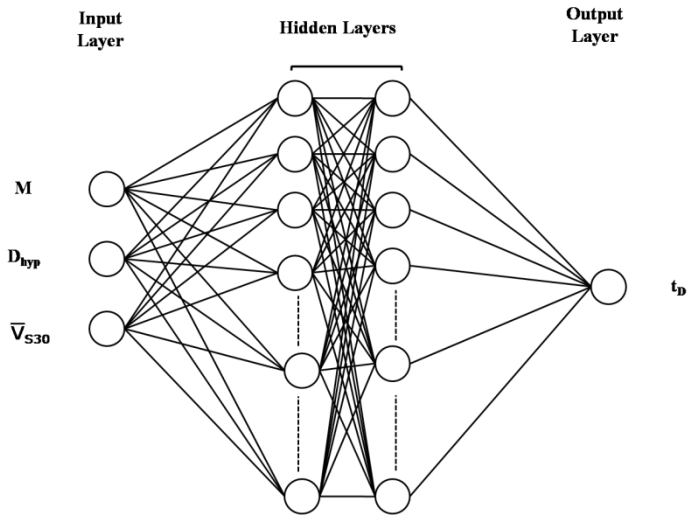

Figure 6.38: Neural network architecture with three nodes on input layer and one node on output layer.

6.4.3.1 Class A

A dataset of 178 was selected randomly from the total set of 214 for training and cross validation and the remaining 36 was used to test the performance of the trained network. Three different data sets of 178 were created and randomized. The three data sets were trained independently and the data set, which gave the minimum network error, was considered for testing the network. Finally ANN model with single hidden layer having 62 neurons, three input neurons and one output neuron showed the best performance. The trained network results and various parameters used for training are mentioned in Table 6.62 and 6.63 respectively. Fig. 6.39 shows training scatter plot for predicted duration to target (real) duration. Fig. 6.40 shows testing scatter-plot for 36 data points which are used to test the prediction capability of above trained model. The result of testing network is defined in terms of R, MAE and RMSE mentioned in Table 6.64. A few test results of three inputs based network for prediction of duration are shown in Table 6.65.

Table 6.62: Network results for 3-62-1 architecture for class A with 3 inputs.

Architecture	Epochs	Correlation	Network Error
3- 62-1	40000	0.895	0.000731

Table 6.63: Parameters used for training neural network 3-62-1 architecture for class A with 3 inputs.

Description	Hidden Layer	Output Layer
Transfer Function	TanhAxon	SigmoidAxon
Learning Rate	0.1	0.1
Momentum	0.6	0.6

Table 6.64: R, MAE, and RMSE values of AAN model used in test performance to predict duration for class A with 3 inputs.

Correlation	MAE	RMSE
0.713	3.10	4.54

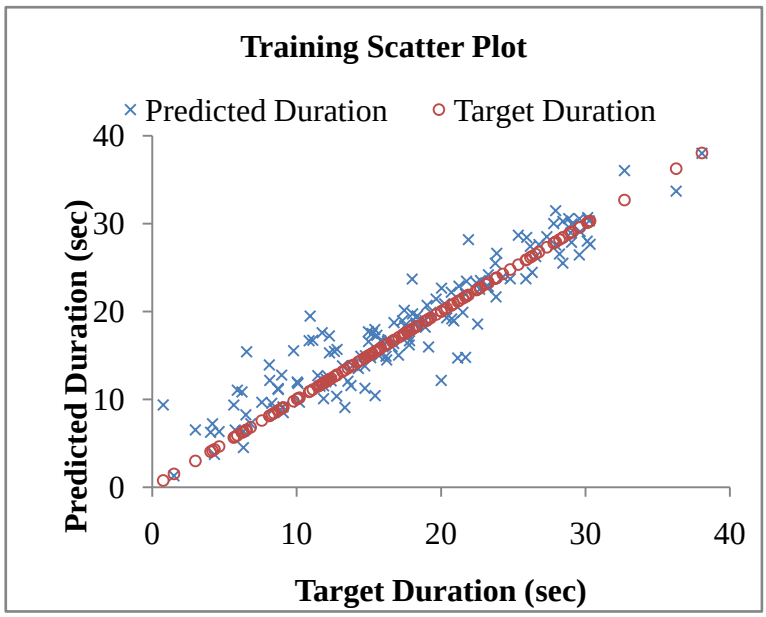

Figure 6.39: Training scatter plot of predicted duration to target duration for site class A with 3 inputs.

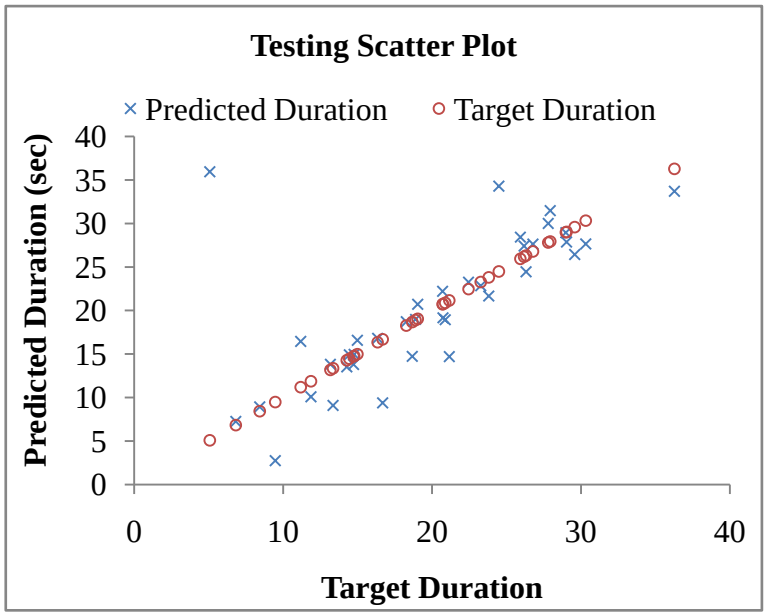

Figure 6.40: Testing scatter plot of predicted duration to target duration for site class A with 3 inputs.

Table 6.65: Few test results of 3- input based network (Duration) for class A.

M	D (in Km)	$\overline{V}_s$ (in m/s)	Desired Duration (in sec)	Network Duration (in sec)
5.3	120	765	5.07	35.96
5.1	134	894	8.42	8.93
6.3	64	817	14.27	13.53
7.2	97	1433	18.27	18.71
5.5	95	1433	23.80	21.67
4.8	76	1433	20.88	18.94
7.0	180	1373	36.28	33.71

6.4.3.2 Class B

A dataset of 1534 was selected randomly from the total set of 1825 for training and cross validation and the remaining 291 was used to test the performance of the trained network. But we were unable to get convergence of network, so we reduced the data by dividing 1825 averaged horizontal earthquake time histories into 4 equals data set each having 456 time histories. These four data sets of 456 were randomized. The four data sets were trained independently and the data set, which gave the minimum network error, was considered for testing the network. A new dataset of 382 was selected randomly from the total set of 456 for training and cross validation and the remaining 74 was used to test the performance of the trained network. Finally ANN model with single hidden layer having 75 neurons, seven input neurons and one output neuron showed the best performance. The trained network results and various parameters used for training are mentioned in Table 6.66 and 6.67 respectively. Fig. 6.41 shows training scatter plot for predicted duration to target duration. Fig. 6.42 shows testing scatter-plot for 74 data points which are used to test the prediction capability of above trained model. The result of testing network is defined in terms of R, MAE and RMSE mentioned in Table 6.68. A few test results of seven inputs based network for prediction of duration are shown in Table 6.69.

Table 6.66: Network results for 3-75-1 architecture for class B with 3 inputs.

Architecture	Epochs	Correlation	Network Error
3- 75-1	43000	0.920	0.001731

Table 6.67: Parameters used for training neural network 3-75-1 architecture for class B with 3 inputs.

Description	Hidden Layer	Output Layer
Transfer Function	TanhAxon	SigmoidAxon
Learning Rate	0.1	0.1
Momentum	0.6	0.6

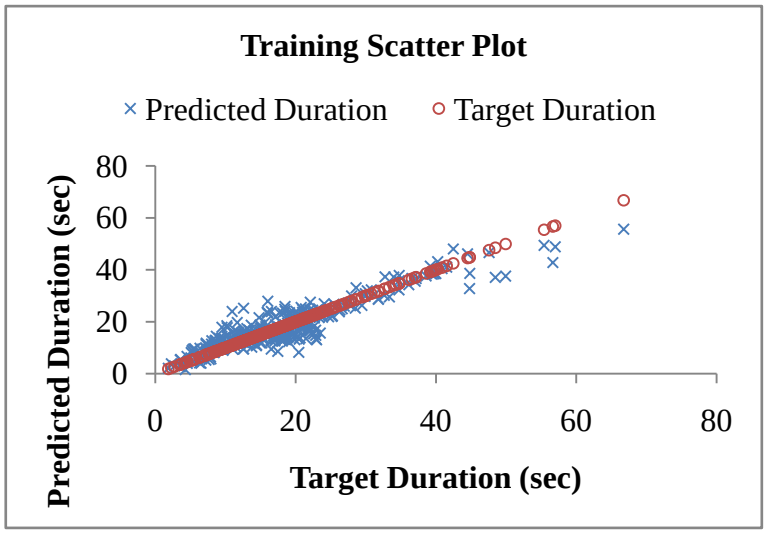

Figure 6.41: Training scatter plot of predicted duration to target duration for site class B with 3 inputs.

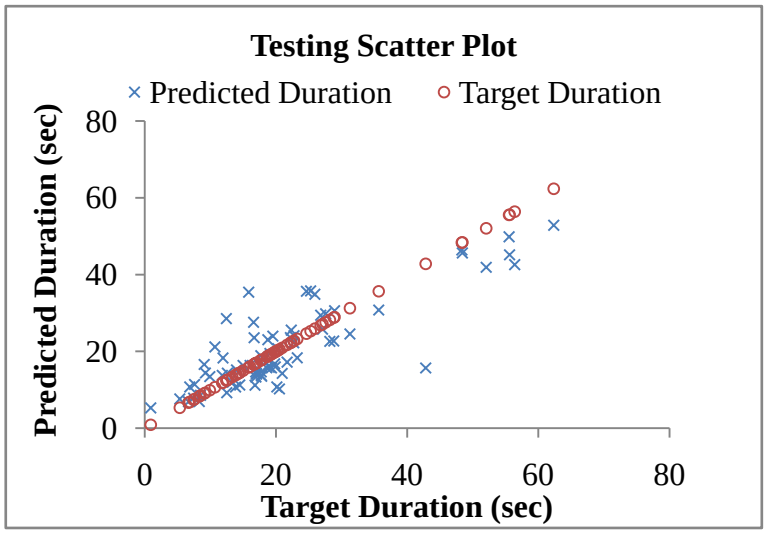

Figure 6.42: Testing scatter plot of predicted duration to target duration for site class B with 3 inputs.

Table 6.68: R, MAE, and RMSE values of AAN model used in test performance to predict duration for class B with 3 inputs.

Correlation	MAE	RMSE
0.843	6.98	7.31

Table 6.69: Few test results of 3- input based network (Duration) for class B.

M	D (in Km)	$\overline{V}_s$ (in m/s)	Desired Duration (in sec)	Network Duration (in sec)
6.1	40	382	8.49	8.58
6.8	159	452	55.55	49.86
5.0	92	412	13.98	15.19
7.3	145	392	18.75	23.04
5.5	185	370	28.20	22.61
4.6	47	421	7.59	11.40
7.0	97	480	16.58	27.60

6.4.3.3 Class C

A dataset of 1618 was selected randomly from the total set of 1926 (Class C) for training and cross validation and the remaining 308 was used to test the performance of the trained network. But we were unable to get convergence of network, to improve the convergence we reduced the data and divided 1926 averaged horizontal earthquake time histories into 4 equal's data set each having 482 time histories. These four data sets of 482 were randomized, trained independently and the data set, which gave the minimum network error, was considered for testing the network. A new dataset of 405 was selected randomly from the total set of 482 for training and cross validation and the remaining 77 was used to test the performance of the trained network. Finally ANN model with single hidden layer having 58 neurons, four input neurons and one output neuron showed the best performance. The trained network results and various parameters used for training are mentioned in Table 6.70 and 6.71 respectively. Fig. 6.43 shows training scatter plot for predicted duration to target duration. Fig. 6.44 shows testing scatter-plot for 77 data points which are used to test the prediction capability of above trained model. The result of testing network is defined in terms of R, MAE and RMSE mentioned in Table 6.72. A

few test results of seven inputs based network for prediction of duration are shown in Table 6.73.

Table 6.70: Network results for 3-58-1 architecture for class C with 3 inputs.

Architecture	Epochs	Correlation	Network Error
3- 58-1	71000	0.910	0.006962

Table 6.71: Parameters used for training neural network 3-58-1 architecture for class C with 3 inputs.

Description	Hidden Layer	Output Layer
Transfer Function	TanhAxon	SigmoidAxon
Learning Rate	0.1	0.1
Momentum	0.6	0.6

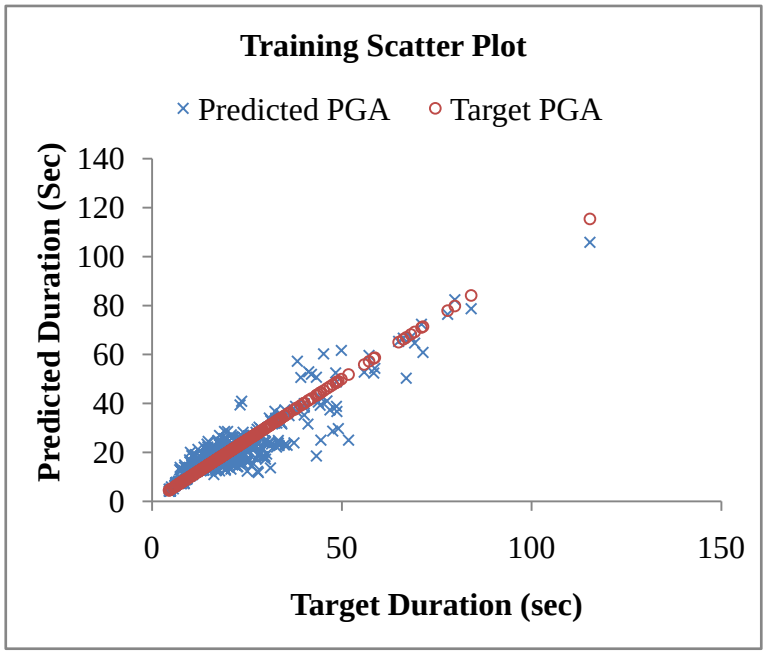

Figure 6.43: Training scatter plot of predicted duration to target duration for site class C with 3 inputs.

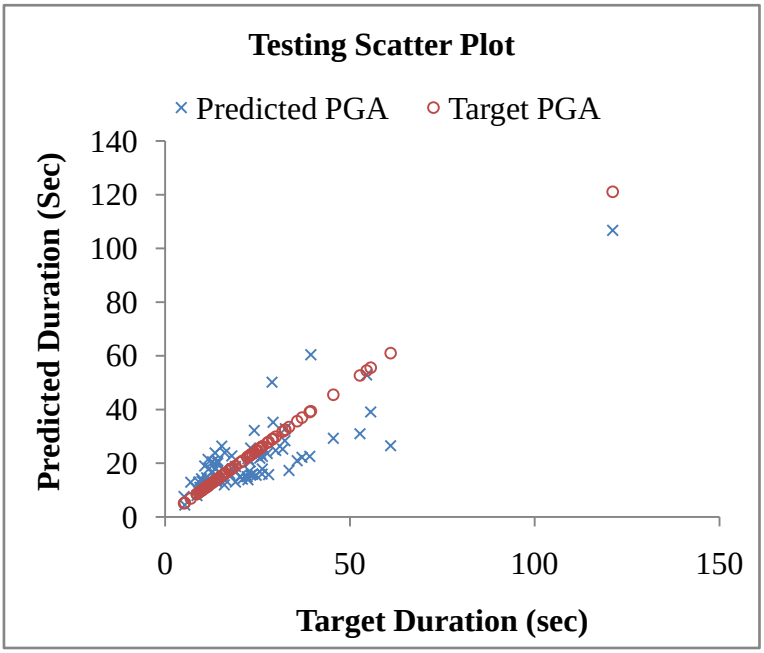

Figure 6.44: Testing scatter plot of predicted duration to target duration for site class C with 3 inputs.

Table 6.72: R, MAE, and RMSE values of AAN model used in test performance to predict duration for class C with 3 inputs.

Correlation	MAE	RMSE
0.841	6.54	14.31

Table 6.73: Few test results of 3- input based network (Duration) for class C.

M	D (in Km)	$\overline{V}_s$ (in m/s)	Desired Duration (in sec)	Network Duration (in sec)
6.1	110	344	5.10	7.55
6.9	156	288	15.5	17.69
7.1	113	231	24.9	23.59
5.0	120	214	26.3	22.54
4.9	136	337	17.5	15.45
5.4	176	360	8.6	7.92
7.2	93	185	121.1	106.72

6.5 RESULTS AND DISCUSSIONS

An ANN model has been developed using three different sets of inputs with seven nodes, four nodes and three nodes in the input layer to make prediction of PGA and t_D for each respective site class and the functional form of model for three different combinations of inputs are shown by Eqn 6.1(a), 6.1 (b), and 6.1 (c). The distribution of data set for class site A, B and C is given in Table 6.1. Cross Validation approach was used for each class dataset and each dataset was divided into three multiple subsets as: (i) The training set, (ii) The validation set, and (iii) The testing set. The training set, consisting of about 68 % of the data set was used to train the network and the validation set, consisting of 16 % of the data set was used for the purpose of monitoring the training process at various stages and to guard against overtraining. The testing set, consists of 16 % of the data set, was used to judge the performance of the trained network. The training was stopped when cross validation error begins to increase and the error has reached minimum value.

Initially, exhaustive search was carried out among a large array of networks with a single and double hidden layer with different number of neurons and based on correlation coefficient, best five performing architectures were chosen. The best performing network in terms of correlation coefficient and network error from the chosen architecture were once again trained for increasing number of epochs, the training was stopped when the validation error was minimum in order to obtain the suitable network model.

The seven nodes architecture consists of the input layer as earthquake magnitude (M), hypo-central distance (D_{hyp}), focal mechanism (FM), average shear wave velocity($\overline{V}_{S30}$); average SPT blow count ($\overline{N}$) ; average shear wave velocity($\overline{V}_{P30}$); and average density of soil ($\overline{\rho}$) and one node on the output layer as PGA. The results of this architecture for all the classes namely A, B, and C are summarized in this section. The sample size considered for the three classes A, B and C are 214(178-36), 1825(1534-291) and 1926(1618-308), respectively. The figures in parenthesis give the number of data selected randomly for training and testing respectively.

The performance of ANN to predict PGA using three types of inputs (7, 4 and 3 input layer) for three classes of soil can be adjudged based on the parameters like correlation (R), MAE and RMSE. The R is a measure of relative correlation and goodness of fit between target and predicted outcome, but extreme values heavily affect it with its range lying between 0 and 1.

Generally, strong correlation exists between two set of variables if it is more than 0.8. The RMSE is the most popular measures of error, which is well suited to iterative algorithms and is a better measure for high value in data set, since it gives a relatively high weight to large errors than small errors. The MAE measure the average magnitude of the errors in a dataset, without considering their direction, gives the same weight to all errors, thus has the advantage that it does not distinguish between the overcome and underestimation and does not get too much influence by higher value.

Table 6.74 lists the values of R, MAE, and RMSE for each AAN models used in test performance to predict PGA and Duration. The values of R are almost ~0.8 for all the cases showing a good correlation between observed and predicted data. However, it may be noted that in all the classes the values of 'R' are at its minimum i.e., less than 0.8 in case of 4 inputs showing that either the reported focal mechanisms do not match with the actual physical process or this parameter is least correlated showing its relatively lesser influence on the predicted value.

Table 6.74: R, MAE, and RMSE values of each AAN models used in test performance to predict PGA.

PGA				
	Inputs	**Correlation**	**MAE**	**RMSE**
Class A	7	0.983	3.86	14.03
	4	0.781	17.30	57.08
	3	0.877	11.20	32.15
Class B	7	0.845	14.81	55.17
	4	0.764	13.98	36.78
	3	0.846	12.92	44.71
Class C	7	0.811	16.53	21.32
	4	0.806	13.50	22.60
	3	0.805	16.55	31.66

The values of parameters used for neural network for various architectures are also given in respective tables along with the scatter diagrams showing the observed and the predicted values. For example, Fig. 6.5 shows testing scatter plot of predicted PGA to target PGA for site class A for 7 inputs. The figure reveals that the prediction is good upto 40 gals. Similar trend

can be observed in Fig. 6.7 showing Testing scatter plot of predicted PGA to target PGA for site class B and Fig. 6.9 Testing scatter plot of predicted PGA to target PGA for site class C. The similar trend is true for 4 and 3 inputs for all the three classes. Based on the observation a conclusion of good prediction in lower range of PGA values can be easily drawn.

A similar exercise to predict SGM duration was carried out for all the three classes with same cases of 7, 4 and 3 input layers. Figure 6.25 to Fig. 6.44 shows the training and testing scatters for the predicted and observed values. The error quantification has been carried out in terms of R, MAE and RSME as given in Table 6.75. The values of R is almost more than 0.8 for all the cases showing a good correlation between observed and predicted data except for two cases of 4 and 3 layers in Class A. The scatter diagram reveals that the duration between 10 to 50 seconds can be predicted faithfully from this approach. The duration definition and its formulae used by various workers generally show much more scatter than the one seen in the prediction diagrams using ANN.

Table 6.75: R, MAE, and RMSE values of each AAN models used in test performance to predict Duration.

PGA				
	Inputs	**Correlation**	**MAE**	**RMSE**
Class A	7	0.936	1.81	4.26
	4	0.720	2.79	3.37
	3	0.713	3.10	4.54
Class B	7	0.986	2.82	6.32
	4	0.887	5.31	5.69
	3	0.843	6.98	7.31
Class C	7	0.938	2.39	3.21
	4	0.878	4.12	4.96
	3	0.841	6.54	14.31

The ANN approach applied to predict PGA and duration in the present study has been tested for the data which was not included in the training part and the error analysis along with the scatter diagrams shows that this approach is a good option to be used as an alternate method to the empirical or theoretical prediction of SGM in terms of PGA and duration.

6.6 SUMMARY

This chapter starts with the formulation of inputs to predict PGA and Duration and then we discuss about the various functional form of ANN model with form with seven, four and three inputs respectively. Then ANN model with seven, four and three input has been developed to predict PGA and Duration for each respective class site which has been defined on the basis of average shear wave velocity. And finally chapter concludes with results and discussion.

Chapter 7

ESTIMATION OF AVERAGE SHEAR WAVE VELOCITY OF SITE USING ANN

7.1 INTRODUCTION

The lessons learnt from the damaging earthquake have not only provided solutions to engineers for the earthquake resistant designs but also helped seismologists to better understand the relation of strong ground motion to the source and media. One of the conspicuous results which are widely accepted amongst the earthquake engineering community is the effects of surface geology on seismic motion. This resulted in a natural conclusion of attributing the severity of damage largely to local site conditions. As a result, site effects need to be given an important consideration in the seismic hazard assessment of an area which is used in prediction of SGM.

Severe consequences of sediment amplification of ground motion during an earthquake are being demonstrated ever since the great 1891 Japan earthquake making this issue as one of the most important questions with respect to understanding and predicting earthquake ground motion. Numerous studies (Bard et al., 1988; Kawase and Aki, 1989; Singh and Ordaz, 1993 and Furumura and Kennett, 1998; Iglesias et al, 2002, 2004, Sitharam et al., 2006, 2007; Sharma et al., 2009, 2012) amply demonstrate large concentration of damage in specific areas due to site-dependent factors related to surface geologic conditions and local soils altering seismic motions. The important observed effects include predominant periods of vibration of soil in situ, large amplification of ground motion in the form of site factors in certain frequency ranges, semi-resonance or resonance of certain building types and consequent deformations or collapses of structures etc. (Kramer, 2003). These evidences show that among all the factors, the local site conditions have a profound influence upon the strong ground motion characteristics. The extent of the influence due to the local site conditions are related to the material properties, geometry of subsurface material, the local topography and the characteristics of ground motion (i.e., amplitude, frequency content and duration) (Vucetic and Dobry, 1991; Borcherdt and Glassmoyer, 1992; Bard and Chavez-Garciaz, 1993; Kramer, 1996; Ansal et al. 2001, Kuo et al., 2009; Krishna et al., 2010; Paul, 2010; Paul et al., 2010). The local soil conditions of a site may substantially alter the subsurface characteristics of

earthquake ground motion by (1) amplifying the ground motion, (2) elongating its duration, (3) generating differential motions (aggravation) (Seed et al. 1976; Chang et al. 1996; Bard, 1997; Sun et al. 2005).

The corollary of the above implicitly necessitate the knowledge of soil section below an earthquake recording station to deconvolve the ground motion for its quantification on hard rock. The local site conditions at a strong motion accelerograph recording station can affect the recorded strong ground motion because the seismic motions at the last moment before reaching the surface of ground or the basement of manmade structures may get strongly amplified. San Francisco (1907) and Mexico City (1985) earthquake are two famous earthquakes in the past that show the consequences of local site effects (Singh et al., 1980; Aki, 1988; Bard, 1988; Singh et al., 1989; Singh et al., 1996). In San Francisco, local amplifications over unconsolidated sediments have shown to be responsible for intensity variation as large as II degrees on MM scale during both the 1907 “big” San Francisco earthquake and the more recent 1989 Loma Prieta earthquake (Chin et al., 1991). Mexico City is situated on very soft lacustrine clay deposits, which led to very large amplification motion during the distant Guerrero Michoacan 1985 earthquake and caused a high death toll and large economic losses (Singh et al., 1988a, 1988b and Lermo et al., 1994). From last two decade destructive earthquakes like Kobe 1995 (Fukushima et al., 2000), Turkey 1999 (Bakir et al., 2002 and Ozel et al., 2002), Bhuj 2001 (Narayan et al., 2004) have clearly demonstrated the additional evidence of the large importance of site effect studies.

There are large numbers of experimental and numerical methods worldwide used to estimate these site effects (Singh et al., 2005; Sitharam et al., 2008a and b; Wen et al., 2008; Mahajan et al., 2004, 2012; Lang et al., 2011; Kuo et al, 2011, 2012 . Most widely accepted method of reflecting the site effects is to classify the recording station based on average shear wave velocity ($\overline{V}_{S30}$). Average shear wave velocity in the top 30 m of soil of a site location is most acceptable parameter to describe soil characteristics; it was also used by many engineering in preparation of design codes (ASCE 7-10, 2000; EN 1998-I, 2004 FEMA 356, 2000, NZS 1170.5, 2001). Thus, geotechnical investigations for determination of average V_s is necessary to be carried out at most of strong motion accelerograph stations installed all over world to characterized the site geology in more refined manner in term of thin and thick deposits.

In India, there are about 500 strong motion instruments and most of them installed in last about 5 to 10 years. Strong ground motion data set in India comprises of at the most 1000 time

histories which are also not centrally available (Singh et al., 2002; Paul et al., 2003, 2005). Other problem of Indian data set is non- availability of geo-technical parameters of the recording site (Samui et al., 2010). Average shear wave velocity for about 30 meter depth is generally available for most of the recording sites in the world. In Japan, all sites have detailed bore log data which is easily available through by registering at their website. Whereas no geotechnical data is available at strong motion recording sites in India except in Gujarat where ISR Gandhinagar has recently done geotechnical investigations at locations of strong motion instruments (including locations of old SRRs installed by IIT Roorkee).

In this scenario, our attempt in present study was to use the huge strong ground motion data set from Japan for understanding the influence of various parameters on ground motion and try to interpolate this understanding in Indian context and then calibrate the same with the recorded data in India. In the present study entire stuff is done in reverse order i.e. instead of predicting PGA and spectral ordinate as output parameter, use them as input parameters and tried to find average shear wave velocity as output parameter by implementing multilayer feed forward Neural Network with back propagation learning scheme using Japanese earthquake. Trained neural networks showed promising performance and were able to predict average shear wave velocities at locations in Japan with very little scatter. Finally trained network based on Japanese dataset was used to predict average shear wave velocity for Indian Himalayan region where multiple strong motion records were available (Sachdeva et al., 2010)

7.2 DEVELOPMENT OF ANN MODEL

7.2.1 Software Support Used

As discussed in previous chapter AlyudaNeuroIntelligence software version 2.2 (677) http://www.alyuda.com/index.html] developed by Alyuda Research, Inc. has been used for development of ANN model.

7.2.2 Forming Inputs and Output

The predictions of average shear wave velocity($\overline{V}_s$) using ANN have been taken up for study. To developed ANN model, a total 18 input variables has been used to made prediction of ($\overline{V}_s$) and the functional form of the model as shown in Fig. 7.1 and also described in Eqn. 7.1

$$\overline{V}_{S30} = f\left(M, D_{hyp}, PGA, \left(\frac{Sa}{g}\right)_{0.03}, \left(\frac{Sa}{g}\right)_{0.05}, \ldots\ldots \left(\frac{Sa}{g}\right)_{3.0}, \left(\frac{Sa}{g}\right)_{4.0}\right)$$

(7.1)

Where, $\overline{V}_{S30}$ = Average shear wave velocity in top 30m of surface layer; M = Earthquake magnitude; D_{hyp} = Hypo-central distance; PGA = Peak ground acceleration and $\left(\frac{Sa}{g}\right)$ = Normalized spectral ordinate at the strong ground motion periods in the range from 0.03 s to 4 s (i.e. 0.03, 0.05, 0.07, 0.1, 0.2, 0.3, 0.4, 0.55, 0.77, 0.75, 1.0, 1.25, 2.0, 3.0, and 4.0).

The distribution of the entire data set w.r.t M, D_{hyp}, PGA and $\overline{V}_{S30}$ is shown in Fig. 7.1. This data set is from Class A sites only. It is pertinent to note that the other data sets from Class B, and Class C consisted of 1825 and 1925 accelerograms respectively were also used to carry out similar analyses as has been done for Class A. However, due to no convergence of neural network could be observed for both class B and C and therefore the results of these two classes are not reported in the present work.

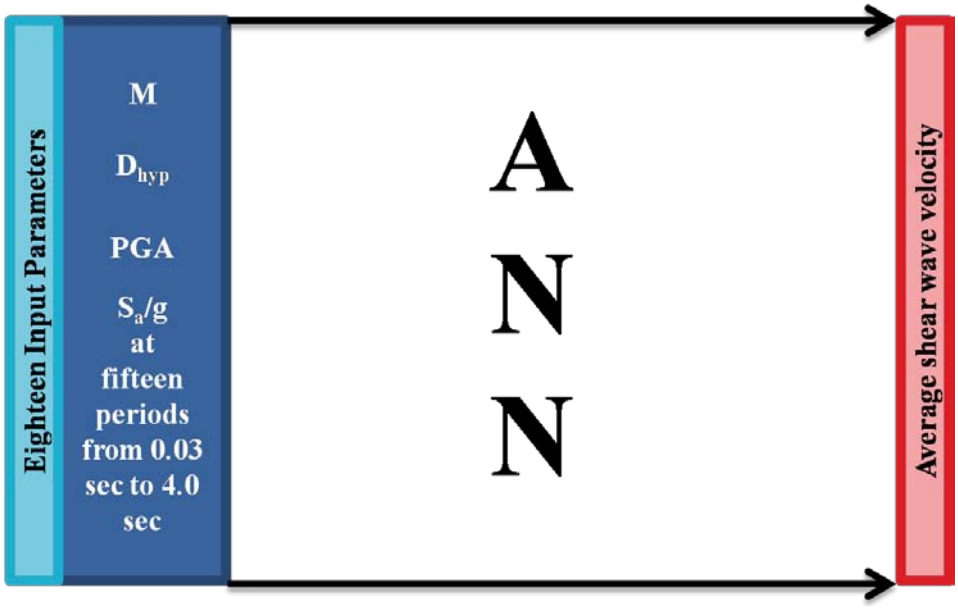

Figure 7.1: Schematic diagram for the Eighteen inputs chosen for prediction of $\overline{V}_{S30}$.

For Class A, 500 averaged horizontal component of recorded time histories varying in Magnitude (M) ranging from 4 -7.4, hypo central distance (D_{hyp}) ranging from 19 - 200 km, PGA ranging from 5 to 1103 cm/s^2, and $\overline{V}_{S30}$ ranging from 770-1433 m/s have been used in this data base. The distribution of the dataset w.r.t M, D_{hyp}, PGA and $\overline{V}_{S30}$ is shown in Fig. 7.2 site class A.

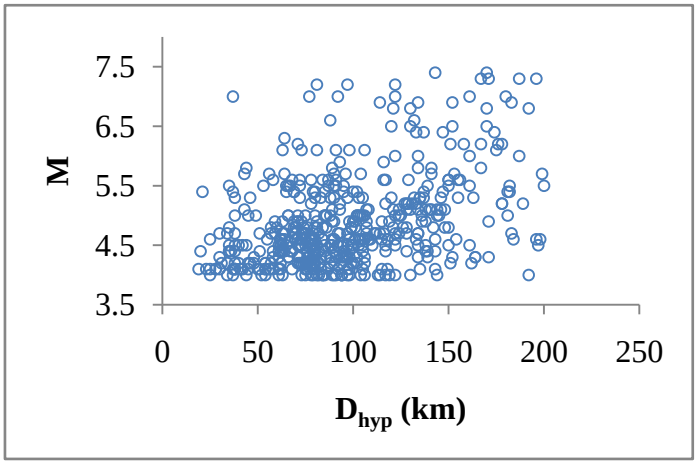

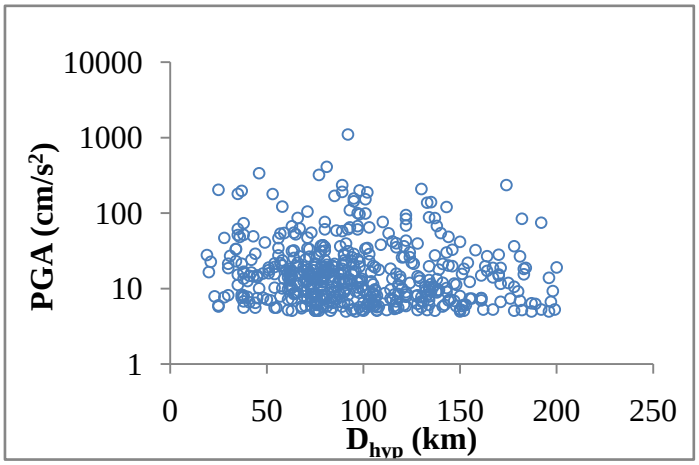

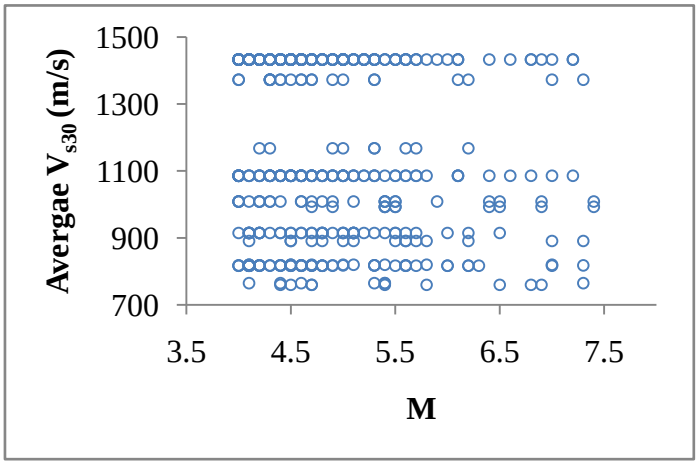

Figure 7.2: Distribution of dataset between M and D_{hyp}, PGA and D_{hyp} , and $\overline{V}_{S30}$ and M for site class A.

7.2.3 Selecting the Training Pairs

The total set of 500 is divided into three multiple subset as: the training set, the validation set, and the testing set. The training set, which consists of about 68 % of the data set, is used to train the network by adjusting the connection weights; the validation set, which is about 16 % of the data set, is used for the purpose of monitoring the training process at various stages and to guard against overtraining. The testing set, which is taken about 16 % of the data set, is used to judge the performance of the trained network. The training is stopped when cross validation error begins to increase i.e. the training is stopped when the cross validation errors is reached minimum value.

7.2.4 Training Phase of ANN

As discussed previously in chapter 3, due to limitation of neural network work only with numeric data and have a limited range of operating value. Therefore, modify the entire dataset before it is fed to a Neural Network. This modification of data is known as pre-processing of data. In pre-processing the whole inputs parameters is converted in the scaling range of -1 to 1 and output parameter is converted in the scaling range of 0 to 1. For conversion of entire data was done using eqn. 7.2 and 7.3 respectively.

$$SF = \frac{(SR_{max} - SR_{min})}{(X_{max} - X_{min})} \tag{7.2}$$

$$X_p = SR_{min} + (X - X_{min}) * SF \tag{7.3}$$

Where, X = actual numeric value of real data ; X_{min} = actual minimum numeric value in data base; X_{max} = actual maximum numeric value in data base; SR_{min} = lower scaling range limit; SR_{max} upper scale range limit; SF = scaling factor and X_p = pre-processed value. After completion of conversion, next step was to decide about the designing of ANN architecture, simply how much number of hidden layers and hidden nodes in each hidden layer required. For this to decide initially an exhaustive search has been carried out among a large array of networks with a single and double hidden layer with different number of hidden neurons to achieved the finest network. From that search, the best performing five architectures were chosen on the basis of correlation coefficient. In the second step, the chosen architecture is then

trained for higher number of epochs with different momentum and learning rate. In the third step the best performing network in terms of correlation coefficient and network error from the chosen architecture are once again trained for increasing number of epochs, the training is stopped when the validation error is minimum in order to obtain the suitable network model. The correlation coefficients (R) and the network error used to evaluate the accuracy of each model are defined as

$$R = \frac{\sum_{i=1}^{n}(X_i - \overline{X}) - (Y_i - \overline{Y})}{\sqrt{\sum_{i=1}^{n}(X_i - \overline{X})^2 \sum_{i=1}^{n}(Y_i - \overline{Y})^2}} \tag{7.4}$$

Where X_i is observed value at i^{th} record, Y_i is predicted value at i^{th} record, n is total number of data points, $\overline{X}$ and $\overline{Y}$is the mean of X_i and Y_i respectively. The correlation coefficient (R) is a statistical measure of strength of the relationship between the actual values and network outputs. The R can range from -1 to +1. The closer R is to 1, the stronger the positive linear relationship, and the closer R is to -1, the stronger the negative linear relationship. When R is near 0 there is no linear relationship. **Network error** is a value in terms of Sum of Squares, it is used to rate the quality of the neural network training process. The smaller the network's error is, the better the network has been trained. Minimization of the error is the main objective of Neural Network training. **Sum-of-Squares** is the most common error function and is the sum of the squared differences between the actual value (target column value) and neural network output.

7.3 EIGHTEEN INPUTS BASED DEVELOPED NETWORK

As described above, the eighteen nodes on the input layer for creating the neural network were the earthquake magnitude (M), hypo-central distance (D_{hyp}), peak ground acceleration (PGA), and 15 normalized spectral ordinates. A set of 421 was selected randomly from the total set of 500 for training and cross validation and the remaining 79 was used to test the performance of the trained networks. Three different data sets of 421 were created and randomized. The three data sets were trained independently and the data set, which gave the minimum network error, was considered for testing the network. Fig. 7.3 shows two hidden layer network model with 39, 35 hidden neurons each layer respectively, eighteen input neurons and one output neuron has been created. The trained network results and various parameters used for training are

mentioned in Table 7.1 and 7.2 respectively. Fig. 7.4 shows training scatter plot for predicted $\overline{V}_{S30}$ to target (observed) $\overline{V}_{S30}$.

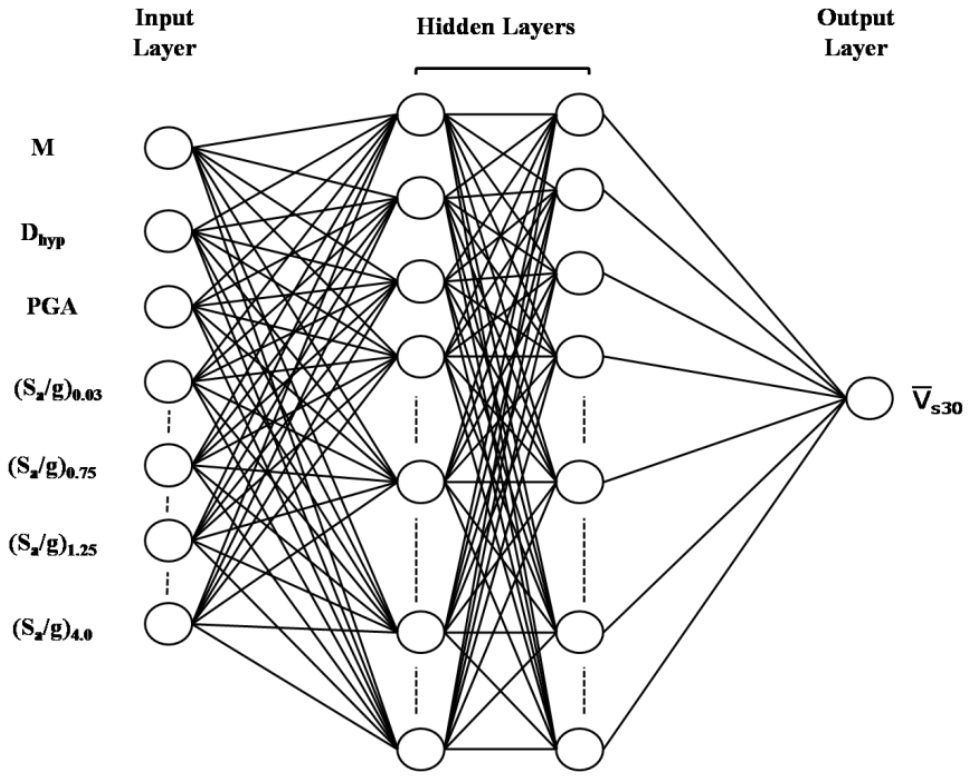

Figure 7.3: Neural network architecture (18-39-35-1) having 18 neurons in input laver, 39, and 35 in 1st and 2nd hidden layers respectively and 1 in output layer for site class A.

Table 7.1: Network results for 18-39-35-1 architecture for class A with 18 inputs.

Architecture	Epochs	Correlation	Network Error
18- 39-35-1	17000	0.987	0.000178

Table 7.2: Parameters used for training neural network 18-39-35-1 architecture for class A with 18 inputs.

Description	Hidden Layer	Output Layer
Transfer Function	TanhAxon	SigmoidAxon
Learning Rate	0.15	0.15
Momentum	0.9	0.9

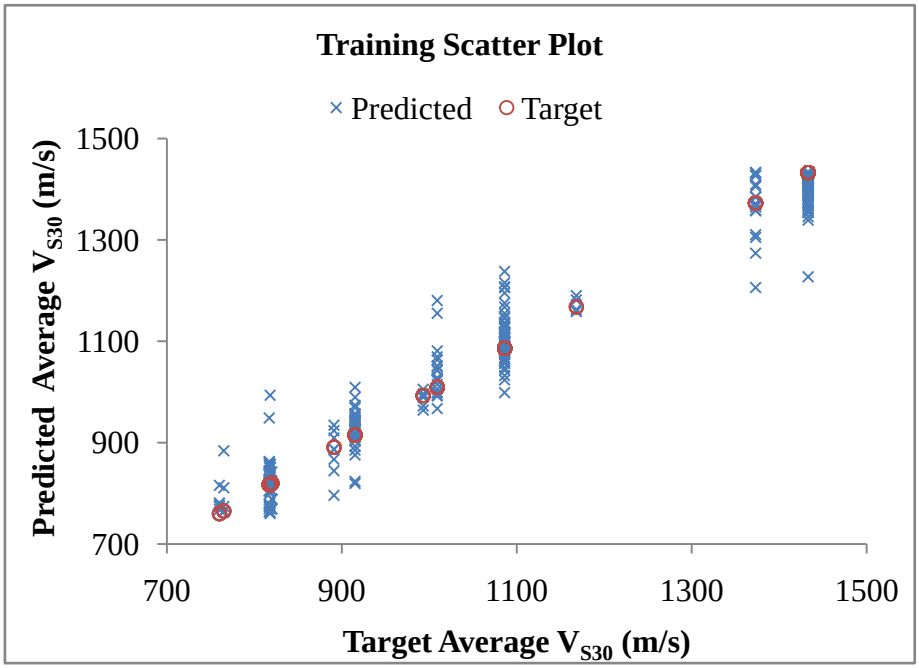

Figure 7.4: Training scatter plot of predicted $\overline{V}_{S30}$ to target $\overline{V}_{S30}$ for site class A.

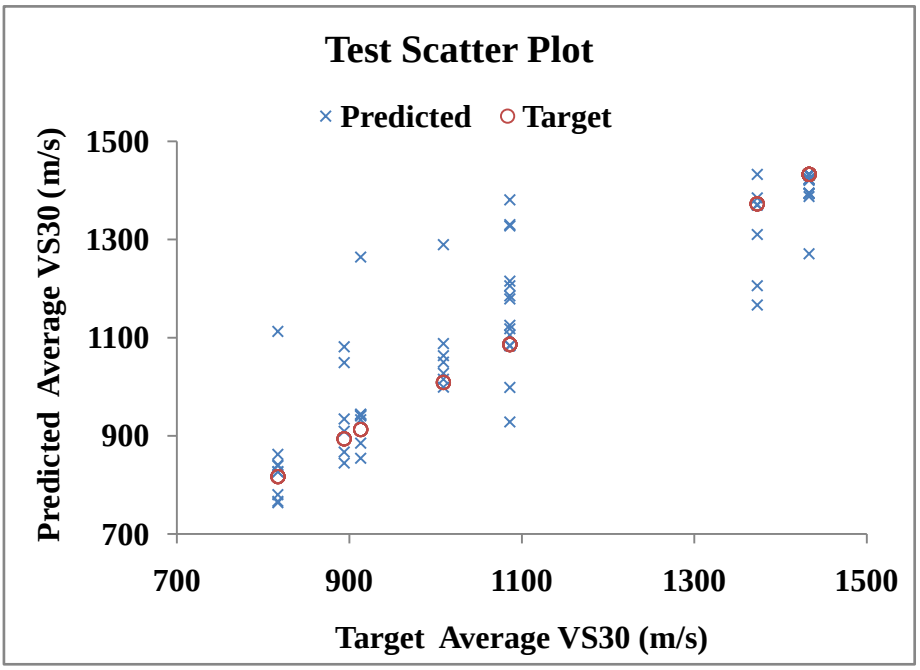

Figure 7.5: Testing scatter plot of predicted $\overline{V}_{S30}$ to target $\overline{V}_{S30}$ for site class A.

Fig.7.5 shows scatter-plot for 77 data points which are used to test the prediction capability of above trained model. The correlation coefficient (R), the root mean square error (RMSE), and the mean absolute error (MAE) used to evaluate the accuracy of model are defined as

$$\mathrm{RMSE} = \sqrt{\frac{1}{n}\sum_{i=1}^{n}(X_i - Y_i)^2} \tag{7.4}$$

$$\mathrm{MAE} = \frac{1}{n}\sum_{i=1}^{n}|(X_i - Y_i)| \tag{7.5}$$

The result of testing network is defined in terms of R, MAE and RMSE mentioned in Table 7.3.

Table 7.3: R, MAE, and RMSE values of AAN model with 18 inputs used in test performance to predict $\overline{V}_{S30}$ for site class A.

Correlation	MAE	RMSE
0.878	4.12	4.96

7.4 RESULTS AND DISCUSSION

As observed from the both training and testing scatter plot Fig. 7.4 and 7.5 respectively for each specific strong ground motion station , a wide range of predicted $\overline{V}_{S30}$ was observed, this is because for each specific station a multiple record of earthquake time histories have been available, and get unique predicted value of $\overline{V}_{S30}$ corresponding to each record of that site. The predicted $\overline{V}_{S30}$ range for each particular recording site is mentioned in column 2 of Table 7.4. To draw some inference from testing scatter plot in Fig. 7.5 a statistical term mean and median to define $\overline{V}_{S30}$ for particular site have been used. Statistical term median show a good representation of predicted $\overline{V}_{S30}$, since it is more close to observed value of $\overline{V}_{S30}$.

Table 7.4: Showing the value of predicted $\overline{V}_{s30}$ at particular sites for testing dataset.

Target $\overline{V}_{S30}$ (m/s) at Particular Site	Predicted $\overline{V}_{S30}$ (m/s) Range at Particular Site	Mean of Predicted $\overline{V}_{S30}$ (m/s) Range at Particular Site	Median of Predicted $\overline{V}_{S30}$ (m/s) Range at Particular Site
1433	1433-1271	1417	1432
1377	1433-1177	1320	1370
1087	1381-928	1172	1152
1009	1290-999	1077	1050
913	1274-854	973	941
894	1081-845	948	922
817	1173-774	847	827

7.4.1 Prediction of $\overline{V}_{S30}$ Using Trained ANN Model for NGA Sites

The generalizing capability of above trained ANN model in this section has been checked. By generalization, simply mean that whether the above trained network work well for outside data that was neither a part of training or testing. To test the prediction capability of above trained for other than Japanese site class A, a new data set was taken from NGA Sites (Pacific Earthquake Engineering Centre (PEER)-NGA (Next Generation Attenuation) database, NGA Flat file Version 7.3, http://peer.berkeley.edu/nga/flatfile.html.) fall in category of site class A. The results of predicted $\overline{V}_{S30}$ for NGA sites are summarized in Table 7.5.

Table 7.5: Showing the value of predicted $\overline{V}_{S30}$ for NGA Site.

Station Name	Target $\overline{V}_{S30}$ (m/s) at site	Predicted $\overline{V}_{S30}$ (m/s) range at site	Mean of predicted $\overline{V}_{S30}$ (m/s) range at site	Median of predicted $\overline{V}_{S30}$ (m/s) range at site	Result (Good/Bad prediction)
Mt Wilson – CITSeisStaion (USA)	822	784-1013	879	797	Good
TTN042 (Taiwan)	845	800-1143	900	848	Good
Vasquez Rocks Park (USA)	997	894-1059	985	1003	Good
TCU085 (Taiwan)	1000	888-1092	977	943	Good
LA - Wonderland Ave (USA)	1223	878-977	918	909	Wrong
Gilroy Array #1 (USA)	1428	792-1077	909	885	Wrong

From Table 7.5 based on estimated value of $\overline{V}_{S30}$ in term of statistical parameter, a concluding remark either the prediction was good or bad have been made. It was easily conclude from the summary of Table 7.5 that given trained model 18-39-35-1 made a successful attempt to predict $\overline{V}_{S30}$ for those NGA sites having $\overline{V}_{s30}$ less than 1100 m/sec. For a site having $\overline{V}_{S30}$ greater than 1100 m/sec, it made a wrong prediction, which may be due to non availability of data for a site having $\overline{V}_{S30}$ between 1100-1400 m/sec used for training purpose (as observed in training scatter plot, Fig. 7.4.).

7.4.2 Prediction of $\overline{V}_{S30}$ Using Trained ANN Model for Indian Sites

Result of estimation of $\overline{V}_{S30}$ from trained ANN model for NGA sites boost the confidence that the above trained model could be useful for Indian sites which fall in category of site class A. In India, Department of Earthquake Engineering, IIT Roorkee has installed a network of 300 strong motion instruments covering North and North East India Himalayan belt (PESMOS, Kumar et al., 2012). But geophysical tests have not been carried out for these sites for $\overline{V}_{S30}$, so attempt has been made to use above trained network to predict $\overline{V}_{S30}$ for those Indian Himalayan sites where at-least 4 past earthquake time histories were available and classified as Class A site (Mittal et al., 2012). Fig. 7.6 shows the predicted $\overline{V}_{S30}$ for Indian sites and the results were summarized in Table 7.6. This estimation of $\overline{V}_{S30}$ for Indian Himalayan sites are first order estimation and need to be validated in future either by borehole method or any other method used for geotechnical investigated at these sites.

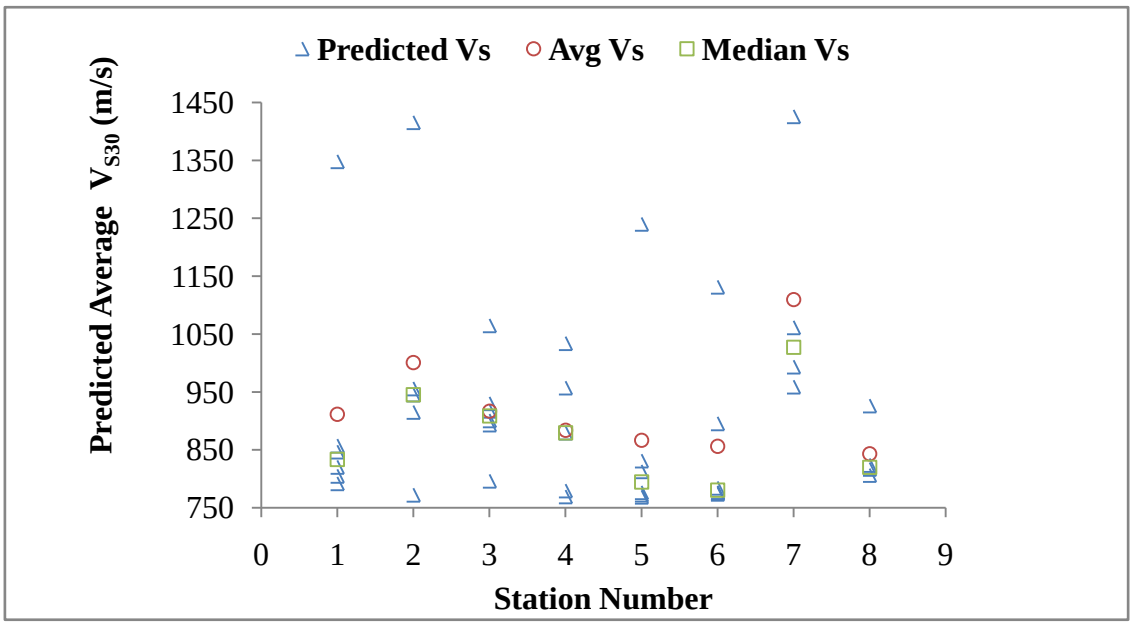

Figure 7.6: Predicted Value of $\overline{V}_{S30}$ by trained ANN model for Indian Himalayan Class A sites.

Table 7.6: Predicted Value of $\overline{V}_{s30}$ by trained ANN model for Indian Himalayan Class A sites.

Station Number	Station Name	Numbers of records available at each site	Predicted $\overline{V}_{S30}$ (m/s) range at each Site	Mean of predicted $\overline{V}_{S30}$ (m/s) range at each Site	Median of predicted $\overline{V}_{S30}$ (m/sec) range at each Site
1	Bageshwar (Uttarakhand)	7	1348-792	911	833
2	Chamba (Himachal Pradesh	5	1417-772	1000	945
3	Gangtok (Sikkim)	7	1075-797	917	909
4	Gairsain (Uttarakhand)	5	1034-779	884	880
5	Kapkot (Uttarakhand)	7	1240-778	877	794
7	Munsayri (Uttarkhand)	7	1131-774	857	780
7	Pithoragarh (Uttarakhand)	4	1427-959	1110	1027
8	Uttarkashi (Uttarkhand)	4	927-807	843	820

7.5 SUMMARY

The main objective of this study was to predict $\overline{V}_{S30}$ of local sites at the strong ground motion recording stations. This aim was achieved by the application of ANN. The experimentally measured $\overline{V}_{S30}$ according to FEMA (357, 2000) for Japan sites as output variable and strong ground motion data of Japan as input (predictor) variables in Eqn.7.1, were used for ANN model development. The study reveals that the developed ANN model has been able to predict $\overline{\mathbf{V}}_{S30}$ based on some of statistical inferences (R, Network Error, Mean, and Median). The overall evaluation of the finding obtained throughout this work reveals that the ANN based model prediction of $\overline{\mathbf{V}}_{S30}$ for strong ground motion recording site are quite impressive. Generally in GMPE's the site condition are incorporated by considering the qualitative description of soil, but using ANN based model the quantitative description of soil property in term of $\overline{\mathbf{V}}_{S30}$ can be used for seismic hazard studies.

Chapter 8

SUMMARY AND CONCLUSIONS

8.1 INTRODUCTION

One of the most challenging issues in earthquake engineering is the prediction of strong ground motion. The prediction is carried out using empirical/semi empirical and/or theoretical procedures but has not been found upto the mark as revealed from the scatter of observed to predicted motion in last few decades. Most of the time, strong ground motion is described in terms of PGA and duration albeit the whole response spectra are used in many of the studies. The empirical prediction requires either a larger set of data set or appropriate methodology to regress the data for developing prediction model. In Indian context, the data set is smaller and the methodologies used in prediction are generally using Ground Motion Prediction Equations which always have some kind of uncertainty associated because in GMPE's always consider the equation form based on prior knowledge of relational information between dependent and independent variable as describe in chapter 2. The literature review made in the present study has amply shown the need of newer technologies like Artificial Intelligence viz., ANN which do not require any prior information about the subtle relation between independent variable (i.e. inputs) and dependent variable (i.e. output). The present chapter summarizes the work carried out in the present study and enumerates various conclusions drawn based on it.

8.2 SUMMARY

The thesis include the background on strong ground motion prediction using GMPEs where detailed discussion have been made of the development of GMPEs and the requirement of dependent and independent parameters. After reviewing the various approaches used for ANN, its feasibility has been worked out to predict SGM. It is of paramount interest to look into the characteristics of strong ground motion before its prediction. The important characteristics of strong ground motion have been described in Chapter 3.

A brief description of Artificial Neural Networks pertaining to present thesis work is presented in Chapter 4. The qualities of ANNs to capture/understand very complex phenomenon and train themselves for prediction form the backbone of generating strong ground motion parameters in

this study. The Multilayer Perceptron neural network model is briefly discussed along with back propagation algorithm.

A brief discussion is presented for Indian strong ground motion database and then a case has been prepared for shifting to compile and process strong motion data from K-NET database of Japan. The influence of soil condition on the shape of response spectra has also been incorporated in discussions. The classification of Japanese earthquake records as per FEMA 356, 2000 as well as IS 1893 (Part 1): 2002 is presented. The chapter concludes with a comparison between the IS 1893 (Part 1): 2002 response spectra and the average and the mean plus one standard deviation spectra for the Japan. In present study, a total of 225978 time histories from 3571 earthquakes recorded at different observatories in Japan having magnitude of 4 and above and source depth less than 200 Km have been downloaded from the internet. Soil profile in term of Standard Penetration Test blow count value, density of soil, including P and S wave velocities structures were also attached to the strong motion data set for further processing. All the **225978** horizontal components of earthquake records were viewed manually and then processed using the software developed for this purpose under this study. To reduce and homogenise the data set for their magnitude, distance, fault parameters, a total of 37046 averaged horizontal components of earthquakes records were finally considered and further classified on the basis of Standard Penetration Test (SPT) blow count ($\bar{N}$) as per IS 1893 (Part1): 2002.

The prime aim of this thesis work was the development of ANN model to predict SGM in terms of PGA and duration that of prime significance in earthquake engineering applications and as well as studies the effect of local site conditions. An ANN model has been developed using three different sets of inputs with seven nodes, four nodes and three nodes in the input layer to make prediction of PGA and duration (t_D) for each respective site class.

For training of ANN dataset, each class has been divided into three multiple sets using cross validation approach as discussed in Chapter 4. The three multiple subsets consists of the training set, the validation set, and the testing set. About 68 % of data constitute the training set which is used to train the network and remaining 32 % was equally dividing into validation and test set. The validation set help to monitor the training of ANN by guard it against overtraining. The training was stopped when cross validation error begins to increase and the error has reached minimum value. Testing set was a set of data which was never exposed to ANN during it training phase once the training phase is over then test set was used to judge the performance

of overall trained network. ANN model generally work on the concept of hidden layers with numbers of neurons it should have, these hidden layer layers perform some non linear function to extract some information from given set of data present to them. So selection of hidden layers with appropriate number of neurons was very critical for the optimum performance of network.

Initially, an exhaustive search was carried out among a large array of networks with a single and double hidden layer with different number of neurons and based on correlation coefficient, best five performing architectures were chosen. The best performing network in terms of correlation coefficient and network error from the chosen architecture were once again trained for increasing number of epochs, the training was stopped when the validation error was minimum in order to obtain the suitable network model.

In first section of work the seven nodes architecture consists of the input layer as earthquake magnitude (M), hypo-central distance (D_{hyp}), focal mechanism (FM), average shear wave velocity ($\overline{V}_{S30}$); average SPT blow count ($\overline{N}$); average shear wave velocity ($\overline{V}_{P30}$); and average density of soil ($\bar{\rho}$) and one node on the output layer as PGA. The results of this architecture for all the classes namely A, B, and C are summarized in this section. The sample size considered for the three classes A, B and C are 214 (142, 36, 36), 1825 (1303, 291, 291) and 1926 (1310, 308, 308), respectively. The figures in parenthesis give the number of data selected randomly for training, validation and testing respectively. The performance of ANN to predict PGA using three cases (with 7 inputs, 4 inputs and 3 three inputs on input layer) for three classes of soil can be adjudged based on the parameters like correlation coefficient (R), root mean squared error (RMSE) and mean absolute error (MAE). The value of R is a measure of goodness of fit between target and predicted outcome, but extreme values heavily affect it with its range lying between 0 and 1. For value of R greater than 0.8, there is a strong correlation exists between two set of variables. For iterative algorithm RMSE is a better choice of measure of error since it gives a relatively large weight to higher errors than small errors whereas, MAE give equal weights to all errors present in dataset, is just simply measure the average magnitude of the errors in a dataset, without considering their direction. MAE have the advantage that it cannot distinguish between overrated and underestimated predicted values, and does not get too much influence by higher value.

For the prediction of PGA, the values of R are observed to be almost ~0.8 for all the cases showing a good correlation between observed and predicted data. However, it may be noted

that in all the classes the values of 'R' are at its minimum i.e., less than 0.8 in case of 4 inputs showing that either the reported focal mechanisms do not match with the actual physical process or this parameter is least correlated showing its relatively lesser influence on the predicted value. The values of parameters used for neural network for various architectures are also given in respective tables along with the scatter diagrams showing the observed and the predicted values. For example, Fig. 6.5 shows testing scatter plot of predicted PGA to target PGA for site class A with 7 inputs. The figures reveal that the prediction is good upto 40 gals. Similar trend can be observed in Fig. 6.7 showing testing scatter plot of predicted PGA to target PGA for site class B and Fig. 6.9 testing scatter plot of predicted PGA to target PGA for site class C. The similar trend is true for inputs 4 and 3 for all the three classes. Based on the observation a conclusion of good prediction in lower range of PGA values can be easily drawn.

In 2nd section a similar exercise to predict SGM duration was carried out for all the three classes with same cases of 7, 4 and 3 inputs on input layer. Figure 6.25 to Fig. 6.44 shows the training and testing scatters for the predicted and observed values. The error quantification has been carried out in terms of R, MAE and RSME as given in Table 6.75. The values of R is almost more than 0.8 for all the cases showing a good correlation between observed and predicted data except for two cases of 4 and 3 layers in Class A. The scatter diagram reveals that the duration between 10 to 50 seconds can be predicted faithfully from this approach. The duration definition and its formulae used by various workers generally show much more scatter than the one seen in the prediction diagrams using ANN.

The ANN approach applied to predict PGA and duration in the present study has been tested for the data which was not included in the training part and the error analysis along with the scatter diagrams shows that this approach is a good option to be used as an alternate method to the empirical or theoretical prediction of SGM in terms of PGA and duration.

In last section of work objective of this study is to predict $\overline{V}_{S30}$ of local sites at the strong ground motion recording stations. This aim is achieved by the application of ANN. The experimentally measured $\overline{V}_{S30}$ according to FEMA (356, 2000) for Japan sites as output variable and strong ground motion data of Japan as input (predictor) variables in Eqn. 7.1, are used for ANN model development. Table 7.5 presented the result to predict $\overline{V}_{S30}$ for NGA sites by above trained eighteen input based model and it was concluded that the given trained model 18-39-35-1 made a successful attempt to predict $\overline{V}_{S30}$ for those sites having $\overline{V}_{S30}$ between 760 - 1100 m/sec. For a site having $\overline{V}_{S30}$ greater than 1100 m/sec made a wrong prediction, this is

due to non availability of data for a site having $\overline{V}_{S30}$ between 1100-1400 m/sec used for training purpose (as observed from Fig. 7.4.). Finally above trained model has been used to predict $\overline{V}_{S30}$ for Himalayan sites where at least four previous recorded earthquake time histories were available. The study results that the developed ANN model is able to predict $\overline{V}_{S30}$ based on some of statistical inferences (R, network error). The overall evaluation of the findings obtained throughout this work reveals that the ANN based model prediction of $\overline{V}_{S30}$ for strong ground motion recording site are quite impressive. Generally in GMPE's the site condition are incorporated by considering the qualitative description of soil, but using ANN based model the quantitative description of soil property in term of $\overline{\mathbf{V}}_{S30}$ can be used for seismic hazard studies.

8.3 CONCLUSIONS

In present study the feasibility of using Artificial Intelligence to Predict Strong Ground Motion Parameter has been carried out. The main objective was to develop ANN's (i.e. Artificial Neural Networks) to predict SGM, duration of SGM and local site condition from the observed SGM at a given site using different combination of inputs i.e. magnitude, hypo-central distance, average shear wave velocity, focal mechanism, average primary velocity, average soil density, average Standard penetration Test (SPT). The results show that the ANN can be used as an alternate methodology instead of prediction through GMPEs. The main conclusions drawn from the present research work are enumerated as below:

1. An alternate methodology for prediction of Strong Ground Motion has been developed in the present study
2. Artificial Intelligence has been critically reviewed for its use in earthquake Engineering and it may be used to predict Strong Ground Motion
3. An ANN has been developed to integrate methodology to predict SGM, local site conditions and duration of SGM from the observed SGM at a given site.
4. The results of the prediction of PGA and SGM based on the Japanese data have been validated using the data set which was not used in training. The trained network has been used for Indian conditions and the error analysis reveal that the same can be used to predict SGM along with its duration for A, B and C class of soil.

5. The ANN with architecture as 18-39-35-1 and with eighteen inputs including magnitude, hypo-central distance, PGA and fifteen normalized spectral ordinates has been developed for predicting average shear wave velocity for the site.
6. The ANN has been applied to NGA model and after validation has been used for Indian conditions, in Himalayas where the error analysis reveals a good match with the observed data.

8.4 SCOPE FOR FURTHER STUDY

There is no limit on the future development of such methodologies but a brief list has been proposed to be the future scope of the present work which is not exhaustive in itself due to limited knowledge of future trends.

1. The performance of networks can be improved by carrying a detailed parametric study on the optimal network to be used to predict strong motion parameters. Future work may also examine the application of hybrid artificial intelligence techniques, Support Vector.
2. The present work can be extend for better performance by further classification of data based on local and regional earthquake.
3. The present work can be extended for the prediction of additional strong motion parameters such as peak ground velocity, peak ground displacements, spectral values etc.
4. The present work can be extended by including additional terms, such as basin depth, if these can be unambiguously supported by data.
5. This work can further be extended for vertical components of earthquake records.

List of Papers Publications

Journals (Published/Accepted)

1. Kumar, A., Mittal, H., **Sachdeva, R.,** and Kumar, A. (2012). Indian strong motion instrumentation network. Seismological Research Letters, 83(1): 59-66.

Conferences (National/International)

1. **Sachdeva, R.,** Kumar, A. and Sharma, M.L. (2010). Prediction of Average Shear Wave Velocity of Site using Strong Ground Motion Records and ANN. In 14th Symposium on Earthquake Engineering, Indian Institute of Technology, Roorkee, Dec 17–19, 2010, 126-137 New Delhi: Elite Publishing.

2. **Sachdeva, R.,** Kumar, A. and Sharma, M.L. (2012). Estimation of Peak Ground Acceleration using Artificial Neural (Paper ID: 1847). 15WCEE, Lisbon, Portugal.

BIBLIOGRAPHY

1. Abrahamson, N.A., Silva, W.J. (1997). Empirical response spectral attenuation relations for shallow crustal earthquakes. Seismological Research Letters, 68 (1): 94-127.

2. Abrahamson, N.A., Shedlock, K. (1997). Overview of ground motion attenuation relations. Seismological Research Letters, 68 (1): 9-23.

3. Adeli, H. (2001). Neural Networks in Civil Engineering: 1989-2000. Computer Aided Civil and Infrastructure Engineering, 16(2): 126-42.

4. Aki, K. (1988). Local site effects on strong ground motion. In: Earthquake Engineering and Soil Dynamics II-Recent Advances in Ground Motion Evaluation, American Society of Civil Engineers (ASCE), 103-155.

5. Alves, E.I. (2006). Earthquake forecasting using neural networks: results and future work. Nonlinear Dynamics, 44(1-4): 341–349.

6. Alyuda NeuroIntelligence (2002). User manual version 2.2, Alyuda Research Company, [http://www.alyuda.com/index.html].

7. Ambraseys, N.N., and Boomer, J.J. (1991). The attenuation of ground accelerations in Europe. Earthquake Engineering and Structural Dynamics, 20: 1179-1202.

8. American Society of Civil Engineers (ASCE 7-10) June (2010). Minimum design loads for buildings and other structures, American Society of Civil Engineers, Reston, Virginia, 658 pp.

9. Amiri, G.G. and Bagheri. A. (2008). Application of wavelet multi resolution analysis and artificial intelligence for generation of artificial earthquake accelerograms. Structural Engineering and Mechanics, 28(2): 153-166.

10. Amiri, G.G. and Bagheri. A. (2008). New method for Generation of Artificial Earthquake Record, The 12th World Conference of International Association for Computer Methods and Advances in Geomechanics (IACMAG), pp. 1763-1769, Goa, India, Oct. 2008.

11. Anbazhagan, P., and Sitharam, T.G. (2008a). Seismic microzonation of Bangalore, India. Journal of Earth System Science 117(2): 833-852.

12. Anbazhagan, P., and Sitharam, T.G. (2008b). Site Characterization and Site Response Studies Using Shear Wave Velocity, Journal of Seismology and Earthquake Engineering, 10(2): 53-67.

13. Anderson, J.A. (2003). An Introduction to Neural Networks. Prentice Hall.

14. Ansal, A.M., Iyisan, R., Gullu, H. (2001). Microtremor measurements for the microzonation of Dinar. Pure Applied Geophysics 158(12): 2525-2541.

15. Araya, R., and Saragoni, G.R. (1984). Earthquake accelerogram destructiveness potential factor, in Proceedings of the Eighth World Conference on Earthquake Engineering, San Francisco, California, U.S.A., pages 835 – 842.

16. Arias, A. (1970). A measure of earthquake intensity, In Seismic Design for Nuclear Power Plants, Hansen, R., Editor, pages 438-469, MIT Press, Cambridge, Massachusetts.

17. Arjun, C.R. (2008). Application of Artificial Neural Networks for Generating Strong Ground Motion Parameters, M.Tech. Thesis, Department of Earthquake Engineering. Indian Institute of Technology, Roorkee, Roorkee

18. Arjun, C.R. and Kumar Ashok (2009). Artificial Neural Network Based Estimation of Peak Ground Acceleration, Journal of Indian Society of Earthquake Engineering, 46(1): 19-28, Paper No. 501.

19. Atkinson, G.M. (1997). Empirical ground motion relations for earthquakes in the Cascadia region, Canadian Journal of Civil Engineering, 64-77.

20. Atkinson, G.M., and Boore, D.M. (1990). Recent trends in ground motion and spectral response relations for North America. Earthquake Spectra, 6(1): 15-35.

21. Atkinson, G.M., and Boore, D.M. (2006). Earthquake ground motion prediction equations for eastern North America. Bull. Seismol. Soc. Am., 96: 2181-2205.

22. Bakir, B.S., Sucuoglu, H., and Yilmaz, T. (2002). An Overview of local site effects and the associated building damage in Adapazari during the 17 August 1999 Izmit earthquake, Bull. Seismol. Soc. Am., 92(1): 509 -526.

23. Bard, P.Y. (1997). Local effects on strong ground motion: Basic physical phenomena and estimation methods for microzoning studies, advanced study course on seismic risk (SERINA), Thessaloniki, Greece, 229-299.

24. Bard, P.Y., Campillo, M., Chavez-Garcia, F.J., and Sanchez-Sesma, F.J. (1988). The Mexico earthquake of September 19, 1985-A theoretical investigation of large and small scale amplification effects in the Mexico City Valley. Earthquake Spectra, 4: 609-633.

25. Bard, P.Y., Chavez-Garciaz, F.J. (1993). On the decoupling of surficial sediments from surrounding geology at Mexico-City, Bull. Seismol. Soc. Am., 83(6): 1979–1991.

26. Barrile, V., Cacciola, M., DAmico,S., Greco, A., Morabito, F.C. and Parrillo, F. (2006). Radial basis function neural networks to foresee aftershocks in seismic sequences related to large earthquakes, in Proceedings of the 13th International Conference on Neural Information Processing, Part II (ICONIP ’06) ,vol. 4233 of Lecture Notes in Computer Science, pp. 909–916, Hong Kong, October 2006.

27. Baziar, M.H. and Ghorbani, A. (2005). Evaluation of lateral spreading using artificial neural networks. Soil Dynamics and Earthquake Engineering, 25(1): 1-9.

28. Berke, L., and Hajela, P. (1991). Application of neural networks in structural optimization. NATO/AGARD Advanced Study Institute, 23(I-II): 731-745.

29. Bernreuter, D. L., J. B. Savy, R. W. Mensing, and D. H. Chung (1984). Development of Eastern United States ground motion models, Appendix C in Seismic Hazard Characterization of the Eastern United States: Methodology and Interim Results [or Ten Sites, U. S. Nuclear Regulatory Commission Rept.NUREG/CR-3756.

30. Bessasson, B. and Kaynia, A.M. (2002). Site amplification in lava rock on soft sediments. Soil Dynamics & Earthquake Eng., 22: 525-540.

31. Biot, M.A. (1941). A mechanical analyzer for the prediction of earthquake stresses, Bull. Seismol. Soc. Am., 31(2): 151-171.

32. BIS (2002). Criteria for earthquake resistant design of structures, IS 1893 (part 1). Bureau of Indian Standards, New Delhi.

33. Bishop, C.M. (1995). Neural Networks for Pattern Recognition, Clarendon Press, Oxford University, UK.

34. Bolt, B.A. (1969). Duration of strong motion, In Proceedings of the Fourth World Conference on Earthquake Engineering, Santiago, Chile, pp 1304-1315.

35. Bommer, J.J. and Martinez-Pereira, A. (2000). Strong Motion Parameters: Definition, Usefulness and Predictability, Proceedings of the Twelfth World Conference on Earthquake Engineering, Auckland, New Zealand, 206.

36. Bommer, J.J., Martinez-Pereira (1999). The effective duration of earthquake strong motion, J Earthquake Eng, 3(2): 127-72.

37. Bommer, J.J., Stafford, P.J., and Alarcon J.E. (2009). Empirical equations for the prediction of the significant, bracketed, and uniform duration of earthquake ground motion, Bull. Seismol. Soc. Am., 99(6): 3192-3201.

38. Boominathan, A., and Krishna Kumar, S. (2010). A Site Specific Study on Evaluation of Design Ground Motion Parameters. International Journal of Geotechnical Earthquake Engineering (IJGEE) 1(1): 1-25.

39. Boominathan, A., Dodagoudar, G.R., Suganthi, A. and Maheswari, R.U. (2008). Seismic hazard assessment of Chennai city considering local site effects, Journal of Earth System Science, 117, S2, 853-863.

40. Boore, D. M., & Joyner, W. B. (1982). The empirical prediction of ground motion. Bulletin of the Seismological Society of America, 72(6), S43–S60. Part B.

41. Boore, D.M., Joyner, W.B., and Fumal, T.E. (1993). Estimation of response spectra and peak acceleration from western North American earthquakes: An interim report, 93-509. U.S. Geological Survey, p 70.

42. Boore, D.M., Joyner, W.B., and Fumal, T.E. (1994). Estimation of response spectra and peak accelerations from Western North American earthquakes, an interim report. Part 2. Open-File Report 94-127. US Geological Survey.

43. Boore, D.M., Joyner, W.B., and Fumal, T.E. (1997). Equations for estimating horizontal response spectra and peak acceleration from western North American earthquakes: A summary of recent works. Seismological Research Letters, 68 (1): 128-153.

44. Borcherdt, R.D. (1970). Effects of local geology on ground motion near San Francisco Bay. Bull. Seism. Soc. Am., 60(1): 29-61.

45. Borcherdt, R.D. (1976). Estimates of Site-Dependent Response Spectra for Design (Methodology and Justification), Earthquake Spectra, 10(4): 617-653. doi:10.1193/1.1585791.

46. Borcherdt, R.D. and Gibbs, J.F. (1976). Effects of local geological conditions in the San Francisco Bay region on ground motions and the intensities of the 1906 earthquake. Bull. Seism. Soc. Am., 66(2): 467-500.

47. Borcherdt, R.D., and Glassmoyer, G. (1992). On the characteristics of local Geology and their influence on ground motions generated by the Loma-Prieata earthquake in the San-Francisco bay region, California. Bull. Seism. Soc. Am., 82(2): 603-641.

48. Building Seismic Safety Council (BSSC) (2003). NEHRP (National Earthquake Hazards Reduction Program) Recommended provisions for seismic regulations for new buildings and other structures (FEMA 450), part 1: provisions, Fedral Emergency Management Agency, National Institute of Building Sciences, Washington,DC, http://www.nehrp.gov/pdf/fema450provisions.pdf.

49. Campbell, K. W., & Bozorgnia, Y. 2003a. Erratum: Updated near-source ground-motion (attenuation) relations for the horizontal and vertical components of peak ground acceleration and acceleration response spectra. Bulletin of the Seismological Society of America, 93(3), 1413.

50. Campbell, K. W., & Bozorgnia, Y. 2003b. Erratum: Updated near-source ground-motion (attenuation) relations for the horizontal and vertical components of peak ground acceleration and acceleration response spectra. Bulletin of the Seismological Society of America, 93(4), 1872.

51. Campbell, K. W., & Bozorgnia, Y. 2003c. Erratum: Updated near-source ground-motion (attenuation) relations for the horizontal and vertical components of peak ground acceleration and acceleration response spectra. Bulletin of the Seismological Society of America, 94(6), 2417.

52. Campbell, K.W. (1981). Near source attenuation of peak horizontal acceleration. Bull. Seism. Soc. Am., 71(6): 2039-2070.

53. Campbell, K.W. (1985). Strong motion attenuation relationships: A ten-year perspective, Earthquake Spectra, 1(4): 759-804.

54. Campbell, K.W. (1997). Empirical near-source attenuation relationships for horizontal and vertical components of peak ground acceleration, peak ground velocity, and pseudo-absolute acceleration response spectra. Seismological Research Letters, 68(1): 154-179.

55. Carpenter, G. And Grossberg, S. (1998). In adaptive resonance theory (ART), the handbook of brain theory and neural networks, (ed. M.A. Arbib), MIT Press, Cambridge, MA., pp 79-82.

56. Chang, S.W., Bray, J.D., Seed, R.B. (1996). Engineering implications of ground motions from the Northridge earthquake. Bull. Seism. Soc. Am., 86: 270-288.

57. Chavez-Garcia, F. J., and Bard, P.Y. (1994). Site effects in Mexico City eight years after the September 1985 Michoacan earthquake. SoilDynamics and Earthquake Engineering, 13: 229–247.

58. Chen, W.F., and Scawthorn, C. (2003). Earthquake Engineering Handbook, CRC Press, New York.

59. Chen, Z. and Stewart, R.R. (2006). A multi-window algorithm for real-time automatic detection and picking of P-phases of microseismic events, CREWES Research paper, 18: 1-9.

60. Chester, D.L. (1990). Why two hidden layers are better than one? International Joint Conference on Neural Networks, 1: 265-268.

61. Chin, B.H., and Aki, K. (1991). Simultaneous study of the source, path, and site effects on strong motion during the 1989 Loma Prieta earthquake: A preliminary result on pervasive nonlinear site effects. Bull. Seismol. Soc. Am., 81: 1859-1884.

62. Clough, R.W., and Penzien, J. (2003). Dynamics of Structures, Third Edition, Computers & Structures, Inc., Berkeley, CA.

63. Dai, H., and Macbeth, C. (1995). Automatic picking of seismic arrivals in local earthquake data using an artificial neural network. Geophysical Journal International, 120(3): 758-774.

64. Dai, H., and Macbeth, C. (1997a). Application of back propagation neural networks to identification of seismic arrival types, Science Direct, Physics of the Earth and Planetary Interiors, 101 (3-4), 177-188.

65. Dai, H., and Macbeth, C. (1997b). The application of back-propagation neural network to automatic picking seismic arrivals from single-component recordings. Journal of Geophysical Research B, 102(B7): 15105–15113.

66. Dawson, C.W. and Wilby, R. (1998). An artificial neural network approach to rainfall-runoff modelling. Hydrological Sciences Journal, 43(1): 47–66,

67. Demuth, H., Beale, M. and Hagan, M. (2006). Neural Network Toolbox 5: User's Guide, The Mathworks, Inc., Natick, Mass, USA.

68. Derras, B., Bekkouche, A. and Zendagui, D. (2010). Neuronal approach and the use of kik-net network to generate response spectrum on the surface. Jordan Journal of Civil Engineering, 4(1): 12-21.

69. Douglas, J. (2001). A comprehensive worldwide summary of strong motion attenuation relationships for peak ground acceleration and spectral ordinates (1969-2000), ESEE Report 01.

70. Douglas, J. (2002). Errata of and additions to ESEE Report No. 01-1: 'A comprehensive worldwide summary of strong-motion attenuation relationships for peak ground acceleration and spectral ordinates (1969 to 2000)'. Dept. report. Department of Civil and Environmental Engineering, Imperial College, London

71. Douglas, J. (2003). Earthquake ground motion estimation using strong motion records: a review of equations for the estimation of peak ground acceleration and response spectral ordinates, Earth Science Reviews, 61(1-2): 43-104.

72. Douglas, J. (2011). Ground-motion prediction equations 1964–2010. PEER Report 2011/102, Pacific Earthquake Engineering Research Center College of Engineering University of California, Berkeley, April 2011.

73. EN1998-1 (Eurocode 8). Design of Structures for Earthquake Resistance, Part 1: General Rules, Seismic Actions and Rules for Buildings. European Committee for Standardization (CEN), Brussels, Belgium, December 2004.

74. Fahlman, S.E. and Lebiere, C. (1988). Faster Learning Variations on Error Backpropagation: An Emprirical Study. Carnegie-Mellon Summer Workshop on Neural Networks.

75. Fallgren, R. B., P. C. Jennings, J. L. Smith, and D. K. Ostrom (1974). Aseismic design criteria for electrical facilities, J. Power Div., Proc. ASCE 100, 1-14.

76. Faraway, J., and Chatfield, C. (1998).Time series forecasting with neural networks: A comparative study using the airline data, Applied Statistics, 47(2): 231-250.

77. Fausett, L.V. (1994). Fundamentals of Neural Networks: Architecture, Algorithms, and Applications, Prentice-Hall, Englewood Cliffs, New Jersey, USA.

78. FEMA (2000). Prestandard and Commentary for the Seismic Rehabilitation of Buildings, FEMA-356, Federal Emergency Management Agency, Washington, DC, U.S.A.

79. Flood, I. (1991). A Gaussian based neural network architecture and complementary training algorithm, Proceedings of the International Joint Conference on Neural Networks, New York, 171-176.

80. Flood, I. and Kartam, N. (1994). Neural network in civil engineering I: Principles and understanding. Journal of Computing in Civil Engineering, 8(2): 131-148.

81. Fukushima and Yoshimitsu et al (1996). A new attenuation relation for strong ground motion in Japan based on recorded data.

82. Fukushima, Y., and Tanaka, T. (1990). A new attenuation relation for peak horizontal acceleration of strong ground motion in Japan. Bull. Seismol. Soc. Am., 80(4): 757-783.

83. Fukushima, Y., Irikura K., Uetake, T., and Matsumoto, H. (2000). Characteristics of Observed Peak Amplitude for Strong Ground Motion from the 1995 Hyogoken Nandu (Kobe) Earthquake. Bull. Seism. Soc. Am., 90(3): 545-565.

84. Furumura T., and Kennett, B. L. N. (1998). On the nature of regional seismic phases-III. The influence of crustal heterogeneity on the wave field for subduction earthquakes: the 1985 Michoacan and 1995 Copala,

85. Galushkin, A.I. (2007). Neural Network Theory, Springer Berlin Heidelberg New York.

86. Garcia, S.R. et.al. (2003). Modeling ground motion in Mexico City using artificial neural networks. Geofisica Internacional, 42(2): 173-183.

87. Garcia, S.R., Miguel, R.P. and Juan, M.M. (2007). Estimation of peak ground accelerations for Mexican subduction zone earthquakes using neural networks. Geofísica international, 46(1): 51-62.

88. Gardner, M.W. and Dorling, S.R. (1998). Artificial neural networks (the multilayer perceptron) - A review of applications in the atmospheric sciences. Atmospheric Environment, 32 (14/15): 2627-2636.

89. Ghaboussi, J., and Lin, C.C.J. (1998). New method of generating spectrum compatible accelerograms using neural networks. Earthquake Engineering and Structural Dynamics, 27(4): 377-396.

90. Giacinto, G., Paolucci, R., and Roli, F. (1997). Application of neural networks and statistical pattern recognition algorithms to earthquake risk evaluation, Pattern Recognition Letters, 18 (11-13): 1353-1362.

91. Goh, A.T.C. (1994b). Seismic liquefaction potential assessed by neural networks, Journal of Geotechnical and Geoenvironmental Engineering, ASCE 120(9): 1467-1480.

92. Grossberg, S. (1976). Adaptive pattern classification and universal recording: parallel development and coding of neural feature detectors, Biological Cybernetics, 23: 121-134.

93. Grossberg, S. (1988a). Competitive learning: From interactive activation to adaptive resonance, in Neural Network and Natural Intelligence. S. Grossberg .ed. Cambridge. MA: MIT Press.

94. Grossberg, S. (1988b).Neural Networks and Natural Intelligence, Cambridge, M.A: MIT Press.

95. Grossberg, S. (1988c). Nonlinear neural networks: principles, mechanisms, and architectures. Neural Networks 1, 17-61.

96. Gullu, H. (2012). Prediction of peak ground acceleration by genetic expression programming and regression: a comparison using likelihood-based measure. Engineering Geology, 141-142: 92-113.

97. Gullu, H. (2013). On the prediction of shear wave velocity at local site of strong ground motion stations: an application using artificial intelligence, Bull. Earthquake Eng., 11: 969-997. DOI 10.1007/s10518-013-9425-8.

98. Gullu, H., and Ercelebi, E. (2007). A neural network approach for attenuation relationships: an application using strong ground motion data from Turkey, Science Direct, Engineering Geology, 93: 65-81.

99. Günaydin, Kemal., and Günaydin, Ayten (2008). Peak Ground Acceleration Prediction by Artificial Neural Networks for Northwestern Turkey, Hindawi Publishing Corporation, Mathematical Problems in engineering, article ID 919420, pp 1-20, Doi. 10.1155/2008/919420.

100. Gurney, K. (2005). An introduction to neural networks. UCL Press Limited is an imprint of the Taylor & Francis Group, London.

101. Guttierez, C. & Singh, S.K., (1992). A site effect study in Acapulco, Guerrero, Bull. Seismol. Soc. Am., 83: 1042-1063.

102. Guzman, R.A. and P.C. Jennings (1976). Design Spectra for Nuclear Power Plants, Journal of the Power Division, ASCE, **102**(PO2), 165-178.

103. Hagan, M.T., Demuth, H.B. and Beale, M. (1996). Neural Network Design, PWS Publishing Company, Boston, U.S.A.

104. Hanks, T.C. (1982). F_{max}. Bull. Seismol. Soc. Am., 72: 1867-1879.

105. Hassoun, M.H. (1995). Fundamentals of Artificial Neural Networks. MIT Press, Cambridge

106. Haykin, S. (1999). Neural Networks: A Comprehensive Foundation, Second Edition, Prentice-Hall, Englewood Cliffs, NJ, USA.

107. Heaton, T. H., and Kanamori, H., (1984). Seismic potential associated with subduction in the north western United States: Seismological Society of America Bulletin, V. 74, p. 933–941.

108. Hebb, D.O. (1949). The organization of behavior: A Neuropsychological Theory, John Wiley, New York.

109. Hecht-Nielsen, R. (1987). "Kolmogrov's mapping neural network existence theorem."

110. Hecht-Nielsen, R. (1989). Theory of the back-propagation neural network. Proceedings of the International Joint Conference on Neural Networks, Washington, DC, 593-605.

111. Hecht-Nielsen, R. (1990). Neurocomputing, Addison-Wesely Publishing Company, Reading, MA.

112. Hertz, J., Krogh, A. and Palmer, R. G. (1991). Introduction to the Theory of Neural Computing. Addison-Wesley Publishing Company.

113. Hopfield, J.J. (1982). Neural Networks and Physical Systems with Emergent Collective Computational Abilities. Proceeding of the National Academy of Science (USA), 79: 2554-2558.

114. Hopfield, J.J., and Tank, T.W. (1985). Neural computation of decisions in optimization problems. Biological Cybernetics, 52:141-152.

115. Housner, G.W. (1941). Calculating the response of an oscillator to arbitrary ground motion. Bull. Seismol. Soc. Am., 31(2): 143-149.

116. Husid, R.L. (1969). Analisis de terremotos: Analisis general, Reviata del IDIEM, Santiago, chile, 8: 21-42.

117. Idriss, I. M. 1978 (Jun). Characteristics of earthquake ground motions. Pages 1151–1265of: Proceedings of the ASCE Geotechnical Engineering Division Speciality Conference:Earthquake Engineering and Soil Dynamics, vol. III.

118. Idriss, I.M., Dobry, R,, and Singh, R.D. (1978). "Nonlinear behavior of soft clays during cyclic loading," *Journal of the Geotechnical Engineering Division*, ASCE, Vol. 104, No. GT12, pp. 1427-1447.

119. Iglesias A., Singh, S.K, Lowry, A., Santoyo, M., Kostoglodov, V., Larson, K.M. and Franco-SÃ¡nchez, S.I. (2004). The silent earthquake of 2002 in the Guerrero seismic gap, Mexico (M_w=7.6): inversion of slip on the plate interface and some implications, GeofÃsica Internacional ,43: 309-317.

120. Iglesias, A., Singh, S.K., Pacheco, J.F. and Ordaz, M. (2002). A source and wave propagation study of the Copalillo, Mexico, earthquake of 21 July 2000 (M_w 5:9): Implications for seismic hazard in Mexico City from inslab earthquakes. Bull. Seismol. Soc. Am., 92: 1060–1071.

121. IS 1893, Criteria for Earthquake Resistant Design of Structures - Part 1: General Provisions and Buildings (Fifth Revision), Bureau of Indian Standards, New Delhi, 2002.

122. Iyengar, R. N. and Ghosh, S. (2004). Microzonation of earthquake hazard in greater Delhi area, Current Science, 87, 1193–1202.

123. Jennings, P.C. (1985). Ground motion parameters that influence structural damage, in R.E. Scholi and J.L. King, eds. Strong Ground Motion Simulation and Engineering Applications, EERI Publication 85 – 02, Earthquake engineering research institute, Berkeley, California.

124. Joyner, W. B. and D. M. Boore (1981). Peak horizontal acceleration and velocity from strong motion records including records from the 1979 Imperial Valley, California, earthquake, Bull. Seism. Soc. Am. ***71***.

125. Joyner, W.B. and Boore, D.M. (1988). Measurement, characterization, and prediction of strong ground motion, in Earthquake Engineering and Soil Dynamics II – Recent Advances in Ground–Motion Evaluation, Geotechnical Special Publication-20, ASCE, New York, pp.43-102.

126. Joyner, W.B. and Boore, D.M. (1993). Methods for regression analysis of strong-motion data. Bull. Seismol. Soc. Am., 83(2): 469-487.

127. Joyner, W.B., Boore, D.M. (1996). Recent developments in strong motion attenuation relationships. Proceedings of the 28th joint meeting of the US-Japan cooperative program in natural resource panel on wind and seismic effects, 101-116.

128. Kaastra, I., and Boyd, M.S. (1995). Forecasting futures trading volume using Neural Networks, Journal of Futures markets, 15(8): 953-970.

129. Kalra, R., Deo, M.C., Kumar, R. and Agarwal, V.K. (2005). RBF network for spatial mapping of wave heights, Marine Structures, 18(3): 289–300.

130. Kamatchi, P. (2008). Neural Network Models for Site-Specific Seismic Analysis of Buildings," Ph. D. thesis, Department of Civil Engineering, Indian Institute of Technology Delhi, Delhi.

131. Kamatchi, P., Rajasankar, J., Ramana, G.V. and Nagpal, A.K. (2010). A neural network based methodology to predict site-specific spectral acceleration values.Earthquake Engineering and Engineering Vibration, 9(4): 459-472 DOI: 10.1007/s11803-010-0028-y.

132. Kanagarathinam, L., Dodagoudar, G.R. and Boominathan, A. (2010).Probabilistic seismic hazard Analysis for Kalpakkam, Tamil Nadu. 14 SEE, Dec 17-19, 2010, Vol. (1-2), pp 192-203, IIT Roorkee.

133. Karunanithi, N., Grenney, W.J., Whitley, D. and Bovee, K. (1994). Neural networks for river flow prediction, Journal of Computing in Civil Engineering, 8(2): 201–220.

134. Katsumata, A. (1996). Comparison of magnitudes estimated by the Japan meteorological agency with moment magnitudes for intermediate and deep earthquakes. Bull. Seismol. Soc. Am., 86(3): 832-842.

135. Kawase, H., and Aki, K. (1989). A study on the response of a soft basin for incident S, P, and Rayleigh waves with special reference to the long duration observed in Mexico City. Bull. Seismol. Soc. Am. **79**: 1361–1382.

136. Kaynia, A.M. (2006). Geotechnical aspects of earthquake design. Proc. Annual Conf. Geotech. Engg. (Geoteknikkdagen), Oslo, 24 Nov. 2006, pp 28.1-28-13.

137. Kerh, T. and Chu, D. (2002). Neural networks approach and microtremor measurements in estimating peak ground acceleration due to strong motion. Advances in Engineering Software, 33(11): 733-742.

138. Kerh, T. and Ting, S.B. (2005). Neural network estimation of ground peak acceleration at stations along Taiwan high-speed rail system. Engineering Applications of Artificial Intelligence, 18(7): 857–866.

139. Kerh, T., Lai, J.S., Gunaratnam, D. and Saunders, R. (2007). Neural Network Examination on Seismic Design Values in the Building Code of Taiwan." In Computer Systems and Applications, AICCSA'07. IEEE/ACS International Conference on, pp. 781-785. IEEE, Amman, Jordan, May 2007.

140. Khameneh, A.Z. and Raimar, J.S. (2008). Generating the Strong Ground Motion based on the First Oncoming Signals using Artificial Neural Network." 8th. World Congress on Computational Mechanics (WCCM8), 5th. European Congress on Computational Methods in Applied Sciences and Engineering (ECCOMAS 2008), Venice, Italy, Jul. 2008.

141. Khattri, K.N. and Teotia, S.S., (2000). Coping of with earthquake hazard and risk in the national capital region (Presented in workshop on Is Delhi prepared from earthquakes, fires and floods held at India International Centre, New Delhi, Sept. 15-16), Construction Journal of India, V. III, issue-3, pp48.

142. Kimball, J.K., (1983). The Use of Site Dependent Spectra, US Geological Survey, Open File Report 83-845, pp. 401-422.

143. Kramer, S. L. (2003). Geotechnical Earthquake Engineering, Pearson Education Publication, pp. 121.

144. Kramer, S.L. (1996). Geotechnical Earthquake Engineering, Prentice Hall, Inc., New Jersey.

145. Krishna Kumar, S. and Boominathan, A. (2010). Seismic Response of Shallow and Deep Stiff Soil Sites. 14 SEE, Dec 17-19, 2010, Vol. (1-2), pp 456-468, IIT Roorkee.

146. Kudrycki, T. P. (1988). Neural network implementation of a medical diagnosis expertsystem, MS thesis, College of Engineering, University of Cincinnati.

147. Kumar, A. (2009). Computer program for processing K-Net strong motion database, unpublished computer program, IIT Roorkee.

148. Kumar, A., Mittal, H., **Sachdeva, R.,** and Kumar, A. (2012). Indian strong motion instrumentation network. Seismological Research Letters, 83(1): 59-66.

149. Kumar, D., Teotia, S.S. and Sriram, V. (2011). Modelling of strong ground motions from 1991 Uttarkashi, India, Earthquake using a hybrid technique. Pure and applied geophysics 168(10): 1621-1643.

150. Kumar, Dinesh and Teotia, S.S. (2008). Prediction of Accelerograms for a Great Earthquake in the Central Seismic Gap Himalaya, National Seminar on Significant Milestones in the growth of Geophysics during the 50 years period (1958-2008), June 25-26, NGRI, Hyderabad.

151. Kuo, C.H., Cheng, D.S., Hsieh, H.H., Chang, T.M., Chiang, H.J., Lin, C.M., Wen, K.L. (2009). Comparison of three different methods in investigating shallow shear-wave velocity structures in Ilan, Taiwan .Soil Dynamics and Earthquake Engineering 29(1):133-143.

152. Kuo, C.H., Wen, K.L., Hsieh, H.H., Chang, T.M., Lin, C.M., Chen, C.T. (2011). Evaluating empirical regression equations for Vs and estimating Vs30 in north eastern Taiwan. Soil Dynamics and Earthquake Engineering, 31: 431-439.

153. Kuo, C.H., Wen, K.L., Hsieh, H.H., Lin, C.M., Chang, T.M., Kuo, K.W. (2012). Site classification and Vs30 estimation of free-field TSMIP stations using the logging data of EGDT. Engineering Geology, 129-130: 68–75.

154. Kyoshin Net (K-NET) Strong Motion Database, National Research Institute for Earth Science and Disaster Prevention, Ibaraki-kenn, Japan, [http://www.k-net.bosai.go.jp].

155. Lachtermacher, G. and Fuller, J.D. (1994). Back-propagation in hydrological time series forecasting. Stochastic and Statistical Methods in Hydrology and Environmental Engineering. K. W. Hipel, A.I. Mcleod, U.S. Panu, and V.P. Singh, eds., Kluwer Academic, Dordecht.

156. Lang, D., Palacios, S.M., Lindholm, C., Balan , S. (2011). Deterministic earthquake damage and loss assessment for the city of Bucharest, Romania, Journal of Seismology, 16(1): 67-88.

157. Lee, S.C., and Han, S.W. (2002). Neural-network-based models for generating artificial earthquakes and response spectra, Computers and Structures, 80(20-21): 1627-1638.

158. Lermo, J., and Chavez-Garcia, F.J. (1994). Site effect evaluation at Mexico City: dominant period and relative amplification from strong motion and microtremor records. Soil Dynamics and Earthquake Engineering, 13: 413-423.

159. Lin, C.C.J., and Ghaboussi, J. (2001). Generating multiple spectrum compatible accelerograms using stochastic neural networks, Earthquake Engineering and Structural Dynamics, 30(7): 1021-1042.

160. Lin, C-CJ, and Ghaboussi, J. (1997). Replicator neural network in generating artificial earthquake accelerograms. Proceeding, International Conference of Artificial Neural Networks in Engineering (ANNIE ’97), St. Louis, Missouri, pp 377–396.

161. Lin, C-CJ, and Ghaboussi, J. (2002). Neural-Network-Based Model for Generating Artificial Earthquake and Response Spectra. Computers And Structures, (80): 1627−1638.

162. Lin, C-CJ. A neural network based methodology for generating spectrum compatible earthquake accelerograms. Ph.D. Thesis, Dept. of Civil and Environmental Engineering, University of Illinois at Urbana-Champaign, Urbana, Illinois.

163. Lin, C-CJ., Liu, Z.M. and Lin, Y.C. (2006). New methodology of generating multiple spectrum compatible earthquake accelerograms for Taiwan area using neural networks. In Proceedings of the 4th International Conference on Earthquake Engineering. Taipei, Taiwan, October 2006.

164. Lin, Tzu Kang., Lin, C.C.J., and Chang, K.C. (2002). A Neural Network based methodology for estimating bridge damage after major earthquakes, Journal of Chinese Institute of Engineers, 25(4): 415-424.

165. Lindholm, C. (1998). Probabilistic and deterministic seismic hazard evaluation. Proceedings of the International Geoscientific Symposium in commemoration of the 25'th Anniversary of the Great Managua Earthquake, December 2-4, 1997, Managua, Nicaragua. 2 pages.

166. Lindholm, C. D., Rojas, W., Bungum, H., Dahle, A., Camacho, E., Cowan, H. and Laporte, M. (1995). A new regional seismic zonation for Central America. In: Proceedings of the fifth Int. Conference on Seismic Zonation, Oct. 17 - 19, Nice, France.

167. Liu, B.Y., Ye, L.Y., Xiao, M.L., and Miao, S. (2006). Peak ground velocity evaluation by artificial neural network for west America region, in Proceedings of the 13th International Conference on Neural Information Processing, Part II (ICONIP '06), vol. 4233 of Lecture Notes in Computer Science, pp. 942–951, Hong Kong, October 2006.

168. Mahajan, A.K., Galiana-Merino, J. J., Lindholm, C. , Arora, B. R., Mundepi, A.K., Chauhan, Neetu and Rai, N. (2011). Characterization of the sedimentary cover at the Himalayan foothills*:* Characterization of the sedimentary cover at the Himalayan foothills using active and passive seismic techniques. Journ of Applied Geophysics, 73: 196-206.

169. Mahajan, A.K., and Kumar, Sushil (2004). Macroseismic field observations of January 26th, 2001 Kachchh earthquake and its seismotectonics. Journal of Asian Earth Sciences 23(1): 17-23.

170. Mahajan, A.K., and Virdi, N.S. (2001). Macroseismic field generated by 29 March, 1999 Chamoli Earthquake and its seismotectonics. Journal of Asian Earth Sciences 19(4): 507-516.

171. Mahajan, A.K., et al (2010). Probabilistic seismic hazard map of NW Himalaya and its adjoining area, India. Natural hazards 53(3): 443-457.

172. Mahajan, A.K., Galiana-Merino, J.J., Lindholm, C., Mundepi, A.K. and Rai, Nitesh (2010). A comparative study of active and passive masw and fk technique and optimum field parameters for site characterization. 14 SEE, Dec IIT Roorkee.

173. Mahajan, A.K., Mundepi, A. K., Chauhan, Neetu., Jasrotia, A.S., Rai, Nitesh and Gachhayat, Tapas Kumar (2012). Active seismic and passive microtremor HVSR for assessing site effects in Jammu city, NW Himalaya, India—A case study. Journal of Applied Geophysics 77: 51-62.

174. Maheshwari, B., Kale, S. and Kaynia, A. (2012). Dynamic properties of Solani sand at large strains: a parametric study International Journal of Geotechnical Engineering 6 (3): 353-358.

175. Maheshwari, B.K., Mahajan, A. K., Sharma, M.L., Paul, D.K., Kaynia, A.M., and Lindholm, Conrad (2013). Relationship between shear velocity and SPT resistance for sandy soils in the Ganga basin, .International Journal of Geotechnical Engineering 7 (1): 63-70.

176. Maier, H. R., and Dandy, G.C. (2000). Neural networks for the prediction and forecasting of water resources variables: A review of modeling issues and applications. Environmental Modeling & Software, 15: 101-124.

177. Manisha, Kumar, Dinesh., and Teotia, S.S. (2011). Seismic Hazard based on Simulated Accelerograms due to Moderate/Strong Earthquakes in National Capital (Delhi) Region. J. Ind. Geophys. Union (April 2011) 15(2): 77-84.

178. Masters, T. (1993). Practical neural network recipes in C++. Academic Press, San Diego.

179. McCulloch, W.S., and Pitts, W.H. (1943). A Logical Calculus of the Ideas Immanent in Nervous Activity. Bulletin of Mathematical Biophysics,5: 115–133.

180. Mcguire, R.K., Becker, A.M., and Donovan, N.C. (1984). Spectral estimates of seismic shear waves," Bulletin of the Seismological Society of America, Vol. 74, No. 4, pp. 1427-1440.

181. Mehrotra, K., Mohan, C.K. and Ranka, S. (1996). Elements of Artificial Neural Networks, Penram International Publishing (India) Pvt. Ltd., Mumbai.

182. Minns, A.W. and Hall, M.J. (1996). Artificial neural networks as rainfall-runoff Models. Hydrological Science Journal, 41(3): 399-417.

183. Minsky, M.L. (1954). Theory of neural-analog reinforcement systems and its application to the brain-model problem, Ph.D. thesis, Princeton University, Princeton, NJ.

184. Mittal, H., Kumar, A. and Ramhmachhuani, Rebecca (2012). Indian national strong motion instrumentation network and site characterization of its station, International Journal of Geosciences, 3: 1151-1167.

185. Mohraz, B. (1976). A Study of Earthquake Response Spectra for Different Geological Conditions, Bull. Seismol. Soc. Am., 61(3): 915–935.

186. Movable Type Scripts, Calculate Distance, bearing and More between Two Latitude/longitude Points, Cambridge, UK. [http://www.movable-type.co.uk/scripts/latlong.html].

187. Mundepi, A.K., Galiana-Merino, J.J., Kamal and Lindholm, C. (2010). Soil characteristics and site effect assessment in the city of Delhi (India) using H/V and f–k methods. Soil Dynamics and Earthquake Engineering, 30(7): 591–599.

188. Naeim, F. (2001). The Seismic Design Hand Book, Second Edition, Kluwer Academic Publishers, Boston, MA.

189. Narayan, J.P., and Sharma, M.L. (2004). Effects of Local Geology on damage severity during Bhuj, India Earthquake, 13th World Conference on Earthquake Engineering, Vancouver, Canada, paper no 2042.

190. National Research Institute for Earth Science and Disaster Prevevtion (NIED), F-NET, Earthquake Mechanism Search, Japan, [http://www.fnet.bosai.go.jp].

191. Nawari, N. O., Liang, R., and Nusairat, J. (1999). Artificial intelligence techniques for the design and analysis of deep foundations. Electronic Journal of Geotechnical Engineeringhttp://geotech.civeng.okstate.edu/ejge/ppr 9909.

192. Neuman, V. J. (1956). Probabilistic logies and the synthesis of reliable organisms from unreliable components, in automata studies, C.E. Shannon and J. McCarthy. Eds., pp. 43-98, Princeton, NJ: Princetc University Press.

193. Neuman, V. J. (1958). The Computer and the Brain, New Haven, ct: Yale University Press, New York.

194. Newmark, N.M. and Hall, W.J. (1982). Earthquake Spectra and Design, EERI Monograph, Earthquake Engineering Research Institute, Berkeley, California, 103 pp.

195. Ortizi, M., Singh, S.K; Kostoglodov, V and Pacheco, J. (2000). Source areas of the Acapulco-San Marcos, Mexico earthquakes of 1962 (M 7.1; 7.0) and 1957 (M 7.7), as constrained by tsunami and uplift records, Geofísica Internacional, 39(4): 337-348.

196. Ozel, O., Cranswick, E., Meremonte, M., and Erdik, M. (2002). Site effects in Avcilar, West of Istanbul, Turkey, from Strong and Weak-Motion Data, Bull. Seism. Soc. Am., 92(1): 499-508.

197. Pacific Earthquake Engineering Research Center (PEER) –NGA database. http://peer.berkeley.edu/nga/flatfile. html.Last accessed on 28 Feb 2014.

198. Pandya, B., Porwal, P. and Banerji, P. (2002). Application of artificial Neural Network in development of site-specific response spectra, Proceedings of the Twelfth Symposium on Earthquake Engineering, Dec. 16-18, 199-207, IIT Roorkee, India.

199. Paolucci, R., Colli, P. and Giacinto, G. (2000). Assessment of seismic site effect in 2-D alluvial valleys using neural networks, Eartquake Spectra, 16 (3): 661-680.

200. Papageorgiou, A.S. and Aki, K. (1983). A specific barrier for the quantitative description of inhomogeneous faulting and the prediction of strong ground motion. II. Applications of the model, Bull. Seismol. Soc. Am., vol. 73: 953 – 978.

201. Patterson, D. (1996). Artificial Neural Networks, Singapore: Prentice Hall.

202. Paul, A. (2010). Current seismic hazard scenario in Garhwal-Kumaun Himalayas. 14 SEE, Dec 17-19, 2010, Vol. (1-2), pp 492-501, IIT Roorkee.

203. Paul, A.,and Kumar, N. (2010). Estimates of source parameters of M4.9 Kharsali earthquake using waveform modelling,J. Earth Syst. Sci., 119(5): 731–743.

204. Paul, A., and Pant, C.C. (2005). Seismicity Pattern of Utaranchal (1999-2004) as recorded by DTSN in Kumaun Himalaya, Geol. Surve. Ind. Spl. Pub. V 85, PP. 89-93.

205. Paul, A., and Pant, P.D. (2003). Seismic hazard estimation in northeastern Kumaun Himalayas, J. Geol. Soc. India, 61: 477–482.

206. PESMOS, Strong Motion Database, Department of Earthquake Engineering-Indian Institute of Technology, Roorkee, [http://pesmos.in/].

207. Principe, J.C., Euliano, N.R., and Lefebvre, W.C. (1999). Neural and Adaptive Systems: Fundamentals through Simulation, John Wiley & Sons, New York, NY, USA.

208. Ramhmachhuani, R. (2011). Site characterization of strong motion accelerographs stations, M.Tech. Thesis, Department of Earthquake Engineering. Indian Institute of Technology, Roorkee, Roorkee.

209. Reed, R.D. and Mark, R.J. (1999). Neural Smithing: Supervised Learning in Feed forward Artificial Neural Networks. The MIT Press.

210. Ripley, B. D. (1996). Pattern recognition and neural networks, Cambridge University Press, Cambridge.

211. Rogers, J.L. (1994). Simulating structural analysis with neural network. Journal of Computing in Civil Engineering, ASCE, 8(2): 252-265.

212. Rosenblatt, F. (1958). The perception: A probabilistic model for information storage and organization in the brain, Psychological Review, 65: 386-408.

213. Rumelhart, D.E., Hinton, G.E., and Williams, R.J. (1986). Learning internal representation by error backpropagation. In Parallel Distributed Processing: Explorations in Microstructure of Cognition (D.E. Rumelhart and J.L. McClelland and PDP research groups, edn., MIT Press, Cambridge, MA), 1: 318–362.

214. **Sachdeva, R.,** Kumar, A. and Sharma, M.L. (2010). Prediction of Average Shear Wave Velocity of Site using Strong Ground Motion Records and ANN. In 14th Symposium on Earthquake Engineering, Indian Institute of Technology, Roorkee, Dec 17–19, 2010, 126-137 New Delhi: Elite Publishing.

215. **Sachdeva, R.,** Kumar, A. and Sharma, M.L. (2012). Estimation of Peak Ground Acceleration using Artificial Neural (Paper ID: 1847). 15WCEE, Lisbon, Portugal.

216. Salchenberger, L. M., Cinar, E. M., and Lash, N. A. (1992). Neural networks: A new tool for predicting thrift failures. Decision Science, 23: 899-916.

217. Samui, Pijush, and Sitharam, T.G. (2010). Site characterization model using artificial neural network and kriging. International Journal of Geomechanics 10(5): 171-180.

218. Sarle, W. S. (1994). Neural networks and statistical models. Proceedings of the 19th Annual SAS Users Group International Conference, Cary, NC: SAS Institute, 1538-1550.

219. Sarles, W.S. (1997). Neural Network FAQ, periodic posting to the Usenet newsgroup comp.ai.neural-net, URL:ftp://ftp.sas.com/pub/neural/FAQ.html.

220. Seed H.B., Ugas, C., and Lysmer, J. (1976). Site-Dependent Spectra for Earthquake-Resistant Design, Bull. Seismol. Soc. Am., 66: 221–243.

221. Seed, H.B., Romo, M.P., Sun, J., Jaime, A. and Lysmer, J. (1987). Relationships between soil conditions and earthquake ground motions in Mexico city in the earthquake September 19, 1985. Report UCB/EERC-87/15. Earthquake Engineering Research Center, University of California, Berkeley, p 112.

222. Seung Chang Lee a, Sang Whan Han b (2002). Neural network based models for generating artificial earthquakes and response spectra. Computers and Structures, 80: 1627–1638.

223. Shahin, M., Jaska, M., and Maier, H. (2008). State of the art of artificial neural networks in Geotechnical engineering. The Electronic Journal of Geotechnical Engineering Bouquest, 8: 1-26.

224. Shahin, M., Maier, H., and Jaska, M. (2004). Data division for developing neural networks applied to geotechnical engineering. Journal of Computing in Civil Engineering 18 (2): 105-114.

225. Shahin, M.A., Jaska, M.B., and Maier, H.R. (2001). Artifical neural network application in geotechanical engineering, *Australian Geomechanics, 36 (1): 49-62.*

226. Sharma, B., Kumar, D., Teotia, S.S., Rastogi, B.K., Gupta, A.K. and Prajapati, S. (2012). Attenuation of Coda Waves in the Saurashtra Region, Gujarat (India). Pure and Applied Geophysics 169(1): 89-100.

227. Sharma, B., Teotia, S.S., Kumar, D. and Raju, P.S. (2009). Attenuation of P-and S-waves in the Chamoli Region, Himalaya, India. Pure and applied geophysics 166(12): 1949-1966.

228. Sharma, M. L. (2003). Seismic hazard in Northern India region Seismological Research Letters, Vol. 74, Number 2, March/April 2003, 140-146.

229. Sharma, M.L. (1998). Attenuation relationship for estimation of peak ground horizontal acceleration using data from strong motion arrays in India. Bull. Seismol. Soc. Am., 88(4): 1063–1069.

230. Sharma, M.L. and Bungum, H. (2006). New strong ground motion spectral acceleration relations for the Himalayan region. In: Proceedings of the1st European conference on earthquake engineering and seismology (ECEES),Geneva, Switzerland, 3-8 september 2006, paper 1312, 8 pp.

231. Shin, A., Takashi, K. and Hiroyuki, F. (2004). Strong motion seismograph network FF Engineering, 4 (3).

232. Shoji, Y., Tanii, K., Kamiyama, M. (2005). A study on the duration and amplitude characteristics of earthquake ground motions, Soil Dynamics and Earthquake Engineering, 25(7-10): 505-12.

233. Singh SK, Lermo JF, Dominguez T, Ordaz M, Espinosa JM, Mena E, Quaas R (1988a) The Mexico earthquake of September 19, 1985 – a study of amplification of seismic waves in the valley of Mexico with respect to a hill zone site. Earthq Spectra 4: 653-673

234. Singh, R.P., Aman, A. and Prasad, Y.J.J. (1996). Attenuation relations for strong seismic ground motion in Himalyan region, Pure and Applied Geophysics, 147(1), 161–180.

235. Singh, S. K., and Ordaz, M. (1993). On the origin of long coda observed in the lake-bed strong-motion records of Mexico City. Bull. Seismol. Soc. Am. **83**, 1298–1306.

236. Singh, S. K., Ordaz, M. and Pérez-Rocha, L.E. (1996). The great Mexican earthquake of 19 June 1858: Expected ground motions and damage in Mexico City from a similar future event. Bull. Seism. Soc. Am., 86: 1655-1666.

237. Singh, S.K, Dattatrayam, R.S., Suresh, G., Iglesias, A., Bansal, B.K., PÃ©rez, Xyoli, Ordaz, M., Gupta, H.K., Baidya, P.R., Gautam, J.L. (2005). The Great Sumatra-Andaman Earthquake of 2004: Regional Broadband Seismograms from India, Seismological Research Letters, 76: 684-692.

238. Singh, S.K., Mena, E., and Castro, R. (1988b). Some aspects of the source characteristics and ground motion amplification in and near Mexico City from acceleration data of the September, 1985, Michoacan, Mexico earthquakes, Bull. Seismol. Soc. Am., 78: 451-477.

239. Singh, S.K., Mohanty, W.K., Bansal, B.K. and Roonwal, G.S. (2002). Ground motion in Delhi from future large/greats earthquakes in the central seismic gap of the Himalayan arc,Bull. Seismol. Soc. Am., 92(2): 555–569.

240. Singh, S.K., Ordaz, M., Anderson, J.G., Rodriguez, M., Quaas, R., Mena, E., Ottaviani, M., and Almora, D. (1989). Analysis of Near-source Strong-motion Recordings along the Mexican Subduction Zone. Bull. Seism. Soc. Am., 79: 1697–1717.

241. Singh, S.K., Reichle, M., and Havskov, J. (1980). Magnitude and epicenter estimations of Mexican earthquakes from isoseismic maps, Geoffs. Int. 19: 269-284.

242. Sitharam, T.G. and Anbazhagan, P. (2008). Site Characterization Using Geotechnical and Geophysical Techniques for Seismic Microzonation of Urban Areas, Key note Lectures, International Conference Development of Urban Areas and Geotechnical Engineering on June 16-19, 2008 in Saint Petersburg, 1: 131-147.

243. Sitharam, T.G., Anbazhagan, P., and Ganesha, K. Raj. (2006). Use of remote sensing and seismotectonic parameters for seismic hazard analysis of Bangalore. Natural Hazards and Earth System Science 6(6): 927-939.

244. Sitharam, T.G., and Anbazhagan, P. (2007). Seismic hazard analysis for the Bangalore region. Natural Hazards 40(2): 261-278.

245. Sitharam, T.G., Samui, Pijush and Anbazhagan, P. (2008). Spatial variability of rock depth in Bangalore using geostatistical, neural network and support vector machine models. Geotechnical and Geological Engineering 26(5): 503-517.

246. Sivanandam, S.N., Sumathi, S., and Deepa, S.N. (2006). Introduction to Neural Networks using Matlab 6.0, Tata McGraw-Hill.

247. Smith, G. N. (1986). Probability and statistics in civil engineering: An introduction, Collins, London.

248. Smith, M. (1993). Neural networks for statistical modeling, Van Nostrand Reinhold,

249. Standards New Zealand (Draft NZS 1170.5), 2001. Structural design actions Part 5: Earthquake actions - New Zealand, Standards New Zealand, Wellington 6020, February 2001.

250. Stone, M. (1974). Cross-validatory choice and assessment of statistical prediction, Journal of Royal Statistical Society, B 36, 111-147.

251. Sun, C.G, Kim, D.S. and Chung, C.K. (2005). Geologic site conditions and site coefficients for estimating earthquake ground motions in the inland areas of Korea, Eng Geol 81: 446-469.

252. Tehranizadeh, M., and Safi, M. (2004). Application of artificial intelligence for construction of design spectra, Science Direct, Engineering Structures, 26: 707-720.

253. Tienfuan, K. and Ting, S.B. (2005). Neural network estimation of ground peak acceleration at stations along Taiwan high-speed rail system. EngineeringApplications of Artificial Intelligence, 18: 857-866.

254. Toflampas, L.M., Spyrakos, C.C., and Koutromanos, L.A. (2009). A new definition of strong motion duration and related parameters affecting the response of medium-long period structures. Soil Dynamics and Earthquake Engineering, 29(4): 752-63.

255. Tokar, S. A., and Johsson, P.A. (1999). Rainfall-runoff modeling using artificial neural networks. Journal of Hydrologic Engineering, 4(3): 232-239.

256. Tokimatsu, K., Arai, H. and Asaka, Y. (1998). Two dimensional shear wave structure and ground motion characteristics in Kobe based on microtremor measurements. Geotech Earthq Eng Soil Dyn III (1): 703-713.

257. Trifunac, M.D, and A.G. Brady (1975). A Study on the duration of strong earthquake ground motion,Bull. Seismol. Soc. Am., 65(3): 581-626.

258. Trifunac, M.D. (1976). Preliminary empirical model for scaling Fourier amplitude spectra of strong ground acceleration in terms of earthquake magnitude, source-to-station distance, and recording site conditions, Bulletin of the Seismological Society of America, Vol. 66, No. 4, pp. 1343-1373.

259. Trifunac, M.D., and Westermo, B.D. (1982). Duration of earthquake shaking, International Journal of Soil Dynamics and Earthquake Engineering, 1(3): 117-21.

260. Tsai, Y.B., and Huang, M.W. (2000). Strong ground motion characteristics of the Chi-Chi, Taiwan earthquake of September 21, 1999. Earthq Eng Seismol 2: 1-21.

261. Turkish Seismic Code (TSC) (2007).Specifications for structures to be built in disaster areas. http://www.koeri.boun.edu.tr/depremmuh/eski/FINAL999.pdf.

262. Twomey, J.M., and Smith, A.E. (1997). Validation and Verification. Artificial neural networks for civil engineers: Fundamentals and applications, N. Kartam, I. Flood and J.H. Garrett, eds, ASCE, new York,44-64.

263. Vanmarcle, E.H. (1976). Structural response to earthquake, Chapter 8 in C. Lomnitz and E. Rosenblueth, eds., Seismic Risk And Engineering Decisions, Elsevier, Amsterdam, pp. 287 - 338.

264. Vucetic, M. and Dobry, R. (1991). ”Effect of Soil Plasticity on Cyclic Response.” *J. Geotech. Engrg.*, 117(1), 89–107.

265. Wang, J. and Teng, T. (1997). Identification and picking of S phase using an artificial neural network. Bull. Seismol. Soc. Am., 87(5): 1140–1149.

266. Wells, D.L. and Coppersmith, K.J. (1994). New empirical relationships among magnitude, rupture length, rupture width, rupture area, and surface displacement. Bull. Seism. Soc. Am., 84: 974-1002.

267. Welstead, S.T. (1994). Neural Network and Fuzzy Logic Application in C++. John Wiley & Sons, Inc.,

268. Wen, K.L., Lin, C.M., Chiang, H.J., Kuo, C.H., Huang, Y.C., Pu, H.C. (2008). Effect of Surface Geology on Ground Motions: The Case of Station TAP056 - Chutzuhu Site. Terr. Atmos. Ocean. Sci., 19(5): 451-462, October 2008.

269. Werner et al. (1976). Geotechnical Investigations at Nuclear Power Plant Sites, Nuclear Engineering and Design 36: 397-409

270. Widrow, B. and Stearns, S.D. (1985). Adaptive signal proceeding England Cliffs, NJ: Prentice-Hall.

271. Widrow, B., and Hoff, M.E. (1960). Adaptive switching circuit. IREWESCON convention record, 4: 96-104.

272. Wirth, W., Wenzel, F., Sokolov, V.Yu. and Bonjer, K.-P. (2003). A uniform approach to seismic site effect analysis in Bucharest, Romania, Soil Dynamics and Earthquake Engineering, 23(8): 737-758.

273. Yamazaki, F., Molas, G.L. and Fatima, M. (1994). Use of neural networks for earthquake damage estimation", Proceeding of the 6th International Conference on Structural Safety and Reliability, pp. 2263-2270, Rotterdam, Netherlands,1994.

274. Yang, C.Y. (1986). Random Vibration 0f Structures, John Wiley and Sons, New York, 295 pp.

275. Yoseph, B and Ramana, G. V. (2008). Earthquake ground-motion parameters at stiff sites in Addis Ababa, Ethiopia, International Journal of Geotechnical Engineering, 2(1): 45-58.

276. Yoseph, B and Ramana, G. V. (2008). Probabilistic seismic hazard analysis at selected sites in Addis Adaba, Ethiopia, to appear in International Journal of Geotechnical Engineering, 3(1).

277. Yu, H.H. and Jenq, N.H. (2002). Handbook of neural network signal processing. CRC Press, ISBN 08493-2359-2.

278. Zurada, J.M. (1992). Introduction to Artificial Neural Systems, West Publishing Company, St. Paul, U.S.A.